THE LIPID HANDLING CAPACITY OF SUBCUTANEOUS FAT REQUIRES MTORC2 DURING DEVELOPMENT

A Dissertation Presented

By

Wen-Yu Hsiao

Submitted to the Faculty of the

University of Massachusetts Graduate School of Biomedical Sciences, Worcester

in partial fulfillment of the requirements for the degree of

DOCTOR OF PHILOSOPHY

June 30, 2020

INTERDISCIPLINARY GRADUATE PROGRAM

THE LIPID HANDLING CAPACITY OF SUBCUTANEOUS FAT REQUIRES MTORC2 DURING DEVELOPMENT

A Dissertation Presented By

Wen-Yu Hsiao

This work was undertaken in the Graduate School of Biomedical Sciences

Interdisciplinary Graduate Program

Under the mentorship of

David A. Guertin, Ph.D., Thesis Advisor

Anthony N. Imbalzano, Ph.D., Member of Committee

Jaime Rivera, Ph.D., Member of Committee

Laura C. Alonso, M.D., Member of Committee

Valentina Perissi, PhD, External Member of Committee

Roger J. Davis MA, MPhil, Ph.D., Chair of Committee

Mary Ellen Lane, Ph.D.,
Dean of the Graduate School of Biomedical Sciences

June 30, 2020

Acknowledgements

First and foremost, I would like to thank my thesis advisor, Dr. David Guertin, for the mentorship he provided to me from the beginning of my rotation in his laboratory through to completion of this degree. Dr. Guertin always brought in inspiring ideas and guided me through my research.

I would also like to thank my committee members, Dr. Roger Davis, Dr. Tony Imbalzano, Dr. Jaime Rivera and Dr. Laura Alonso for providing support and suggestions to my research and my career plan. I would like to give my special thanks to the chair, Dr. Davis, for always being supportive and hosting every meeting. I would also like to show my appreciation to Dr. Valentina Perissi for serving as an external member of my committee and providing innovative ideas.

I would also like to thank all the members in the Guertin lab. It wouldn't be such a warm, interactive and fun place to work and stay without you. There have also been laughs and jokes and good science in the lab.

Finally, I would like to thank my parents, Fu-Hsing and Chiung-Hua, in Taiwan and my husband, Jui-Fu. You made this journey possible.

Abstract

Overweight and obesity are associated with Type 2 Diabetes, non-alcoholic fatty liver disease, cardiovascular disease and cancer, but all fat is not equal as storing excess lipid in subcutaneous white adipose tissue (SWAT) is more metabolically favorable than in visceral fat. Here, we uncover a critical role for mTORC2 in setting SWAT lipid handling capacity. We find that subcutaneous white preadipocytes differentiating without the essential mTORC2 subunit *Rictor* express mature adipocyte markers but develop a striking lipid storage defect. *In vivo,* this results in smaller adipocytes, reduced tissue size, lipid re-distribution to visceral and brown fat, and sex-distinct effects on systemic metabolic fitness. Mechanistically, mTORC2 promotes transcriptional upregulation of select lipid metabolism genes controlled by PPARγ and ChREBP. These include genes that control lipid uptake, synthesis, and degradation pathways as well as *Akt2*, the gene encoding its substrate and insulin effector. Finally, we reveal a potential novel mTORC2 target, ACSS2, which might control intracellular acetyl-CoA availability and regulate metabolic gene expression by altering histone modification in white adipocytes. Exploring this pathway may uncover strategies to promote safe lipid storage and improve insulin sensitivity.

Author Contributions

In Chapter II, Dr. Yuefeng Tang performed the *Adiponectin-Cre;Rictor*$_{loxP/loxP}$ mouse experiments. Dr. Joan Sanchez-Gurmaches developed the *Prx1-Cre* project and Huawei Li assisted with mouse housing and breeding. Dr. Camila Martinez Calejman, Dr. Chien-Min Hung, Dr. Su Myung Jung and Dr. Amelia Luciano assisted with biochemical analysis. Dr. Rui Li and Dr. Lihua Julie Zhu performed the bioinformatics analysis of RNA-seq. John Haley performed Seahorse assays and data analysis. Victoria DeMambro and Dr. Clifford Rosen from Maine Medical Center performed bone structure and bone marrow imaging and analysis. Dr. Kathryn Wellen from University of Pennsylvania Perelman School of Medicine shared the ACLY constructs and participated in the design and discussion.

In Chapter III, Dr. Sophie Trefely and Dr. Nathaniel Snyder from University of Pennsylvania and Drexel University performed the acetyl-CoA measurement and labeling experiments.

Table of Contents

List of Tables

List of Figures

Chapter IV

List of copyrighted Materials Produced by the Author

The following figures were reproduced from journals:

Figure Number	Publisher
Figure I-3	Elsevier
Figure I-4	Springer
Figure III-1	Springer

List of Third Party Copyrighted Material

Figure Number	Publisher	License Number
Figure I-5	Elsevier	4855680142366

The following figures were reproduced from journals:

Figure Number	Publisher
Figure I-1	Elsevier

List of Symbols, Abbreviations or Nomenclature

ACC – Acetyl-CoA carboxylase

ACLY – ATP citrate lyase

ACSS2 – Acyl-CoA Synthetase Short Chain Family Member 2

Adipoq – Adiponectin

AGPAT1 – 1-acylglycerol-3-phosphate O-acyltransferase 1

ATGL – Adipose triglyceride lipase

C/EBPα – CCAAT-enhancer-binding protein α

C/EBPβ – CCAAT-enhancer-binding protein β

C/EBPδ – CCAAT-enhancer-binding protein δ

ChREBP – Carbohydrate-responsive element binding protein

DGAT1 – Diacylglycerol O-acyltransferase 1

DGAT2 – Diacylglycerol O-acyltransferase 1

EHHADH – Enoyl-CoA hydratase and 3-hydroxyacyl-CoA dehydrogenase

FABP4 – Fatty acid binding protein 4

FASN – Fatty acid synthase

GLUT1 – Glucose transporter type 1

GLUT4 – Glucose transporter type 4

GPAT – Glycerol-3-phosphate acyltransferase

HSL – Hormone-sensitive lipase

Insig1 – Insulin induced gene 1

LPL – Lipoprotein lipase

MCAD – Medium-chain acyl-CoA dehydrogenase

mTORC2 – the Mammalian/mechanistic target of rapamycin complex 2

PPARγ – Peroxisome proliferator-activated receptor γ

PRX1 – Paired-related homeobox 1

SCD1 – Stearoyl-CoA desaturase 1

SREBP1 – Sterol regulatory element binding protein 1

UCP1 – Uncoupler protein 1

CHAPTER I – General Introduction

This chapter contains materials published in Current Diabetes Reports from

Springer:

Hsiao, W.-Y., Guertin, D.A., 2019. *De Novo* Lipogenesis as a Source of Second Messengers in Adipocytes. Curr. Diab. Rep. 19, 138.
https://doi.org/10.1007/s11892-019-1264-9

1.1 Obesity and Type 2 Diabetes

Overweight and obesity affect much of the US population and their global prevalence is increasing (Hales et al. 2017). Body mass index (BMI) of 25-30 kg/m_2 is defined as overweight, and obesity is defined as BMI over 30 kg/m_2. One-third of adults in the US are considered obese, or approximately 93.3 million people affected as of 2015-2016 (Hales et al. 2017). Obesity is a major risk factor for Type 2 Diabetes (T2D), cardiovascular diseases and several cancer types (Van Gaal, Mertens, and De Block 2006). The onset of T2D, in particular, parallels with obesity in all ethnic groups (Sullivan et al. 2005; Eckel et al. 2011), and more than 80% of T2D cases can be attributed to obesity (Willett, Dietz, and Colditz 1999).

T2D is characterized by hyperglycemia, which is caused by blunted insulin sensitivity of metabolic tissues. Impaired insulin sensitivity decreases glucose uptake and utilization in muscle cells and adipocytes leading to increased circulating glucose. In the earlier disease stage, this drives pancreatic beta cells to secret more insulin in response to the higher glucose level. Persistent hyperinsulinemia can lead to beta cell dysfunction, causing decreased insulin secretion in late-stage disease (Ashcroft and Rorsman 2012). Indeed, insulin resistance and hyperinsulinemia occur before the onset of hyperglycemia (Tabák et al. 2012). Lifestyle change and therapeutic intervention in the early stage of the disease is the preferred treatment strategy. However, the current treatments

are unsatisfactory, as evidenced by the high rates of patients with unregulated blood sugar, and there is an unmet need for new antidiabetic therapeutics. To this end, understanding the molecular pathogenesis of insulin resistance is critical.

Center stage in the obesity epidemic is body fat, or adipose tissue. This is the body's main long-term energy storing tissue and a critical source of endocrine signals (called adipokines) that regulate systemic metabolic homeostasis (Rosen and Spiegelman 2014; Luo and Liu 2016). Adipose tissue has become the culprit of the obesity and T2D epidemics even though a main function of adipose tissue expansion is to protect against over-nutrition. Nevertheless, excessive adipose tissue can lead to its dysregulation and is thought to drive insulin resistance and pre-diabetes (Kusminski, Bickel, and Scherer 2016; Longo et al. 2019). Notably, having too little adipose tissue, such as in lipodystrophy disorders, can also cause insulin resistance and metabolic disease (Joffe, Panz, and Raal 2001). Thus, understanding how adipose tissue responds to and regulates metabolism is essential for understanding and treating T2D.

1.2 Anatomical location and function of adipose tissues

Adipose tissue morphology and function vary based on its anatomical location (Kwok, Lam, and Xu 2016; Sebo and Rodeheffer 2019; Kahn, Wang, and Lee 2019). Generally speaking, there are two distinct classes of adipose

tissue: brown adipose tissue (BAT) and white adipose tissue (WAT) [Figure I-1]. Brown adipocytes in BAT contain multilocular lipid droplets and produce energy via uncoupled respiration in mitochondria [Figure I-2]. WAT is generally considered energy storing and can be further subcategorized as subcutaneous adipose tissue (SWAT) or visceral adipose tissue (VWAT) based on its location [Figure I-1]. However, even this is an oversimplification as different SWAT depots can have different developmental origins, gene expression profiles and metabolic functions (Sanchez-Gurmaches, Hung, and Guertin 2016; Chau et al. 2014; Macotela et al. 2012; M.-J. Lee, Wu, and Fried 2013). SWAT, which resides under the skin, is often considered a “healthy” adipose tissue as studies show that some obese individuals with higher amounts of SWAT have normal insulin sensitivity and less tissue inflammation (Primeau et al. 2011; Scherer 2019). Moreover, a portion of white adipocytes in SWAT can adopt brown adipocyte-like characteristics, becoming what is called brite or beige adipocytes, in response to cold stimulation, exercise, and other stresses [Figure I-2] (Ikeda, Maretich, and Kajimura 2018; Fox et al. 2007). This so-called “browning” potential might also make SWAT more metabolically beneficial. In contrast, excess VWAT, which is adjacent to internal organs, is often metabolically unhealthy. Clinical studies reveal that expanding VWAT (as seen in central obesity) positively correlates with the development of insulin resistance (Verboven et al. 2018; André Tchernof and Després 2013).

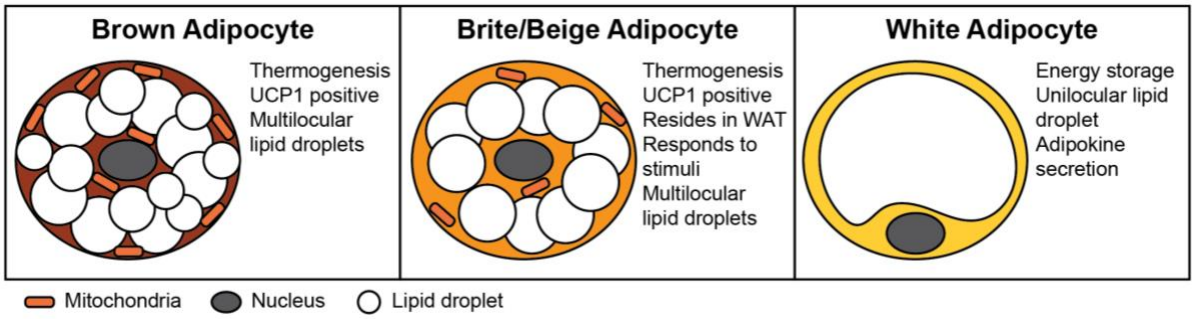

Figure I-1 Comparisons of morphology and function between brown, brite/beige and white adipocytes. This figure was adapted from the following publication:
Sanchez-Gurmaches, J., Hung, C.-M., Guertin, D.A., 2016. Emerging Complexities in Adipocyte Origins and Identity. *Trends Cell Biol.* 26, 313–326.

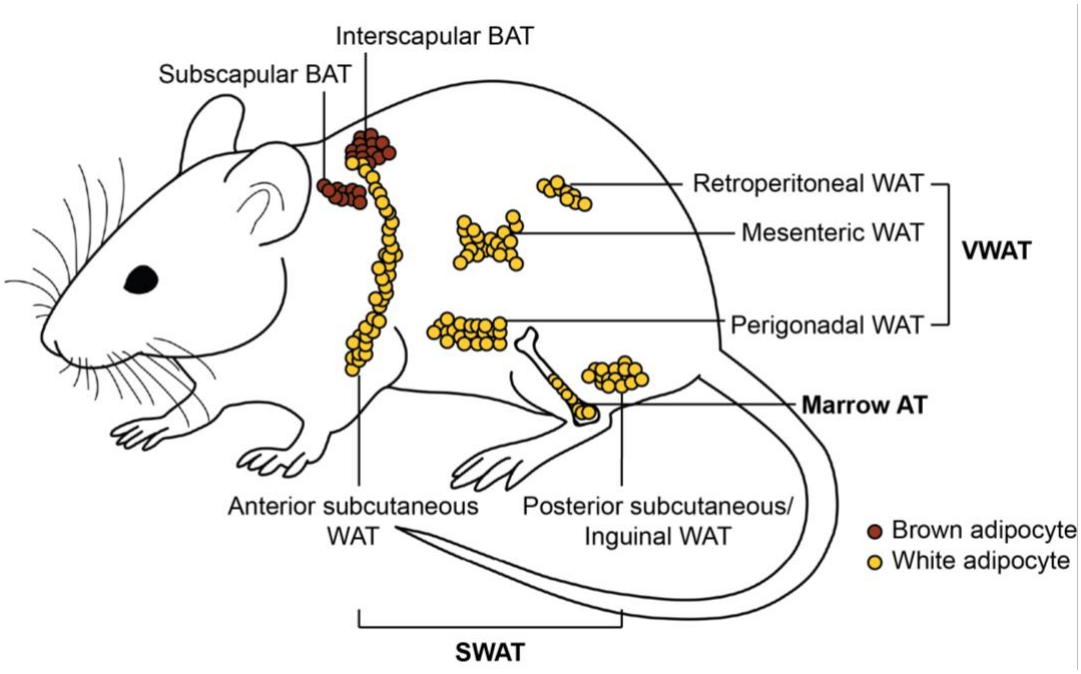

Figure I-2 Anatomical distribution of major adipose tissues in mouse. WAT: white adipose tissue; VWAT: visceral white adipose tissue; SWAT: subcutaneous white adipose tissue; BAT: brown adipose tissue; Marrow AT: marrow adipose tissue.

SWAT and VWAT also differ in their mechanism of growth (Bjørndal et al. 2011; Vishvanath and Gupta 2019). Some human studies suggest that SWAT preadipocytes have greater adipogenic capacity and differentiate into new adipocytes, thereby expanding tissue size by increasing cell number, especially in women (Drolet et al. 2008; Veilleux et al. 2011; Verboven et al. 2018; Lessard and Tchernof 2012; Macotela et al. 2012). VWAT, on the other hand, expands by increasing individual adipocyte size (called hypertrophy) (Lessard and Tchernof 2012). Curiously, a mouse study marking newly-synthesized adipocytes shows that, upon high-fat diet feeding, VWAT formed new adipocytes from precursors, whereas SWAT expanded mainly by hypertrophy (Q. A. Wang et al. 2013). Thus, how adipose tissues grow may vary depending upon stimuli, sexes, or species. Interestingly, transplantation of donor SWAT to either visceral or subcutaneous site in recipient mice improves glucose tolerance and insulin sensitivity (M. T. Foster et al. 2011; 2013; Hocking, Chisholm, and James 2008; T. T. Tran et al. 2008; Stanford et al. 2015). This suggests that there are also intrinsic properties of each depot that are independent of anatomical location. Other studies argue that increasing individual adipocyte size in either or both depots correlates with insulin resistance (Tulloch-Reid et al. 2004), and expanding SWAT by this modality may also promote insulin resistance. In addition to SWAT and VWAT, bone marrow adipose tissue (MAT) also secrets adiponectin and plays a role in regulating whole-body metabolism (Scheller et al. 2015). The contribution of

different fat depots to energy storage, adipokine production, and overall insulin sensitivity is complex and thorough research still needs to be done.

Targeting selective adipose tissue with Cre-Lox recombination system

Tissue-specific Cre driver (Cre recombinase controlled by a tissue-specific promoter), combined with *LoxP*, allows us to manipulate genes of interests in a tissue-specific manner (H. Kim et al. 2018). In the field of adipose tissue studies, *Adiponectin-Cre* targets mature adipocytes in both BAT and WAT, with fewer off-target effects in other organs which is superior to a previously used *aP2-Cre* [Table I-1]. For selectively targeting BAT, *Ucp1-Cre* is available for targeting mature brown adipocytes and *Myf5-Cre* as well as *Pax7-Cre* for targeting brown adipocyte precursor cells (APCs) [Table I-1 and I-2]. However, a challenge exists that there had been no Cre drivers that selectively target white APCs. Emerging drivers have been shown to target in a variety of stages in adipocyte precursors, such as *Pdgfra-Cre*, *Pdgfrb-Cre* and *Wt1-Cre* drivers, but these Cre drivers also target other cell types during embryogenesis other than APCs and might complicate the phenotypes seen in adipocytes [Table I-2]. Recently we reported that *Prx1-Cre* (the paired related homeobox1 promoter-driven Cre), which is induced in mesenchyme, selectively targets the APCs in SWAT as well as in adipose tissue in bone marrow [Figure I-3] (Sanchez-Gurmaches, Hsiao, and Guertin 2015). Thus, acknowledging that there is no tool without caveats, *Prx1-*

Cre may be the most useful Cre driver for selectively studying adipose tissue development *in vivo* and understanding the distinct metabolic functions of SWAT.

Table I-1 Summary of existing Cre drivers targeting mature adipocytes.

Targeting mature adipocytes				
	Driver	**Target depots**	**Other tissue expression**	**References**
aP2-Cre	*aP2* promoter	BAT and WAT	Liver, Skeletal muscle, Brain, Lung, Testis	(Abel et al. 2001; Barlow et al. 1997; He et al. 2003)
Retn-Cre	BAC transgenic containing up and downstream of *resistin* gene (*Retn*)	BAT and WAT	Brain	(Mullican et al. 2013)
Adipoq-Cre	Adiponectin promoter or BAC transgenic sequence of *adiponectin* (*adipoq*)	BAT and WAT	Osteoblasts	(Z. V. Wang et al. 2010; Eguchi et al. 2011)
Ucp1-Cre	*Ucp1* promoter and coding region	BAT and brite/beige fat		(Guerra et al. 2001)

BAT: brown adipose tissue; WAT: white adipose tissue.

Table I-2 Summary of existing Cre drivers targeting adipocyte precursors.

Targeting adipocyte precursor cells (APCs)			
	Target depots	**Other tissue expression**	**References**
Prx1-Cre	APCs from psWAT, asWAT (regional), MAT	Bone, other tissues derived from limb bud mesenchyme	(Sanchez-Gurmaches, Hsiao, and Guertin 2015; Logan et al. 2002; Krueger et al. 2014)
PdgfRa-Cre	APCs from all WATs	Fibroblasts with other differentiation potentials (e.g. myofibroblasts) in many tissues	(Berry and Rodeheffer 2013; Roesch et al. 2008)
PdgfRb-Cre	IngWAT, rWAT	Mural cells in vasculature (mainly in adipose tissue)	(W. Tang et al. 2008; Foo et al. 2006)
Pax3-Cre	BAT, rWAT, asWAT (50%), pgWAT*	Skeletal muscles	(Lang et al. 2005; Liu et al. 2012)
HoxB6-Cre	ingWAT, mWAT, pgWAT**, asWAT	Spleen	(Sebo et al. 2018)
Meox1-Cre	APCs from BAT, rWAT, pgWAT*	Skeletal muscles	(Sebo et al. 2018)
Wt1-Cre	APCs from VWATs	Mesoderm-derived tissues: kidneys, gonads, peri-/epicardium, spleen, mesentery, omentum	(Chau et al. 2011; 2014)
Myf5-Cre	APCSs from BAT, asWAT and rWAT***	Skeletal muscles	(Sanchez-Gurmaches et al. 2012; Tallquist et al. 2000)
Pax7-Cre	BAT	Skeletal muscles	(Sebo et al. 2018; Lepper and Fan 2010; Lepper, Conway, and Fan 2009)
VE-cadherin-Cre	BAT, ingWAT, pgWAT	Endothelial cells of vasculature, hematopoietic cells	(Alva et al. 2006; Monvoisin et al. 2006; K.-V. Tran et al. 2012)

* More labeled cells in this depot from male mice.
** More labeled cells in this depot from female mice.
*** Around 50% of cells labeled in these white depots.
BAT: brown adipose tissue; WAT: white adipose tissue; psWAT: posterior subcutaneous WAT; asWAT: anterior subcutaneous WAT; ingWAT: inguinal WAT; pgWAT: perigonadal WAT; mWAT: mesenteric WAT; rWAT: retroperitoneal WAT; VWAT: visceral WAT; MAT: bone marrow adipose tissue.

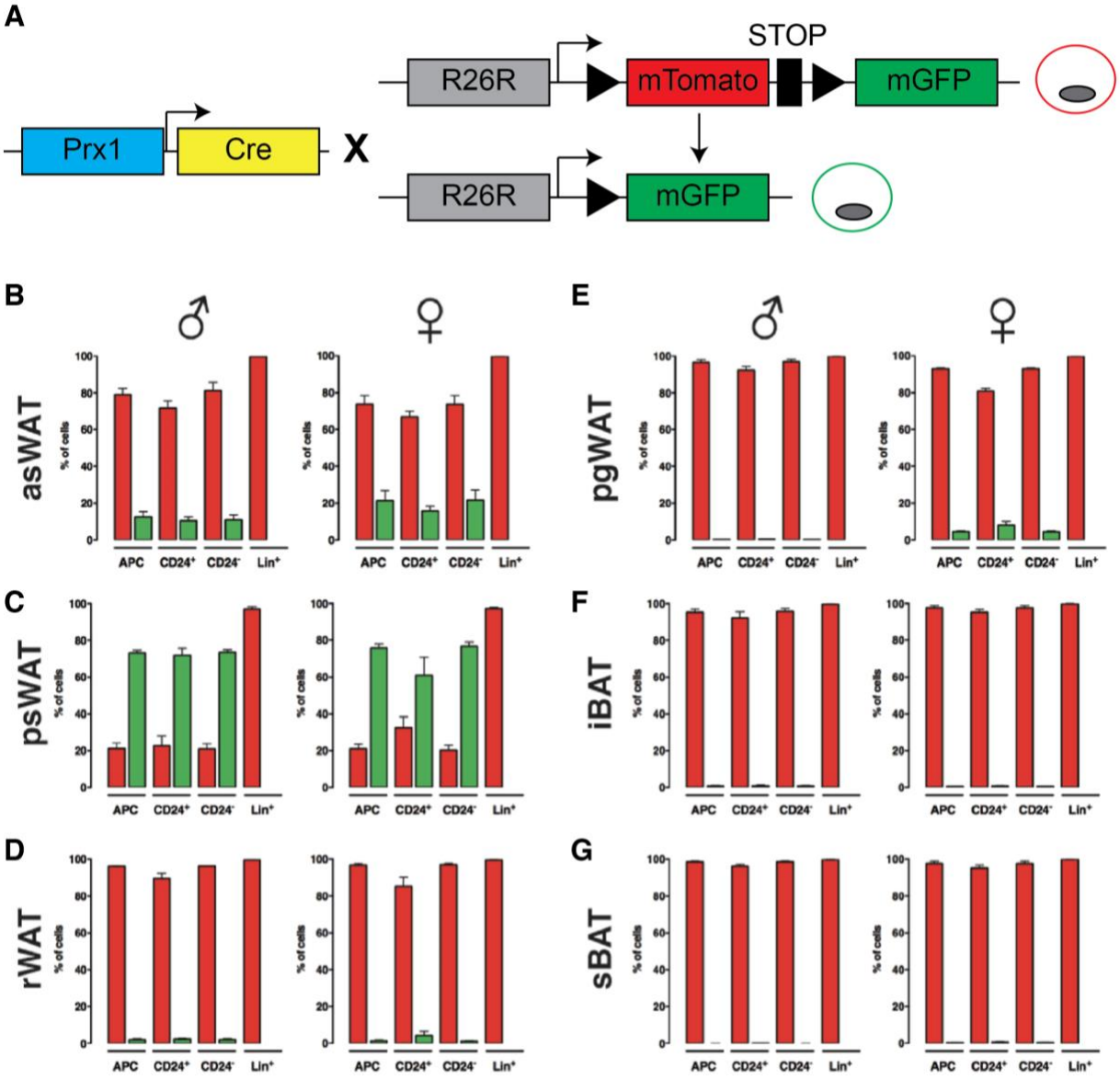

Figure I-3 *Prx1-Cre* selectively targets subcutaneous white adipocyte precursors. A. Schematic diagram of alleles of the mouse model used in this study. **B-G.** Percentage of mTomato+ or mGFP+ cells in the subvascular fraction (SVF) of indicated depot. The SVFs were analyzed by flow cytometry with the following cell surface markers: Lin(CD45/CD31), CD34, Sca1 and CD24. Lin+ cells were considered non-APCs. Lin- were further sorted into APCs (CD34+ and Sca1+) and other non-APC cells. The APCs were further classified into CD24+ and CD24- populations. asWAT: anterior subcutaneous white adipose tissue; psWAT: posterior subcutaneous WAT; rWAT: retroperitoneal WAT; pgWAT: perigonadal WAT; iBAT: interscapular brown adipose tissue; sBAT: subscapular BAT. This figure was adapted from the following publication:
Sanchez-Gurmaches, J., Hsiao, W.-Y., Guertin, D.A., 2015. Highly selective *in vivo* labeling of subcutaneous white adipocyte precursors with Prx1-Cre. *Stem Cell Reports* 4, 541–550.

1.3 Mechanisms of adipose tissue insulin resistance

The ability of an adipocyte to balance anabolic and catabolic lipid metabolism is essential for overall metabolic health. In the post-prandial (fed) state, insulin stimulates the transport of circulating glucose and lipids into adipocytes and suppresses lipolysis. Lipolysis occurs when stored lipids in the form of triacylglycerol (TAG) are hydrolyzed into free fatty acids (FFAs) and glycerol. During fasting, anabolic pathways abate while glucagon stimulates lipolysis. Following lipolysis, FFAs are released into circulation to provide fuel for other tissues while glycerol is used by the liver for gluconeogenesis or TAG synthesis. In insulin resistance, these tightly regulated metabolic processes fail to respond normally to increased circulating insulin following a meal. In adipocytes, this translates into insulin's inability to stimulate glucose uptake and suppress lipolysis. When adipocytes cannot normally store lipids, these lipids can "spillover" and accumulate in other tissues such as liver and skeletal muscle, causing toxicity (Sattar and Gill 2014; Unger et al. 2010; Scherer 2019). Obesity also impairs the synthesis and/or secretion of important adipokines, such as adiponectin, which normally promotes insulin sensitivity in other tissues (Kwon and Pessin 2013).

Understanding how diet, lifestyle, and genetics influence the carbohydrate and lipid handling capacity of adipocytes and their endocrine functions is critical to advancing new therapies. Yet despite many major advances, a key question

still under intense investigation is how exactly adipose tissue dysfunction promotes insulin resistance in obesity. Both reduced glucose uptake and increased lipolysis have been shown to drive systemic insulin resistance (Samuel and Shulman 2012; Morigny et al. 2016; Guilherme et al. 2019). Obesity is also associated with adipose tissue inflammation, which can promote insulin resistance by interfering with insulin signaling (Huh et al. 2014; Chatzigeorgiou and Chavakis 2016; Xia, Rao, and Zhong 2017). Both innate and adaptive immune functions, mediated by macrophages and T cells respectively, are dysregulated in obesity, which leads to proinflammatory cytokine secretion (Appari, Channon, and McNeill 2017; Kang et al. 2016; Olefsky and Glass 2010; Deng et al. 2017; McLaughlin Tracey et al. 2014). In this thesis, we will focus on how altered glucose and lipid metabolism in adipocytes affects systemic insulin sensitivity.

In the fed state, insulin promotes glucose uptake into adipocytes by triggering the translocation of the glucose transporter, GLUT4, to the plasma membrane [Figure I-4]. This is regulated at least in part by insulin-stimulated AKT-dependent inhibitory phosphorylation of the AS160 Rab-GTPase, which allows Rab protein to remain GTP-bound and facilitates translocation of GLUT4-containing vesicles to the plasma membrane (Mîinea et al. 2005; Brewer et al. 2011; Ramm et al. 2006, 14; Shuai Chen et al. 2011). AKT and AS160-independent pathways also reportedly contribute to GLUT4 translocation

(Gonzalez and McGraw 2006). Within adipocytes, glucose has several potential fates [Figure I-4]. It can be used to synthesize glycerol-3-phosphate (G3P) from glycolytic metabolites, which was recently shown to be stimulated by insulin in 3T3L1 adipocytes (Krycer et al. 2017). G3P is required to make glycerol for the esterification of FFAs, which is an essential step in TAG synthesis. Glucose can also enter the hexosamine biosynthetic pathway (HBP), a branch of glycolysis, in which O-linked N-acetylglucosamine (O-GlcNAc) is generated. O-GlcNAc can be used for post-translational modification of proteins by a process called O-GlcNAcylation. Key regulators of insulin signaling including IRS-1 and AKT can be O-GlcNAcylated (Whelan et al. 2010; Park, Ryu, and Lee 2005, 2), as can PPARγ, the master transcription factor in adipocyte differentiation (Ji et al. 2012). Glycosylation is thought to affect protein activity and insulin sensitivity in adipocytes (Wells, Vosseller, and Hart 2003; Mondoux et al. 2011; C. Sun et al. 2016; Wollaston-Hayden et al. 2014). Glucose metabolites also contribute to the pentose phosphate pathway (PPP) in adipocytes, which generates NADPH needed for lipogenesis (Krycer et al. 2017). Fatty acids are also synthesized *de novo* from glucose-derived carbons via a pathway called *de novo* lipogenesis (DNL, discussed below). Thus, metabolite flux through these pathways dynamically reflects glucose availability and utilization by adipocytes, which is coupled to hormonal signaling.

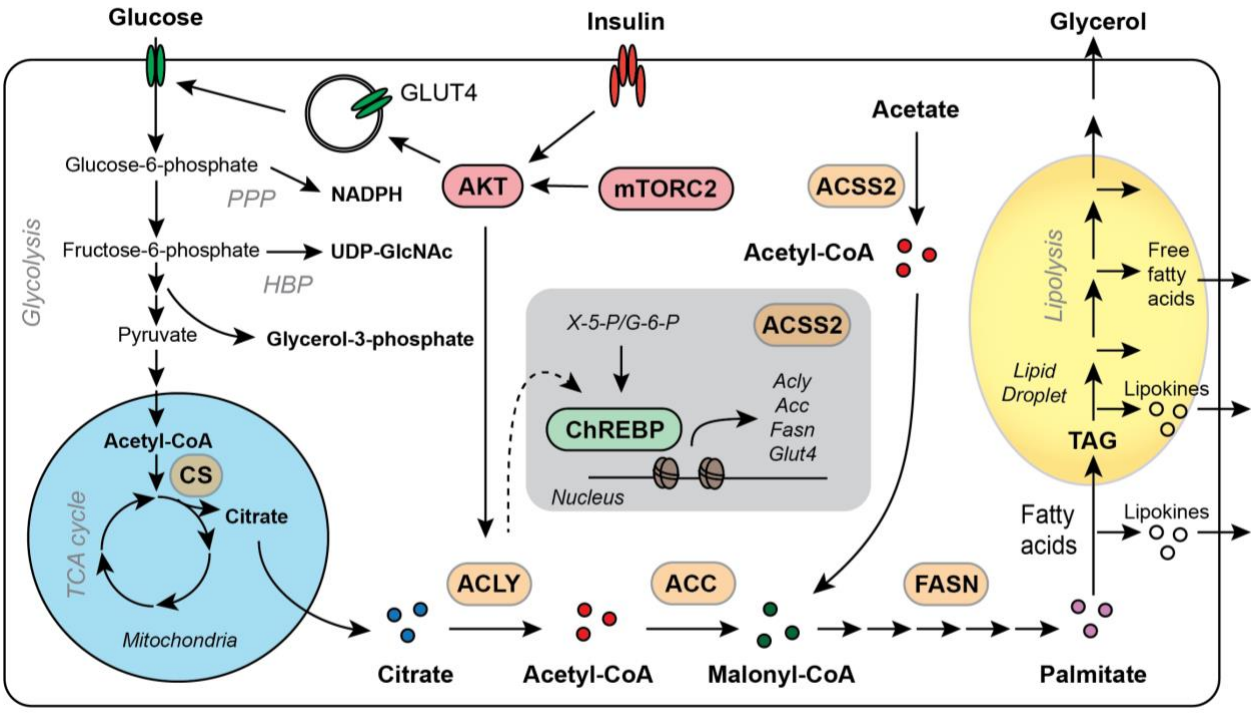

Figure I-4 Glucose Metabolism and *De Novo* Lipogenesis (DNL) in Adipocytes. Model depicting major metabolic routes of glucose metabolites in adipocytes. In the fed state, insulin stimulates GLUT4 translocation to the plasma membrane and facilitates glucose uptake. Metabolites of glucose generated during glycolysis can enter the pentose phosphate pathway (PPP), which generates NADPH for lipid synthesis; the hexosamine biosynthetic pathway (HBP), which generates UDP-N-acetylglucosamine (UDP-GlcNAc) and promotes O-GlcNAcylation of proteins; and the glycerol-3-phosphoate pathway, which is required to make the glycerol backbone for assembling triacylglycerides (TAGs). Glucose carbons that enter into the mitochondrial TCA cycle as pyruvate are converted to citrate by citrate synthase (CS). Citrate can remain in the TCA cycle, or in times of nutrient abundance, be exported into the cytoplasm and enter the DNL pathway. The major DNL enzymes are ATP citrate lyase (ACLY), which generates acetyl-CoA; acetyl-CoA carboxylase (ACC), which generates malonyl-CoA; and fatty acid synthase (FASN), which synthesizes palmitate. Palmitate is the primary end product of DNL, which can be further processed by desaturases and elongases. DNL enzymes and Glut4 transcription are regulated by ChREBP. Other glycolytic-derived metabolites, such as xylulose-5-phophate (X-5-P) and glucose-6-phosphate (G-6-P), are thought to directly stimulate ChREBP activity. Acetyl-CoA can also be produced from acetate by ACSS2 although ACSS2's function in adipocytes is not well understood. Note that a large fraction of the lipid stored in TAGs is derived from circulating lipids taken up into the adipocytes, which is discussed in the text but excluded from the figure for simplicity. This figure was adapted from the following publication:
Hsiao, W.-Y., Guertin, D.A., 2019. *De Novo* Lipogenesis as a Source of Second Messengers in Adipocytes. *Curr. Diab. Rep.* 19, 138.

1.4 *De novo* lipogenesis in adipocytes and insulin sensitivity

The DNL pathway is positively correlated with insulin sensitivity in human obesity. For example, human and mouse models of obesity have a downregulated DNL pathway in the adipose tissue, and reduced GLUT4 gene expression (Eissing et al. 2013; Herman et al. 2012; Roberts et al. 2009; Guilherme et al. 2017). In healthy individuals, DNL in adipocytes is thought to contribute relatively little to overall TAG content (around 20% based on $^{2}H_{2}O$-tracing study in human); most TAG is derived from the uptake and esterification of exogenous lipids from circulation (Strawford et al. 2004). However, only subcutaneous depots have been carefully examined and differences in DNL between depots at different anatomical sites are not well defined. Notably, the positive correlation between DNL and insulin sensitivity is specific to adipocytes. For example, in the liver, increased DNL drives nonalcoholic fatty liver disease (NAFLD) and insulin resistance (Chiu, Mulligan, and Schwarz 2018; Eissing et al. 2013; Sanders and Griffin 2016).

How does DNL in adipocytes link to insulin sensitivity? One possibility is that adipocytes synthesize special signaling lipids that have systemic insulin sensitizing functions. One such “lipokine” that has been reported is palmitoleate (16:1n17), a mono unsaturated fatty acid which has been shown to attenuate adipose tissue inflammation and promote insulin sensitivity in mice (H. Cao et al. 2008). Another is a novel class of lipids called branched fatty acid esters of

hydroxyl fatty acids (FAHFAs). FAHFAs have also been shown to sensitize the insulin response and have anti-inflammatory function (Yore et al. 2014; Syed et al. 2018; Kuda et al. 2016). Among these lipids, palmitic acid esters of hydroxyl-stearic acids (PAHSAs) are enriched specifically in adipose tissue, and their level decreases in humans with adipose tissue hypertrophy and insulin resistance (Yore et al. 2014; Hammarstedt et al. 2018). GLUT4 overexpression in mouse adipose tissue correlates with elevated serum PAHSA levels (Yore et al. 2014). Moreover, PAHSA supplementation in mice with insulin resistance can improve insulin sensitivity (Yore et al. 2014). These studies suggest one potential mechanism by which DNL can influence insulin sensitivity, and this exciting area of research has been recently reviewed elsewhere (Yang, Vijayakumar, and Kahn 2018; Song, Xiaoli, and Yang 2018).

In adipocytes, three key enzymes that mediate glucose-derived *de novo* lipid synthesis are ATP-citrate lyase (ACLY), acetyl-CoA carboxylase (ACC) and fatty acid synthase (FASN) [Figure I-4]. Metabolized glucose that enters the mitochondria via pyruvate can exit the TCA cycle in the form of citrate, which is exported to the cytosol. Once in the cytosol, citrate is cleaved into acetyl-CoA and oxaloacetate by ACLY. Cytosolic acetyl-CoA serves as the 2-carbon building block for subsequent lipogenesis. ACC, especially the cytosolic isoform ACC1 (Harada et al. 2007), then converts acetyl-CoA to malonyl-CoA. FASN, through a multi-step reaction, then assembles malonyl-CoA units into the first lipogenic end

product, the 16-carbon palmitate. Palmitate can then be processed into different lipid species via the action of elongases and desaturases.

ACLY, ACC, and FASN are transcriptionally regulated by a glucose metabolite-sensing transcription factor called carbohydrate-responsive element-binding protein (ChREBP), and by sterol regulatory element-binding protein (SREBP) [Figure I-4] (Iizuka et al. 2004). Overexpressing GLUT4 in adipose tissue promotes glucose uptake, which increases DNL enzyme expression by stimulating ChREBP activity. In response, ChREBPα stimulates expression of a shorter isoform, called ChREBPβ, which is transcribed from an alternative start site, and has greater transcriptional activity (Yore et al. 2014). Deleting *Glut4* in adipose tissue, on the other hand, causes systemic insulin resistance despite preserved adipose tissue mass (Abel et al. 2001). Similarly, adipocyte-specific ChREBP KO mice develop insulin resistance upon chow diet feeding, which is exacerbated by high fat diet (HFD). Interestingly, mice lacking fat ChREBP also have impaired glucose uptake (Vijayakumar et al. 2017), suggesting ChREBP may function both upstream and downstream of glucose uptake in a feed-forward loop. The findings of these animal model are consistent with observations in obese humans that low GLUT4 and ChREBP activity, particularly in SWAT, correlate with insulin resistance (Kursawe et al. 2013; Herman et al. 2012).

ChREBP regulation involves multiple processes (Ortega-Prieto and Postic 2019). One of the mechanisms appears direct sensing of glucose-derived metabolites. It is reportedly activated by glycolytic metabolites such as xylulose-5-phosphate (T. Kawaguchi et al. 2001; Kabashima et al. 2003) and possibly glucose-6-phosphate (Dentin et al. 2012). Another possible regulation is via signaling pathways. For example, the mechanistic target of rapamycin complexes 2 (mTORC2), which phosphorylates and activates AKT, is required in adipose tissue for ChREBPβ expression and for expression of the entire DNL pathway [Figure I-4] (Tang et al. 2016). Moreover, mice lacking mTORC2 in adipose tissue exhibit insulin resistance (Hung et al. 2014a; Tang et al. 2016, 2; Jung et al. 2019). How mTORC2 and AKT regulate ChREBP expression is still not well understood; however, adipose tissue mTORC2 loss phenotypically shows partial overlap with the effects of HFD on ChREBPβ and the DNL pathway expression (Tang et al. 2016), potentially suggesting a common mechanism. ChREBP can also be inhibited by phosphorylation mediated by protein kinase A (PKA) and AMP phosphorylated protein kinase (AMPK) (Davies, O'Callaghan, and Towle 2008; Takumi Kawaguchi et al. 2002). Understanding ChREBP regulation remains an important area of investigation.

1.5 mTORC2 and adipose tissue metabolism

Mechanistic or mammalian target of rapamycin (mTOR) has an important role in sensing environmental cues and regulating cell growth and survival (Saxton and Sabatini 2017). mTOR is a serine/threonine kinase and exists in two functionally distinct complexes: complex 1 (mTORC1) and complex 2 (mTORC2). mTORC1, with specific binding proteins Raptor and PRAS40, senses amino acid availability and growth factor signals, and regulates protein synthesis and cell growth by phosphorylating its targets such as p70S6 Kinase 1 (S6K1) and eIF4E Binding protein (4EBP) [Figure I-5] (Brunn et al. 1997; Burnett et al. 1998). mTORC2, compared to the other complex, is not well understood. mTORC2, which contains Rictor, mSin1 and mLST8, responds to insulin and growth factor stimulation and phosphorylates several members of AGC kinases, such as AKT (at S473 site), SGK and PKC [Figure I-5]. These kinases also control cell proliferation and survival [Table I-3]. Thus, both complexes have the ability to sense and respond to environmental stimuli and coordinate with intracellular signaling pathways to regulate cell functions.

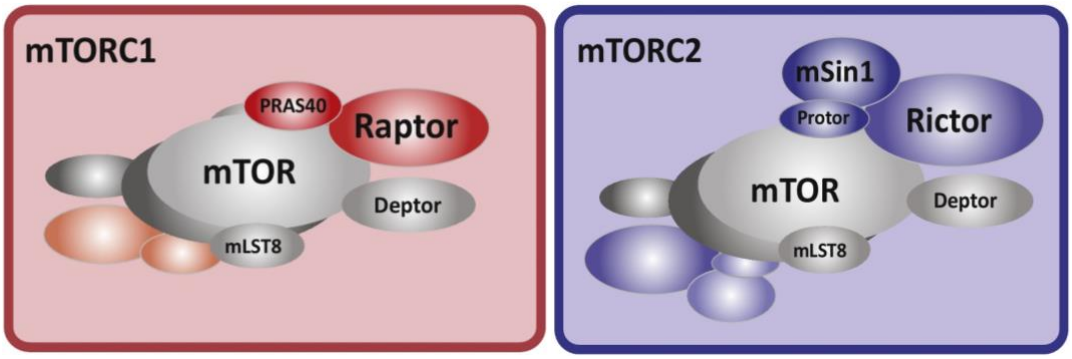

Figure I-5 The mTOR complexes and the components of each complex. This figure was adapted from the following publication: Lee, P.L., Jung, S.M., Guertin, D.A., 2017. The Complex Roles of Mechanistic Target of Rapamycin in Adipocytes and Beyond. *Trends Endocrinol. Metab.* 28, 319–339.

Table I-3 Classical mTORC2 substrates and functions.

Substrates	Reported Functions	References
AKT	Controlling cell growth, proliferation, survival, and glucose/lipid metabolism	(Sarbassov et al. 2005)
SGK1	Functioning in sodium homeostasis and cellular stress responses	(García-Martínez and Alessi 2008)
PKCα	Controlling cell migration, proliferation, apoptosis, and adhesion	(Guertin et al. 2006; Ikenoue et al. 2008; Dos D. Sarbassov et al. 2004; Facchinetti et al. 2008)

This table was adapted from the following publication: Lee, P.L., Jung, S.M., Guertin, D.A., 2017. The Complex Roles of Mechanistic Target of Rapamycin in Adipocytes and Beyond. *Trends Endocrinol. Metab.* 28, 319–339.

Emerging evidence highlights the essential role of mTORC2 in regulating glucose and lipid metabolism in a variety of metabolic tissues and cancers. In brown adipose tissue, it regulates DNL and promotes diet-induced thermogenesis. In mature white adipocytes, on the other hand, mTORC2 regulates glucose uptake and DNL in part through regulating ChREBP expression (Guo et al., 2019; Guri et al., 2017; Jung et al., 2019; Tang et al., 2016). Conditionally deleting *Rictor* in mice with *Adiponectin-Cre*, which targets

all mature adipocytes, causes insulin resistance (Tang et al. 2016; Yu et al. 2019). The requirement of mTORC2 for regulating glucose homeostasis can also been seen in other metabolic organs such as liver, muscle and pancreas [Table I-4 for tissue-specific deletion models and references]. The mechanisms have been mainly explored in cancer cells. In glioblastoma, mTORC2 regulates glycolytic metabolism via regulating c-MYC level and activity which might be partially through a FoxO1-dependent pathway, which is essential for proliferation and survival (Masui, Cavenee, and Mischel 2014). The mechanisms of how mTORC2 regulates glucose and lipid metabolism under physiological conditions require more investigation.

Table I-4 Mouse models of tissue-specific *Rictor* deletion.

Organ/Tissue	Genetic model	Phenotypes	References
Liver	*Alb-Cre$^{Tg/0}$;rictor$^{fl/fl}$*	Systemic hyperglycemia and hyperinsulinemia Constitutive gluconeogenesis, impaired glycolysis, glucose uptake and lipogenesis in liver	(Hagiwara et al. 2012; Yuan et al. 2012)
Muscle	*MCK-Cre;rictor$^{fl/fl}$*	Insulin resistance Decreased glucose uptake in muscle	(Kumar et al. 2008)
Pancreatic β cells	*Ins2-Cre;*rictor$^{fl/fl}$ *RIP-Cre;*rictor$^{fl/fl}$	Decreased insulin secretion Decreased β cell proliferation and cell mass	(Gu et al. 2011; Xie et al. 2017)
Brown adipose tissues	*Myf5-Cre;rictor$^{fl/fl}$* *UCP1-Cre;rictor$^{fl/fl}$*	Increased diet-induced thermogenesis Decreased *de novo* lipogenesis (DNL) in adipose tissue	(Hung et al. 2014; Jung et al. 2019)
White adipose tissue	*aP2-Cre;rictor$^{fl/fl}$* *Adiponectin-Cre; rictor$^{fl/fl}$*	Systemic insulin resistance Decreased glucose uptake in adipose tissue Decreased DNL in adipose tissue	(Kumar et al. 2010; Tang et al. 2016)

1.6 AKT and adipocyte development and function

AKT, one of the canonical mTORC2 substrates, is essential for regulating cell proliferation, cell survival and metabolism (Manning and Cantley 2007). AKT consists of three isoforms, AKT1, AKT2 and AKT3, which are encoded by three independent genes (Dummler and Hemmings 2007). Despite different genes of origin, they share common structural domains: a pleckstrin homology domain (PH domain) at N terminus, a catalytic (or kinase) domain, and a C-terminal extension containing hydrophobic motif (HM) [Figure I-6], and the amino acid sequences of these three have up to 80% similarity (C. C. Kumar and Madison 2005). However, the PH-linker domain and the C-terminal region share less commonality, which might explain intracellular localization differences and substrate specificities between the isoforms (C. C. Kumar and Madison 2005; Santi and Lee 2010). All three isoforms also share a common activation mechanism in response to insulin: insulin signal enriches phosphatidylinositol 3,4,5 trisphosphate (PIP_3) in the plasma membrane, and AKT is recruited to the plasma membrane where AKT is phosphorylated at T308/309/307 (on AKT1/2/3) by PDK1 and at S473/474/472 by mTORC2 (Alessi et al. 1996). The phosphorylated AKT then activates its classical downstream targets as well as mTORC1 [Figure I-7].

Despite sharing a common structure and overlapping partially in function, the three isoforms are distinguished by tissue distribution and activity (Gonzalez

and McGraw 2009). AKT1 is ubiquitously expressed and is essential for cell survival (W. S. Chen et al. 2001; H. Cho et al. 2001). *In vitro* study shows that deleting AKT1 in preadipocytes abrogates adipogenesis possibly by inhibiting G1-to-S phase progression during early days of differentiation (Yun et al. 2008). However, mice with whole-body *Akt1* deletion are generally smaller in size but do not develop insulin resistance or glucose metabolism defect (H. Cho et al. 2001). Similar results were seen in BAT: adipocyte size or systemic insulin sensitivity remains unchanged when *Akt1* is deleted in brown fat precursors (Sanchez-Gurmaches et al. 2019). AKT2, the major isoform in mature adipocyte and other insulin-sensitive tissues, is indispensable for adipocyte development and glucose metabolism in response to insulin. Deleting *Akt2* in cultured human preadipocytes attenuates adipogenesis and glucose utilization (Fischer-Posovszky et al. 2012). Whole-body *Akt2* KO mice develop hyperglycemia and insulin resistance as well as age-dependent lipodystrophy, and ablating AKT2 specifically in brown adipocytes causes lipodystrophy and insulin resistance (Sanchez-Gurmaches et al. 2019; Han Cho et al. 2001; Garofalo et al. 2003). Despite having distinct functions in adipocytes, AKT1 and AKT2 might partially compensate for each other as co-deletion of both isoforms cause more severe phenotypes (Sanchez-Gurmaches et al. 2019; Shearin et al. 2016; 2016; Peng et al. 2003). This compensatory effect suggests that although *Akt1* single deletion does not cause significant phenotypes in adipose tissue or whole-body metabolism, AKT1 still in part contributes to adipose tissue development and

function. *Akt3* is mainly expressed in brain (Nakatani et al. 1999), and it does not compensate for co-deletion of *Akt1* and *Akt2* (Sanchez-Gurmaches et al. 2019). The discrepancies between *in vitro* and *in vivo* studies suggest the complexity of AKT signaling in regulating adipose tissue function and whole-body metabolism and more studies are required to elucidate the mechanisms.

Figure I-6 The schematic of AKT structure.

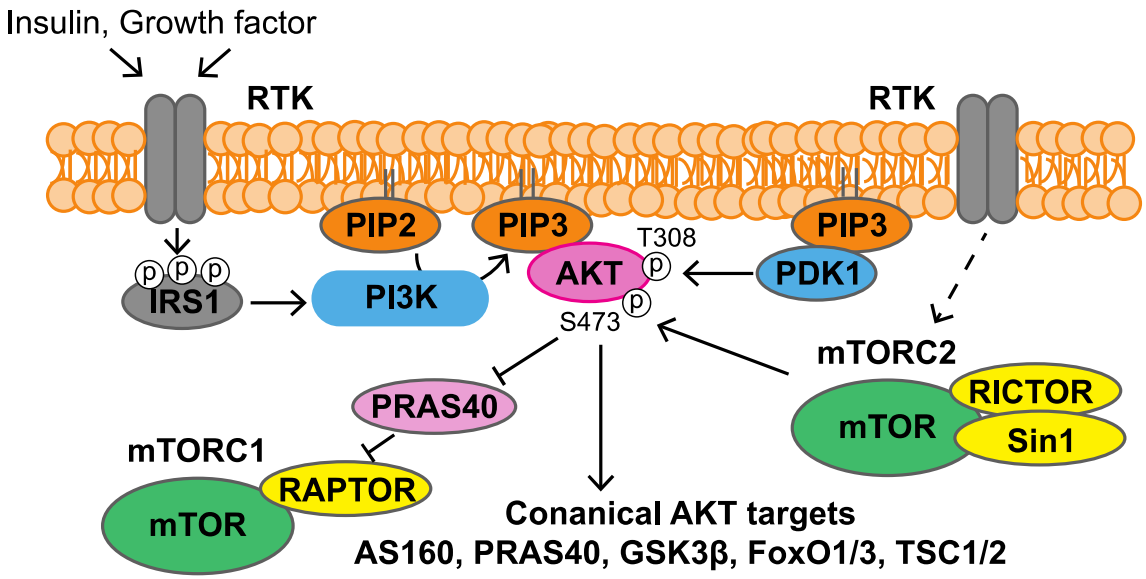

Figure I-7 The mTORC2-AKT signaling pathway. Upon insulin or growth factor stimulation, receptor trypsin kinases (RTKs) phosphorylate Insulin receptor substrate 1 (IRS1) and then activate phosphatidylinositol 3-kinase (PI3K). Activated PI3K phosphorylates phosphatidylinositol-4,5-bisphosphate (PIP2) to generate phosphatidylinositol-3,4,5-triphosphate (PIP3), which recruits AKT and PDK1 to the plasma membrane where PDK1 phosphorylates AKT at T308. RTK might be able to directly activate mTORC2, which phosphorylates AKT at S473. Activated AKT then phosphorylates its canonical downstream targets such as AS160, PRAS40, GSK3β, FoxO1/3 and TSC1/2. AKT activates mTORC1 via inhibitory phosphorylation of PRAS40, which then release the suppressing function of PRAS40 toward mTORC1.

The link between AKT and mTORC2

Phosphorylation of S473/474 at the C-terminal hydrophobic motif (HM) by mTORC2 in AKT1/AKT2 is considered essential for maximizing AKT activity (Sarbassov et al. 2005; Hresko and Mueckler 2005). However, several *in vitro* and *in vivo* models suggest that phosphorylation of S473 might be dispensable for overall AKT activity. Global downstream AKT signaling appears unaffected in animal models with *Rictor* deletion specifically in mature adipose tissues and brown adipose tissues, in which the phosphorylation of HM is diminished (Hung et al. 2014a; Tang et al. 2016; Jung et al. 2019; Calejman et al. 2020). One study shows that replacing S474-AKT2 with an inactive mutant (S474A) in cultured adipocytes does not affect either insulin-stimulated glucose uptake or mTORC1 activity (Beg et al. 2017). Another study replacing S474A-AKT2 mutant in cultured adipocytes reveals a different observation: HM phosphorylation is required for maximal AKT signaling to TSC2, PRAS40, FoxO1/3 and AS160, which is essential for GLUT4 translocation and glucose transport (Kearney et al. 2019). A recent study in cultured brown preadipocytes shows that mTORC2 is required for phosphorylation of ACLY via an AKT-dependent mechanism (Calejman et al. 2020), and this observation has also been detected in multiple breast cancer cells (Y. Chen et al. 2016). The differences between *in vitro* and *in vivo* models and even between cell types can be explained by the different chronicity of *Rictor* loss between *in vivo* and *in vitro*, the complexity of the environment in tissues, and the possible different dependency on mTORC2-AKT

signaling in different cell types. Nevertheless, previous *in vivo* studies mainly focused on mTORC2's role in mature white adipocytes and brown adipocytes and whether the role of *Rictor*/mTORC2 in white adipose tissue development is unclear.

1.7 PPARγ and adipocyte differentiation and function

The core transcriptional regulator of adipocyte differentiation (also referred to adipogenesis) is peroxisome proliferator-activated receptor γ (PPARγ), which is a ligand activated nuclear hormone receptor and the target of the synthetic thiazolidinediones (TZDs) agonists (Schoonjans et al. 1997; Fujita et al. 1983; Yki-Järvinen 2004). When activated in preadipocytes, PPARγ binds to PPARγ Responsive Elements (PPREs) and cooperates with CCAAT/enhancer binding protein α (C/EBP α) to drive adipogenesis (Schoonjans, Staels, and Auwerx 1996; Tontonoz et al. 1994; Lefterova et al. 2008). Other transcription factors aid PPARγ during adipogenesis including C/EBPβ and C/EBPδ (involved in early PPARγ induction) (Z. Cao, Umek, and McKnight 1991); RXR (which binds PPARγ as an obligate heterodimer) (Gearing et al. 1993; IJpenberg et al. 1997); ChREBP and SREBP (expressed later during adipogenesis and best known for driving lipogenesis gene expression) (J. B. Kim et al. 1998; Witte et al. 2015); and chromatin modifiers such as CBP/P300 and the Mediator complex (Steger et al. 2010; Badri et al. 2008; Gelman et al. 1999; S. Chen et al. 2000). In mature adipocytes, PPARγ regulates insulin sensitivity, lipid handling, and adipocyte

survival (Cristancho and Lazar 2011). Thus, PPARγ has been dubbed the "master regulator of adipocyte biology". However, current understanding in PPARγ and adipogenesis are based on cell culture models, mainly by 3T3-L1 (Green and Meuth 1974; Farmer 2006). It raises an argument that whether the mechanisms framed by cell culture can represent the adipose tissue development in vivo, since the environment in vivo is more complicated (Pope et al. 2016). Besides, the hormonal and metabolic signals that both enable and fine-tune PPARγ activity in response to nutrient availability remain less well defined.

1.8 Summary and hypothesis

In this dissertation, I utilized both *in vitro* and *in vivo* systems to study the role of mTORC2 in regulating white adipocyte development and function. My hypothesis is that mTORC2 is required for responding to differentiation signals and reprograms the cells to become committed mature adipocytes. In the third part of the dissertation, I explored the possible mechanisms of how mTORC2 regulates adipocyte differentiation and lipid metabolism.

CHAPTER II - The lipid handling capacity of subcutaneous fat is programmed by mTORC2 during development

This chapter contains materials submitted in Cell Reports from Cell Press (June, 2020).

2.1 Introduction

White adipose tissue (WAT) stores energy and secretes endocrine factors that control metabolism (Guilherme et al. 2019; P. L. Lee, Jung, and Guertin 2017; Lefterova et al. 2014; Scherer 2019). WAT expands in response to over-nutrition so that the excess calories can be safely stored as triacylglycerol (TAG) preventing toxic lipid accumulation in non-adipose tissues (Almandoz et al. 2013; Snel et al. 2012; Unger et al. 2010). However, in overweight and obese individuals, white adipocytes become dysregulated and contribute, through mechanisms incompletely understood, to obesity-related comorbidities including type 2 diabetes (T2D), non-alcoholic fatty liver disease (NAFLD), cardiovascular diseases (CVDs) and cancer (Van Gaal, Mertens, and De Block 2006). Thiazolidinediones (TZDs) are oral insulin sensitizing drugs used to treat T2D. They act by stimulating PPARγ, the master transcriptional regulator of adipogenesis, to enhance insulin sensitivity and promote glucose utilization and lipid synthesis and storage (Hauner 2002). Although TZDs are commonly prescribed, serious side effects have limited their efficacy (Cariou, Charbonnel, and Staels 2012). Thus, a better understanding of PPARγ regulation may lead to improved therapies.

Importantly, not all WAT depots are equal. For example, the health risks of metabolic syndrome and cardiovascular events for overweight patients with excessive visceral white adipose tissue (VWAT) is higher than for individuals with

excess subcutaneous white adipose tissue (SWAT) (Ferrara et al. 2019; Lessard and Tchernof 2012; McLaughlin et al. 2011). An individual's body fat set point, and their ability to grow adipose tissue during development and upon over nutrition, is also variable in the population and between sexes (Tramunt et al. 2019; Fitzgerald et al. 2018; Tchoukalova et al. 2010). Such complexities suggest anti-obesity therapies will likely have greater success when personalized. Thus, understanding depot and sex differences in adipose tissue biology is also clinically relevant.

In mature white adipocytes, the mechanistic target of rapamycin complex 2 (mTORC2) regulates glucose uptake and *de novo* lipogenesis (DNL) *in vivo* in part through regulating the carbohydrate response element binding protein (ChREBP) transcription factor (Guo et al. 2019; Guri et al. 2017; Jung et al. 2019; Tang et al. 2016). In humans, a positive correlation between DNL in SWAT and systemic insulin sensitivity has been shown (Calejman et al. 2020; Cybulski et al. 2009; Hung et al. 2014b; Jung et al. 2019; Tang et al. 2016). Consistently, conditionally deleting *Rictor* in mice with *adiponectin-Cre*, which targets all mature adipocytes, causes insulin resistance (Tang et al. 2016; Yu et al. 2019). The AKT kinases (AKT1, AKT2 and AKT3), which are canonical mTORC2 substrates, are phosphorylated by mTORC2 in their C-terminal hydrophobic motif (HM) sites (Ser473, Ser474, and Ser472 respectively) (Sarbassov et al. 2005; Hresko and Mueckler 2005). However, global downstream AKT signaling

appears minimally affected *in vivo* in Adiponectin-Cre;*Rictor* knockout mice (*Rictor*$_{adipoq}$) despite the lack of AKT HM phosphorylation (Calejman et al. 2020; Cybulski et al. 2009; Hung et al. 2014b; Jung et al. 2019; Tang et al. 2016). Mutating AKT2-S474 to alanine *in vitro* in 3T3L1 adipocytes (AKT2 being the major WAT isoform) also revealed that HM phosphorylation is dispensable for insulin-stimulated glucose uptake and mTORC1 activity (Beg et al. 2017); while another study using AKT2-S474 mutant 3T3L1 adipocytes showed that HM phosphorylation is required for maximal AKT signaling to TSC2, PRAS40, FoxO1/3 and AS160 (Kearney et al. 2019). Possible explanations for the observed differences between *in vitro* and *in vivo* models, which are not necessarily exclusive, are that AKT signaling compensation occurs with prolonged *Rictor* loss *in vivo*, but not equally across all AKT substrates or functions; that individual AKT substrates inherently differ in their mTORC2 dependency; or that AKT-independent mechanisms contribute to WAT dysfunction. Moreover, mutating S474 is also not identical to deleting *Rictor* as mTORC2 regulates other AKT phosphorylation sites and AGC family kinases (Ikenoue et al. 2008; Facchinetti et al. 2008; Hiraoka, Okumura, and Kishimoto 2011), and thus variables in experimental strategy also likely contribute to some of these differences. Nevertheless, previous studies focus largely on mTORC2's role in mature white adipocytes and whether *Rictor*/mTORC2 is required for white adipose tissue development is not known.

Here, I investigated the role of mTORC2 in subcutaneous fat development using both *in vitro* and *in vivo* models. In both primary and immortalized cells, I found that *Rictor*/mTORC2 was not required to induce PPARγ during differentiation, but that it was required for stimulating PPARγ activity towards a subset of target genes that encode regulators of lipid uptake and storage. mTORC2 did not appear to stimulate PPARγ through ChREBP, but rather in coordination with ChREBP to promote maximum lipid storing capacity. To show physiological relevance, I also deleted *Rictor in vivo* in precursor cells that give rise to SWAT, but not to visceral WAT or brown adipose tissue (BAT). Consistent with my *in vitro* findings, this impaired the expression of select PPARγ target genes that encode regulators of lipid handling, in addition to attenuating expression of ChREBP/SREBP1c target genes that control *de novo* lipid synthesis. This resulted in reduced subcutaneous white adipocyte size, reduced overall SWAT mass, and redistribution of lipids to the visceral and brown fat depots. Interestingly, this caused insulin resistance in males. However, females were able to maintain normal insulin sensitivity despite *Rictor* loss causing a similar but milder effect on SWAT mass and lipid re-distribution. Overall, these data suggested a model in which mTORC2 acts upstream of the adipogenic transcriptional machinery during SWAT development to program lipid handling capacity. Since the ability to store lipid in SWAT is correlated with improved metabolic health, these findings may have important implications for developing T2D treatments.

2.2 Results

mTORC2 promotes lipid filling during subcutaneous white adipogenesis *in vitro*.

To investigate the role of mTORC2 in subcutaneous white adipose tissue (SWAT) development I first generated a primary subcutaneous white adipocyte differentiation model by isolating stromal vascular fraction (SVF) cells, which contain preadipocytes, from the inguinal WAT depots of *UBC-Cre$_{ERT2}$;Rictor$_{loxP/loxP}$* mice and briefly treating them with 4-hydroxy tamoxifen (4-OHT) to induce *Rictor* deletion [Figure II-1A]. Following 4-OHT washout, primary *Rictor*-inducible knockout SVF cells (*Rictor-iKO$_{primary}$* preadipocytes hereafter) and their isogenic vehicle-treated controls were differentiated following a standard protocol (Zebisch et al. 2012). Staining of differentiated primary adipocytes with Oil Red O [Figure II-1B] or by LipidTOX and Perilipin 1 (PLIN1) immunofluorescence [Figure II-1C] indicated decreased lipid droplet accumulation in the *Rictor-iKO$_{primary}$* cells. Quantification of the Oil Red O-stained lipid droplets after isopropanol extraction indicated ~20% less neutral lipid in the *Rictor-iKO$_{primary}$* cells [Figure II-S1A]. The total cell number [Figure II-S1B] and percentage of PLIN1 positive cells [Figure II-S1C] was unchanged by *Rictor* loss suggesting a defect in intracellular lipid accumulation. I also induced *Cre$_{ERT2}$* activity in otherwise wild type SVF cells (i.e. having no floxed *Rictor* alleles) to confirm that neither brief tamoxifen exposure nor temporal recombinase activity alone in the undifferentiated cells affected Oil Red O staining, RICTOR level, or AKT phosphorylation upon differentiation [Figure II-1A, S1D and S1E]. These

data suggested that mTORC2 positively regulates subcutaneous white adipocyte lipid accumulation.

I observed no difference in *Pparg2*, *Cebpa*, *Cebpb* and *Cebpd* mRNA expression during differentiation in *Rictor-iKO*$_{primary}$ cells [Figure II-1D], and consistently, PPARγ2 protein expresses normally [Figure II-1E]. I did observe that the PPARγ2 cofactor C/EBPα expresses at higher than normal protein level following differentiation in *Rictor-iKO*$_{primary}$ cells despite having an unchanged mRNA expression profile [Figure II-1D and 1E]. Primary cells lacking *Rictor* had decreased AKT hydrophobic motif phosphorylation (S473 on AKT1; S474 on AKT2) and AKT turn motif phosphorylation (T450 on AKT1; T451 on AKT2) throughout differentiation, confirming *Rictor* ablation [Figure II-1E and 1F]. AKT1-T308/AKT2-T309 phosphorylation decreased by ~50% in *Rictor-iKO*$_{primary}$ cells at day 0 and day 2 of differentiation but increased at day 8 relative to controls [Figure II-1F and 1G]. This is consistent with previous *in vivo* observations in adipocytes that mTORC2 facilitates but is not essential for AKT-T308 phosphorylation (Hung et al. 2014b; Jung et al. 2019; Tang et al. 2016). Interestingly, isoform specific AKT1 and AKT2 analysis showed a decrease in AKT2 mRNA induction during differentiation resulting in reduced AKT2 protein at D8 [Figure II-1F and S1F]. Transcriptional regulation of *Akt2* was not observed in *Rictor* deleted mature adipocytes (Tang et al. 2016). Nevertheless, the decrease in AKT2 level did not prevent insulin (100 nM) from stimulating phosphorylation of

AKT substrates such as FoxO1 (T24), GSK3β (S9) or PRAS40 (T246) in the *Rictor*-deficient cells [Figure II-1F and 1G]. Collectively, these data suggested that lipid accumulation during adipogenesis, but not differentiation requires mTORC2.

I also immortalized *UBC-Cre$_{ERT2}$;Rictor$_{loxP/loxP}$* SVF cells (hereafter *Rictor-iKO$_{immortal}$* preadipocytes) to test whether immortalization alters differentiation dynamics and mTORC2 dependency. Like their primary cell counterparts, *Rictor-iKO$_{immortal}$* preadipocytes had a lipid filling defect, exhibiting a 60% decrease in Oil Red O staining after differentiation compared to controls [Figure II-S1G]. Similar to the *Rictor-iKO$_{primary}$* cells, the D8 *Rictor-iKO$_{immortal}$* cells showed reduced RICTOR and AKT-S473/4 phosphorylation, slightly higher p-AKT-T308/9, decreased AKT2 protein, and increased C/EBPα protein [Figure II-S1H]. Notably, AKT1 mRNA and protein levels also increased in the D8 *Rictor-iKO$_{immortal}$* cells, which was not detected in the *Rictor-iKO$_{primary}$* cells, and this appeared at least partly due to increased *Akt1* transcription [Figure II-S1H and S1I]. There was also a slight difference in PPARγ2 induction in the immortalized cells, which transcriptionally induces normally at day 2—as in primary cells—but fails to maximally amplify thereafter [Figure II-S1J and S1K]. Nevertheless, *Rictor-iKO$_{immortal}$* preadipocytes exhibited many of the same features as *Rictor-iKO$_{primary}$* preadipocytes with the observed differences likely resulting from the immortalization procedure.

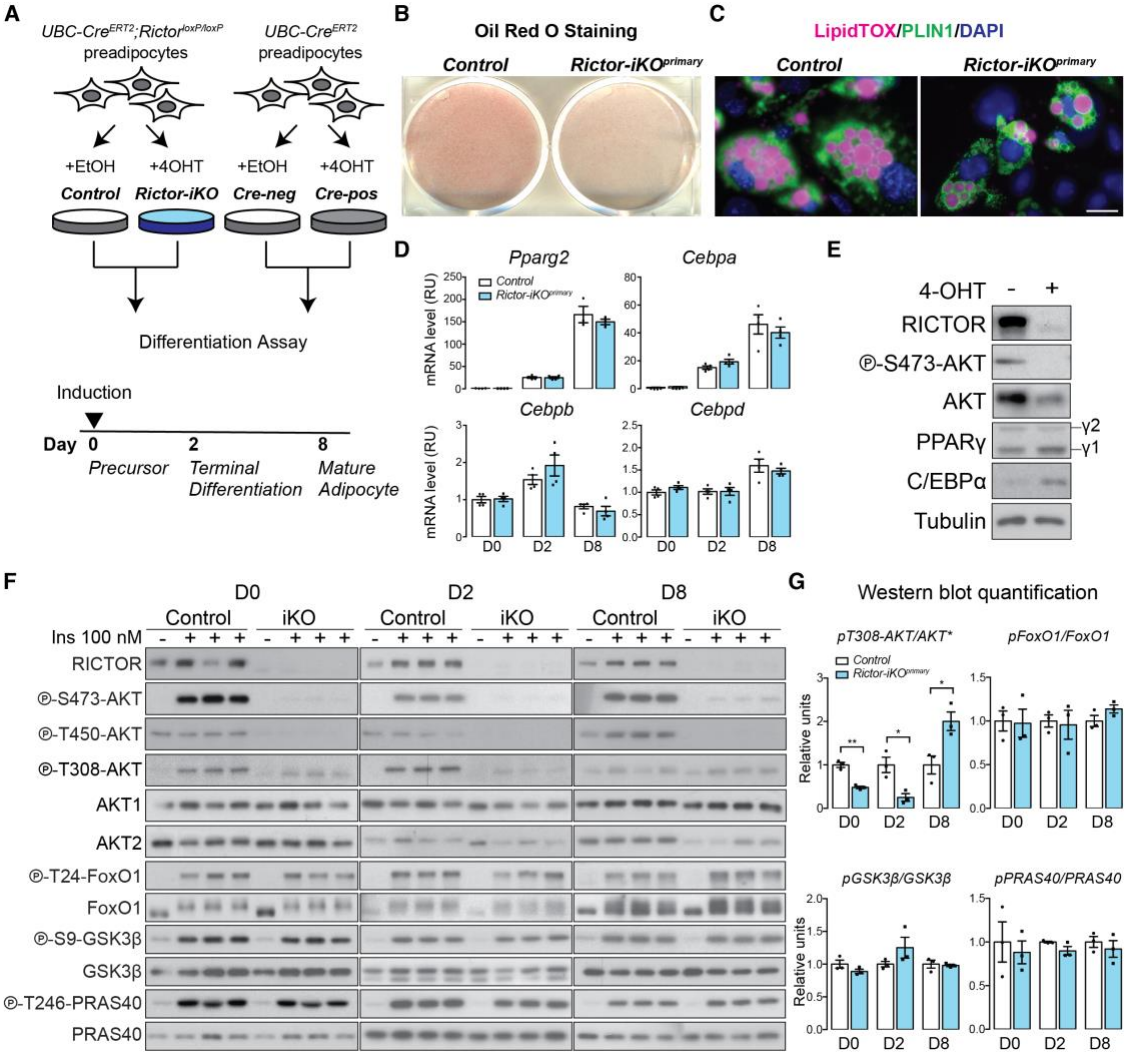

Figure II-1 mTORC2 promotes lipid filling during subcutaneous white adipogenesis *in vitro.* **A** Model of *in vitro* experimental strategy. 4-OHT: 4-hydroxytamoxifen. Cre-neg: Cre-negative cells; Cre-pos: Cre-positive cells. **B** Oil Red O (ORO) staining of differentiated (Day 8) isogenic control and *Rictor-iKO* primary (*Rictor-iKO*^{primary}) cells. **C** LipidTOX and Perilipin 1 (PlIN1) immunofluorescence staining of differentiated (Day 8) control and *Rictor-iKO*^{primary} cells. Scale bar = 100 μm. **D** Relative mRNA expression by RT-PCR of differentiation marker genes at the indicated differentiation days (N = 4; data represent mean ± SEM). **E** Representative western blot of lysates from differentiated (Day 8) cells. N = 3. γ1: PPARγ1 isoform; γ2: PPARγ2. **F** Western blot of the indicated total and phospho-proteins in lysates with or without 100 nM insulin (ins) stimulation at day 0, 2 and 8 of differentiation. N= 3 for insulin-stimulated samples. **G** Quantification of the indicated total and phosphorylated protein levels. Total AKT (*) reflects AKT1 and AKT2 levels (N = 3; data represent mean ± SEM; $*p < 0.05$, $**p < 0.01$).

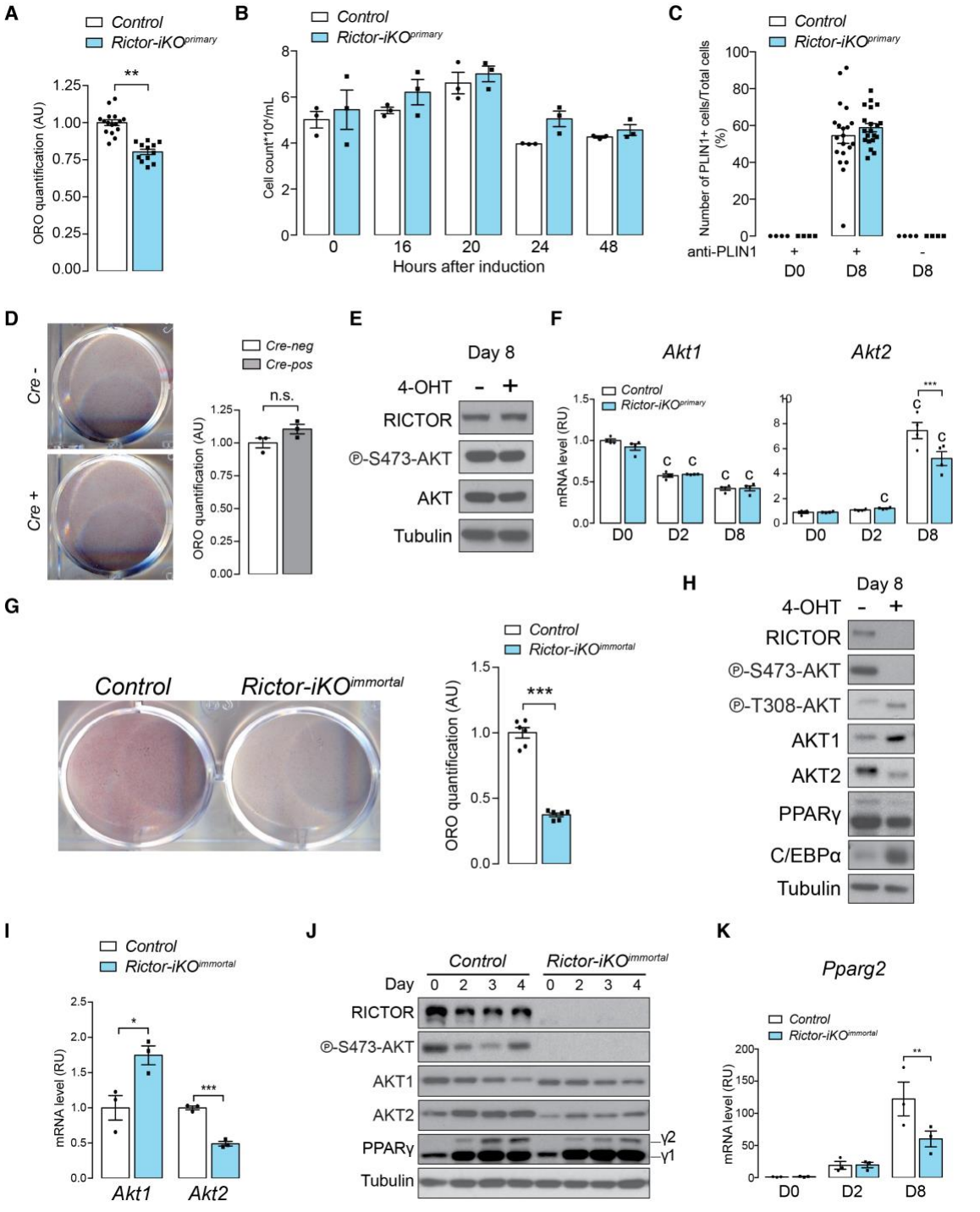

Figure II-S1 mTORC2 promotes lipid filling during white adipogenesis in both primary-cultured and immortalized cells, related to Figure 1. A Quantification (quant) of the Oil Red O (ORO) staining of differentiated control (EtOH) and *Rictor-iKO*^{primary} (4-OHT) cells after isopropanol extraction and direct ORO content measurement (data represent mean ± SEM; $^{**}p < 0.01$). See also **Figure 1B**.

Figure II-S1 (Cont.) B Cell number quantification of control *and Rictor-iKO^{primary}* cells at indicated time points during the first 48 hours of differentiation (data represent mean ± SEM). **C** Percentage of Perilipin 1-positive (PLIN1+) cells per image taken from the immunofluorescence staining in **Figure 1C** (data represent mean ± SEM). **D** ORO staining of differentiated primary *preadipocytes isolated from a UBC-Cre^{ERT2}* mouse. *Right panel*: quantification (quant) of the Oil Red O (ORO) staining. (data represent mean ± SEM; $^{**}p < 0.01$). Cre-: cells treated with EtOH (without Cre). Cre+: cells treated with 4-OHT (with Cre expression). n.s.: not significant. **E** Representative western blot of lysates from differentiated (Day 8) *UBC-Cre^{ERT2}* cells with (4-OHT-treated) or without (EtOH-treated) Cre expression. N = 3. **F** Relative mRNA expression by RT-PCR of *Akt* isoforms in control and *Rictor-iKO^{primary}* cells at the indicated differentiation days (data represent mean ± SEM; $^{***}p < 0.001$; c: $^{***}p < 0.001$ when compared to D0 cells). **G** ORO staining of differentiated control and *Rictor-iKO^{immortal}* cells. *right panel*: Quantification of the ORO staining of differentiated control and *Rictor-iKO^{immortal}* cells after isopropanol extraction and direct ORO content measurement (data represent mean ± SEM; $^{***}p < 0.001$). **H** Representative western blot of lysates from differentiated (Day 8) control and *Rictor-iKO^{immortal}* cells. N = 3. **I** Relative mRNA expression by RT-PCR of *Akt* isoforms in differentiated control and *Rictor-iKO^{immortal}* cells (data represent mean ± SEM; $^{*}p < 0.05$, $^{***}p < 0.001$). **J** Representative western blot of lysates from control and *Rictor-iKO^{immortal}* cells at early differentiation time points (day 0 through day 4). N =3. γ1: PPARγ1 isoform; γ2: PPARγ2. **K** Relative mRNA expression by RT-PCR of *Akt* isoforms in control and *Rictor-iKO^{immortal}* cells at indicated differentiation days (data represent mean ± SEM; $^{**}p < 0.01$).

mTORC2 promotes expression of lipid handling genes.

To begin exploring how mTORC2 regulates lipid accumulation during differentiation, I generated RNA-seq transcriptomes from the control and *Rictor-iKO$_{primary}$* SVF cells in the precursor stage (D0), the terminal differentiation stage (D2, when PPARγ2 is induced), and the mature adipocyte stage (D8) [Figure II-1A]. By first making pair-wise comparisons between the control and knockout cells at each differentiation day examined, I found that most of the differential gene expression occured between D2 and D8 [Figure II-2A]. For example, I identified 141 genes significantly down-regulated in *Rictor-iKO$_{primary}$* cells at D8 compared to only 52 and 38 genes at D0 and D2, respectively and 37, 76, and 78 up-regulated genes at D0, D2 and D8 respectively [Figure II-2A]. I classified the down-regulated genes as requiring *Rictor* for normal induction (*Rictor-*

required genes), and the up-regulated genes as being suppressed by *Rictor* (*Rictor*-suppressed genes) [Figure II-2A]. Gene ontology (GO) term and KEGG pathway enrichment analysis for D0 and D2 *Rictor*-required genes (those down-regulated) revealed genes thought to function in cell adhesion (N=8) and extracellular matrix receptor interaction pathways (N=6) [Table II-1]. In contrast, the D8 *Rictor*-required genes were enriched for metabolic processes especially lipid metabolism (N=22) [Table II-1]. Among the *Rictor*-suppressed genes was an over-representation of inflammation pathway genes [Table II-1]. Notably, genes that suppress adipogenesis such as *Pref1* and *Pdgfra* were not increased by *Rictor* loss consistent with *Rictor-iKO*$_{primary}$ cells having a defect in metabolic gene expression but not in differentiation. Thus, mTORC2 is a positive regulator of lipid metabolic gene expression during adipocyte differentiation.

I also compared the D8 and D0 control transcriptomes to identify adipogenic genes, which I defined as genes upregulated >1.4 fold at FDR <0.05 in D8 vs D0. This identified 825 adipogenic genes in the control primary cells. Among the D8 *Rictor*-required genes, 77 of them (54.6%) were also adipogenic genes based on this analysis. GO analysis identified lipid metabolism genes as being highly overrepresented among the D8 *Rictor*-required adipogenic genes [Figure II-2B]. KEGG analysis further identified the PPAR signaling pathway as the top scoring pathway among the D8 *Rictor*-required genes (KEGG results based on 10 out of 77 genes) [Figure II-2C]. Notably, *Rictor*-required genes in

the PPAR signaling pathway encoded regulators of both anabolic and catabolic lipid metabolism such as fatty acid uptake, fatty acid oxidation, *de novo* lipogenesis and TAG synthesis [Figure II-S2A]. By comparing the D8 *Rictor*-required genes to a published database of PPARγ targets, I identified several additional *Rictor*-required genes (41/141) as likely PPARγ targets [Figure II-2D]. In addition, 6 and 20 of *Rictor*-required genes were also classified as ChREBP and/or SREBP1 targets, respectively, based on published data (Ortega-Prieto and Postic 2019; Oki and Ohta 2016) [Figure II-2D].

For several of the *Rictor*-required genes identified by RNA-seq I developed RT-PCR assays to confirm their D8 expression differences in primary cells [Figure II-2E]. I focused on genes that regulate lipid metabolism including previously reported PPARγ target genes (*Scd1, Dgat1, Glut4, Cd36, Lpl, Fabp4, Hsl* and *Mcad*), *de novo* lipogenesis genes (*Acaca, Fasn, Scd1*), and as controls, *Rictor*-independent adipogenic genes (*Plin1* and *Adipoq*). As predicted from the RNA-seq data, genes encoding regulators of several lipid anabolic pathways such as fatty acid and TAG synthesis *(Acaca, Fasn, Scd1*, *Dgat1* and *Dgat2*) and glucose and fatty acid uptake (*Glut4, Cd36, Lpl, Fabp4*) were decreased in D8 *Rictor-iKO*$_{primary}$ cells [Figure II-2E]. I also detected attenuation of genes that encode regulators of lipid catabolic processes such as lipolysis (*Hsl*) and beta-oxidation (*Mcad*) in *Rictor-iKO*$_{primary}$ cells [Figure II-2E]. I confirmed decreased CD36, FABP4, ACC, FASN, and SCD1 protein expression by Western blot

[Figure II-2F]. In contrast, the PPARγ targets *Plin1* and *Adipoq* were unaffected by *Rictor* loss [Figure II-2E], which was also consistent with normal Perilipin 1 positive staining in the D8 adipocytes [Figure II-1C and S1C]. Importantly, the control Cre_{ERT2} cells [Figure II-1A] showed no defects in *Acaca, Fasn, Scd1, Cd36, Lpl, Fabp4* or *Glut4* expression [Figure II-S2B]. I confirmed that decreased expression of the PPARγ targets *Cd36* and *Fabp4* required *Rictor* deletion prior to differentiation as deleting *Rictor* after differentiation did not attenuate their expression despite ablating AKT-S473 phosphorylation [Figure II-S2C and II-S2D]. In contrast, *de novo* lipogenesis genes (*Acaca* and *Fasn*) required *Rictor* both during differentiation and in mature adipocytes [Figure II-S2D] consistent with our previous *in vivo* findings (Tang et al. 2016). Thus, without *Rictor*, differentiating SWAT preadipocytes cannot establish their normal lipid metabolic gene expression program, which included regulators of lipid synthesis, uptake, breakdown and oxidation pathways.

To confirm that the observed gene expression differences reflect metabolic changes, I performed functional assays. Using ^{14}C-glucose I showed that lipid synthesis increased 65-fold from D0 to D8 in control cells and confirmed that D8 *Rictor-iKO*$_{primary}$ cells had a 92% reduction in *de novo* lipid synthesis with the D0 cells also showing a slight decrease [Figure II-S2E]. Consistent with reduced *Glut4* expression, I also measured a 25% and 35% decrease in insulin-stimulated 3H-2-DG glucose uptake at D0 and D8, respectively [Figure II-S2F].

However, non-insulin stimulated glycolysis and glycolytic capacity measured on a Seahorse Extracellular Flux Analyzer exhibited higher and normal capacity, respectively, based on extracellular acidification rate [Figure II-S2G], which was consistent with RNA-seq data showing normal glycolysis gene expression in *Rictor-iKO*$_{primary}$ cells [Figure II-S2A]. Using BODIPY as a probe to measure lipid uptake, I also measured a 25% and 35% decrease in lipid uptake after 10 and 30 minutes of labeling, respectively, in *Rictor-iKO*$_{primary}$ cells [Figure II-S2H]. These data were consistent with a model in which mTORC2 sets the general lipid handling capacity of SWAT during adipogenesis by modulating expression of both anabolic and catabolic lipid metabolism genes.

Table II-1: Gene ontology biological processes and KEGG pathway enrichment analysis of *Rictor*-dependent genes.

GO term Biology Processes			
Rictor-required (Down-regulatory) genes			
GO term	GO #	Gene count	FDR
D2			
Cell adhesion	0007155	8	3.20E-02
D8			
Lipid metabolic process	0006629	22	9.80E-09
Metabolic process	0008152	19	4.90E-06
Oxidation-reduction process	0055114	21	6.10E-05
Fatty acid metabolic process	0006631	10	2.10E-03
Triglyceride metabolic process	0006641	6	1.10E-02
Inflammatory response	0006954	12	4.20E-02
Rictor-suppressed (Up-regulatory) genes			
GO term	GO #	Gene count	FDR
D2			
Complement activation	0006956	6	7.70E-06
Immune system process	0002376	11	1.50E-02
KEGG pathways			
Rictor-required (Down-regulatory) genes			
Pathway		Gene count	FDR
D0			
ECM*-receptor interaction		6	2.90E-03
D2			
ECM-receptor interaction		6	9.40E-04
D8			
PPAR signaling pathway		12	1.10E-07
Fatty acid metabolism		8	8.40E-05
Metabolic pathways		30	2.00E-03
Propanoate metabolism		5	7.10E-03
Glycerolipid metabolism		6	1.20E-02
Fat digestion and absorption		5	9.40E-04
Rictor-suppressed (Up-regulatory) genes			
Pathway		Gene count	FDR
D2			
Staphylococcus aureus infection		7	1.70-E04
Complement and coagulation cascades		6	4.00E-02

*ECM: extracellular matrix

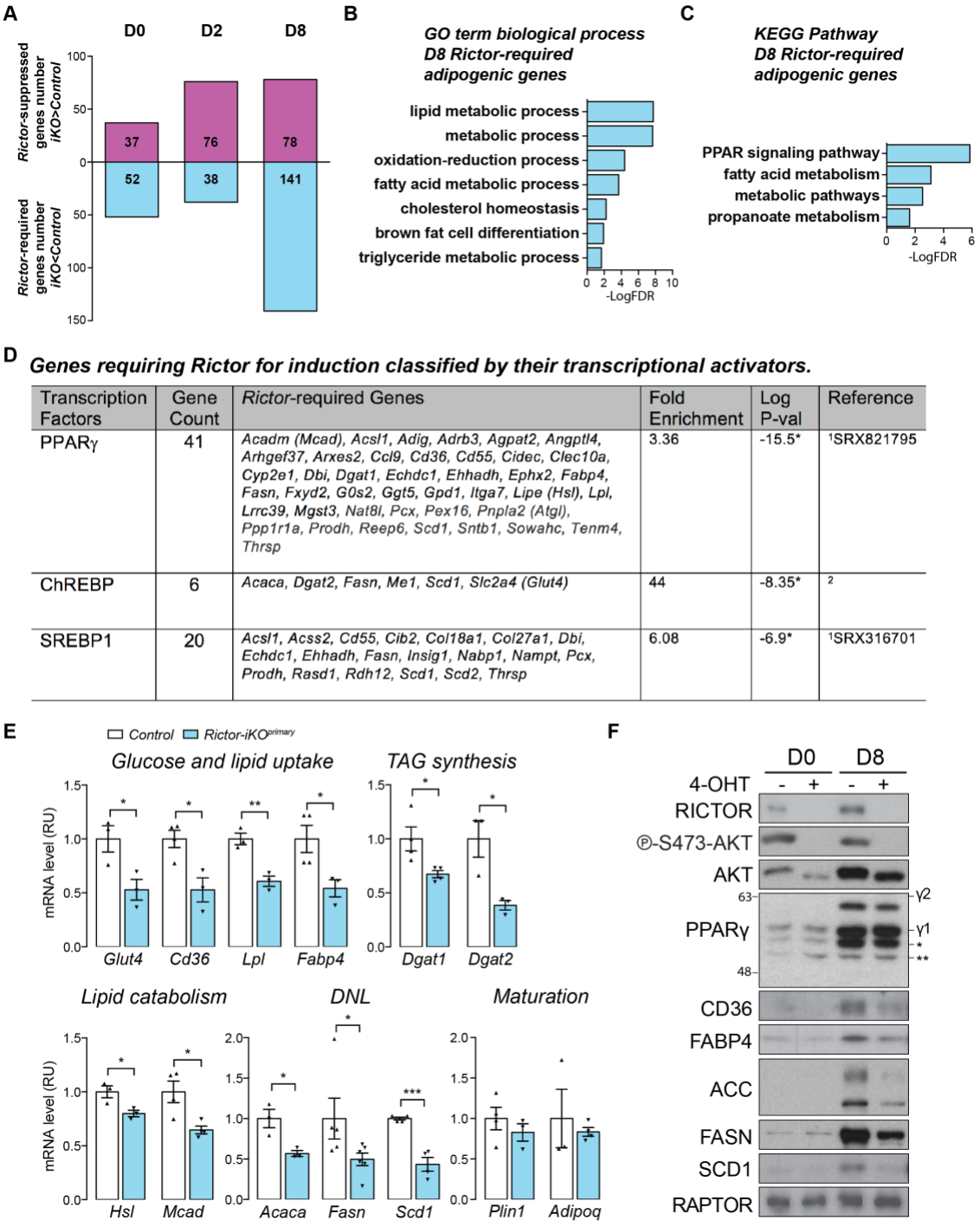

Transcription Factors	Gene Count	*Rictor*-required Genes	Fold Enrichment	Log P-val	Reference
PPARγ	41	*Acadm (Mcad), Acsl1, Adig, Adrb3, Agpat2, Angptl4, Arhgef37, Arxes2, Ccl9, Cd36, Cd55, Cidec, Clec10a, Cyp2e1, Dbi, Dgat1, Echdc1, Ehhadh, Ephx2, Fabp4, Fasn, Fxyd2, G0s2, Ggt5, Gpd1, Itga7, Lipe (Hsl), Lpl, Lrrc39, Mgst3, Nat8l, Pcx, Pex16, Pnpla2 (Atgl), Ppp1r1a, Prodh, Reep6, Scd1, Sntb1, Sowahc, Tenm4, Thrsp*	3.36	-15.5*	[1]SRX821795
ChREBP	6	*Acaca, Dgat2, Fasn, Me1, Scd1, Slc2a4 (Glut4)*	44	-8.35*	[2]
SREBP1	20	*Acsl1, Acss2, Cd55, Cib2, Col18a1, Col27a1, Dbi, Echdc1, Ehhadh, Fasn, Insig1, Nabp1, Nampt, Pcx, Prodh, Rasd1, Rdh12, Scd1, Scd2, Thrsp*	6.08	-6.9*	[1]SRX316701

Figure II-2 mTORC2 promotes expression of lipid handling genes. A Up-regulated (*Rictor*-suppressed) and down-regulated (*Rictor*-required) genes at the indicated differentiation days (fold change >1.4; adjusted p value < 0.05). **B** Gene ontology (GO) term enrichment analysis of day 8 *Rictor*-required adipogenic genes analyzed by the Database for Annotation, Visualization and Integrated Discovery (DAVID).

Figure II-2 (Cont.) C KEGG pathway enrichment analysis of D8 *Rictor*-required adipogenic genes analyzed by DAVID). **D** Gene requiring *Rictor* for induction classified by their published transcriptional activators. [1]Compared to ChIP-atlas database (Oki and Ohta, 2016); [2]Compared to the ChREBP targets listed in Iizuka, 2017. * p value < 0.05). Full gene names are listed in **Figure II-S2A** legend. **E** Relative mRNA expression by RT-PCR of the indicated genes in day 8 control and *Rictor-iKO*^{primary} cells (N ≥ 3; data represent mean ± SEM; $*p < 0.05$, $**p < 0.01$, ***p < 0.001). **F** Representative western blot of the indicated total proteins in lysates from undifferentiated (D0) and differentiated (D8) control and *Rictor-iKO*^{primary} cells. N = 3. γ1: PPARγ1 isoform; γ2: PPARγ2. * and ** are background bands. Numbers at the left: protein size in kDa.

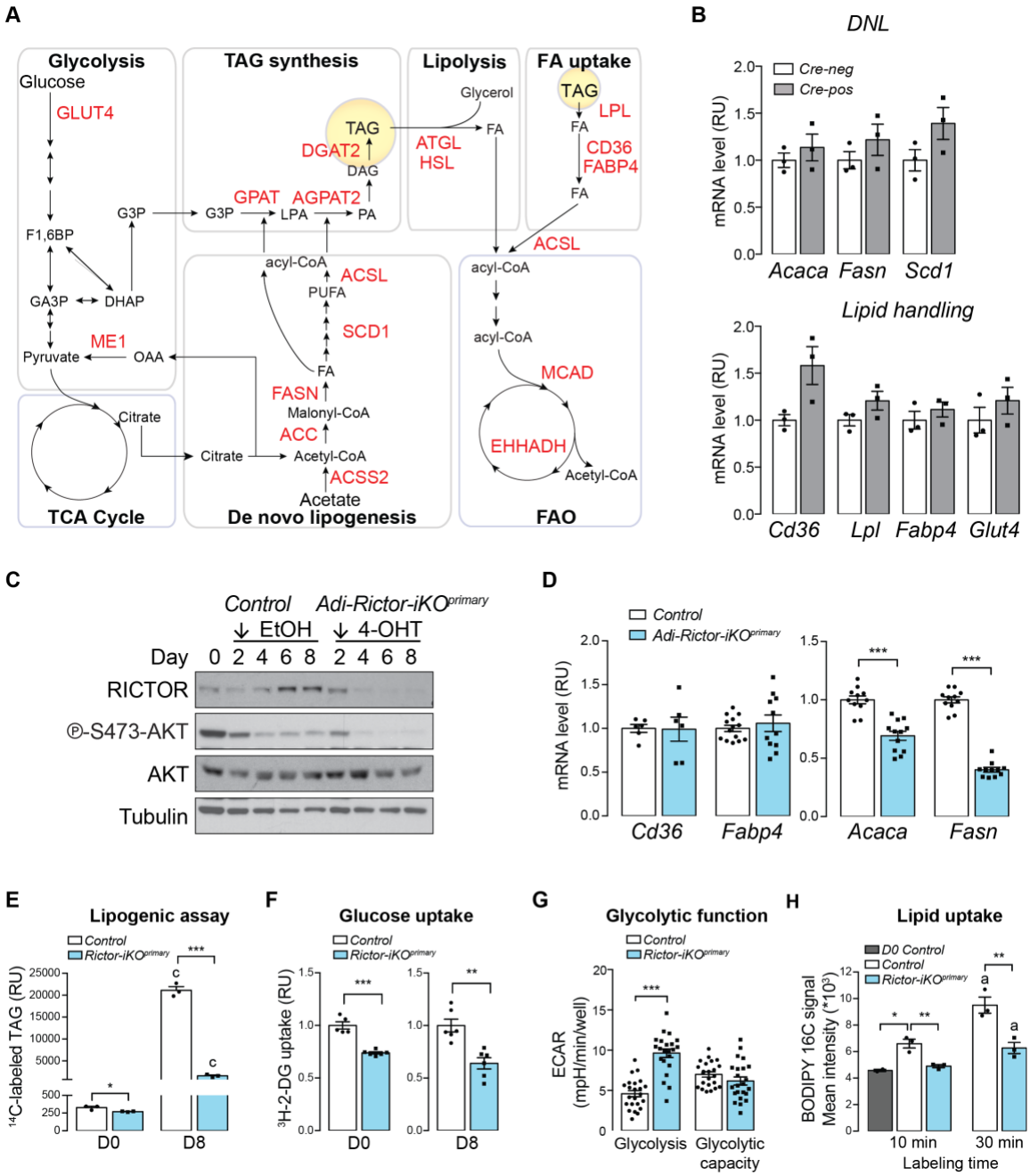

Figure II-S2 mTORC2 promotes expression of PPARγ regulated lipid handling genes, related to Figure 2. **A** Pathway clusters of the *Rictor*-required adipogenic genes modified by KEGG pathway analysis. Genes highlighted in red: down-regulatory genes identified as PPARγ/ChREBP/SREBP1 targets. Also see **Figure 2C**.

Figure II-S2 (Cont.) FAO: fatty acid oxidation, TCA cycle: tricarboxylic acid *cycle*; Abbreviations of metabolites: F1,6BP: fructose-1,6-bisphosphate, GA3P: glyceraldehyde 3-phosphate, DHAP: dihydroxyacetone phosphate, LPA: lysophosphatidic, PA: phosphatidic acid, DAG: diacylglycerol, TAG: triacylglycerol, FA: fatty acid, PUFA: polyunsaturated fatty acid. Abbreviations of gene names: GLUT4: Glucose transporter type 4, ME1: Malic enzyme 1, GPAT: Glycerol-3-phosphate acyltransferase, AGPAT2: 1-acylglycerol-3-phosphate O-acyltransferase 2, DGAT2: Diacylglycerol O-acyltransferase 1, ACSS2: Acyl-CoA Synthetase Short Chain Family Member 2, ACC: Acetyl-CoA carboxylase, FASN: Fatty acid synthase, SCD1: Stearoyl-CoA desaturase 1, ACSL: Acyl-CoA synthetase long-chain, HSL: Hormone-sensitive lipase. ATGL: Adipose triglyceride lipase, LPL: Lipoprotein lipase, FABP4: Fatty acid binding protein 4, MCAD: Medium-chain acyl-CoA dehydrogenase, EHHADH: Enoyl-CoA hydratase and 3-hydroxyacyl-CoA dehydrogenase. **B** Relative mRNA expression by RT-PCR of genes in the DNL and lipid handling pathways in differentiated *primary UBC-Cre^{ERT2}* cells with (Cre-pos, 4-OHT-treated) or without (Cre-neg, EtOH-treated) Cre expression (data represent mean ± SEM). See also **Figure 1A**. **C** Western blot of lysates from control and *Rictor-iKO^{primary}* cells with *Rictor* deleted from D2 (*Adi-Rictor-iKO^{primary}*) at indicated differentiation time points. Arrow: Starting point of 4-OHT exposure. **D** Relative mRNA expression by RT-PCR of genes in the DNL and lipid handling pathways in control and *Adi-Rictor-iKO^{primary}* cells. Data represent mean ± SEM; $^{***}p < 0.001$. **E** Lipogenic assay measured by 14C-glucose incorporation into 14C-TAG of undifferentiated (D0) and differentiated (D8) control *and Rictor-iKO^{primary}* cells. Data represent mean ± SEM; $*p < 0.05$, $^{***}p < 0.001$. c: $p < 0.001$ relative to its D0 counterpart. RU: relative unit (calculated from CPM per μg of protein). **F** ^{3}H-2-deoxyglucose (^{3}H-2-DG) uptake of undifferentiated (D0) and differentiated (D8) control *and Rictor-iKO^{primary}* cells. Data represent mean ± SEM; $^{*}p < 0.01$, $^{***}p < 0.001$. RU: relative unit (calculated from CPM per minute per μg of protein). **G** Glycolytic function determined by extracellular acidification rate (ECAR) of differentiated control *and Rictor-iKO^{primary}* cells. Data represent mean ± SEM; $^{***}p < 0.001$. **H** BODIPY FL C16 lipid uptake of undifferentiated (D0) and differentiated (D8) control *and Rictor-iKO^{primary}* cells incubated in either 10 or 30 minutes. Mean intensity was determined by flow cytometry. Data represent mean ± SEM; $*p < 0.05$, $^{**}p < 0.01$. a: $p < 0.05$ when compared to its counterpart in 10-minute group.

Specific PPARγ targets require *Rictor* for full induction

To further explore the connection between mTORC2 and PPARγ, I expressed a PPARγ activity reporter construct that contains three PPRE elements in the luciferase promoter (J. B. Kim et al. 1998) in control and *Rictor-iKO$_{immortal}$* cells and quantified reporter gene activity at D2 of differentiation. As expected, reporter activity increased 2-fold when the activity at D2 is compared to that in undifferentiated cells (D0) [Figure II-S3A]. Reporter activity decreased by 53% when *Rictor* was deleted [Figure II-S3A], and while supplementing the PPARγ agonist rosiglitazone enhanced reporter activity 1.8-fold in control cells, it

had no effect in the *Rictor-iKO*$_{immortal}$ cells [Figure II-S3A]. Similarly, overexpressing recombinant HA-PPARγ2 enhanced reporter activity 2-fold over baseline in D2 control cells, and this was reduced by 58% in the *Rictor-iKO*$_{immortal}$ cells despite recombinant HA-PPARγ2 expressing at similar levels in the control and knockout cells [Figure II-S3A and S3B]. Moreover, overexpressing HA-PPARγ2 did not rescue lipid droplet accumulation in *Rictor*-deficient cells upon differentiation [Figure II-S3C]. It also failed to restore expression of *Cd36*, *Lpl, Fabp4, Acaca, Fasn,* or *Scd1* [Figure II-S3D] or ACLY, ACC or FASN protein expression [Figure II-S3E], although lipid content and *Cd36* expression did show minor increases relative to *Rictor*-deficient cells expressing the empty vector control. I also tested whether supplementing rosiglitazone during the full differentiation assay would improve the *Rictor* KO phenotype. Rosiglitazone did increase Oil Red O staining and target gene expression in both control and *Rictor-iKO*$_{immortal}$ cells, but lipid accumulation and gene expression remained significantly attenuated in *Rictor-iKO*$_{immortal}$ cells relative to control [Figure II-S3F, S3G, S3H]. Overall, these data were consistent with *Rictor* loss impairing PPARγ activity.

Next, I used chromatin IP (ChIP) assay to examine endogenous PPARγ target gene promoters in primary cells for both PPARγ binding to PPRE elements and for histone H3K9 acetylation, which is associated with PPARγ target gene activity (Lefterova et al. 2008; Steger et al. 2010; Xiao Wang et al. 2019; Salma

et al. 2004). I examined the PPRE regions in *Rictor*-dependent (*Cd36* and *Fabp4*) and a *Rictor*-independent (*Pkm2*) PPARγ target [Figure II-S4A, S4B and Appendix II for primer sequences]. At differentiation D2, PPARγ-PPRE binding was unchanged at the promoters of *Cd36, Fabp4* and *Pkm2* when *Rictor* is absent; however, at D8, PPARγ binding at the *Cd36* and *Fabp4* PPREs decreased by 40% and 33%, respectively, in the absence of *Rictor* [Figure II-3A]. In contrast, but consistent with our gene expression analysis, PPARγ binding to the *Pkm2* promoter (Panasyuk et al., 2012), was unaffected by *Rictor* loss [Figure II-3A]. Deleting *Rictor* also decreased H3K9ac by 40% and 44%, respectively, in the PPREs of *Cd36* and *Fabp4* at D2, preceding measurable loss of PPARγ binding [Figure II-3B]. H3K9ac further decreased at both promoters by 73% and 80%, respectively, at D8 while remaining unaffected in the *Pkm2* PPRE throughout differentiation [Figure II-3B]. Similar results were obtained using the *Rictor-iKO*$_{immortal}$ system; for example, PPARγ binding to the *Fabp4*-PPRE decreased in *Rictor-iKO*$_{immortal}$ cells although the defect occurred 2 days earlier in the immortalized cells than in the primary cells [Figure II-S4C]. This was consistent with the immortalized cells but not the primary cells, showing greater dependency on *Rictor* for PPARγ amplification [Figure II-S1J and S1K]. Total histone H3 levels and global H3K9 acetylation appeared unaffected by *Rictor* loss [Figure II-S4D]. These data were consistent with specific PPARγ targets requiring *Rictor* for full induction during differentiation.

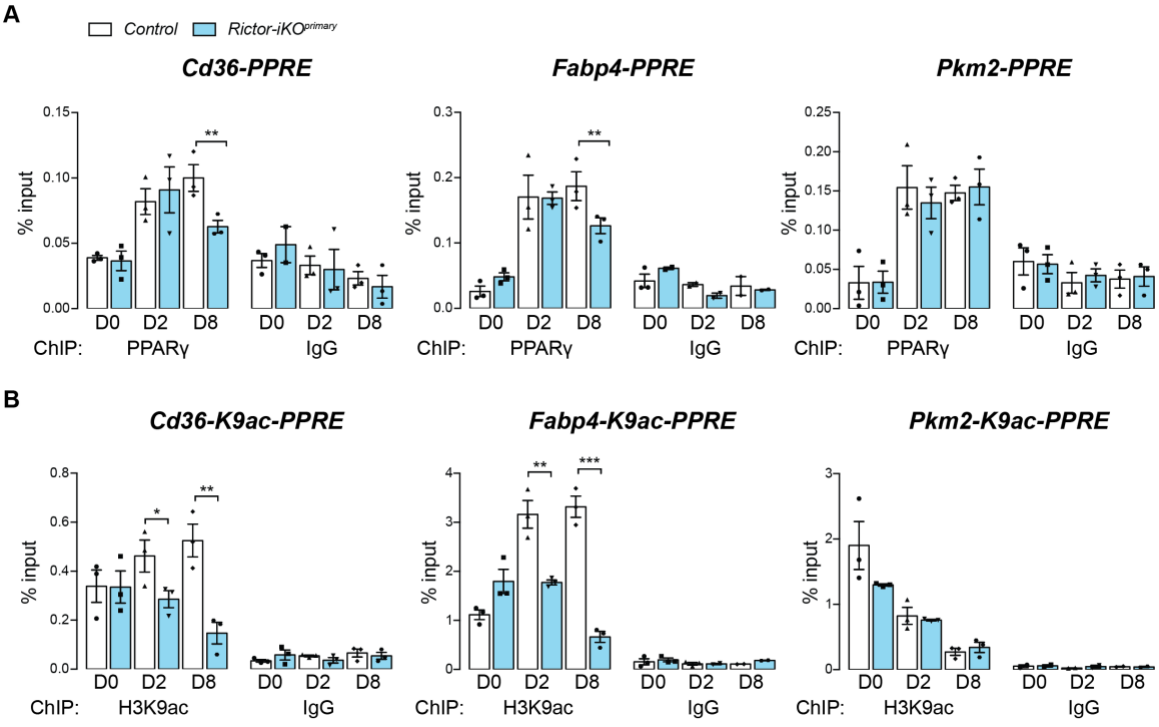

Figure II-3 Specific PPARγ targets require *Rictor* for full induction. A PPARγ/PPAR-responsive element (PPRE) interaction identified by chromatin IP (ChIP) at *Cd36, Fabp4* and *Pkm2* promoters in control and *Rictor-iKO*^{primary} cells (N = 3 for PPARγ ChIP, N = 3 for IgG ChIP; data represent mean ± SEM; $^{**}p < 0.01$). ChIP with IgG were used as negative controls. **B** H3K9 acetylation (H3K9ac) by ChIP analysis at *Cd36, Fabp4* and *Pkm2* promoters in control and *Rictor-iKO*^{primary} cells (N = 3 for PPARγ ChIP, N = 3 for IgG ChIP; data represent mean ± SEM; $^{*}p < 0.05$, $^{**}p < 0.01$, ***p < 0.001). ChIP with IgG were used as negative controls.

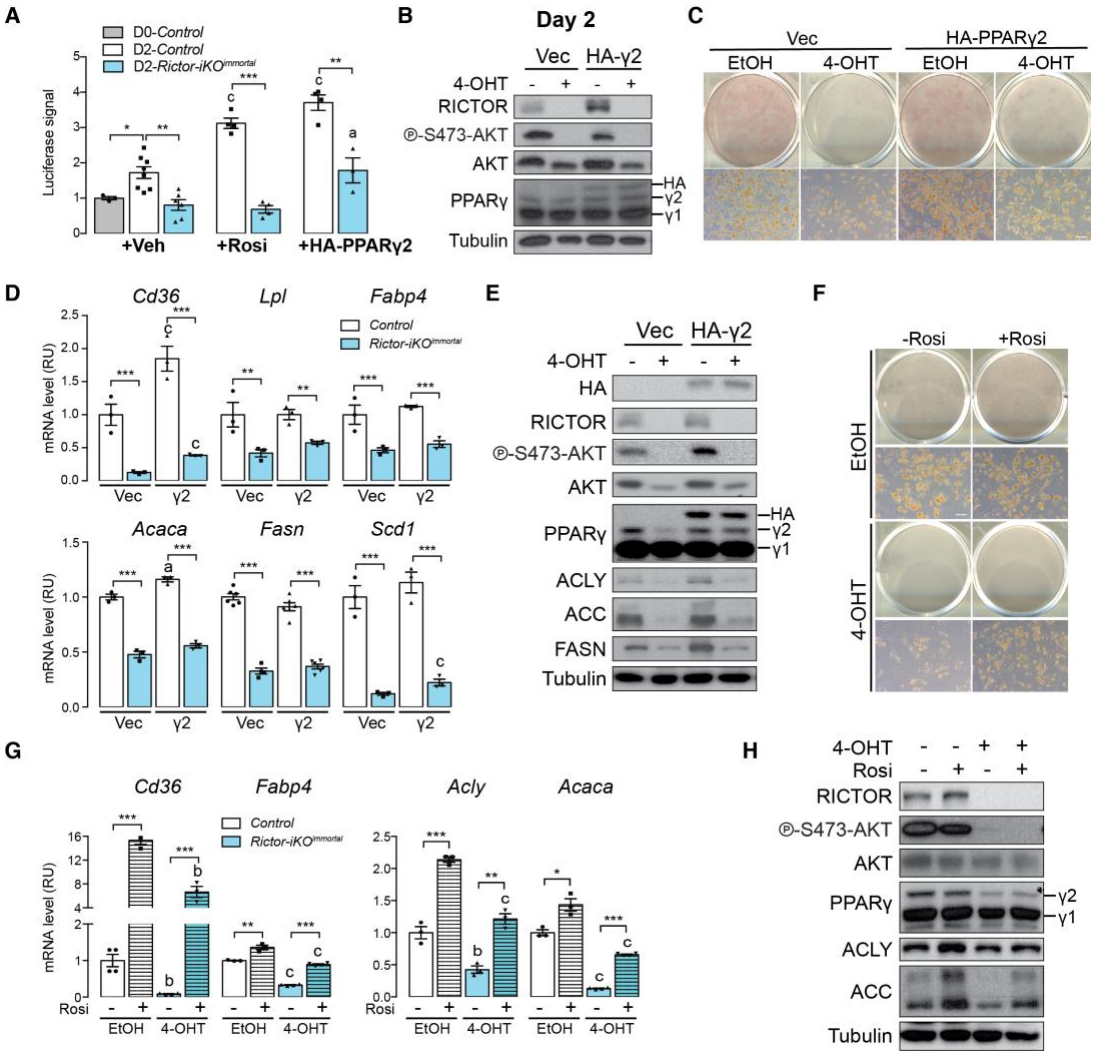

Figure II-S3 Specific PPARγ targets require *Rictor* for full induction, related to Figure 3. A Luciferase reporter gene assay with PPRE-responsive element (PPRE-Luc) in control and *Rictor-iKO*^{immortal} cells with indicated treatment or transduction at day 2. Rosi: Rosiglitazone (data represent mean ± SEM; $*p < 0.05$, $^{**}p < 0.01$, $^{***}p < 0.001$; a: $*p < 0.05$ when compared to vehicle-treated cells; c: $^{***}p < 0.001$ when compared to vehicle-treated cells). **B** Representative western blot of lysates from control and *Rictor-iKO*^{immortal} at day 2. N = 3. HA-γ2: cells transduced with HA-PPARγ2. **C** ORO staining of differentiated control and *Rictor-iKO*^{immortal} cells overexpressing empty vector (Vec) or HA-PPARγ2 plasmid (scale bar = 50 μm). **D** Relative mRNA expression of indicated genes from differentiated control and *Rictor-iKO*^{immortal} cells overexpressing empty vector (vec) or HA-PPARγ2 (γ2) plasmid (data represent mean ± SEM; $^{**}p < 0.01$, $^{***}p < 0.001$; a: $*p < 0.05$ when compared to vector-expressing cells; c: $^{***}p < 0.001$ when compared to vector-expressing cells). **E** Representative western blot of lysates from differentiated control and *Rictor-iKO*^{immortal} cells overexpressing empty vector (Vec) or HA-PPARγ2 (HA-γ2) plasmid. N = 3. **F** ORO staining of differentiated control and *Rictor-iKO*^{immortal} cells (4-OHT-treated) with or without rosiglitazone (Rosi) supplement during differentiation (scale bar = 50 μm).

Figure II-S3 (Cont.) G Relative mRNA expression of indicated genes from differentiated control and *Rictor-iKO*^{immortal} cells (4-OHT-treated) with or without Rosiglitazone (Rosi) supplement (data represent mean ± SEM; $^{**}p < 0.01$, $^{***}p < 0.001$; a: $*p < 0.05$ when compared to its counterpart in non-Rosi group; b: $^{**}p < 0.01$; c: $^{***}p < 0.001$). **H** Representative western blot of lysates from differentiated control and *Rictor-iKO*^{immortal} cells with or without rosiglitazone (Rosi) supplement. N = 3.

Neither ChREBPβ nor SREBP1n overexpression is sufficient to rescue PPARγ target genes

In mature adipocytes, mTORC2 positively regulates expression of the transcription factor ChREBPβ and its target genes in the *de novo* lipogenesis pathway, e.g. *Acly*, *Acc*, and *Fasn* (Tang et al. 2016). ChREBPβ has also been shown to regulate PPARγ expression and activity in 3T3L1 cells during adipogenesis (Witte et al. 2015). Therefore, I asked whether over-expressing recombinant ChREBPα or ChREBPβ in *Rictor-iKO*$_{immortal}$ cells could rescue lipid accumulation and PPARγ gene expression. In the control cells, over-expressing recombinant ChREBPβ increased lipid amount by 20% determined by Oil Red O staining [Figure II-4A]; however, lipid accumulation was unaffected in *Rictor-iKO* cells over-expressing ChREBPα or ChREBPβ [Figure II-4A]. Notably, expressing ChREBPβ partially restored the mRNA and protein expression of ACLY, ACC, and FASN [Figure II-4B and 4C], but it had no impact on the PPARγ target genes *Cd36, Lpl, Fabp4*, *Dgat1* or *Dgat2* [Figure II-4C]. Expressing ChREBPα had no effect on PPARγ target genes and minimal effects on DNL gene expression [Figure II-4A-C]. The SREBP1 lipogenic transcription factor shares targets with

ChREBP and its activity is positively linked to mTORC2 in the liver (Hagiwara et al. 2012; Yuan et al. 2012). Interestingly, however, I observed an increase in the level of nuclear SREBP1 (SREBP1n) in both *Rictor-iKO*$_{primary}$ and *Rictor-iKO*$_{immortal}$ cells [Figure II-4D and 4F] suggesting increased SREBP1 processing. Consistent with this, the gene encoding the SREBP-processing inhibitor *Insig1* was a *Rictor*-required gene [Figure II-2D and Table II-1]. Moreover, over-expressing the transcriptionally actived SREBP1n cleavage product in *Rictor-iKO*$_{immortal}$ cells had little effect on PPARγ target gene expression and failed to restore lipid droplet formation [Figure II-4E-4G]. Thus, neither ChREBPα/β nor SREBP1n overexpression was sufficient to restore defects in lipid metabolic gene expression when cells differentiated in the absence of *Rictor*.

In contrast to our findings in this study, previous work using a brown preadipocyte differentiation model showed that *Rictor* is required for PPARγ2 induction (Calejman et al. 2020; Hung et al. 2014b) suggesting that brown and white preadipocyte differentiation may have different mTORC2 requirements *in vitro*. Consistent with this notion, I recently showed that overexpressing ACLY or ACLY-S455D partially and completely rescues *Rictor* loss in the brown preadipocyte model (Calejman et al. 2020); however, in *Rictor*-deficient subcutaneous white preadipocytes, stably overexpressing recombinant ACLY, ACLY-S455D or ACLY-S455E did not rescue lipid accumulation [Figure II-S4E], *Pparg2*, *Cd36*, or *Fabp4* gene expression [Figure II-S4F] or ACC protein levels

during differentiation [Figure II-S4G]. In fact, overexpressing ACLY enhanced the suppressive effect of *Rictor* loss on gene expression in the white preadipocyte model [Figure II-S4F]. This is consistent with these models of brown and subcutaneous white adipogenesis having different mTORC2 requirements.

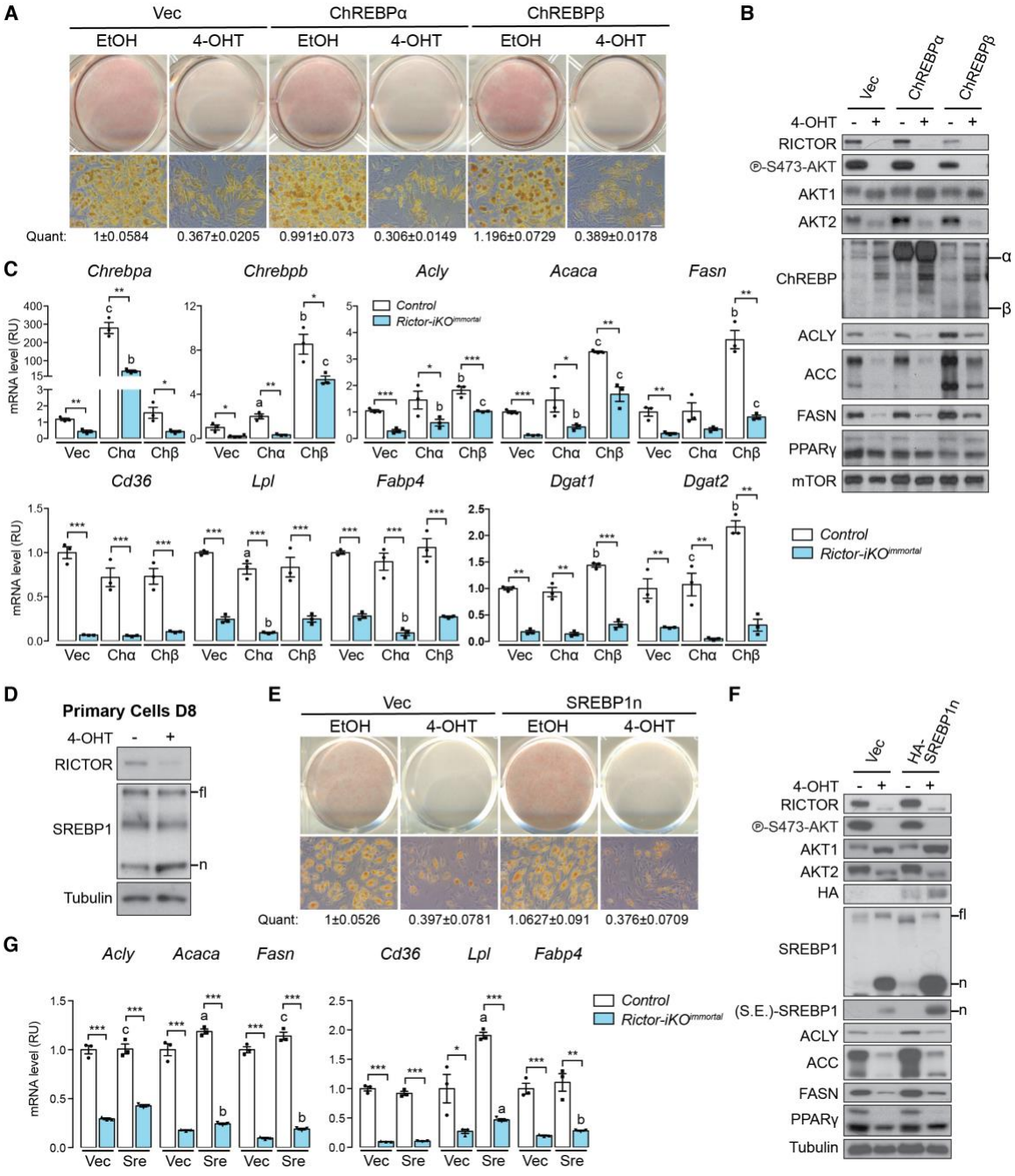
A
Vec
ChREBPα
ChREBPβ
EtOH
4-OHT
Quant:
1±0.0584
0.367±0.0205
0.991±0.073
0.306±0.0149
1.196±0.0729
0.389±0.0178
B
Vec
ChREBPα
ChREBPβ
4-OHT
RICTOR
Ⓟ-S473-AKT
AKT1
AKT2
ChREBP
α
β
ACLY
ACC
FASN
PPARγ
mTOR
C
Chrebpa
Chrebpb
Acly
Acaca
Fasn
Cd36
Lpl
Fabp4
Dgat1
Dgat2
mRNA level (RU)
Control
Rictor-iKOimmortal
Vec
Chα
Chβ
D
Primary Cells D8
4-OHT
RICTOR
SREBP1
fl
n
Tubulin
E
Vec
SREBP1n
EtOH
4-OHT
Quant:
1±0.0526
0.397±0.0781
1.0627±0.091
0.376±0.0709
F
Vec
HA-SREBP1n
4-OHT
RICTOR
Ⓟ-S473-AKT
AKT1
AKT2
HA
SREBP1
fl
n
(S.E.)-SREBP1
n
ACLY
ACC
FASN
PPARγ
Tubulin
G
Acly
Acaca
Fasn
Cd36
Lpl
Fabp4
mRNA level (RU)
Control
Rictor-iKOimmortal
Vec
Sre

Figure II-4 Overexpressing ChREBPβ or SREBP1n does not rescue *Rictor* loss. A Oil Red O (ORO) staining of differentiated control (EtOH) and *Rictor-iKO*^{immortal} (4-OHT) cells expressing empty vector (Vec), ChREBPα, or ChREBPβ. The number below represents quantification (quant) of Oil Red O after isopropanol extraction (scale bar = 50 μm; data represent mean ± SEM). **B** Representative western blot of lysates corresponding to panel A. N = 3. **C** Relative mRNA expression by RT-PCR of the indicated genes corresponding to panel A (N = 3; data represent mean ± SEM; $*p < 0.05$, $**p < 0.01$, $***p < 0.001$). a-c: comparison of over-expressing cells to vector-containing cells; a: $p < 0.05$; b: $p < 0.01$; c: $p < 0.001$. **D** Representative western blot of lysates from differentiated (D8) control and *Rictor-iKO*^{primary} cells. N = 3. fl: full-length SREBP1; n: processed nuclear SREBP1 product. **E** Oil Red O (ORO) staining of differentiated control and *Rictor-iKO*^{immortal} cells expressing empty vector (Vec) or SREBP1n. The number below represents quantification (quant) of Oil Red O after isopropanol extraction (data represent mean ± SEM). **F** Representative western blot of lysates from differentiated control and *Rictor-iKO*^{immortal} cells corresponding to panel E. N = 3. S.E: shorter exposure. **G** Relative mRNA expression by RT-PCR of indicated genes in control and *Rictor-iKO*^{immortal} cells corresponding to panel E. (N = 3; data represent mean ± SEM; $*p < 0.05$, $**p < 0.01$, $***p < 0.001$). a-c: comparison of over-expressing cells to vector-containing cells; a: $p < 0.05$; b: $p < 0.01$; c: $p < 0.001$.

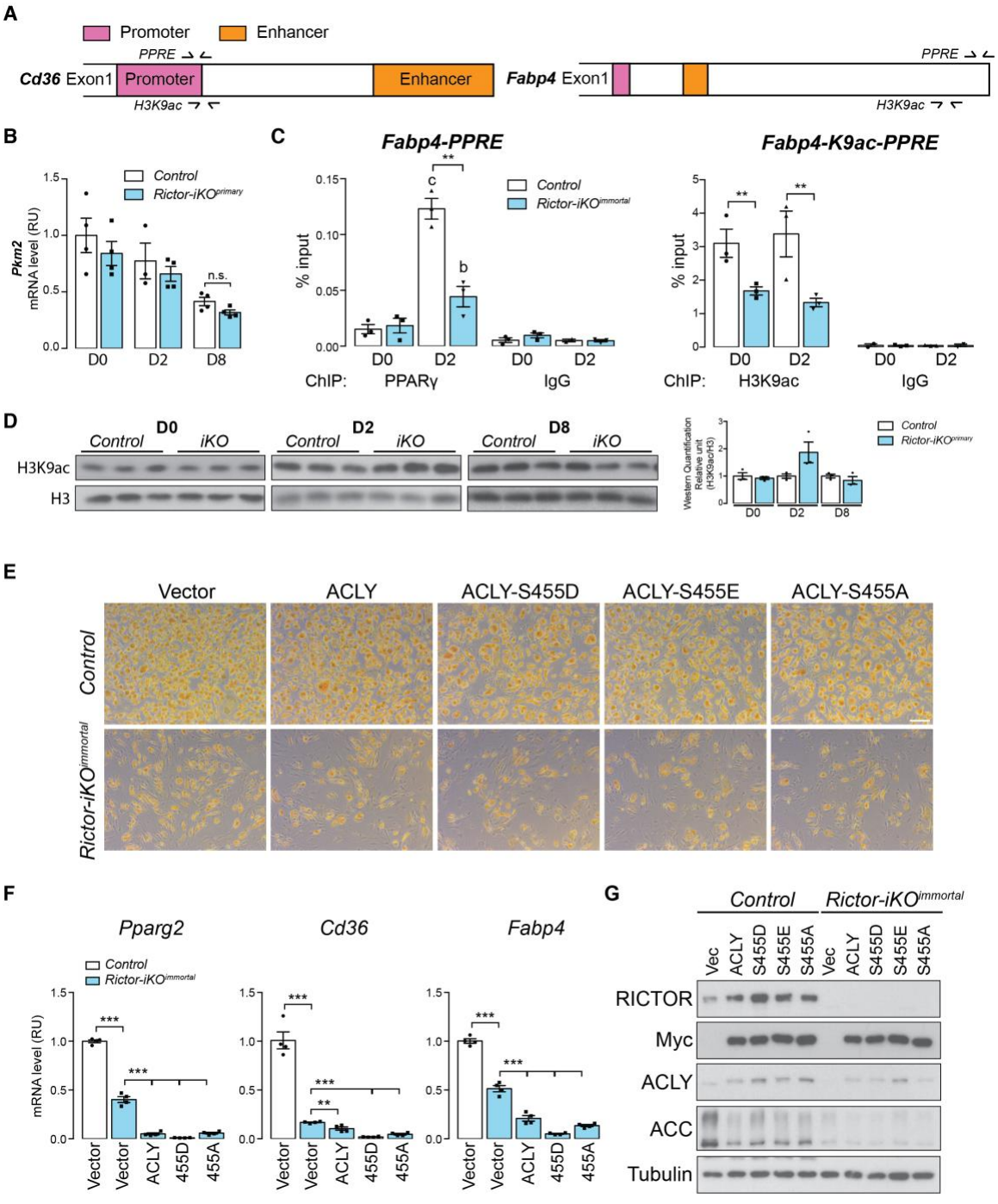

Figure II-S4 ACLY over-expression does not rescue *Rictor-iKO* phenotypes, related to Figure 3 and Figure 4. A Graphic showing the primer binding site (arrows) used in the ChIP assays relative to the promoter and enhancer regions of indicated genes. **B** Relative mRNA expression of *Pkm2* in differentiated control and *Rictor-iKO*^{primary} cells (data represent mean ± SEM; n.s: not significant).

Figure II-S4 (Cont.) C PPARγ/PPAR-responsive element (PPRE) interaction and H3K9 acetylation (H3K9ac) identified by chromatin IP (ChIP) at *Fabp4* promoter in control and *Rictor-iKO*^{immortal} cells (data represent mean ± SEM; $^{**}p < 0.01$; b: $^{**}p < 0.01$ when compared to D0 cells; c: $^{***}p < 0.001$ when compared to D0 cells). ChIP with IgG were used as negative controls. **D** Western blot of extracted histones from control and *Rictor-iKO*^{primary} cells at indicated days during differentiation. Right panel: quantification of H3K9 acetylation signals compared to total H3 (N = 3, data represent mean ± SEM). **E** Oil Red O (ORO) staining of differentiated control (EtOH) and *Rictor-iKO*^{immortal} (4-OHT) cells overexpressing empty vector (Vec), Myc-ACLY, Myc-ACLY-S455D, Myc-ACLY-S455E, or Myc-ACLY-S455A (scale bar = 100 μm). **F** Relative mRNA expression by RT-PCR of indicated genes in differentiated control and *Rictor-iKO*^{immortal} cells overexpressing empty vector (Vec), ACLY, ACLY-S455D, ACLY-S455E, or ACLY-S455A (data represent mean ± SEM; $^{**}p < 0.01$, $^{***}p < 0.001$). **G** Representative western blot of lysates from differentiated control and *Rictor-iKO*^{immortal} cells overexpressing empty vector (Vec), ACLY or indicated ACLY mutants. N = 3.

AKT1-S473D restores PPARγ target gene expression

Next, I asked whether rescuing AKT hydrophobic motif phosphorylation could restore PPARγ target gene expression by generating *Rictor-iKO*$_{immortal}$ cells expressing recombinant HA-AKT1-S473D or HA-AKT2-S474D phospho-mimetics or their HA-AKT1 and HA-AKT2 wildtype and HA-AKT1-S473A phospho-deficient controls. Only HA-AKT1-S473D restored lipid accumulation in differentiating *Rictor-iKO*$_{immortal}$ cells [Figure II-5A and 5B]. Western blot confirmed expression of each recombinant AKT construct [Figure II-5C]. Overexpressing HA-AKT1-S473D also increased *Chrebpb*, *Acaca, Pparg2*, *Fabp4* and *Cd36* expression as well as ACC protein expression in *Rictor-iKO*$_{immortal}$ cells [Figure II-5C and 5D]. HA-S474D-AKT2 and to a lesser extent HA-AKT2 wildtype also increased *Chrebpb* expression consistent with a recent study linking AKT2 and ChREBP-dependent DNL in brown fat [Figure II-5D] (Sanchez-Gurmaches et al. 2019) and suggesting that AKT1 and AKT2 may cooperate or compensate for each other in

ChREBP regulation. Notably, HA-AKT2 and HA-S474D-AKT2 increased *Pparg2* mRNA level but not rescue its target expression, suggesting PPARγ activity might function independently of AKT2 [Figure II-5D]. In sum, these data were consistent with AKT being the key mTORC2 substrate linking mTORC2 to lipid metabolic gene expression.

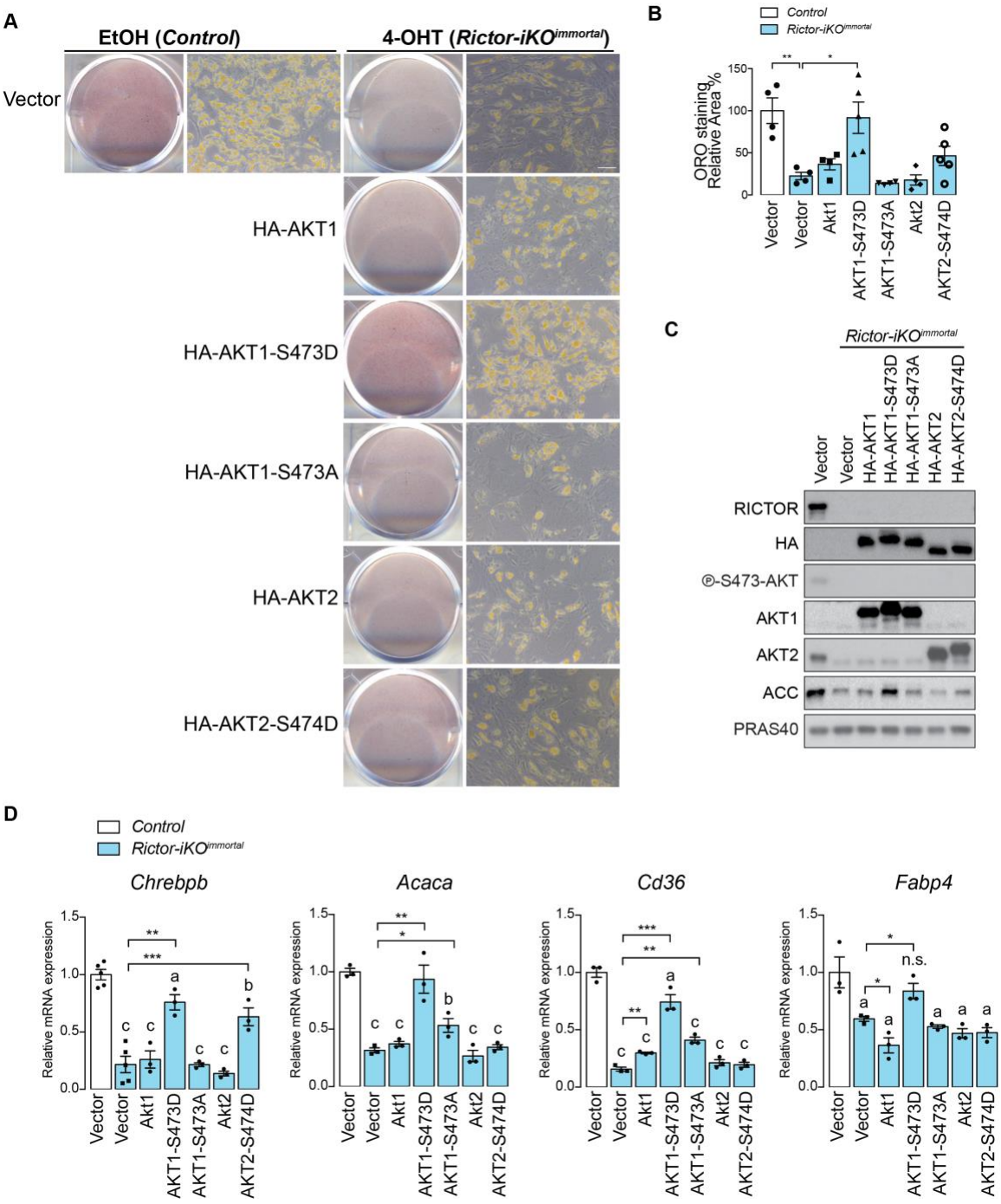

Figure II-5 AKT1-S473D is sufficient to rescue lipid accumulation defect in *Rictor* KO cells. A Oil Red O (ORO) staining of differentiated control (EtOH) and *Rictor-iKO*^{immortal} (4-OHT) cells expressing empty vector, HA-AKT1, HA-AKT1-S473D, HA-AKT1-S473A, HA-AKT2, or HA-AKT2-S474D. **B** Quantification of Oil Red O from **A** after isopropanol extraction (scale bar = 50 μm; data represent mean ± SEM; $*p < 0.05$, $**p < 0.01$, $***p < 0.001$).

C Representative western blot of lysates from differentiated control (EtOH) and *Rictor-iKO*^{immortal} (4-OHT) cells expressing empty vector, HA-tagged AKT1, AKT1-S473D, AKT1-S473A, AKT2 or AKT2-S474D. N = 3. **D** Relative mRNA expression by RT-PCR of the indicated genes corresponding to panel A (N = 3; data represent mean ± SEM; $*p < 0.05$, $**p < 0.01$, $***p < 0.001$). a-c: comparison of over-expressing cells to vector-containing cells; a: $p < 0.05$; b: $p < 0.01$; c: $p < 0.001$.

SWAT development requires mTORC2 *in vivo*

To examine the physiological relevance of these findings, I generated *Prx1-Cre;Rictor*$^{fl/fl}$ mice (*Rictor*$^{Prx1\text{-}Cre}$) in which *Rictor* is deleted *in vivo* in a precursor cell population that gives rise to posterior SWAT, but not to visceral WAT (VWAT) or BAT (Sanchez-Gurmaches, Hsiao, and Guertin 2015; Krueger et al. 2014). *Rictor*$^{Prx1\text{-}Cre}$ mice weighed significantly less than controls starting at 6 and 12 weeks of age for females and males respectively [Figure II-6A]. Food intake was equivalent between groups [Figure II-S5A]. In both sexes, the SWAT weighed significantly less in *Rictor*$^{Prx1\text{-}Cre}$ mice (65% less in males and 57% less in females) [Figure II-6B and 6C]. H&E staining and imaging of the whole SWAT depot showed reduced adipocyte size in *Rictor*$^{Prx1\text{-}Cre}$ mice [Figure II-6D and 6E]. Reciprocally, VWAT and BAT masses in the male *Rictor*$^{Prx1\text{-}Cre}$ mice increased by 60% and 35%, respectively, as a result of adipocyte hypertrophy [Figure II-6B-E]. On the other hand, VWAT mass increased by only 40% in the female *Rictor*$^{Prx1\text{-}Cre}$ mice [Figure II-6B and 6C], due to milder cell hypertrophy [Figure II-6D and 6E], but there was no significant difference in female BAT mass [Figure II-6B and 6C]. I determined that reduced tissue mass was mainly a result of smaller cell size by calculating total depot cellularity (Parlee et al. 2014), which revealed a

linear relationship between tissue weight and average adipocyte volume (r_2=0.97 in male SAT and r_2=0.80 in female SAT) suggesting no significant difference in cellularity [Figure II-S5B]. Moreover, adipocyte precursor cell (APC) number was unchanged between the SWAT of *Rictor*$^{Prx1\text{-}Cre}$ mice and controls [Figure II-S5C] consistent with the SWAT partial-lipodystrophy phenotype originating from a lipid accumulation defect during adipogenesis. Western blotting confirmed that *Rictor*$^{Prx1\text{-}Cre}$ mice lack RICTOR and p-AKT-S473 in posterior SWAT, but not in VWAT or BAT [Figure II-6F]. Neither male nor female *Rictor*$^{Prx1\text{-}Cre}$ mice had enlarged livers [Figure II-S5D] or evidence of hepatic steatosis based on direct TAG measurement [Figure II-S5E]. Analysis of neonates indicated that SWAT lipodystrophy occurred as early as postpartum day 7 (P7) at which point the SWAT weighed 40% less and contains smaller adipocytes [Figure II-S5F-S5H]. This is in stark contrast to deleting *Rictor* in mature adipocytes (e.g. with *Adiponectin-Cre*), which does not affect adipose tissue mass or adipocyte size through 20 weeks of age under standard chow (Tang et al. 2016). These data were consistent with *Rictor* also being required for SWAT development *in vivo*, and further reveals a sex difference in how adipose tissue lipids are redistributed following *Rictor* loss.

Prx1-Cre expressing precursors also give rise to some bone marrow adipocytes as well as osteoblasts and chondrocytes (Krueger et al. 2014; Logan et al. 2002). Consequently, computed tomography (CAT) scanning showed that

the femur and tibia of male *Rictor*$^{Prx1\text{-}Cre}$ mice were 10% and 5% shorter, respectively, correlating with thinner cortical and trabecular bone, which was more prominent in males [Figure II-S5I and Table II-2] (W. Sun et al. 2016; D.-M. Liu et al. 2016; J. Chen et al. 2015). Reduced bone length may explain why quadriceps also weighed slightly less in *Rictor*$^{Prx1\text{-}Cre}$ mice despite the muscle having normal morphology and RICTOR expression [Figure II-S5J-S5L]. *Rictor*$^{Prx1\text{-}Cre}$ male mice also had less bone marrow volume (MV) in the proximal region and a trending decrease in marrow adipose tissue (MAT) especially in females, as shown by osmium staining combined with CAT scanning [Table II-3] (Scheller et al. 2015). Gene expression analysis confirmed reduced *Rictor* mRNA expression but normal *Pparg2* expression in the marrow adipocytes of both male and female *Rictor*$^{Prx1\text{-}Cre}$ mice [Figure II-S5M]. These data are consistent with previous studies showing that *Prx1-Cre* also targets bone marrow mesenchyme (Krueger et al., 2014) and MAT (Sun et al., 2016) in *Rictor*$^{Prx1\text{-}Cre}$ mice, the latter exhibiting characteristics similar to the SWAT in *Rictor*$^{Prx1\text{-}Cre}$ mice.

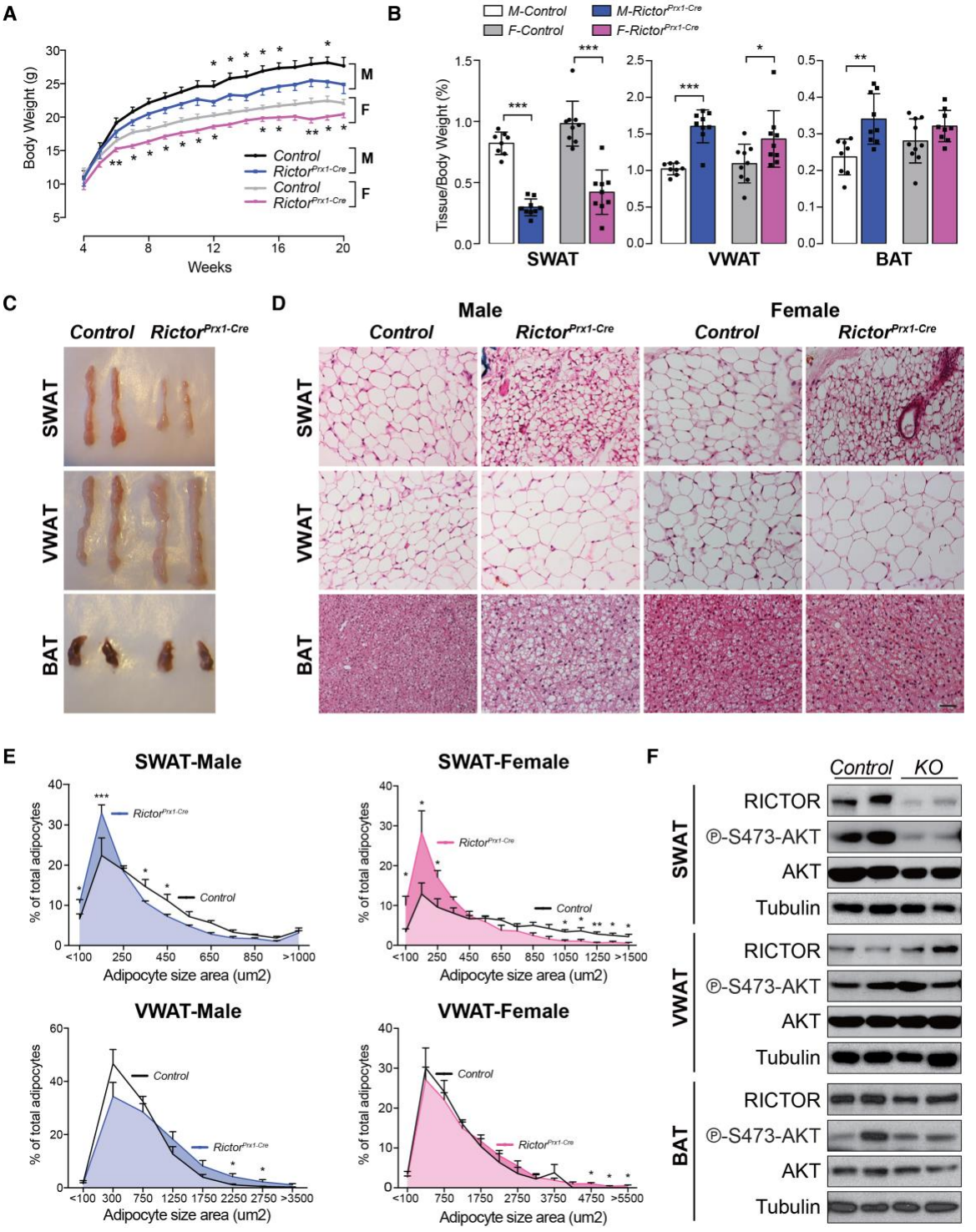

Figure II-6 Subcutaneous white adipose tissue growth requires mTORC2 *in vivo.* A Growth curves of male (M) and female (F) control and *Rictor*^{Prx1cKO} mice (N = 10-14; data represent mean ± SEM; t test; $*p < 0.05$).

Figure II-6 (Cont.) **B** Tissue weight relative to body weight of subcutaneous white adipose tissue (SWAT), visceral white adipose tissue (VWAT) and brown adipose tissue (BAT) (N = 8-10; data represent mean ± SEM; ⁎p < 0.05, ⁎⁎p < 0.01, ***p < 0.001). **C** Representative images of the indicated fat depots from 8-week-old male control and *Rictor*$^{Prx1\text{-}Cre}$ mice. **D** H&E stains corresponding to the tissues in panel C for both male and female mice (scale bar = 100 μm). **E** Individual adipocyte cell size distribution in each indicated depot (N = 4 mice; > 1000 and 500-1000 individual adipocytes measured from SWAT and VWAT of each mouse, respectively; data represent mean ± SEM; ⁎p < 0.05, ⁎⁎p < 0.01, ***p < 0.001). **F** Representative western blot of lysates from SWAT, VWAT and BAT of 8-week-old male control and *Rictor*$^{Prx1\text{-}Cre}$ mice. N = 2.

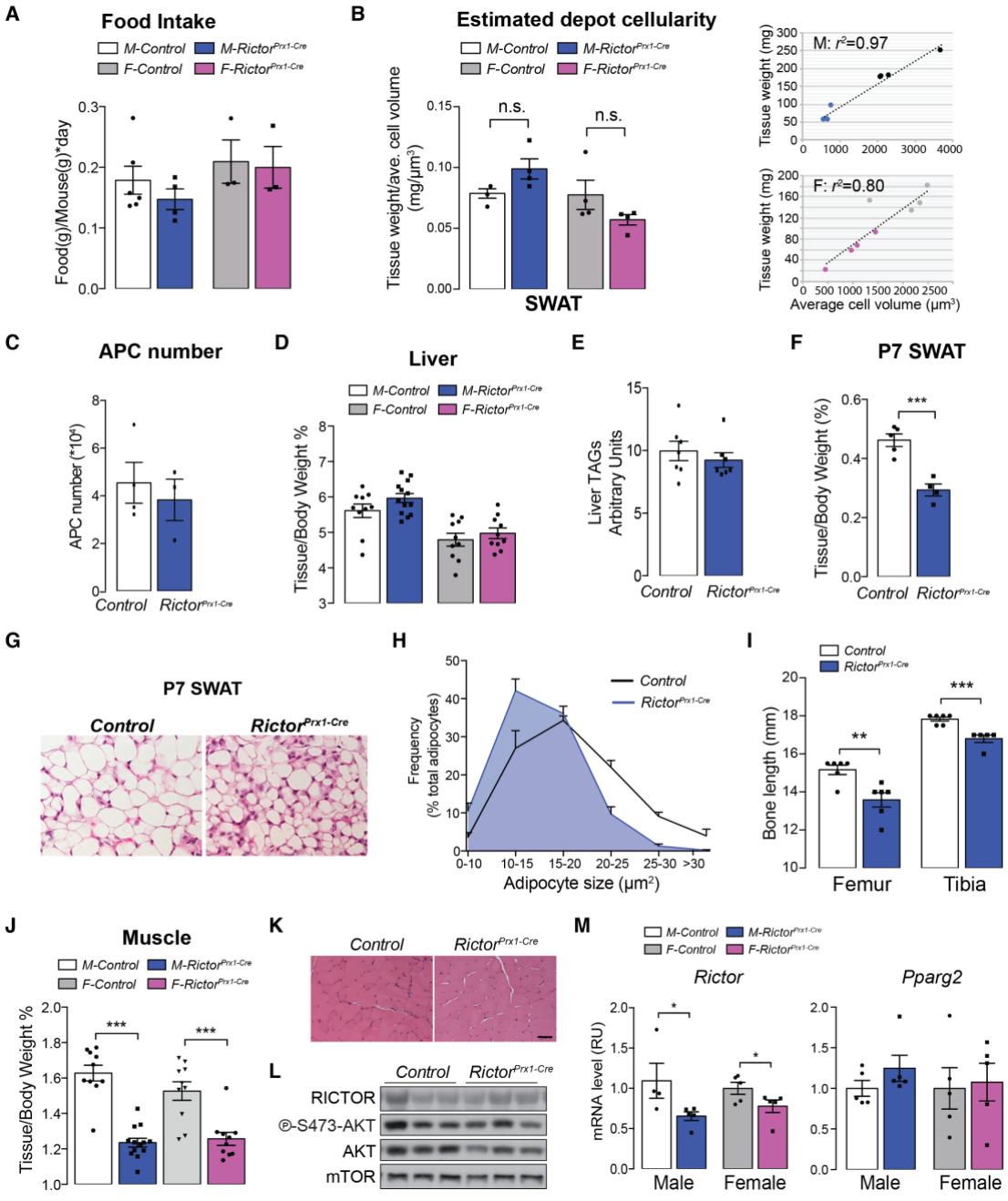

Figure II-S5 Other tissue involvement in *Rictor$^{Prx1\text{-}Cre}$ mice*, related to Figure 6. **A** Food intake of control and *Rictor$^{Prx1\text{-}Cre}$* mice at 8 weeks of age (N = 3-6; data represent mean ± SEM). **B** Estimated depot cellularity in SWAT from control and *Rictor$^{Prx1\text{-}Cre}$* mice at 8 weeks of age (N = 4; data represent mean ± SEM). *right panel*: linear correlation of tissue weight versus average cell volume. r^2 = square of correlation. n.s.: not significant, M: male, F: female. **C** Adipocyte precursor (APC) number isolated from SWAT using cell surface markers staining followed by FACS analysis (N= 4; data represent mean ± SEM). **D** Liver weight relative to body weight of control and *Rictor^{prx1cKO}* mice at 8 weeks of age (N= 10-11; data represent mean ± SEM). **E** TAG content of livers from 8-week-old female mice. Data represent mean ± SEM. **F** SWAT weight relative to body weight of control and *Rictor$^{Prx1\text{-}Cre}$* mice at postpartum day 7 (P7) (N =4; data represent mean ± SEM; ***p < 0.001). **G** H&E stains of adipose tissues from postpartum day 7 (P7) mice. **H** Adipocyte size distribution in indicated depot (N = 4; more than 100 adipocytes were calculated from each mouse; data represent mean ± SEM). **I** Femur and Tibia length from 8-week-old male mice (N =6; data represent mean ± SEM; **p < 0.01, ***p < 0.001). **J** Muscle (quadriceps) weight relative to body weight of control and *Rictor$^{prx1\text{-}Cre}$* mice at 8 weeks of age (N= 10-11; data represent mean ± SEM; ***p < 0.001). **K** H&E stains of muscles from 8-week-old mice (scale bar = 100 μm). **L** Western blot of lysates from muscles of control and *Rictor$^{Prx1\text{-}Cre}$* mice. N = 3. **M** Relative mRNA expression by RT-PCR of *Rictor* and *Pparg2* in bone marrow adipose tissues isolated from control and *Rictor$^{Prx1\text{-}Cre}$* mice (N= 4-5; data represent mean ± SEM; *p < 0.05).

Table II-2: Bone structure analysis.

	Male			Female		
	Control	*Rictor$_{Prx1\text{-}Cre}$*	*P*-Value	Control	*Rictor$_{Prx1\text{-}Cre}$*	*P*-Value
Tb thickness (mm)	0.0513±0.00584	0.04334±0.00496	0.0396*	0.0407±0.00819	0.0397±0.00328	0.782
Tb spacing (mm)	0.246±0.0218	0.289±0.147	0.500	0.362±0.0919	0.376±0.0603	0.785
Tb number (1/mm)	4.132±0.321	4.006±1.459	0.840	2.975±0.829	2.721±0.364	0.529
BV/TV	0.101±0.225	0.0986±0.0702	0.938	0.037±0.0259	0.0275±0.0091	0.421
Cort thickness (mm)	0.185±0.00850	0.1426±0.0178	0.00127**	0.171±0.00985	0.1315±0.00706	0.00073***
Cort/Total Area	0.529±0.00371	0.500±0.0335	0.223	0.540±0.0517	0.501±0.0233	0.134
Marrow Area (mm^2)	0.610±0.00985	0.505±0.0461	0.0578	0.4133±0.0271	0.387±0.0399	0.272

*P <0.05; **P<0.01; P<0.001

Tb: trabecular; BV: bone volume; TV: total volume; Cort: cortical.

Table II-3: Bone marrow analysis and osmium stain quantification.

		Male			Female		
		Control	*Rictor*$^{Prx1\text{-}Cre}$	*P*-Value	Control	*Rictor*$^{Prx1\text{-}Cre}$	*P*-Value
Prox.	MV (mm_3)	6.659±0.723	4.564±0.678	0.00287**	3.895±0.437	3.59±0.409	0.316
	MAT (mm_3)	0.03465±0.04	0.0788±0.088	0.405	0.0693±0.0673	0.0077±0.00816	0.039*
Dist.	MV (mm_3)	1.429±0.0856	1.218±0.281	0.196	1.184±0.222	1.104±0.110	0.462
	MAT (mm_3)	0.82±0.289	0.771±0.687	0.876	0.789±0.377	0.579±0.239	0.306

*P <0.05; **P<0.01.
Prox.: proximal; Dis.: distal; MV: marrow volume; MAT: marrow adipose tissue.

Male *Rictor*$^{prx1\text{-}Cre}$ mice become insulin resistant.

I next asked if SWAT dysfunction due to *Rictor* loss causes insulin resistance. Interestingly, 8-week-old male *Rictor*$^{Prx1\text{-}Cre}$ mice developed insulin intolerance as indicated by a 30% increase in glucose AUC relative to controls [Figure II-S6A]. This correlated with a trending increase in serum insulin level in males [Figure II-S6E]. This was not observed in females [Figure II-S6B], and neither sex showed defects in glucose tolerance [Figure II-S6C and S6D]. Adiponectin, leptin and non-esterified fatty acids (NEFAs) were unchanged in *Rictor*$^{Prx1\text{-}Cre}$ male mice fed *ad libitum* [Figure II-S6E]. The propensity for male *Rictor*$^{Prx1\text{-}Cre}$ to develop insulin resistance was consistent with their greater accumulation of visceral fat.

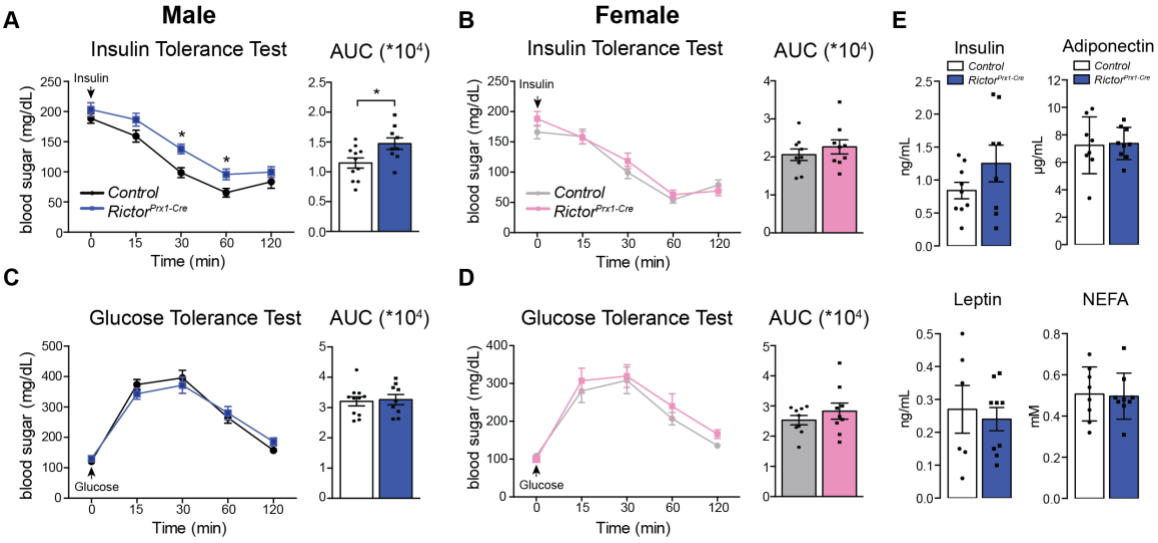

Figure II-S6 Male *Rictor*$^{Prx1\text{-}Cre}$ mice develop insulin resistance, related to Figure 6. A-B Insulin tolerance test (left) with area under curve (AUC, right) from 8-week-old male (**A**) and female (**B**) mice (n = 9-11; data represent mean ± SEM; ∗p < 0.05). **C-D** Glucose tolerance test (left) with area under curve (AUC, right) from 8-week-old male (**C**) and female (**D**) mice (n = 9-11; data represent mean ± SEM; ∗p < 0.05)**. E** Plasma insulin, adiponectin, leptin, and non-esterified fatty acids (NEFA) levels ad libitum fed 8-week-old male mice (n = 7-9; bars represent mean ± SEM).

Rictor is required *in vivo* during SWAT development for lipid metabolic gene expression

Similar to what I observed *in vitro* (i.e. in the D8 primary cells that were differentiated in the absence of *Rictor),* the SWAT of *Rictor*$_{Prx1\text{-}Cre}$ mice expressed PPARγ and C/EBPα *in vivo* as well as insulin receptor beta (IRβ, which was elevated over control) [Figure II-7A]. Also, similar to the *in vitro* models, the SWAT from *Rictor*$_{prx1\text{-}Cre}$ mice had reduced AKT2 mRNA and protein expression [Figure II-7A and S7A]. *In vivo*, reduced AKT2 expression correlated with reduced p-AKT-T308, which was expected as AKT2 is the major AKT isoform in mature adipocytes. Interestingly, p-AS160-T642, p-GSK3β-S9 and p-FoxO1-T24

remain intact *in vivo*, even though p-AKT-T308 is reduced [Figure II-7A]. However, phosphorylation of PRAS40 at T246 was reduced in *Rictor*$^{Prx1\text{-}Cre}$ SWAT. Since PRAS40 is a negative regulator of mTORC1 and T246-PRAS40 phosphorylation releases the inhibition, decreased p-T246-PRAS40 could explain the concomitant reduced phosphorylation of a direct mTORC1 substrate p-S6K1-T389 [Figure II-7A]. I did not observe this effect *in vitro* [Figure II-1F and S7B] or *in vivo* when *Rictor* is deleted in mature adipocytes with *Adiponectin-Cre* (Tang et al. 2016), suggesting the mTORC1 signaling defect was a secondary effect caused by reduced AKT2 induction during differentiation and therefore, reduced total AKT signaling.

I next asked whether SWAT lipid-handling genes require *Rictor* during development for their expression *in vivo*. This was indeed the case for all of the *Rictor*-required anabolic and catabolic lipid metabolism genes as well as their products that I examined and that were previously identified by RNA-seq in primary cells [Figure II-7A, 7B]. *Adiponectin*, however, was reduced in expression *in vivo* but not in the primary cell model [Figure II-7B]. This is consistent with previous observations showing that adiponectin levels may be sensitive to prolonged adipocyte *Rictor* loss *in vivo* (Cybulski et al. 2009; Tang et al. 2016). Notably, SWAT primary SVF preadipocytes isolated from *Rictor*$^{prx1\text{-}Cre}$ mice and differentiated *in vitro* also showed reduced lipid accumulation [Figure II-S7C], decreased lipogenic and TAG synthesis gene and/or protein expression [Figure

II-S7D and S7E], and decreased AKT2 expression [Figure II-S7D and S7E] after differentiation. Moreover, *Adiponectin* mRNA expression was unaffected in primary *Rictor*$^{Prx1\text{-}Cre}$ preadipocytes that are differentiated [Figure II-S7E], consistent with down-regulation of *Adiponectin* mRNA occurring secondary to *Rictor* loss. Consistent with previous data, *Rictor*-deficient SWAT also had defective insulin-stimulated glucose uptake and increased basal lipolysis [Figure II-S7F and S7G]. These data confirmed the physiological relevance of our *in vitro* findings and the role of mTORC2 in establishing the lipid handling capacity of SWAT.

In our previous study of *Rictor*$^{Adipoq\text{-}Cre}$ mice, in which *Rictor* was deleted in mature adipocytes rather than in precursors like this study, the expression of the PPARγ target genes *Cd36, Lpl* and *Fabp4* were unchanged between the control and *Rictor*-deficient SWAT depots when mice were eating standard chow ad libitum (Tang et al. 2016). Reasoning that the difference could be explained by SWAT development placing a greater demand on mTORC2-regulated PPARγ activity, I wondered whether challenging *Rictor*$^{Adipoq\text{-}Cre}$ mice to store more lipid in SWAT would reveal the PPARγ gene expression defects. To this end, I re-examined PPARγ gene expression in *Rictor*$^{Adipoq\text{-}Cre}$ mice that were refed following a fast or given a high fat diet. Indeed, challenging *Rictor*$^{Adipoq\text{-}Cre}$ mice with a prolonged fast followed by 6 hours of refeeding resulted in 36%, 50% and 60% reductions in *Cd36, Lpl,* and *Dgat2* expression respectively, corresponding

to a 33% reduction in tissue mass relative to controls [Figure II-7C and 7D]. Similarly, placing *Rictor*$_{Adipoq\text{-}Cre}$ on high fat diet (HFD) for 12 weeks failed to increase *Cd36, Lpl,* and *Fabp4* expression in the *Rictor* knockout fat [Figure II-7E], consistent with reduced adipose tissue lipid accretion and overall smaller adipocytes [Figure II-7F] (Tang et al. 2016). I concluded that mTORC2 is required to maximally stimulate expression of PPARγ-dependent lipid storage genes in subcutaneous white adipocytes when they are challenged with physiological states that draw high demand on lipid storage pathways, such as tissue development, refeeding after a fast, and chronic obesogenic diets.

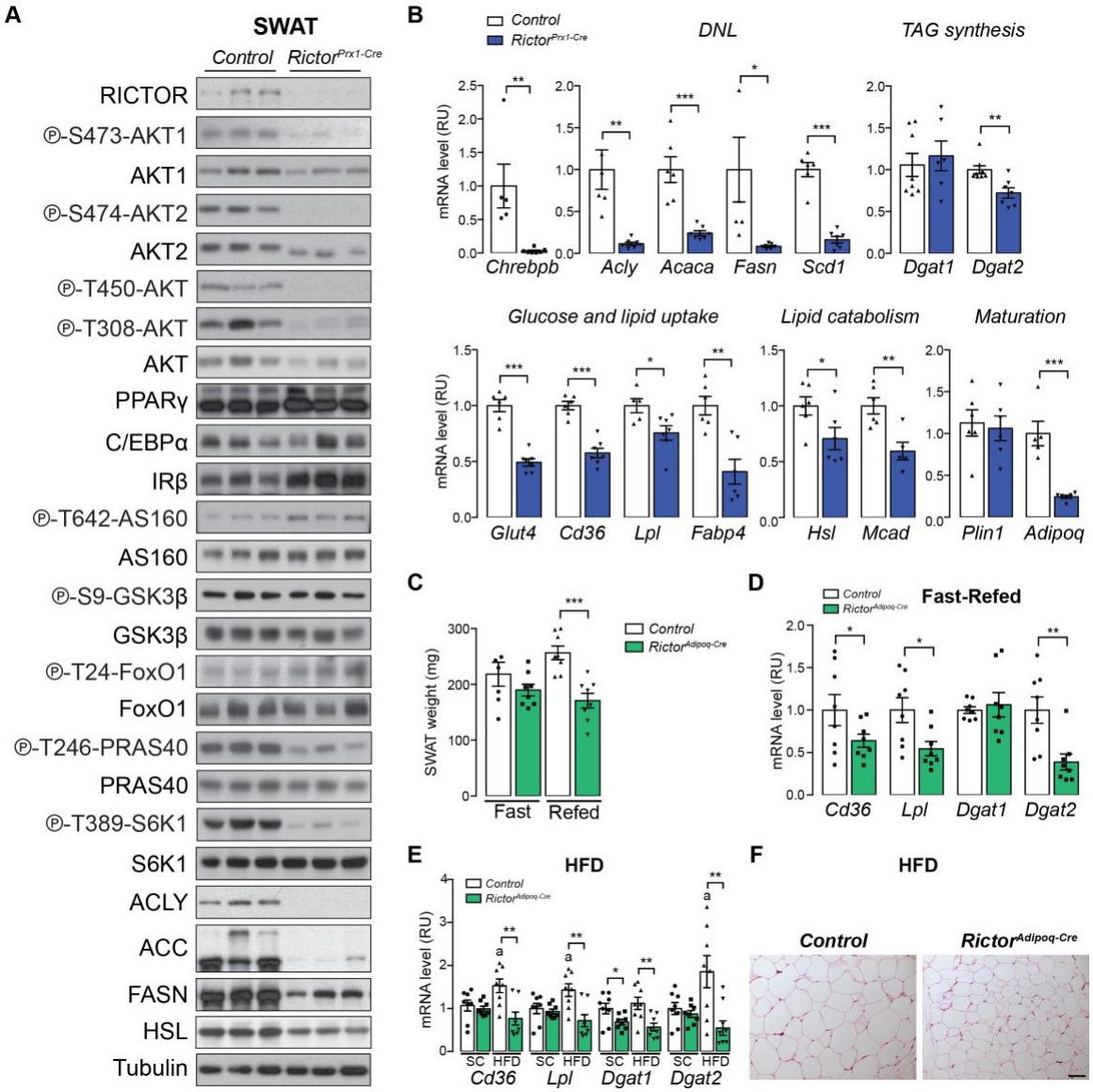

Figure II-7 *Rictor* regulates expression of lipid handling genes during SWAT growth. A Western blot of lysates from the subcutaneous white adipose tissue (SWAT) of 8-week-old control and *Rictor*$^{Prx1\text{-}Cre}$ mice. N= 3. **B** Relative mRNA expression by RT-PCR of indicated genes from SWAT of 8-week-old control and *Rictor*$^{Prx1\text{-}Cre}$ mice (N = 6-8; data represent mean ± SEM; $*p < 0.05$, $**p < 0.01$, ***p < 0.001). **C** Tissue weight of SWAT of 8-week-old control and *Rictor*$^{Adipoq\text{-}Cre}$ mice refed for 6 hours following 24-hour fasting (N = 8; data represent mean ± SEM; ***p < 0.001). **D** Relative mRNA expression by RT-PCR of indicated genes from SWAT of 8-week-old control and *Rictor*$^{Adipoq\text{-}Cre}$ mice refed for 6 hours following 24-hour fasting (N = 8; data represent mean ± SEM; $*p < 0.05$, $**p < 0.01$, ***p < 0.001). **E** Relative mRNA expression by RT-PCR of indicated genes from SWAT of control and *Rictor*$^{Adipoq\text{-}Cre}$ mice after 12-week HFD or standard chow (SC) feeding (N= 7-8; data represent mean ± SEM; *p < 0.05, **p < 0.01; a: p < 0.05 when HFD samples were compared to SC samples). **F** H&E stains of SWAT from control and *Rictor*$^{Adipoq\text{-}Cre}$ mice after 12-week HFD or chow (SC) feeding (scale bar = 100 μm).

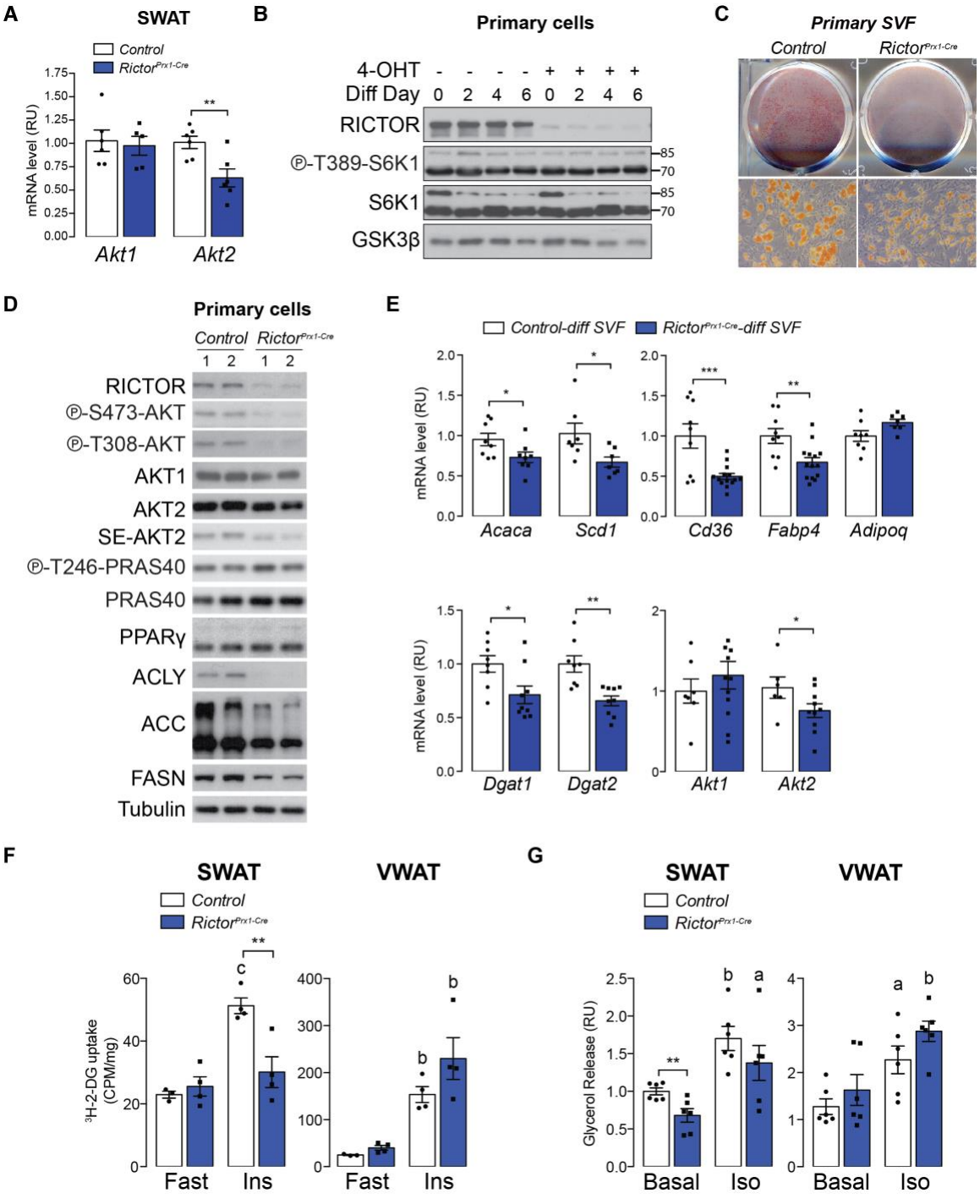

Figure II-S7. *Rictor* is also required in special conditions in mature adipocytes for lipid metabolic gene expression, related to Figure 7. A Relative mRNA expression by RT-PCR of *Akt* isoforms in SWAT from 8-week-old control and *Rictor*$^{Prx1\text{-}Cre}$ mice (N= 6-7; data represent mean ± SEM; **p < 0.01).

Figure II-S7 (Cont.) B Western blot of total and phospho-S6K1 in lysates from controls and *Rictor-iKO*^{primary} cells at indicated time points during adipogenesis. **C** Oil Red O (ORO) staining of differentiated primary preadipocytes isolated from control and *Rictor*$^{Prx1\text{-}Cre}$ mice. **D** Western blot of lysates from differentiated primary preadipocytes isolated from control and *Rictor*$^{Prx1\text{-}Cre}$ mice. Each sample is from an individual mouse with the indicated genotype. **E** Relative mRNA expression by RT-PCR of indicated genes from differentiated primary preadipocytes isolated from control and *Rictor*$^{Prx1\text{-}Cre}$ mice (N= 8; data represent mean ± SEM; *p < 0.05, **p < 0.01, ***p < 0.001). **F** ^{3}H-2-Deoxyglucose uptake (^{3}H-2-DG) of SWAT and VWAT with or without insulin (ins) stimulation from control and *Rictor*$^{Prx1\text{-}Cre}$ mice. Data represent mean ± SEM; **p < 0.01. b: p < 0.01 while its fasted counterpart is compared; c: p < 0.001. **G** Lipolytic function measured by glycerol release from SWAT and VWAT with or without isoproterenol (iso) stimulation from control and *Rictor*$^{Prx1\text{-}Cre}$ mice. Data represent mean ± SEM; **p < 0.01. a: p < 0.05 while its counterpart under basal condition is compared; b: p < 0.01.

Rictor deletion in SWAT protects the mice from HFD-induced obesity and insulin resistance.

Previous studies show that SWAT has a protective effect against insulin resistance in both human and mouse models (McLaughlin et al. 2011; Booth et al. 2018; M. T. Foster et al. 2013). Next, we asked if selective SWAT lipodystrophy will aggravate high fat diet (HFD)-induced metabolic disturbances. To explore this, we fed both control and *Rictor*$^{Prx1\text{-}Cre}$ mice a 60% HFD for 12 weeks starting at 8 weeks of age and compared them with age-comparable standard chow diet (SCD)-fed mice. *Rictor*$^{Prx1\text{-}Cre}$ male mice consuming SCD for 20 weeks weighed 10 % less compared to control mice. Interesting, *Rictor*$^{Prx1\text{-}Cre}$ mice were resistant to HFD-induced weight gain and are grossly leaner [Figure II-8A and 8C]. When relative weight gains were compared, *Rictor*$^{Prx1\text{-}Cre}$ mice fed with HFD gained only 3.2 grams in average compared to chow-fed mice, which was ~45% less than the weight gain in control [Figure II-8A]. Similarly, the female *Rictor*$^{Prx1\text{-}Cre}$ mice were also resistant to diet-induced weight gain [Figure II-8B].

The control and *Rictor*$^{Prx1\text{-}Cre}$ mice consumed comparable amount of food [Figure II-8D] and defecated similar amount of lipid in feces, which is determined by fecal glycerol content [Figure II-8E]. When relative depot mass-to-body weight ratio was calculated, the percentage of adipose tissue weight increased in every analyzed depot in response to 12-week HFD feeding [Figure II-8G]. The percentage of SWAT mass in *Rictor*$^{Prx1\text{-}Cre}$ male mice was 70% less than the SWAT of control mice fed with HFD. VWAT in *Rictor*$^{Prx1\text{-}Cre}$ mice, on the other hand, was trending increased under HFD [Figure II-8F and 8G]. The compensatory increase in VWAT and BAT masses (in which *Rictor* is present) of *Rictor*$^{Prx1\text{-}Cre}$ mice fed a chow diet was significant under chow condition, and HFD feeding blunted this effect [Figure II-8G]. Consistently, histology showed that HFD feeding increased general adipocyte size in the control SWAT [Figure II-8H]. The SWAT from *Rictor*$^{Prx1\text{-}Cre}$ mice contained more smaller adipocytes, and the cell size did not respond as significantly as that in control depot [Figure II-8H]. No significant histology change was detected in neither VWAT nor BAT [Figure II-8I]. Western blot confirmed *Rictor* deletion and phospho-AKT-S473 ablation selectively in SWAT [Figure II-8J]. There were no differences in liver, pancreas and muscle tissue-to-body weights [Figure II-8K], and the liver TAG contents were similar between control and *Rictor*$^{Prx1\text{-}Cre}$ mice under either SCD or HFD fed condition [Figure II-8L].

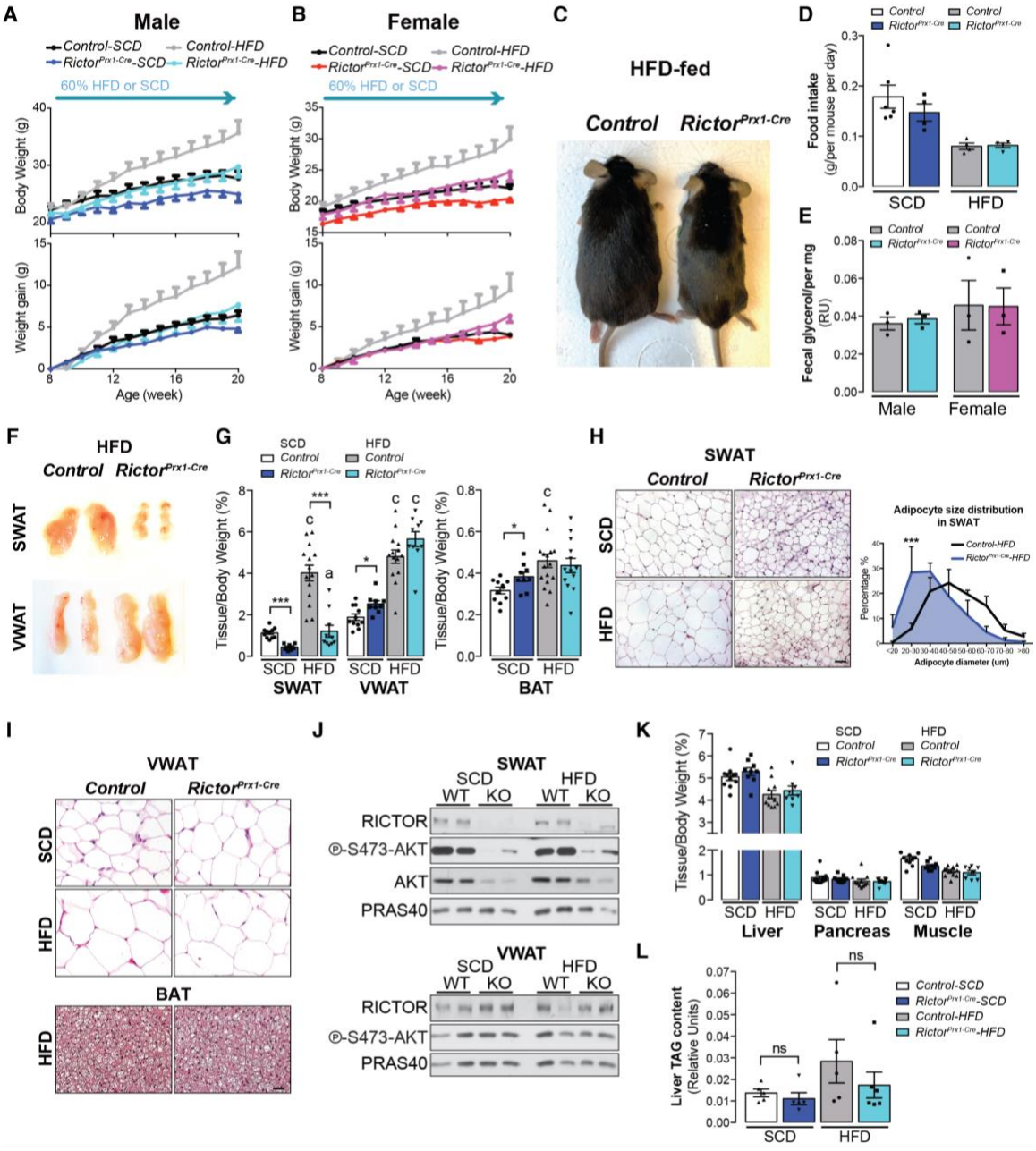

Figure II-8 Basic *Rictor* deletion in SWAT protects the mice from HFD-induced obesity and insulin resistance. A-B Growth curves of male **(A)** and female **(B)** control and *Rictor*$^{Prx1\text{-}Cre}$ mice fed with standard chow diet (SCD) or high fat diet (HFD) (N = 5-14; data represent mean ± SEM). *lower panel*: weight gain in average compared to the weight at 8 weeks of age. **C** A representative picture of control and *Rictor*$^{Prx1\text{-}Cre}$ mice fed with HFD. **D** Food intake of SCD or HFD-fed mice. Data represent mean ± SEM. **E** Fecal glycerol content of indicated mouse group. Data represent mean ± SEM. **F** Representative images of the indicated fat depots from HFD-fed mice. **G** Tissue weight relative to body weight of subcutaneous white adipose tissue (SWAT), visceral white adipose tissue (VWAT) and brown adipose tissue (BAT). Data represent mean ± SEM. $*p < 0.05$, $***p < 0.001$). c: $p<0.001$ when compared to its SCD-fed counterpart.

Figure II-8 (Cont.) H H&E stains of SWAT (scale bar = 100 μm). *right panel*: size distribution of adipocytes in SWAT. **I** H&E stains of VWAT and BAT (scale bar = 100 μm). **J** Representative western blot of lysates from SWAT and VWAT of SCD- or HFD-fed control (WT) and *Rictor*$^{prx1\text{-}Cre}$ (KO) mice. N = 2. **K** Tissue weight relative to body weight of liver, pancreas and muscle. Data represent mean ± SEM. L Liver TAG content. Data represent mean ± SEM. ns: not significant.

HFD-fed *Rictor*$^{Prx1\text{-}Cre}$ mice have better systemic glucose tolerance

Next, we explored how deleting *Rictor* in SWAT affects systemic health. 12-week HFD exposure induced systemic insulin resistance in control male mice. *Rictor*$_{Prx1\text{-}Cre}$ male mice developed mild insulin resistance on SCD, and HFD feeding did not exacerbate the insulin intolerance [Figure II-9A]. These mice were also protected from diet-induced glucose intolerance [Figure II-9B]. In female mice, the *Rictor* deletion effects on insulin sensitivity and glucose tolerance were not as significant as those seen in the male mice [Figure II-9C and 9D]. Unlike the male mice, 20-week-old female *Rictor*$_{Prx1\text{-}Cre}$ mice were not relatively insulin resistant compared to control mice, which is similar to 8-week-old female mice on SCD [Figure II-S6B]. HFD induced significant insulin resistance in both control and *Rictor*$_{Prx1\text{-}Cre}$ female mice [Figure II-9C]. Moreover, female *Rictor*$_{Prx1\text{-}Cre}$ mice were slightly protected from diet-induce glucose intolerance [Figure II-9D]. These results suggested that the sex differences proceeded through aging and diet challenges. We further explored how *Rictor* loss in SWAT mechanistically caused these phenotypes in male mice. Interestingly, *Rictor* deletion in SWAT promoted diet-induced *Ucp1* mRNA and protein expression [Figure II-9E and 9F]. It is consistent with the finding in brown adipose tissue in which *Rictor* deletion increases diet-induced UCP1 expression and thermogenesis (Hung et al. 2014a;

Jung et al. 2019). We also determined the inflammatory status of these depots since adipose tissue inflammation also contributes to insulin resistance in obese mice (Guilherme et al. 2008; Verboven et al. 2018). HFD feeding increased F4/80 mRNA level, a marker of adipose tissue macrophage, in both SWAT and VWAT from control and *Rictor*$^{Prx1\text{-}Cre}$ mice, with no significant differences between genotypes [Figure II-9G]. It suggested that the protective effect on HFD seen in *Rictor*$^{Prx1\text{-}Cre}$ mice might not be attributed to decreased tissue inflammation. More detailed works need to be done to address this correlation.

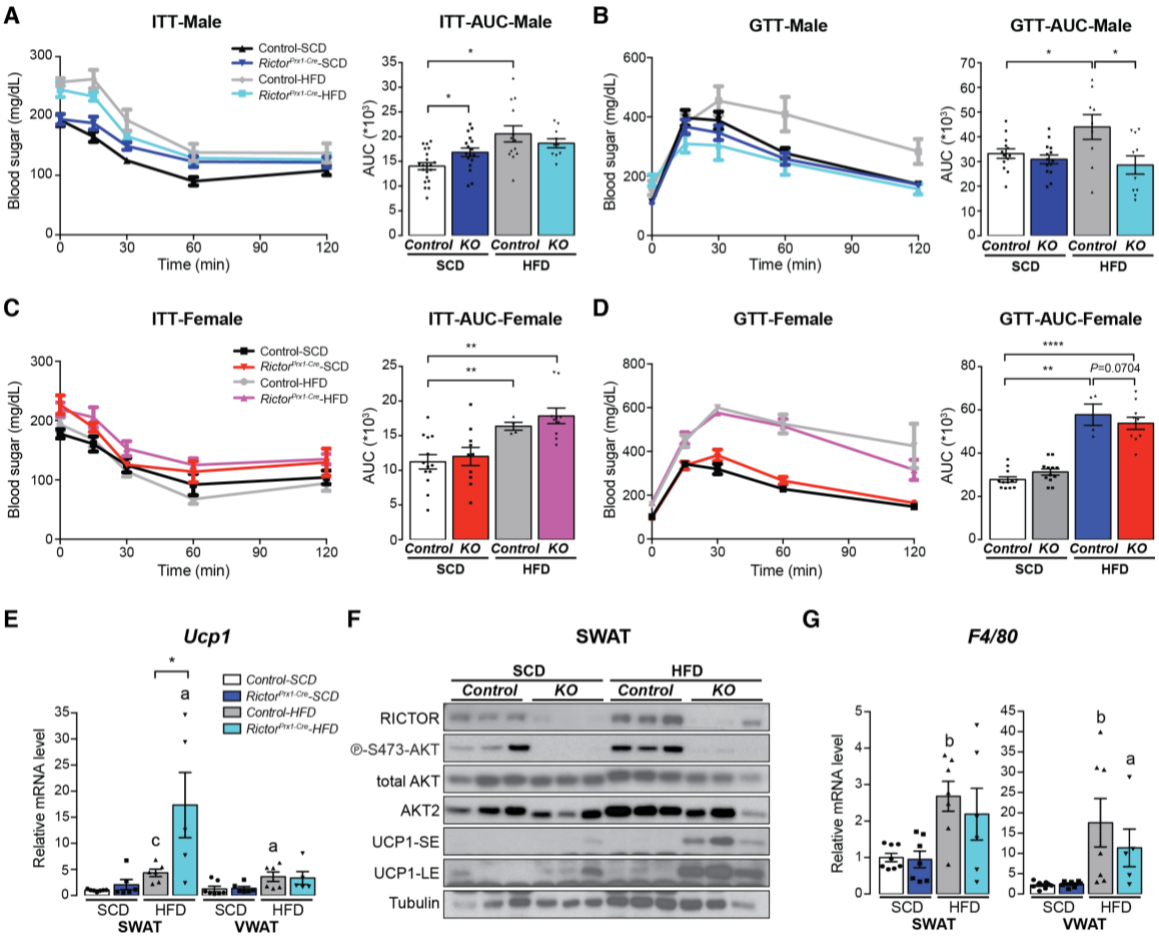

Figure II-9 *Rictor*$^{prx1\text{-}Cre}$ male mice are protected from diet-induced glucose intolerance. A-D insulin tolerance test (ITT) in male **(A)** and female **(C)** mice and glucose tolerance test (GTT) in male **(B)** and female **(D)** mice. *right panel*: area-under-curve of indicated curve (data represent mean ± SEM; *p < 0.05, **p < 0.01, ***p < 0.001, ****p < 0.0001). **E** Relative mRNA expression of *Ucp1* in SWAT and VWAT of standard chow diet (SCD) or HFD (high fat diet)-fed control and *Rictor*$^{prx1\text{-}Cre}$ mice. Data represent mean ± SEM; *p < 0.05; a: p < 0.05 when compared to its SCD counterpart, c: p < 0.001. **F** Western blot of lysates from SWAT of control and *Rictor*$^{prx1\text{-}Cre}$ (KO) mice fed with SCD or HFD. N = 3. SE: a film with shorter exposure, LE: a film with longer exposure. **G** Relative mRNA expression of *F4/80* in SWAT and VWAT of standard chow diet (SCD) or HFD (high fat diet)-fed control and *Rictor*$^{prx1\text{-}Cre}$ mice. Data represent mean ± SEM. a: p < 0.05 when compared to its SCD counterpart, b: p < 0.01.

Deleting *Akt1* in subcutaneous adipocyte precursors causes mild lipogenic defect selectively in female mice.

Previous *in vitro* studies showed that AKT1 is required for adipogenesis in white (Yun et al. 2008) and phosphomimetic AKT1-S473D mutant, not AKT2-S474D, rescued *Rictor-KO* lipogenic defect [Figure II-5A] (Calejman et al. 2020; Hung et al. 2014b). However, how AKT1 regulates white adipose tissue development is unclear. Therefore, I generated *Prx1-Cre;Akt1*$^{fl/fl}$ mice (*Akt1*$^{Prx1\text{-}Cre}$) to examine this in both male and female mice. *Akt1*$^{Prx1\text{-}Cre}$ mice weighed similarly when compared to control mice [Figure II-10A]. Interestingly, AKT1 was required for SWAT growth *in vivo*, but only in female mice as SWAT mass and individual SWAT adipocyte size were smaller selectively in *Akt1*$^{Prx1\text{-}Cre}$ female mice but not in males [Figures II-10B and 10C]. I confirmed *Akt1* deletion in SWAT from *Akt1*$^{Prx1\text{-}Cre}$ by mRNA expression [Figures II-10D], without compensatory overexpression of other *Akt* isoforms [Figures II-10E]. I also confirmed AKT1 protein ablation specifically in mature adipocytes by analyzing the floating fraction of the tissue, in which mature adipocytes were enriched

[Figures II-10F]. This female-specific SWAT growth defect may be more related to a *de novo* lipogenesis defect because *Chrebpb*, *Acly*, and *Acaca* mRNA, and ACLY, ACC, and FASN protein levels were decreased in *Akt1*$^{Prx1\text{-}Cre}$ female SWAT [Figures II-10G and 10H], but PPARγ levels and the expression of *Cd36*, *Lpl, Glut4, Scd1* and *Fabp4* were normal [Figures II-10I]. No significant change in DNL or PPARγ target gene expression was detected in *Akt1*$^{Prx1\text{-}Cre}$ male SWAT [Figures II-10J and 10K]. Thus, the phenotypes seen in *Akt1*$^{Prx1\text{-}Cre}$ female mice suggested that AKT1 was required for maximal induction of *de novo* lipogenesis *in vivo*.

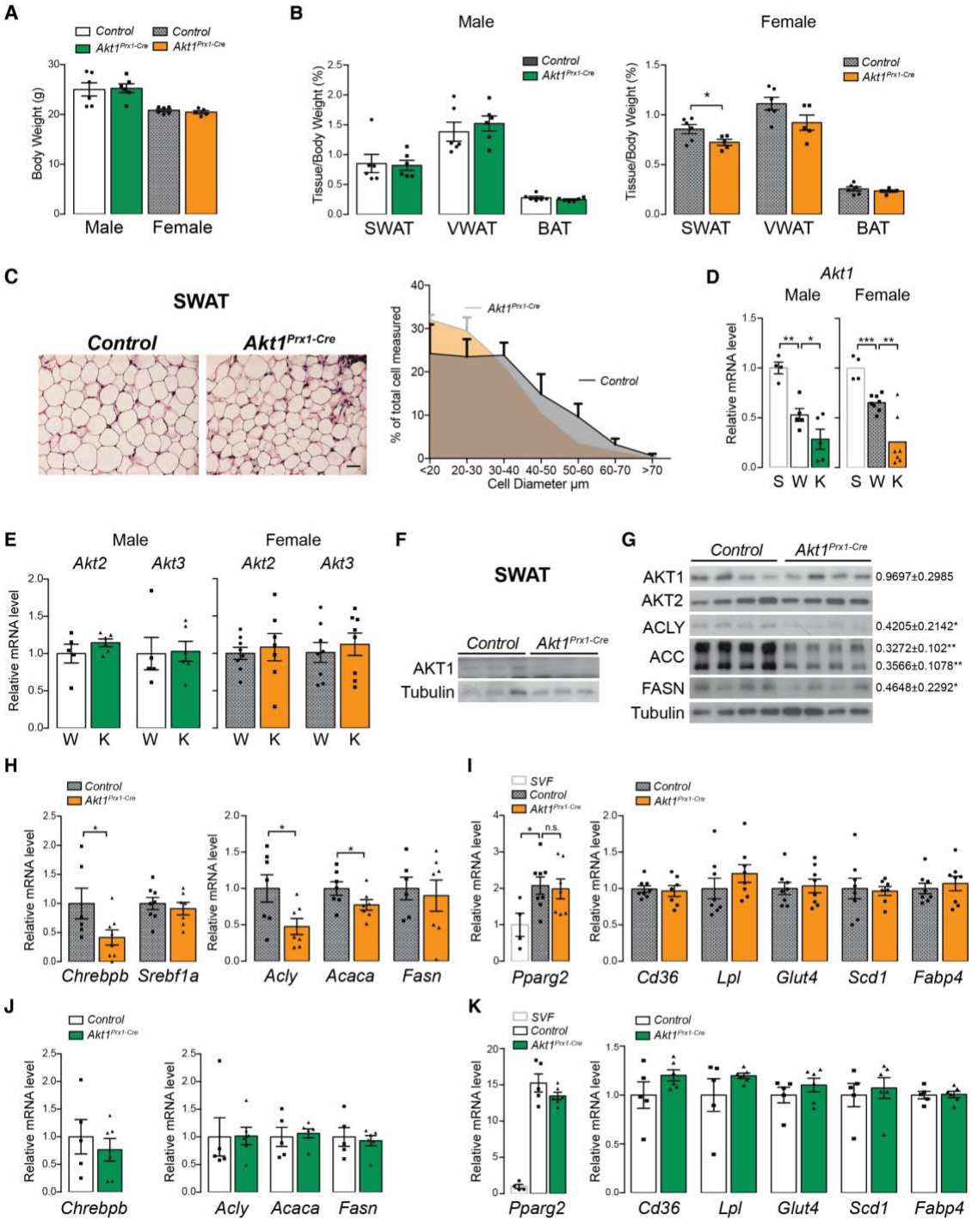
A
Control
Akt1Prx1-Cre
Body Weight (g)
Male
Female
B
Male
Female
Tissue/Body Weight (%)
SWAT
VWAT
BAT
C
SWAT
Control
Akt1Prx1-Cre
% of total cell measured
Cell Diameter μm
D
Akt1
Relative mRNA level
S W K
E
Akt2
Akt3
F
AKT1
Tubulin
G
AKT1
AKT2
ACLY
ACC
FASN
0.9697±0.2985
0.4205±0.2142*
0.3272±0.102**
0.3566±0.1078**
0.4648±0.2292*
H
Chrebpb
Srebf1a
Acly
Acaca
Fasn
I
SVF
n.s.
Pparg2
Cd36
Lpl
Glut4
Scd1
Fabp4
J
K

Figure II-10 *Akt1*$^{Prx1\text{-}Cre}$ female mice have mild lipogenic defect. A Body weight of 8-week-old control and *Akt1*$^{Prx1\text{-}Cre}$ mice. Data represent mean ± SEM. **B** Adipose tissue weight relative to body weight from male (left panel) and female (right panel) 8-week-old control and *Akt1*$^{Prx1\text{-}Cre}$ mice**.** Data represent mean ± SEM; *p < 0.05. **C** Representative H&E stains of SWAT from 8-week-old control and *Akt1*$^{Prx1\text{-}Cre}$ female mice (scale bar = 100 μm). *right panel*: cell size distribution in indicated SWAT calculated from the H&E stains. **D-E** Relative mRNA expression by RT-PCR of *Akt* isoforms of isolated SVFs (S) and floating fractions from SWAT of control (W) and *Akt1*$^{Prx1\text{-}Cre}$ (K) mice. Data represent mean ± SEM. *p < 0.05; **p < 0.01; ***p < 0.001. **H** Adipocyte size distribution in indicated depot (N = 4; more than 100 adipocytes were calculated from each mouse; data represent mean ± SEM). **F** Western blot of lysates from floating fractions of SWAT from control and *Akt1*$^{Prx1\text{-}Cre}$ mice. N = 3. **G** Western blot of lysates from SWATs of control and *Akt1*$^{Prx1\text{-}Cre}$ mice. N = 4. Data represent mean ± SEM. *p < 0.05. **H-K** Relative mRNA expression by RT-PCR of indicated genes from SWAT of control and *Akt1*$^{Prx1\text{-}Cre}$ male (**H** and **I**) and female (**J** and **K**) mice. Data represent mean ± SEM. *p < 0.05; **p < 0.01; ***p < 0.001.

2.3 Discussion

In this study, I investigated the role of mTORC2 in SWAT development. My findings supported a model in which differentiating subcutaneous white adipocytes required *Rictor*/mTORC2 to establish maximum lipid handling capacity during development. This was mediated in part by positively regulating PPARγ-activity towards specific genes that encode regulators of lipid storage, which may occur independently or downstream of ChREBP, and likely acted through AKT signaling. Moreover, mTORC2 was required for maximum PPARγ target gene expression in mature subcutaneous white adipocytes particularly during dietary challenges that promoted rapid lipid storage and adipose tissue growth, such as consuming a high fat diet. Thiazolidinedions (TZDs), which are drugs used to treat Type 2 diabetes, work by binding and stimulating PPARγ, but they have negative side effects including potential heart failure (Cariou, Charbonnel, and Staels 2012). Thus, our study may help identify alternative

mechanisms to stimulate PPARγ activity and/or safe lipid storage in subcutaneous fat, which is more metabolically favorable than storing lipid in visceral fat or non-adipose tissue.

In contrast to my current findings in white adipose tissue, *Rictor* is required for PPARγ mRNA induction in a brown preadipocyte differentiation model, and therefore, *Rictor*-deficient brown preadipocytes are completely incapable of differentiating and synthesizing lipid droplets when subjected to standard *in vitro* differentiation assays. In brown preadipocytes, this is linked to a deficiency in ATP citrate lyase (ACLY) phosphorylation (S455) and acetyl-coA production. This phenotype is partially rescued by overexpressing recombinant ACLY, and completely rescued by overexpressing the phosphor-mimetic construct ACLY-S455D (Calejman et al. 2020). A recent study using a non-adipocyte model (primary bovine mammary epithelial cells) also reports blocked PPARγ2 expression when *Rictor* is knocked down by shRNA (Guo et al. 2019). Consistent with the brown and white preadipocyte differentiation models showing different requirements for mTORC2 (i.e. *Rictor* is not required for PPARγ2 mRNA induction here), overexpressing ACLY-S455D did not rescue gene expression and lipid accumulation defects in the *Rictor*-deficient subcutaneous white preadipocytes in this study. One explanation for why these brown and white adipocyte differentiation models differ is that they are different cell types derived from the natural precursor cell population in their respective depots (i.e.

interscapular BAT and inguinal WAT). Alternatively, the brown preadipocytes are immortalized using the SV40-Large T antigen protocol (Fasshauer et al. 2000), which could change the metabolic requirements for PPARγ induction. Determining how mTORC2 signaling regulates metabolism and gene expression across different cell types is an important ongoing area of research.

How might mTORC2 regulate PPARγ activity? One possibility is that a PPARγ post-translational modification(s), such as phosphorylation, acetylation, SUMOylation, or O-GlcNAcylation, could be sensitive to mTORC2 signaling (Brunmeir and Xu 2018). For example, phosphorylation of PPARγ increases or decreases its activity depending on the sites and the upstream regulators (Choi et al., 2014, 2010; Compe et al., 2005; Helenius et al., 2009; Hu et al., 1996; Iankova et al., 2006). Acetylation of PPARγ, on the other hand, has been shown to positively regulate lipid synthesis (Tian et al. 2014). Another possibility is that mTORC2 regulates the ability of PPARγ to bind certain co-factors (Miard and Fajas 2005), which could include histone acetyltransferases (HATs) or deacetylases (HDACs) (Miard and Fajas 2005). mTORC2 could also regulate PPARγ's ability to bind certain targets by affecting the chromatin landscape or chromatin remodeling factors, evidenced by decreased H3K9ac in *Rictor* KO PPREs shown here. The detailed mechanisms of how mTORC2 regulates PPARγ activity requires more investigation.

Another interesting finding in our study was that male and female mice respond differently to *Prx1-Cre* mediated *Rictor* deletion with respect to fat re-distribution and insulin sensitivity. For example, only male *Rictor*$^{Prx1\text{-}Cre}$ mice developed insulin resistance. Interestingly, while *Rictor*$^{Adipoq\text{-}Cre}$ mice did not exhibit lipodystrophy, they are also insulin resistant, and this is more pronounced in male mice (Tang et al. 2016; Yu et al. 2019). Thus, adipose mTORC2 may play a greater role in controlling systemic insulin sensitivity in males than in females, and the SWAT may be particularly important to this phenomenon. The mechanism controlling this is currently unknown. However, these observations add to the growing appreciation for sex differences in adipose tissue metabolic regulation. For example, female *Adiponectin-Cre;Acly*^{floxed} mice were recently reported to have a more severe metabolic phenotype than their male KO counterparts (Fernandez et al. 2019). Understanding sex differences in adipose tissue metabolism is an exciting ongoing research area.

One limitation of our study is that *Prx1-Cre* to targets other cell lineages in addition to SWAT including some bone lineages and marrow adipocytes. Importantly for this study however, *Prx1-Cre* does not target precursors of brown fat or visceral white fat (Sanchez-Gurmaches, Hsiao, and Guertin 2015; Krueger et al. 2014). To the best of our knowledge, there are no other Cre-drivers that selectively target SWAT precursor cells in this manner. Our use of three different *in vitro* differentiation models that exhibit overlapping phenotypes with each other and the *in vivo* model, including primary SVF preadipocytes from the *Rictor*^{Prx1cKO}

mice, greatly strengthens the ability to distinguish the mTORC2 functions that are specific to SWAT. Nevertheless, effects caused by *Rictor* loss in non-adipose tissue cells cannot be ruled out in the *in vivo* model. Unfortunately, there is also no reciprocal Cre driver that is as efficient at targeting only the VWAT precursors. Therefore, I cannot make conclusions about how mTORC2 might function in VWAT development.

Overall, our study reveals previously unknown mTORC2 functions in regulating SWAT growth, adipose tissue gene expression, and sex dependent metabolic homeostasis. These conclusions may have important implications for understanding and treating Type 2 diabetes and other obesity related metabolic diseases.

(The discussion for Figure II-8 – II-10 is in Chapter IV)

2.4 Acknowledgments

I thank members of the Guertin lab for valuable discussions. I thank Tony Imbalzano for reading the manuscript, and Norm and Hyun Cheol for technical assistance. D.A.G. is supported by grants from the NIH (R01DK094004 and R01CA196986) and a Leukemia and Lymphoma Society Career Development Award. S.M.J. is supported by a postdoctoral fellowship from the American Diabetes Association (1-18-PDF-128). J.S.-G. was supported by a postdoctoral

fellowship from the American Heart Association (15POST25550079). C.M.C. was supported by a postdoctoral fellowship from the American Diabetes Association (1-16-PMF-008).

2.5 Materials and Methods

Cell Culture

I utilized the white preadipocytes residing in stromal vascular fraction (SVF) of *Ubc-Cre$_{ERT2}$;Rictor$_{floxed}$* mice for *in vitro* studies. The SVFs are isolated by digesting the inguinal WAT in digestion buffer (123 mM NaCl, 5 mM KCl, 1.3 mM CaCl2, 5 mM glucose, 100 mM HEPES, 1% antibiotics and 4% BSA at pH 7.4 containing 1.5 mg/mL of collagenase A). The isolated cells were cultured directly as primary cells or immortalized by 3T3 immortalization protocol as previously described to generate cell lines (Tang et al. 2016). Cells were maintained in 25mM glucose (high-glucose), pyruvate and glutamine-containing DMEM in incubators at 37°C and 5% CO_2. For adipocyte differentiation (Zebisch et al. 2012), cells were seeded at medium density and allowed to proliferate to confluence in the presence of high-glucose DMEM containing 10% FBS and 1% antibiotics (called complete medium). Two days after the cells reached confluency, cells were induced to differentiate by adding induction media (high-glucose DMEM containing 10% FBS, 1% antibiotics, 100 nM insulin, 2 µg/mL dexamethasone, 0.5mM 3-isobutyl-1-methylxanthine (IBMX) and 1 nM Rosiglitazone) for 2 days and the medium was replaced with complete medium containing 100 nM insulin for another two days and the cells were maintained in complete medium since then until day 8. Deletion of *Rictor* in preadipocytes was achieved by treating the cells with one dose of 4-hydroxytamoxifen (4-OHT, 1µM) for two constitutive days before induction for early deletion as previous described

(Hung et al. 2014b; Tang et al. 2016). The cells were exposed to 4-OHT for only 2 days before differentiation and remained 4-OHT-free thereafter, which also minimizes the effects of 4-OHT on the cells. For *Rictor deletion* in differentiating adipocytes (*Ad-Rictor-iKO*), 4-OHT was supplemented in culture medium for two constitutive days from D2 to D4 after the differentiation was induced. Control cells received equivalent volume of ethanol (EtOH) as vehicle-treated controls. SVF isolated from *Ubc-Cre$_{ERT2}$* mice was treated either by EtOH or 4-OHT to address the effect of Cre. At different time points during differentiation, cells were collected for protein, mRNA or Oil-Red-O staining analysis. To analyze the signaling, cells were serum starved in high-glucose DMEM for 3 hours and stimulated with 100 nM insulin for 15 minutes.

Immunofluorescence and LipidTOX staining

Cells seeded on coverslips were fixed with iced-cold methanol at -20C for 15 min. Fixed cells were then blocked with PBS containing 3% BSA and 0.3% Triton for 30 min at room temperature, and incubated with primary anti-perilipin 1 (CST, 1:200 diluted in 1% BSA and 0.1% Triton) at 4°C overnight. After washed with PBS three times, the coverslips were stained with secondary antibodies (AlexaFluor-488-conjugated goat anti-rabbit IgG, Invitrogen, 1:400) mixed with HCS LipidTOX deep red neutral lipid stain (Invitrogen, H34477) at room temperature for an hour followed by DAPI staining and mounted on glass slides with Prolong Gold. Cells were examined with a laser-scanning microscope (Zeiss

Axio imager). At least 6 images were obtained for each condition and the images were analyzed by ImageJ.

Oil Red O staining

The differentiated cells were washed three times with PBS and fixed with 10% buffered formalin at 4 °C overnight. Cells were incubated in propylene glycol and then stained with a filtered Oil Red O solution (0.5% Oil Red O in propylene glycol) for 10 min at 37 °C, washed with 85% propylene glycol and three times with distilled water, and visualized under a microscope (Zeiss). Oil Red O contents were then quantified by direct extraction of Oil Red O from stained cells using isopropanol and absorbance at 510 nM using a microplate reader (Tecan Safire2).

Western blot analysis and immunoprecipitation assays

Cells were harvested in cold PBS and lysed in protein lysis buffer (1% Triton X-100, 50 mM HEPES at pH 7.4, 150 mM NaCl, 5% glycerol, 2 mM EDTA, protease/phosphatase inhibitor cocktails). For immunoblot analysis of surgically dissected fat tissue depots, tissues were homogenized and lysed in RIPA buffer (150 mM NaCl, 50 mM HEPES at pH 7.4, 0.1% SDS, 1% Triton X-100, 2 mM EDTA, 0.5% Na-deoxycholate) containing protease and phosphatase inhibitor cocktails. For floating fractions from depots, WATs were digested in digestion buffer (123 mM NaCl, 5 mM KCl, 1.3 mM CaCl2, 5 mM glucose, 100 mM

HEPES, 1% antibiotics and 4% BSA at pH 7.4 containing 1.5 mg/mL of collagenase A). and were centrifuged at 500g for 10 minutes in cold. The upper layers were obtained as floating fractions. Protein lysates were mixed with 5X SDS sample buffer and boiled, separated by SDS-PAGE, transferred to polyvinylidene difluoride (PVDF) membrane filters and subjected to immunoblot analysis. Antibodies used in this study are listed in Appendix I.

Gene expression analysis

Total RNA was isolated from cells or tissues using QIAzol (QIAGEN, #79306) and an RNeasy kit (QIAGEN). Equal amounts of RNA were retro-transcribed to cDNA using a High capacity cDNA reverse transcription kit (#4368813, Applied Biosystems). Quantitative RT-PCR (qRT-PCR) was performed in 10 µL reactions using a StepOnePlus real-time PCR machine from Applied Biosystems using SYBR Green PCR master mix (#4309156, Applied Biosystems, or 2XUlrtraSYBR from CWBio) according to manufacturer instructions. TATA-box binding protein (Tbp) gene expression was used as a normalization gene in all conventional RT-PCR experiments. Data analysis was performed on web-based software provided by the manufacturer. Primer sequences are shown in Appendix II.

RNA-sequencing (RNA-seq)

RNAs were extracted from primary culture cells as described. Extracted RNA (3ug) was processed for mRNA isolation using NEBNext Poly(A) mRNA

Magnetic Isolation Module (NEB, #E7490). Isolated mRNA was used to generate a cDNA library using NEBNext Ultra II Directional RNA Library Prep Kit for Illumina according to the manufacturer's instructions. For the multiplex purpose, the libraries were barcoded using commercially available primers for Illumina system (NEB). The quantity and quality were checked using Qubit and a fragment analyzer (a service provided by Molecular Biology Core Lab, MCBL at UMMS), respectively. The sequence was done by paired end read 100 bases using HiSeq 4000.

Bioinformatics analysis

With star_2.5.3a (Dobin et al. 2013), paired-end reads were aligned to mouse genome mm10 (GRCm38.p6), which is annotated with Ensembl annotation GRCm38.94 (Zerbino et al. 2018). Aligned exon fragments with mapping quality higher than 20 were counted toward gene expression with featureCounts_1.5.2 (Liao, Smyth, and Shi 2014). Differential expression (DE) analysis was performed with DESeq2_1.20.0 (Love, Huber, and Anders 2014). Within DE analysis, mouse was taken as a known batch variable. Also, 'ashr' was used to create log2 Fold Change (LFC) shrinkage for each comparison (Stephens 2017). Significant DE genes (DEGs) were filtered with the criteria FDR < 0.05 and absolute log2 fold change (|LFC|) > 0.485 (fold change > 1.4). Gene set enrichment analysis was performed using DAVID Bioinformatics Resources online (D. W. Huang,

Sherman, and Lempicki 2009a; 2009b) and ChIP-atlas for transcription factor interaction (Oki and Ohta 2016).

Chromatin immunoprecipitation (ChIP) analysis

Nuclei were isolated using nuclei preparation buffer supplemented with protease inhibitor and deacetylase inhibitor (Trichostatin A, TSA), and nuclei were pelleted by centrifugation. Cells were cross-linked with 1% paraformaldehyde for 10 minutes at room temperature and quenched for 10 minutes by adding 0.125 M glycine. After three washes with cold PBS, cells were lysed with lysis buffer (1% SDS, 20 mM EDTA pH8, 50 mM Tris-HCl pH8) supplemented with protease inhibitor and deacetylase inhibitor and placed on ice for 10 minutes. Fractionation of chromatin was done by Bioruptor (setting: 2 cycles, 15 minutes each with high intensity 30-30 seconds on-off interval). ChIP was done using the indicated primary antibodies and incubated overnight. Pull down of antibody-bound fragments was done by adding agarose protein G beads (Prometheus), followed by serial washes two times each with RIPA low salt buffer (0.1% SDS, 1% Triton x-100, 1 mM EDTA, 2 0mM Tris-HCl pH 8, 140 mM NaCl and 0.1% Na Deoxycholate), RIPA high salt buffer (0.1% SDS, 1% Triton x-100, 1 mM EDTA, 2 0mM Tris-HCl pH 8, 500 mM NaCl and 0.1% Na Deoxycholate), LiCl buffer (250 mM LiCl, 0.5% NP40, 0.5% Na Deoxycholate, 1 mM EDTA, 10 mM Tris-HCl pH8) and TE buffer (10mM Tris-HCl pH8 and 1 mM EDTA). DNA fragments were eluted by 100 mM NaHCO3 and 1% SDS, uncrosslinked, and treated with

protease K and RNase. Fragments were eluted by phenol-chloroform extraction. Eluted fragments were analyzed by RT-PCR using the primers listed in Appendix II.

Luciferase Reporter Gene assay

The luciferase reporter containing PPRE (PPRE X3-TK-luc) was a gift from Bruce Spiegelman(Kim et al., 1998). The PPRE-firefly luc-containing plasmid is transiently co-transfected with RL-TK (containing Renilla-Luc as reference for transfection efficiency) into preadipocytes. *Rictor* was deleted 24 hours after the transfection and differentiation was done as previously described. At day 2 of differentiation, cells were lysed and enzymic reactions were done using Dual Luciferase Reporter Assay (DLR from Promega). The relative firefly luciferase/Renilla luciferase signals were determined by a microplate reader (Tecan Safire2).

Construction of overexpression by retroviral infection

To generate retroviruses, HEK293T cells were transfected with pMSCV-retroviral vectors subcloned with PPARg2, ChREBPa, ChREBPb, SREBP1n, ACLY with mutants, and AKT with mutants in combination with the retroviral packaging DNA (pCL-Ampho). Culture media was changed 12 hours after transfection and the virus-containing supernatant was collected 48 hours after transfection and passed through a 0.45 μm (PVDF) filter. Preadipocytes were transduced in

medium containing 8 µg/mL of polybrene by centrifugation at 1700 RPM for 30 min. After 24 hours, cells were subjected to antibiotic selection and future analysis. The plasmids used in this study are listed in Appendix I.

Glucose uptake measurement

Cells were preincubated for 3 h in KRH medium without glucose (120 mM NaCl, 5 mM KCl, 1.3 mM $CaCl_2$, 1.3 mM $MgSO_4$, 1.3 mM KH_2PO_4 and Hepes 25mM with pH 7.4 plus 0.5% BSA + 2 mM pyruvate). For insulin stimulated group, cells were treated with 100 µM insulin for 15 minutes at the end of incubation. Deoxy-D-glucose 2-[1,2-^{3}H(N)] mixed with unlabeled 2-DOG was then added, and incubation was continued for an additional 10 min. The medium was then removed and cells were washed three times with KRH medium without glucose and BSA to terminate the assay. Cells were then lysed in 1% triton, mixed with scintillation buffer, and the uptake of 3H glucose was quantified in counts per minute (cpm) using a scintillation counter. The cpm values were normalized to the protein concentration of each sample. For *in vivo* glucose uptake measurement, mice were fasted for 6 hours and were received an intraperitoneal injection of 10 mCi of Deoxy-D-glucose 2-[1,2-^{3}H(N)] in a total volume of 150 mL. Two hours following the injection, mice were euthanized and tissue samples were collected, weighed and homogenized. Specific fractional uptakes of ^{3}H-deoxyglucose were determined by scintillation counter.

De novo lipogenesis assay

Cells were incubated with 25 mM DMEM in which 0.01% of the total glucose concentration of the medium was comprised of D-[U-^{14}C]-glucose for three days. Chloroform extraction was performed, and labeled lipids were measured using a scintillation counter. Each sample was normalized to total protein concentration.

BODIPY FL C16 uptake

BODIPY FL C16, a fluorescence analogue of palmitic acid, were utilized for measuring lipid uptake as previously described (Dubikovskaya et al. 2014). Primary preadipocytes were cultured and induced into differentiation as previously described. At the end of differentiation, cultured medium was replaced by HBSS with 0.1% fatty acid free BSA containing 2 μM BODIPY FL C16 and the cells were incubated for 10 minutes or 30 minutes. The reaction was stopped by washing with cold PBS with 0.2% BSA. Cells were then trypsinized and diluted with FACS buffer (HBSS with 10% FBS, 10 mM EDTA, 50 μg/mL propidium *iodide) and proceeded to FACS analysis (LSRII A-5 Laser).*

Glycolytic stress test

Glycolytic ability was measured using a Seahorse XFe96 analyzer (Agilent Technologies). Mouse primary preadipocytes were seeded in a XFe96 cell culture microplate (Agilent Technologies) and differentiation was induced as previously described. At differentiation day 8, cells were washed and incubated

with assay medium for 1 h at 37°C in a CO_2-free incubator. Plates were then transferred to a Seahorse Bioscience XFe96 analyzer. Extracellular acidification rate (ECAR) were measured at baseline, followed by adding 10 mM glucose, oligomycin (1.5 μM), and 50 mM 2-deoxyglucose. indicates glycolytic capacity. The ECAR was normalized to cell number determined by Cytation™ 5.

Measurement of lipolysis in adipose tissue

For measurement of lipolysis, cultured adipocytes or adipose tissues from mice were harvested and incubated in DMEM with or without isoproterenol at 10 μM for 4 or 6 hours and the medium were collected to measure glycerol concentration using commercial kit (Free glycerol reagent, Sigma). The glycerol level was normalized with protein concentration of the tissue mass.

Histone extraction

Cells were washed 2 times with PBS and lysed with Triton extraction buffer (PBS containing 0.5% Triton X 100, protease inhibitor and 1 μM TSA) for 10 minutes at 4°C with gentle swirling. Lysates were pelleted and the pellets were resuspended in 0.2N HCl and incubated at 4°C overnight. Centrifugation was done in the next day and supernatants were collected for western blots.

Mice and Mice Housing

Rictor-floxed mice were described previously (Shiota et al. 2006) and were crossed with mice expressing either *Prx1-Cre* (JAK #005584), *Adiponectin-Cre*

(JAK #028020) or *Ubc-Cre*$_{ERT2}$ (JAX #007001) mice to generate conditional or inducible KO models. *Akt1*-floxed mice were kindly provided by Dr. Morris Birnbaum in University of Pennsylvania. Floxed Cre-negative mice were used as controls. All the mice were in C57BL/6 background. The mice used for all studies were between 8–20 weeks old. Mice were housed in the Animal Medicine facilities of the UMMS in a clean room set at 22°C and 45% humidity under daily 12h light/dark cycles in ventilated racks with cages changed every two weeks, and fed a normal chow diet (Prolab® Isopro® RMH 3000) from Lab Diet *ad libitum. For HFD challenge, diet was switched from normal chow to 60% HFD* (D12492 Harlan Laboratories) when the mice were 8 weeks old. The mice were monitored for 12 weeks and the body weight was recorded weekly. All animal experiments were approved by Institutional Animal Care and Use Committee of University (IACUC) of Massachusetts Medical school (UMMS). No animals were excluded from any experiments, unless they displayed obvious wounds from fighting as determined by our veterinarians.

Tissue harvest and histology

Adipose tissue depots and other organs/tissues were carefully dissected to avoid contamination from surrounding tissues. Organs/tissues were weighed by a microscale (XS105, Mettler Toledo). Samples for RNA or protein were frozen down immediately in liquid nitrogen and stored at 80 °C for further analysis. For signaling, mice were fasted for 6 hours in the morning without changing other

husbandry conditions. The same amount of normal chow diet was provided for an hour after fasting period and the indicated tissues were harvested and stored as described above. For histology, tissue pieces were fixed by 10% formalin. Embedding, sectioning and Hematoxylin & Eosin (H&E) staining were done by the UMass Medical School Morphology Core. Liver samples were embedded in O.C.T. compound (Tissue-Tek) before sectioning and Oil Red O staining. Images were taken by Zeiss Axio microscope. For cell size measurements, tissue slices were scanned by Zeiss Axio Scan.Z1 (N = 4 for wild-type and 4 for conditional KOs) and the adipocyte size was automatically measured by ImageJ with plug-in (Adipose). More than 1000 cells were analyzed for each depot. For estimating adipocyte number in a depot, average adipocyte volume was calculated from more than 800 cells which were imaged as described above. The adiposity was then determined by depot weight-to-average adipocyte volume ratio.

Glucose Tolerance Test / Insulin Tolerance Test

Animals subjected for glucose tolerance test (GTT) were fasted overnight, followed by intraperitoneal glucose (2 g/kg of body weight) injection. For insulin tolerance test animals were fasted for 5 hours in the morning without changing other husbandry conditions, followed by intraperitoneal insulin (0.75 U/kg of body weight, Novolin) injection. Blood glucose levels were measured by tail bleeding with a commercially available glucose meter (GE) at indicated time points.

Liver TAG measurement

The protocol is modified from a previously described method (Jouihan 2012). For each sample, 100-300mg of liver was taken and lysed in ethanolic KOH (2 parts of ethanol and 1 part of 30% KOH) at 55 overnight. Digested lysates were diluted with 50% EtOH and centrifuge for 5 minutes. 200 uL of lysate were taken and mixed with 215 uL 1M MgCl2, then the mixture was left on ice for 10 minutes and followed by centrifugation for 5 minutes. Mixtures were mixed with Free Glycerol Reagent (Sigma) and incubated for 15 minutes at 37°C. The samples were measured by a microplate reader at 540 nm absorbance.

Serology

Blood was collected from animals by cardiocentesis. Serum was collected from the supernatant after centrifugation. The analysis of insulin, NEFA, leptin and adiponectin was performed by National Mouse Metabolic Phenotyping Center (MMPC) at UMMS.

Marrow fat quantification by osmium staining and CT

The protocol was modified from a previously described method (Scheller et al. 2014). Bones were fixed for 24–48 hours in 10% neutral-buffered formalin (VWR, Radnor, PA; cat. no. 16004-128), washed with water and decalcified in 14% EDTA, pH 7.4, for 14 days. After washing again with water, 600 µl Sorensen's phosphate buffer (pH 7.4) was added to one bone (tibia) in a 1.5-ml microtube.

Four per cent osmium tetroxide (200 µl) solution (Electron Microscopy Services, Hatfield, PA; cat.no. 19170) was added to each tube to make a 1% solution. Bones were stained in the fume hood 48 hours at room temperature. Osmium solution was carefully removed to a small liquid waste container that had been filled with corn oil to ~25% of the volume. Any used pipet tips were 'rinsed' of active osmium tetroxide by pipeting corn oil. All tips and tubes were discarded as osmium solid waste. Bones were washed, in the same tube, by incubating in 1 ml of Sorensen's buffer for 3 h at room temperature. This was repeated twice and the last wash was left in the hood overnight. Stained bones were then moved to a fresh set of 1.5 ml microtubes containing 1 ml Sorensen's buffer each. The used tubes were discarded as solid osmium waste. At this point, the bones and tubes were removed from the fume hood and used for CAT scan.

MicroCT

Specimens were embedded in 1% agarose and placed in a 19-mm diameter tube. The length of the bone was scanned using a µCT system (µCT100 Scanco Medical, Bassersdorf, Switzerland). Scan settings are as follows: voxel size 12 µm, medium resolution, 70 kVp, 114 µA, 0.5 mm AL filter and integration time 500 ms. Density measurements were calibrated to the manufacturer's hydroxyapatite phantom. Analysis was performed using the manufacturer's evaluation software and a threshold of 400 for MAT.

APC quantification

APCs were isolated as previously described (Rodeheffer, Birsoy, and Friedman 2008). In brief, stromal-vascular fraction (SVF) was prepared from SWAT by collagenase (1.5mg/mL) treatment and the pellets were resuspended in erythrocyte lyses buffer (0.15 M NH_4Cl and 0.01 M $KHCO_3$ in water). Cells were then pelleted and resuspended in staining media (Hanks' balanced salt solution (HBSS) with 2% fetal bovine serum) and labelled with the following primary antibodies: PE-Cy7-conjugated anti-CD31, PE-Cy7-conjugated anti-CD45, A700-conjugated anti-CD29, A647-conjugated anti-CD34 and LybA/E-conjugated anti-Sca1 Antibodies. After staining, cells were filtered through a 35-µm cell-strainer capped tube (#352235, BD Falcon) to ensure single-cell suspension and stained with live/dead Blue (L34962, Invitrogen). Live single cells were gated according to the expression of surface markers ($CD31^-CD45^-CD29^+CD34^+Sca1^+$) in a BD LSRII analyser. Data were analysed with FlowJo.

Quantification and Statistical Analysis

Data are presented as mean + SEM, unless stated otherwise. Student's t test, or non-parametric Mann-Whitney test, were used to determine statistical significance. Statistical analysis was done using GraphPad Prism. The number of mice used per experiment is stated in each figure legend.

Data and Code availability

Unprocessed data from this manuscript have been deposited to Gene Expression Omnibus (GEO; GSE146470).

CHAPTER III –The role of mTORC2 in acetyl-CoA metabolism during adipocyte development

This chapter contains materials published in Current Diabetes Reports from

Springer:

Hsiao, W.-Y., Guertin, D.A., 2019. *De Novo* Lipogenesis as a Source of Second Messengers in Adipocytes. Curr. Diab. Rep. 19, 138.
https://doi.org/10.1007/s11892-019-1264-9

3.1 Introduction

Adipose tissue stores excess energy in the form of triacylglyceride (TAG). TAG is composed of fatty acids and glycerol. Fatty acids can be obtained from uptake of extracellular fatty acids or be synthesized *de novo* through a process called *de novo* lipogenesis (Song, Xiaoli, and Yang 2018; Wong and Sul 2010). *De novo* lipogenesis (DNL) utilizes acetyl-CoA as a building block to generate fatty acids. Nutrients such as glucose, glutamine and acetate can be used to generate acetyl-CoA through this process. In cultured human white adipocytes, glucose is the major source for DNL which is determined by stable isotope labeling (~45%), whereas acetate contributes around 35% of carbons for lipogenesis (Collins et al. 2011). There is a minor role for glutamine in DNL in white adipocytes, which is different from brown adipocytes (Yoo, Stephanopoulos, and Kelleher 2004). In contrast, glucose provides most of the carbons for glycerogenesis (Collins et al. 2011). Thus, processes altering intracellular glucose and acetate flux into acetyl-CoA might affect lipogenesis and lipid metabolism in white adipocytes.

The amount of acetyl-CoA is a key dynamic indicator of nutrient availability (Shi and Tu 2015; J. V. Lee, Shah, and Wellen 2013). In addition to providing the initial two-carbon unit for DNL, nuclear-cytoplasmic acetyl-CoA is the precursor for acetylation of lysine residues on histones and non-histone proteins, such as transcription factors and metabolic enzymes (Pietrocola et al. 2015). The effect of

cellular acetyl-CoA level on histone acetylation profiles has been shown in budding yeast, in which decreased intracellular acetyl-CoA levels results in downregulation of global histone acetylation and transcription (Takahashi et al. 2006; Galdieri and Vancura 2012; Galdieri et al. 2013; 2014). In the context of mammalian cells, such as stem cells and cancer cells, altering acetyl-CoA level affects metabolism, proliferation, and differentiation by modulating histone acetylation (Wellen et al. 2009; Cai et al. 2011; J. V. Lee, Shah, and Wellen 2013; J. V. Lee et al. 2014; Campbell and Wellen 2018). These studies lead to a hypothesis that compartmentalization of acetyl-CoA is linked to nutrient availability. For example, in the fed state, the nuclear-cytoplasmic acetyl-CoA generated from glycolysis and the mitochondrial export of citrate can alter histone acetylation in addition to driving lipid synthesis (Takahashi et al. 2006; Wellen et al. 2009). On the other hand, in the fasted state mitochondrial acetyl-CoA is generated from the oxidation of pyruvate, lipids, and amino acids and is used for ATP synthesis (Shi and Tu 2015). Many studies support a link between histone acetylation and insulin sensitivity (Muka et al. 2016; Xiaoqing Wang et al. 2017), and there is also a link between acetyl-CoA level and adipocyte function (Oliva-Olivera et al. 2018). Thus, acetyl-CoA dynamics are likely critical for regulating adipocyte gene expression and maintaining metabolic flexibility.

Acetyl-CoA in the cytoplasm and nucleus is generated by the cleavage of mitochondrial-exported citrate by ATP-citrate lyase (ACLY) in a reaction that

additionally generates oxaloacetate. Another nuclear-cytoplasmic enzyme, called Acyl-CoA synthetase short chain family member 2 (ACSS2), can also generate acetyl-CoA from an acetate [Figure III-1]. The levels of these acetyl-CoA-generating enzymes correlate with body adiposity and insulin sensitivity. For example, a recent mouse study suggests that HFD may reduce acetyl-CoA level and the acetyl-CoA/CoA ratio in adipose tissue, and this correlates with reduced ACLY expression and histone acetylation (Carrer et al. 2017). In obese patients with abnormal glucose and lipid profiles, ACLY level is also decreased in adipocyte precursors isolated from these individuals (Oliva-Olivera et al. 2018). Notably, a recent study in brown adipocytes show that mTORC2/AKT regulates ACLY activity through phosphorylation on Serine 455 site, which links to intracellular acetyl-CoA level and histone acetylation during brown adipocyte development (Calejman et al. 2020). ACSS2, on the other hand, also plays a role in lipid synthesis under certain stress conditions. In cancer cells, ACSS2 can provide a significant portion of carbon for fatty acid and phospholipid synthesis during hypoxic and/or nutrient-deprived conditions (X. Li et al. 2017; Schug et al. 2015). This is likely because ACSS2 selectively regulates genes involved in lipid metabolism (Vysochan et al. 2017; Z. Huang et al. 2018a, 2). The physiological role of ACSS2 in adipose tissue is not known. Whole-body *Acss2-null* mice are protected from HFD-induced weight gain. These mice have less liver steatosis, smaller adipocytes and decreased whole-body lipid content (Z. Huang et al. 2018a). More evidence also shows that ACSS2 functions in the nucleus to

recapture the nuclear acetate retrieved from HDAC and preserves histone acetylation in oxygen and nutrient-deprived conditions in cancer cells (Bulusu et al. 2017) [Figure III-1]. These studies support that ACSS2 promotes the systemic storage or metabolism of fat according to the fed or fasted state through the selective regulation of genes involved in lipid metabolism. The signaling upstream of ACSS2 and how it regulates lipogenesis still remain to be elucidated.

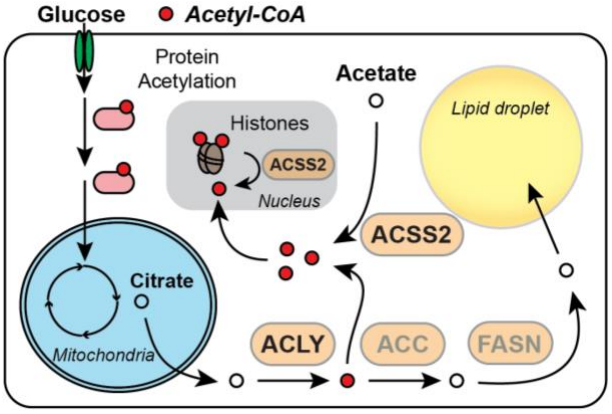

Figure III-1 Pathways for acetyl-CoA metabolism. Nuclear-cytoplasmic acetyl-CoA can be generated from an ACLY-dependent or an ACSS-dependent pathway.

In the previous chapter, I showed that mTORC2 is required for maximal induction of genes regulating lipid metabolism which might be due to enhancing histone acetylation selectively at these genes in early adipogenesis (D0 and D2, [Figure II-3B and 3C]). I also revealed that phosphomimetic ACLY at S455 site is not sufficient for rescuing the gene expression and lipogenic defects in *Rictor-iKO* white adipocytes, suggesting an alternative mechanism exists. Here, I explored the possible mechanisms of how mTORC2 regulates lipid filling program during white adipocyte differentiation.

3.2 Results

mTORC2 regulates acetyl-CoA level during white adipocyte differentiation

Acetyl-CoA can be derived from glucose metabolites and our previous study showed that glucose uptake requires mTORC2 signaling in brown preadipocytes and mature white adipocytes (Tang et al. 2016; Calejman et al. 2020). First, I determined whether glucose uptake is affected by *Rictor* deletion in primary white SVFs (hereinafter *Rictor-iKO*$_{primary}$), which contain preadipocytes. Inducible *Rictor* ablation was achieved by introducing 4-OHT as described in [Figure II-1A]. *Rictor-iKO*$_{primary}$ cells had ~25% and ~13% reduction in insulin-stimulated ^{3}H-labled 2-deoxyglucose (^{3}H-2-DG) uptake at day 0 and day 2 of differentiation, respectively [Figure III-2A]. This result was consistent with our previous finding suggesting that mTORC2 is required for glucose uptake in adipocytes. Next, I directly measured the intracellular acetyl-CoA, which reduced by 20% in *Rictor-iKO*$_{primary}$ preadipocytes (D0), and remains unchanged at differentiation day 2 [Figure III-2B]. Since acetyl-CoA is generated mainly at least from two nutrient sources: glucose via an ACLY-dependent pathway and acetate via an ACSS2-dependent process, I traced which nutrient contributes to the acetyl-CoA pool with ^{13}C isotope-labeled acetate and glucose [Figure III-2C]. At day 0, the decreased total acetyl-CoA level might be due to decreased glucose contribution [Figure III-2D], corresponding with the similar level of glucose uptake reduction [Figure III-2A]. At day 2, acetate contributed less to acetyl-CoA level in *Rictor-iKO*$_{primary}$ cells, with no change in glucose contribution [Figure III-2D].

Interestingly, acetyl-CoA depended approximately 2-fold more on acetate than on glucose at day 2 [Figure III-2D], which might suggest a switch in nutrient flux during adipogenesis. These data indicated that mTORC2 regulates intracellular acetyl-CoA production during adipogenesis.

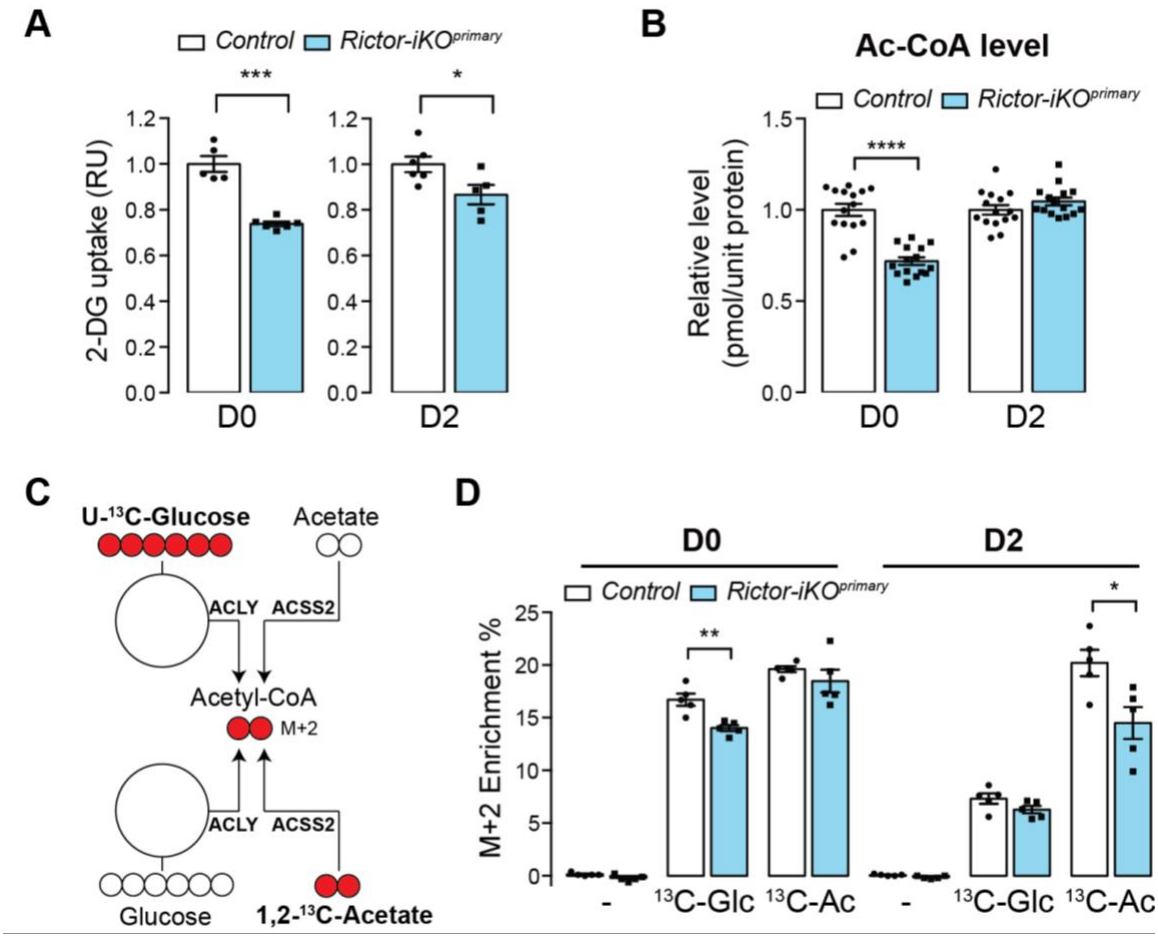

Figure III-2 mTORC2 regulates acetyl-CoA level in white adipocytes. A ^{3}H-labled 2-deoxyglucose (2-DG) uptake of control and *Rictor-iKO*^{primary} cells at D0 and D2 of differentiation. **B** Intracellular acetyl-CoA level (ac-CoA) in control and *Rictor-iKO*^{primary} cells at D0 and D2. **C** Overview of isotope labeling experiment. Red circles indicate carbon-13 (^{13}C) in indicated nutrients. Open circles indicate non-labeled (^{12}C) carbons. **D.** M+2 enrichment of acetyl-CoA from isotope-labeled glucose (U-^{13}C-Glucose, as ^{13}C-Glc) or isotope-labeled acetate (1,2-^{13}C-acetate, as ^{13}C-Ac) in control and *Rictor-iKO*^{primary} cells at D0 and D2. -: medium contains non-labeled glucose and acetate. Data represent mean ± SEM; $*p < 0.05$, $**p < 0.01$, $***p < 0.001$, $****p < 0.0001$.

Enhancing glucose influx is not sufficient to rescue lipid filling defect in *Rictor-iKO* adipocytes

Stable isotope tracing with different nutrients revealed that glucose contributes the majority of carbons for lipogenesis in cultured white adipocytes (Collins et al. 2011). *Rictor* loss causes glucose transport defect which might lead to decreased lipogenesis. To access that, I forced glucose influx by overexpressing GLUT1 to test whether glucose uptake defect is the primary cause of decreased lipid formation in *Rictor-iKO* cells. I immortalized SVFs isolated from *Ubc-Cre$_{ERT2}$;Rictor$_{floxed}$* mice (hereinafter *Rictor-iKO$_{immortal}$* cells) for further mechanistic studies (Tang et al. 2016). GLUT1 expression increased glucose uptake by 3-5 fold at basal state and by 1.5-2 folds upon insulin stimulation [Figure III-3A]. Consistently, overexpressing GLUT1 increased glucose incorporation into lipid by 7 fold in control and 3 fold in mature *Rictor-iKO$_{immortal}$* adipocytes, which was determined by ^{14}C-U-glucose lipogenic assay [Figure III-3B]. Although glucose transport and lipogenesis increased in both control and *Rictor-iKO$_{immortal}$* cells, there was a 60% reduction in glucose-derived lipid formation in GLUT1-overexpressing *Rictor-iKO* cells, which was even more significant when compared to cells without GLUT1 overexpression (~30% reduction in *Rictor-iKO* cells). Moreover, Oil Red O staining showed no improvement in lipid filling of *Rictor-iKO$_{immortal}$* cells when GLUT1 was overexpressed [Figure III-3C], despite the fact that *Rictor-iKO$_{immortal}$* cells with GLUT1 overexpression had similar glucose uptake compared to that in control

cells without exogenous GLUT1 [Figure III-3A]. GLUT1 overexpression was confirmed by western blot [Figure III-3D]. The DNL pathway (ACC and ACLY protein level) and the selective PPARγ targets (*Cd36* and *Lpl* as the representative) were not rescued, or even down-regulated, in *Rictor-iKO*$_{immortal}$ cells [Figure III-3D and III-3E]. This suggested that increasing glucose influx is not sufficient to restore the lipid filling defect in *Rictor-iKO*$_{immortal}$ adipocytes.

Exogenous acetate supplementation is not sufficient to restore lipid filling defect in *Rictor-iKO* adipocytes.

While glucose provides the majority of acetyl-CoA for lipogenesis and protein modification, acetate can also be used to generate acetyl-CoA via an ACSS2-dependent pathway for these purposes [Figure III-1]. In brown preadipocytes, exogenous acetate partially rescues differentiation and lipid accumulation during adipogenesis in the context of *Rictor* loss (Calejman et al. 2020). I tested whether acetate supplementation during adipogenic process is sufficient to rescue the lipid accumulation defect in *Rictor*-null white adipocyte. Oil Red O staining showed increased neutral lipid accumulation by ~60% in primary control cells with 2.5 mM sodium acetate (NaOAc) supplementation. *Rictor-iKO*$_{primary}$ cells, however, did not respond to NaOAc supplementation in the aspect of lipid accumulation [Figure III-3F]. Higher concentration of NaOAc (10 mM) inhibited lipid content in both control and *Rictor-iKO*$_{primary}$ cells [Figure III-3F]. I chose 5 mM NaOAc supplementation for further analysis since this

concentration has been widely utilized for adipogenic assay and histone acetylation in many cultured adipocyte systems (Wellen et al. 2009; Calejman et al. 2020). I confirmed the exogenous acetate influx and utilization by identifying an increase in histone acetylation [Figure III-3G]. Western blot showed decreased AKT2 and DNL enzymes such as ACC and FASN protein expression without changing in PPARγ2, an indicator of adipocyte differentiation, in *Rictor-iKO*$_{primary}$ cells with no acetate supplement [Figure III-3H]. This finding is consistent with previously reported data [Figure II-1E]. With the presence of acetate, no major protein expression changed in control cells, but the affected proteins in *Rictor-iKO*$_{primary}$ cells were not rescued. Moreover, PPARγ2 was decreased in *Rictor-iKO*$_{primary}$ cells when compared to the level in control cells with NaOAc supplementation [Figure III-3H]. This finding indicated that *Rictor-iKO*$_{primary}$ cells might have an acetate utilizing defect that exogenous acetate exposure causes more significant defect in adipogenic protein expression. Thus, these data suggested that increasing acetate availability is not sufficient to restore the lipid filling defect in *Rictor-iKO*$_{immortal}$ adipocytes.

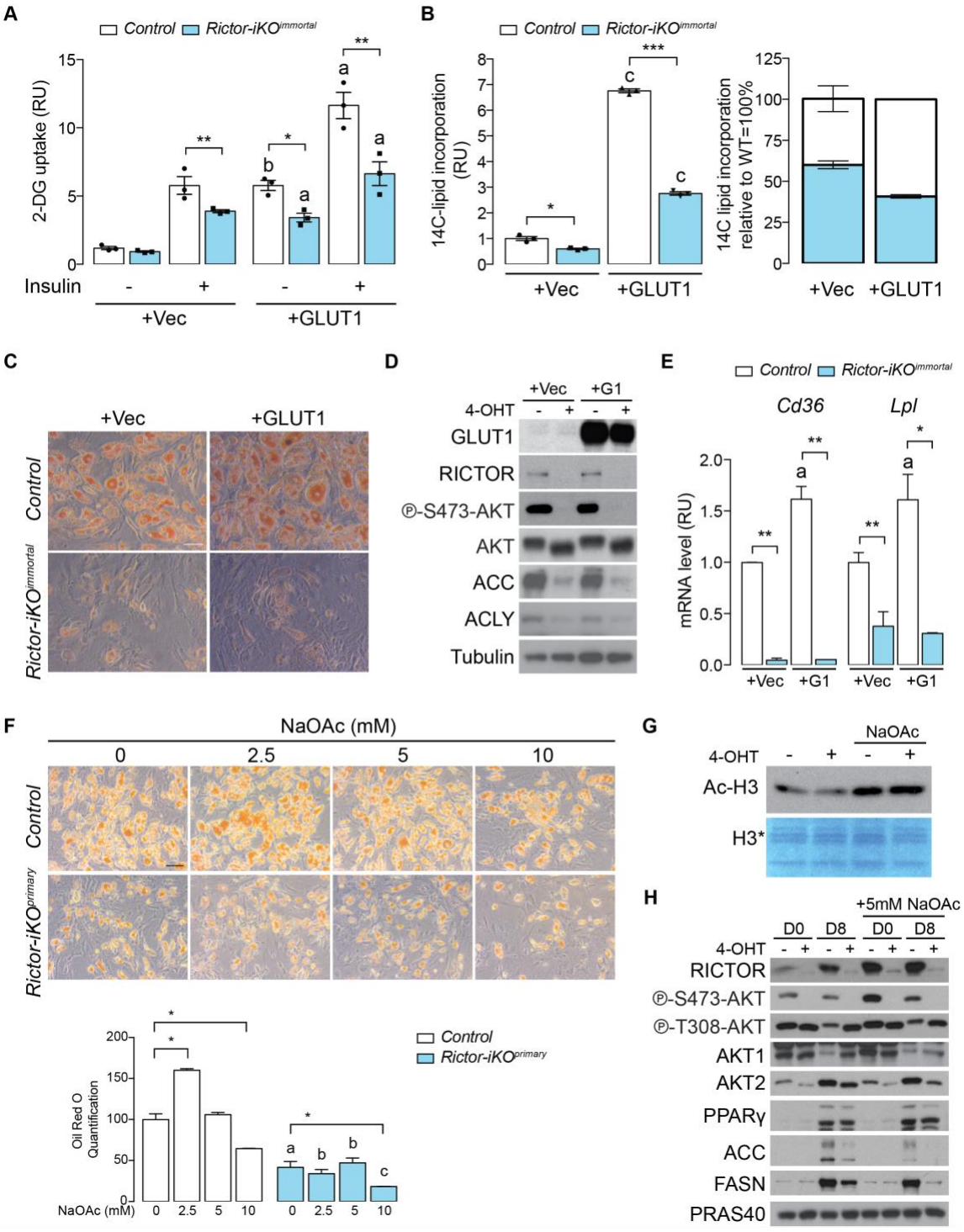

Figure III-3 Enhancing glucose or acetate flux is not sufficient for rescuing lipogenic defect in *Rictor-iKO* white adipocytes. A ^{3}H-labled 2-deoxyglucose (2-DG) uptake of differentiated control and *Rictor-iKO^{immortal}* cells with GLUT1 or empty vector (vec) expression. Data represent mean ± SEM.

Figure III-3 (Cont.) B (*left panel*) Lipogenesis assay measuring D-[U-^{14}C]-glucose labeling of *de novo* synthesized lipids in differentiated control and *Rictor-iKO^{immortal}* cells with GLUT1 or empty vector (vec) expression. (*right panel*) Relative ^{14}C-incorporated lipid in *Rictor-iKO^{immortal}* cells compared to control cells (set as 100%). Data represent mean ± SEM. **C** Oil Red O staining of differentiated control and *Rictor-iKO^{immortal}* cells with GLUT1 or empty vector (vec) expression. Scale bar = 100 μm. **D** Representative western blot of lysates from differentiated cells with or without GLUT1 (G1) overexpression. N = 3. 4-OHT: hydroxytamoxifen. **E** Relative mRNA expression of indicated genes in differentiated cells with or without GLUT1 (G1) overexpression. Data represent mean ± SEM**. F** *(upper panel)* Oil Red O staining of differentiated control and *Rictor-iKO^{primary}* cells with or without sodium acetate (NaOAc) supplement. Scale bar = 50 μm. *(lower panel)* Quantification of Oil Red O signals in indicated conditions. Data represent mean ± SEM. a: $p < 0.05$ compared to control cells with same NaOAc supplement; b: $p < 0.01$ compared to the control; c: $p < 0.001$. **G** Western blot of lysates from isolated histones of undifferentiated control and *Rictor-iKO^{primary}* cells. *: H3 band at the coomassie-stained gel. **H** Representative western blot of lysates from undifferentiated (D0) and differentiated (D8) control and *Rictor-iKO^{primary}* cells with indicated sodium acetate (NaOAc) supplement. PRAS40 as internal control. $*p < 0.05$, $**p < 0.01$, $***p < 0.001$.

mTORC2 regulates ACSS2 expression and localization during adipogenesis

From our RNA-sequencing analysis (addressed in Chapter 2), I uncovered *Acyl-CoA synthetase short chain family member 2* (*Acss2)* as both an adipogenic gene and one the most downregulated D8 genes in *Rictor-iKO$_{primary}$* cells (FC=2.64, FDR= 4.24419E-12) [Figure III-4A]. I confirmed that *Acss2* mRNA and protein level increase during differentiation, and were *Rictor*-dependent—indicated by a nearly 50% reduction in mRNA expression by D4 in *Rictor-iKO$_{primary}$* cells [Figure III-4B] and a corresponding decrease in total ACSS2 protein level by Western blot [Figure III-4C]. ACSS2 was recently linked to fat storage (Huang et al. 2018; Vysochan et al. 2017; Xu et al. 2018), and hypoxia or glucose deprivation induces ACSS2 nuclear translocation which might be required for lipogenic gene expression in cancer cells (Chen et al. 2017; Li et al.

2017). Therefore, I wondered if ACSS2 might promote lipid metabolic gene expression downstream of mTORC2 during adipogenesis.

I first examined ACSS2 localization during primary cell differentiation. By immunofluorescence staining using an antibody recognizing endogenous ACSS2, I observed a diffuse ACSS2 localization in undifferentiated precursors; however, it began accumulating in the nucleus by D2 of differentiation where it remained enriched through D8 [Figure III-4D]. I validated the specificity of this antibody using ACSS2-deficient cells [Figure III-4E]. In contrast, ACSS2 nuclear accumulation was markedly reduced in *Rictor-iKO*$_{primary}$ cells [Figure III-4D]. To confirm this, I also fractionated the cells into cytoplasmic and nuclear parts and performed Western blots for endogenous ACSS2. Consistently, both ACSS2 and PPARγ accumulated in the nucleus during early differentiation (at day 4); however, only nuclear ACSS2 levels were reduced in the *Rictor-iKO*$_{primary}$ cells [Figure III-4F]. Further analysis showed that the translocation defect occurs as early as differentiation day 3 (reduced by 20%), without change in cytoplasmic ACSS2 level [Figure III-4G]. Thus, ACSS2 translocated into the nucleus during early subcutaneous white adipocyte differentiation and this appeared to be regulated by mTORC2.

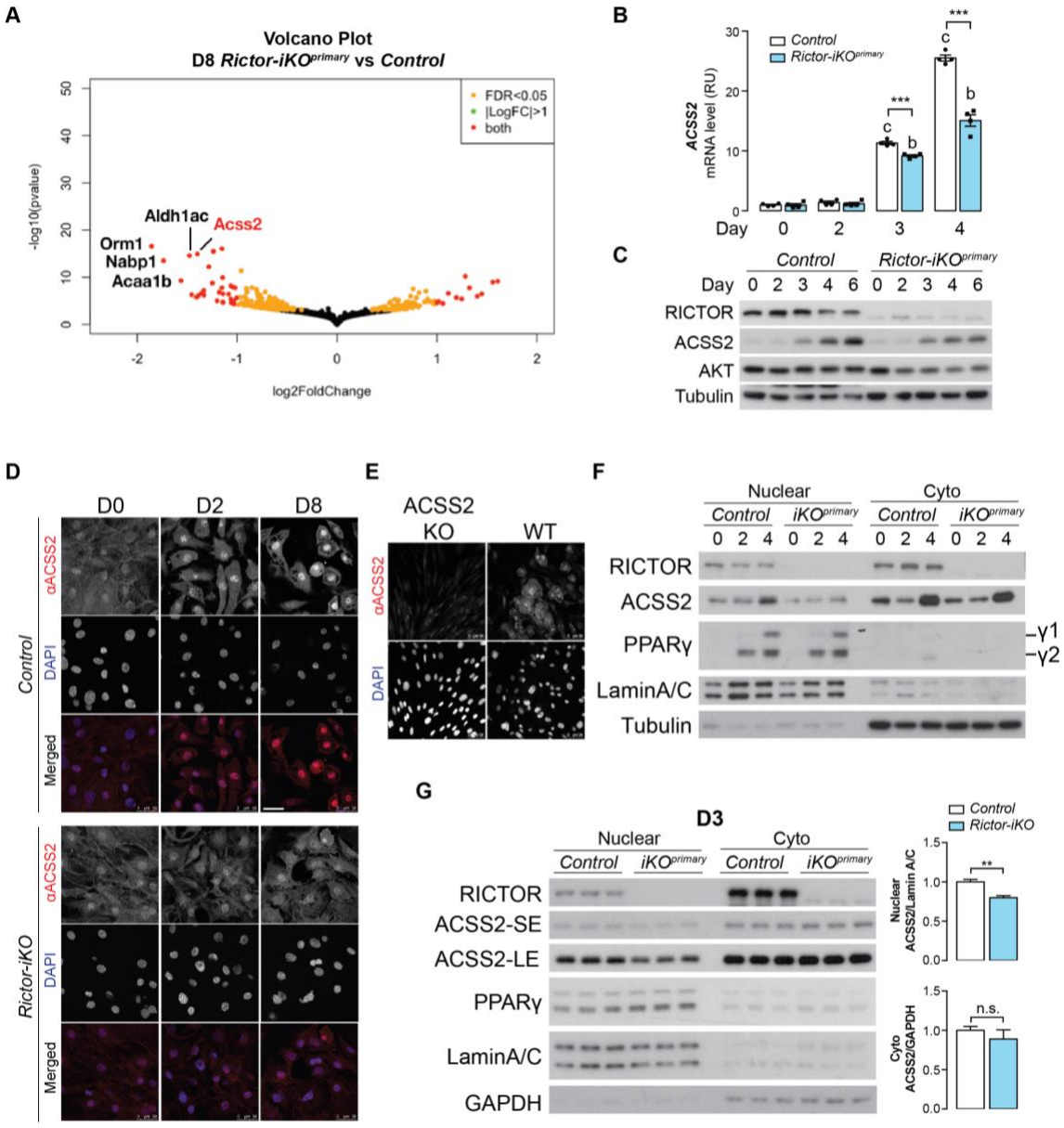

Figure III-4 mTORC2 regulates ACSS2 expression and localization during adipogenesis. A Volcano plot of RNA-seq transcriptome data displaying the pattern of gene expression values for *Rictor-iKO relative to primary control* differentiated adipocytes (data analyzed from Chapter 2, please see materials and methods for details). Significantly differentially expressed genes (FDR<0.05 and $|\log_2 FC| > 1$) are highlighted in red. Selected genes which are significantly decreased in *Rictor-iKO* cells are indicated. **B** Relative mRNA expression of *Acss2* in control and *Rictor-iKO*^{primary} cells at indicated day during differentiation. Data represent mean ± SEM. **C** Representative western blot of lysates from control and *Rictor-iKO*^{primary} cells at indicated day during differentiation. N =3. **D** Immunofluorescence staining of control and *Rictor-iKO*^{primary} cells for endogenous ACSS2 at indicated day during differentiation. Scale bar = 50 μm.

Figure III-4 (Cont.) E Validation of anti-ACSS2 antibody with immunofluorescence staining. KO: ACSS2 KO. **F** Representative western blot analysis of the nuclear and cytoplasmic (cyto) fractions of control and *Rictor-iKO*^{primary} cells at indicated day during differentiation. N = 3. **G** (*left panel*) Western blot analysis of the nuclear and cytoplasmic (cyto) fractions of control and *Rictor-iKO*^{primary} cells at day 3 during differentiation. N = 3. (*right panel*) Quantitative measurement of ACSS2 levels relative to internal controls shown in left panel (Lamin A/C as nuclear protein loading control and GAPDH as cytoplasmic loading control). Data represent mean ± SEM. $*p < 0.05$, $**p < 0.01$, $***p < 0.001$.

ACSS2 promotes lipid accumulation in adipocytes

To determine whether ACSS2 functions in adipogenesis, I used CRISPR-Cas9 gene editing to delete *Acss2* with two independent guides (hereinafter *Acss2*$_{CrisprKO}$) in subcutaneous white preadipocytes [Figure III-5A]. When differentiated, the *Acss2*$_{CrisprKO}$ cells showed a 22% reduction in lipid content as determine by quantifying Oil Red O staining [Figure III-5B]. Most strikingly, deleting *Acss2* attenuated expression of *Chrebpb*, *Acaca, Fasn, Scd1, Pparg2, Glut4, Cd36* and *Fabp4* [Figure III-5D and III-5E]. I further confirmed downregulation of ACLY, ACC, and FASN expression by Western blot but did not see a detectable difference in PPARγ protein by Western blot [Figure III-5F].

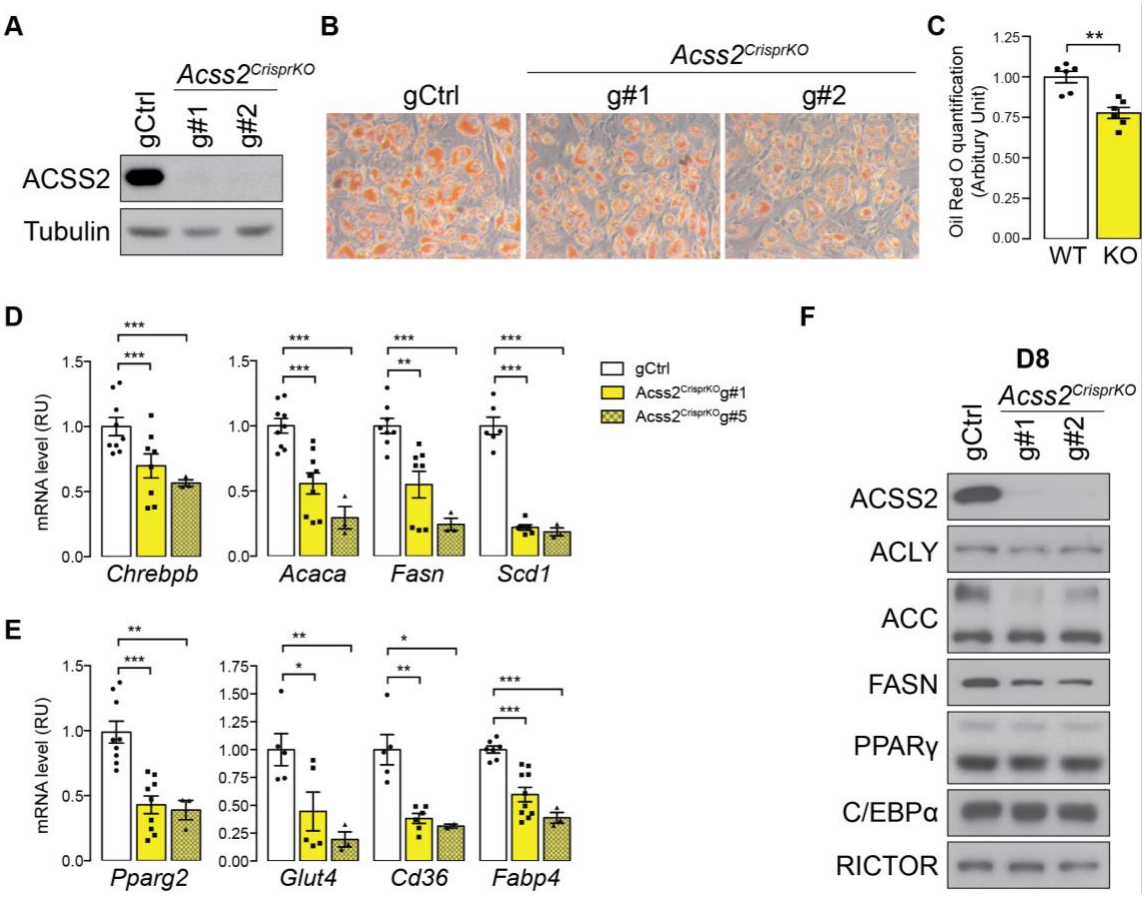

Figure III-5 ACSS2 promotes lipid accumulation in adipocytes. A Confirmation of ACSS2 KO by CRISPR/Cas9. Western blot of lysates from preadipocytes containing a guide targeting *Acss2* (2 distinc guides) or *Gfp* (control). **B** ORO staining of differentiated control and ACSS2-KO adipocytes (*Acss2*^{CrisprKO}). **C** Quantification of ORO staining determined by isopropanol extraction. Data represent mean ± SEM. $^{**}p < 0.01$. **D-E** Relative mRNA expression of indicated genes in differentiated control and *Acss2*^{CrisprKO} cells. Data represent mean ± SEM. $^{*}p < 0.05$, $^{**}p < 0.01$, $^{***}p < 0.001$. **F** Western blot of lysates from differentiated (D8) control and *Acss2*^{CrisprKO} cells. N = 2.

Nuclear-localizing ACSS2 is not sufficient to rescue lipid filling defect in the *Rictor-iKO* white adipocytes.

Finally, to test the hypothesis that ACSS2 functions downstream of mTORC2 during adipogenesis, I expressed in *Rictor-iKO*$_{immortal}$ cells either empty

vector, HA-ACSS2, HA- ACSS2-NLS containing a nuclear targeting sequence, or cytoplasm-localizing ACSS2 (HA-ACSS2-Cyto) with S659A mutation (X. Li et al. 2017) and asked if this could rescue lipid accumulation and gene expression. I confirmed the localization of these recombinant ACSS2 under glucose-rich (25 mM) and glucose-deficient conditions (1 mM) by immunofluorescence. Wildtype ACSS2 protein was present in both cytoplasm and nucleus under high glucose condition, and was enriched in nucleus when the glucose was deprived [Figure III-6A]. This translocation was consistent with the result described previously (Li et al. 2017; Chen et al. 2017). ACSS2-NLS recombinant protein was distributed mainly in the nucleus when the cells were exposed to either high or low glucose [Figure III-6A]. ACSS2-Cyto protein could still be present in the nucleus under glucose-rich condition, which was not seen in the previous study in cancer cells (X. Li et al. 2017). Interestingly, ACSS2-Cyto was not further enriched in the nucleus under low glucose condition [Figure III-6A], suggesting that this mutation blunted the nuclear translocation effect in response to glucose deprivation. Next, I stably expressed these constructs into immortalized preadipocytes with or without *Rictor* deletion. In control cells, expressing any of the ACSS2 constructs decreased lipid accumulation determined by Oil Red O staining, and none of the constructs rescued lipid filling defect in *Rictor-iKO*$_{immortal}$ cells [Figure III-6A]. I confirmed the expression of these recombinant ACSS2 constructs and *Rictor* deletion by western blot [Figure III-5B].

Since *Acss2* is an adipogenic gene which is induced during differentiation, stable ACSS2 overexpression in preadipocytes might be not be physiological. To address this, I modified the rescue experiment by transiently transduced these ACSS2 constructs into preadipocytes one day prior to the initiation of differentiation. The transduced construct was significantly expressed 48 hours after transduction, and the level increased thereafter [Figure III-6C]. By this strategy, overexpressing either ACSS2, ACSS2-NLS or ACSS2-cyto partially rescued lipid accumulation in *Rictor-iKO*$_{immortal}$ cells compared to vector-expression cells [Figure III-6D]. Interestingly, cells expressing ACSS2-NLS protein accumulated slightly more lipid when compared to other *Rictor-iKO*$_{immortal}$ cells [Figure III-6D]. I confirmed the ACSS2 expression and *Rictor* deletion by western blot. ACC and FASN in the DNL pathway were increased in cells expressing ACSS2, ACSS2-NLS or ACSS2-cyto [Figure III-6E]. However, the mRNA expression did not have corresponding changes in these cells [Figure III-6F]. The *Pparg2* and PPARγ targets such as *Cd36*, *Fabp4* and *Scd1* were not sufficiently rescued by ACSS2 overexpression [Figure III-6F]. Thus, despite having a positive role downstream of mTORC2 in adipogenesis, restoring ACSS2 expression and nuclear localization in *Rictor*-deficient cells was also insufficient to rescue them.

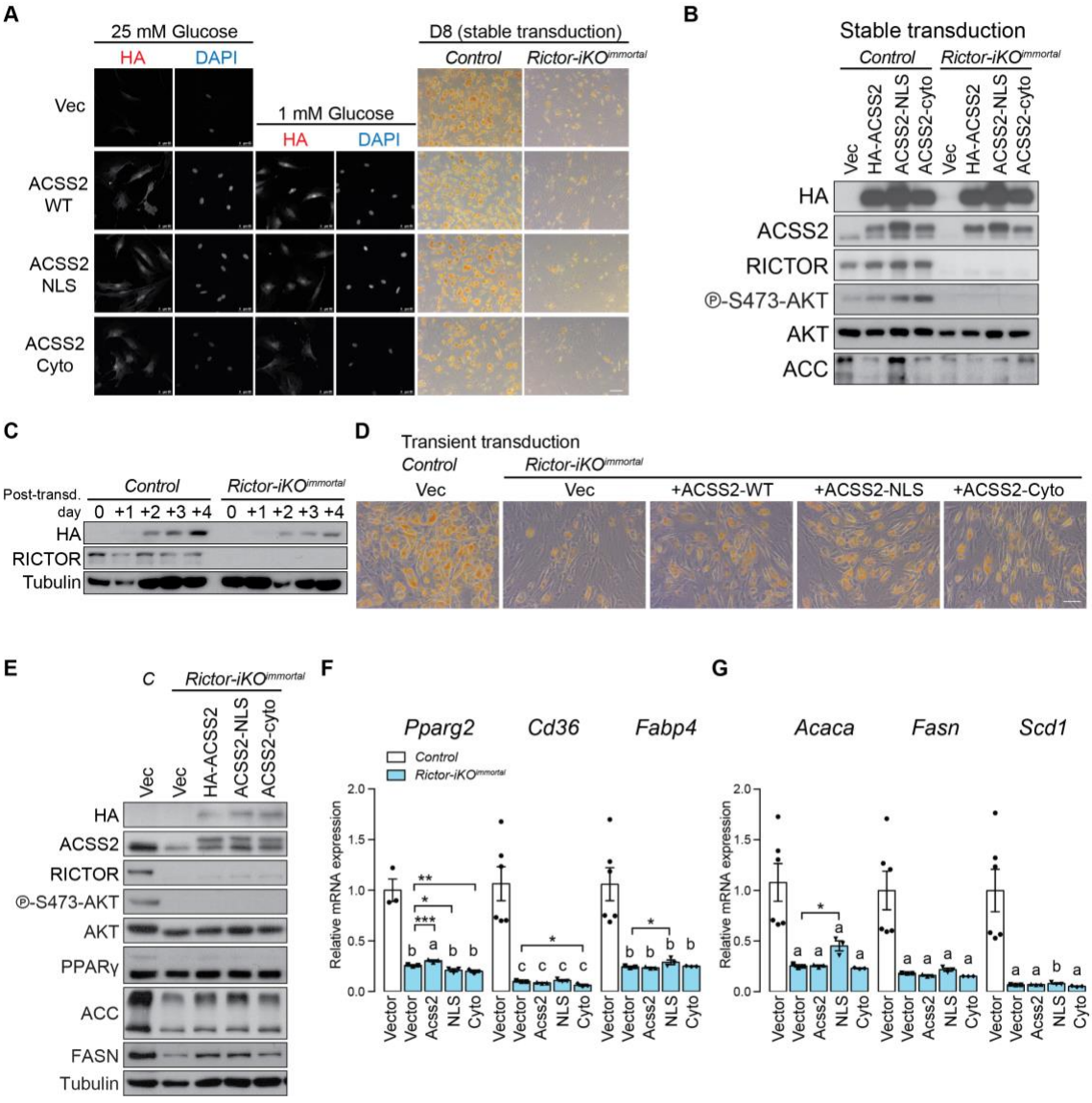

Figure III-6 Nuclear-localizing ACSS2 is not sufficient to rescue lipid accumulation defect in *Rictor-iKO* white adipocytes. A Immunofluorescence staining of undifferentiated control and *Rictor-iKO*^{immortal} cells expressing empty vector (vec), ACSS2-WT, ACSS2-NLS or ACSS2-Cyto constructs. Antibody targeting HA was used to recognize these HA-tagged recombinant proteins. Scale bar = 50 μm. *right side of the panel*: ORO staining of differentiated control and *Rictor-iKO*^{immortal} cells stably expressing indicated constructs. Scale bar = 50 μm. **B** Western blot of lysates from differentiated control and *Rictor-iKO*^{immortal} cells stably expressing empty vector (vec), HA-ACSS2-WT, HA-ACSS2-NLS or HA-ACSS2-Cyto constructs. **C** Western blot of lysates from control and *Rictor-iKO*^{immortal} cells at indicated time points after transient transduction (transd.) of HA-ACSS2 construct. **D** ORO staining of differentiated control and *Rictor-iKO*^{immortal} cells with transiently expression of indicated constructs. Scale bar = 50 μm.

Figure III-6 (Cont.) E Western blot of lysates from differentiated control and *Rictor-iKO*^{immortal} cells with transient expression of indicated constructs. **F-G** Relative mRNA expression of indicated genes in control and *Rictor-iKO*^{immortal} cells with transient expression of indicated ACSS2 constructs. Data represent mean ± SEM. $*p < 0.05$, $**p < 0.01$, $***p < 0.001$. a: $p < 0.05$ when compared to control group; b: $p < 0.01$; c: $p < 0.001$.

3.3 Discussion

In this chapter, I uncovered the role of mTORC2 in regulating intracellular acetyl-CoA flux in white adipocytes. Based on the RNA-seq transcriptome analysis performed in Chapter 2 [Figure III-4A], I identified that ACSS2 requires mTORC2 for maximal induction during adipocyte development. Moreover, ACSS2 was enriched in the nucleus during adipogenesis and knocking out *Rictor* ablates this phenomenon. These results showed the link between mTORC2 and *Acss2* at transcriptional level and/or protein nuclear localization during adipogenesis. Although the mechanism of how mTORC2 regulates ACSS2 expression and function remains unclear, I provided a new evidence of acetyl-CoA regulatory function of mTORC2 and a promising target in this pathway.

Emerging evidence highlights the role of ACSS2 in maintaining intracellular acetyl-CoA pool during metabolic stress. Many cancer cells, which have high biosynthetic demands due to rapid cell growth, depend on cytosolic ACSS2 to provide sufficient carbons for generating fatty acid and phospholipid (Schug et al. 2015; Mashimo et al. 2014). These cancer cells have up-regulated ACSS2 expression and the level correlates with disease progression in some

types of cancer (Schug et al. 2015; Comerford et al. 2014; Mashimo et al. 2014). In addition to the role in the cytosol, recent studies show that ACSS2 translocates to the nucleus under hypoxia or glucose deprivation. The nuclear ACSS2 utilizes nuclear acetate, which is produced by HDAC from histone deacetylation, to generate acetyl-CoA for histone modification which alters gene expression under these stress conditions (Li et al. 2017; Chen et al. 2017; Zlotorynski 2017). The role of ACSS2 in adipocytes is not well understood. Whole-body *Acss2* KO mice showed that ACSS2 might be required for lipogenic gene expression (Huang et al. 2018). Knocking-down ACSS2 in human preadipocytes diminished lipogenesis (Oliva-Olivera et al. 2018). Another model using cytomegalovirus-infected human fibroblasts, which have increased lipogenic capacity, also showed that ACSS2 is required for lipogenic gene expression (Vysochan et al. 2017). However, more careful investigation is required to understand how ACSS2 regulates adipocyte differentiation and function. I hypothesize that adipogenesis in white preadipocytes has higher glucose demand for turning on lipogenic programs, which might create a similar stress conditions seen in cancer or virus-infected cells and requires ACSS2. A study in cultured 3T3-L1 adipocytes supports this hypothesis: the demand for glucose increases by 4-5 folds during early differentiation (Jackson et al. 2017). In line with this finding, it might explain the observation in this dissertation: ACSS2 is enriched in the nucleus during differentiation [Figure III-4]. Although nuclear-localizing ACSS2 was not sufficient to rescue the lipogenic defect in

Rictor-deficient adipocytes, it suggested that mTORC2 might regulate ACSS2 through mechanisms other than translocation such as post-translational modification, protein stability, or other factors that affect the protein activity. Further investigation *in vivo* can be done by generating APCs-specific *Acss2* KO using the *Prx1-Cre* reported here to address the role in adipose tissue development and function.

In summary, altering acetyl-coA production closely correlates with glucose and lipid metabolism in adipocytes, and mTORC2 potentially contributes to this process through regulating acetyl-CoA-producing enzymes.

Materials and Methods

Acetyl-CoA labeling

Cells were fasted for 12 h and then incubated in DMEM without glucose plus 5mM of non-labeled or $_{13}$C-6-glucose and 100 μM non-labeled or $_{13}$C-2-acetate at 37 °C for 1 h. Samples were harvested in cold PBS, centrifuged at 1000 × g for 5 min, and the pellet was quenched in 10% (w/v) ice cold trichloroacetic acid in water, and then frozen at −80 °C until extraction and analysis on a QExactive Plus (Thermo) mass spectrometer coupled to an Ultimate 3000 high-performance LC. For quantitation, the abundance of acyl-CoA species was determined by interpolation to a linear standard curve. For isotopic tracer analysis, isotopic

enrichment was calculated to compensate for the non-linearity of isotopic enrichment using the FluxFix calculator (Trefely, Ashwell, and Snyder 2016).

Construction of small guide RNAs and lentiviral infection

Gene-specific custom designed single guide RNAs were cloned into the lentiCRISPRv2 vector (Addgene). The sgRNA sequences were determined by an online CRISPR Design Tool (http://chopchop.rc.fas.harvard.edu/) and sequences for sgRNAs targeting *Acss2* genes are shown in Appendix II. To generate lentiviruses, HEK293T cells were transfected with lentiviral vectors expressing the sgRNA of interest in combination with VSV-G envelope plasmid and Delta-Vpr packing plasmid. Culture media was changed 12 hours after transfection and the virus-containing supernatant was collected 48 hours after transfection and passed through a 0.45 mm filter to remove host cells. White preadipocytes were transduced in medium containing 4 mg/mL of polybrene (Sigma) by centrifugation at 1800 RPM for 30 min. 24 hours after the infection, cells were trypsinized and subjected to antibiotic (puromycin) selection.

The followings methods have been mentioned in Chapter 2

Cell culture

Immunofluorescence staining

Oil Red O staining

Construction of overexpression by retroviral infection

Gene expression analysis by RT-PCR

Western immunoblot analysis

Histone extraction and Western immunoblot analysis

CHAPTER IV - General Discussion and Future Directions

This chapter contains materials published in Current Diabetes Reports from

Springer:

Hsiao, W.-Y., Guertin, D.A., 2019. *De Novo* Lipogenesis as a Source of Second Messengers in Adipocytes. Curr. Diab. Rep. 19, 138.
https://doi.org/10.1007/s11892-019-1264-9

4.1 Metabolic signals and metabolic reprogramming

Abnormal nutrient fluxes in metabolic pathways have been detected in cancer and insulin resistance, but it is still unclear that whether these fluxes are the causes or the consequences. In the field of cancer research in the past, it had been proposed that aberrant metabolism in cancer cells is a passive response to rapid cell growth caused by up-regulation of oncogenes and/or down-regulation of tumor suppressor genes (Hanahan and Weinberg 2011). Evidence for an alternative concept has been built up in the past several years: these gene expression changes are secondary to an upstream signaling, which alters metabolic influx and triggers metabolic reprogramming to meet the requirements of increasing biosynthesis (Ward and Thompson 2012). Recent studies support that altered metabolic influx can provide signals to the cells. For example, the level of nuclear-cytoplasmic acetyl-CoA, which is at the center of many biosynthetic pathways, reflects the nutrient status of the environment and regulates gene expression and protein activity by histone and non-histone protein acetylation, respectively (Shi and Tu 2015; Wellen and Thompson 2012; Kaelin and McKnight 2013). Protein acetylation is modulated by lysine acetyltransferases (KATs) and deacetylases (DACs), which are sensitive to intracellular acetyl-CoA level (Sivanand, Viney, and Wellen 2018). It has been proposed that increased acetyl-CoA level promotes protein acetylation by activating KATs (Daitoku, Sakamaki, and Fukamizu 2011; J. V. Lee et al. 2014;

Pietrocola et al. 2015). Thus, factors that alter intracellular acetyl-CoA might change gene expression and protein activities which reprogram metabolism.

In the context of adipocytes, emerging evidence shows that protein/histone acetylation correlates with systemic insulin resistance. For example, forkhead box 1 (FoxO1) is one of the transcription factors which senses nutrient status and its activity is regulated by acetylation in addition to its classic regulation by insulin-stimulated phosphorylation. Acetylation, like phosphorylation, promotes FoxO1 accumulation in the cytoplasm thereby preventing FoxO1-driven catabolic activity (Perrot and Rechler 2005; Jing, Gesta, and Kahn 2007, 2; Gonzalez et al. 2011; Jung et al. 2019). Another example is CIDEC, which is required for forming lipid droplets. Deacetylation of CIDEC by HDAC6 inhibits its activity and destabilizes lipid droplets in adipocytes (Qian et al. 2017). The same study showed that HDAC6 is down-regulated in adipocytes from obese mice and adipocyte-specific HDAC6 KO mice have increased lipid accumulation and reduced insulin sensitivity (Qian et al. 2017). Thus, acetylation of non-histone proteins may also be related to nutrient status and can modulate metabolism to fit environmental demands. Many studies suggest that altering KAT or DAC activity may affect insulin sensitivity by regulating protein and/or histone acetylation in liver and adipose tissue. Several histone deacetylase inhibitors (or HDAC inhibitors) have been shown to improve insulin sensitivity in mouse models (Sharma and Taliyan 2016; Ye 2013). Moreover, a recent study

links diets and intracellular acetyl-CoA level and histone modification. HFD-fed mice have a decreased nuclear-cytosolic acetyl-CoA level and a global reduction in histone acetylation in adipose tissue and pancreas (Carrer et al. 2017). These studies support that the acetyl-CoA pool in adipocytes tightly links to cell metabolism.

4.2 The role of mTORC2 in sensing metabolic signals and metabolic reprogramming

Based on the results in this dissertation, I concluded that mTORC2 regulates lipid metabolic gene expression by an AKT1-dependent and possibly by regulating intracellular acetyl-CoA flux and histone acetylation in white adipocytes. First, I showed in Chapter II that acetylation of H3K9 sites at selective PPARγ target gene promoters was decreased in *Rictor*-deficient preadipocytes during differentiation [Figure II-3 and II-S4]. Second, I provided the evidence showing that there might be changes in glucose/acetyl-CoA influx in differentiating white preadipocytes [Figure III-2]. Last but not least, I identified an acetyl-CoA generating enzyme, ACSS2, as a possible target of mTORC2 which regulates its gene expression and/or protein translocation during differentiation [Figure III-4]. These results are in line with our recent findings in brown preadipocytes: mTORC2 is required for intracellular acetyl-CoA production and proper histone acetylation (Calejman et al. 2020). However, there are several distinct features between brown and white preadipocytes. First, in brown

preadipocytes, the authors detected a global reduction histone acetylation especially at H3K27 site (Calejman et al. 2020). These authors also detected a decreased H3K27 acetylation at the promoter of *Pparg2* during earlier differentiation, which may contribute to the *Pparg2* induction defect. In my white preadipocyte differentiation model, I did not detect significant changes in global histone acetylation [Figure II-S4D] or *Pparg2* induction defect in differentiating adipocytes. However, I identified changes in H3K9 acetylation at selective PPARγ targets regulating lipid metabolism [Figure II-3B]. Second, mTORC2 regulates acetyl-CoA production and lipogenesis via an AKT-ACLY-dependent pathway in brown preadipocytes (Calejman et al. 2020). However, the phosphomimetic ACLY mutant (S455D, an AKT-sensitive site) was not sufficient to rescue lipid accumulation defect in white adipocytes [Figure S4E-4G]. Interestingly, I detected a significant reduction in *Acss2* gene expression in *Rictor-iKO* white adipocytes. A similar finding has also been seen in brown preadipcytes, in which *Rictor* deletion blunts the compensatory ACSS2 expression upon ACLY loss (Calejman et al. 2020; Wellen et al. 2009). These differences suggest that mTORC2 regulates acetyl-CoA possibly by multiple pathways [Figure IV-1].

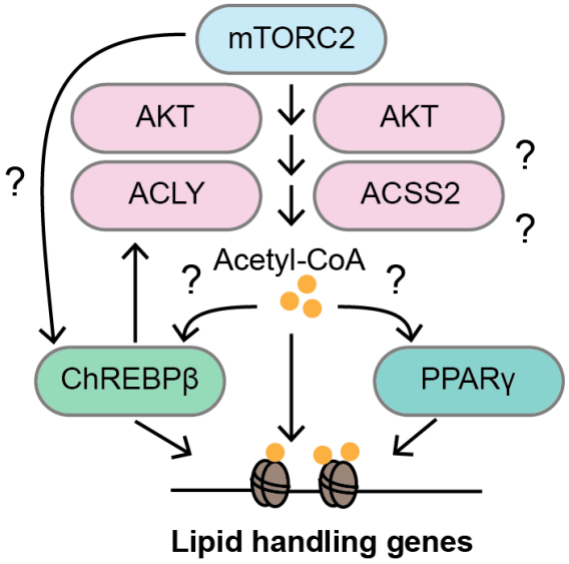

Figure IV-1 The working model of how mTORC2 regulates acetyl-CoA flux and lipid handling gene expression during adipocyte differentiation.

4.3 How does mTORC2 regulate PPARγ activity?

In this dissertation, I uncovered that ablation of mTORC2 signaling in precursors decreased PPARγ activity without affecting PPARγ2 induction, expression and translocation in primary cultured white adipocytes and white adipose tissues. I also correlated the histone acetylation of PPRE regions of selective PPARγ targets and PPARγ activity toward lipid metabolic genes. The mechanisms of how mTORC2 regulates PPARγ activity still require further investigation. Here, I propose a possible explanation [Figure IV-2]. First, PPARγ can be post-translationally modified and these modifications can regulate its activity. One of the well-known modifications is phosphorylation at S112, which can either up- or down-regulate PPARγ activity depending the upstream signals (Compe et al., 2005; Helenius et al., 2009; Hu et al., 1996; Iankova et al., 2006).

Another phosphorylation site is at serine S273, which is phosphorylated by Cdk5 and has inhibitory effect (Choi et al. 2010; 2014). Other modifications such as acetylation and sumoylation have also been reported and might regulate its activity (Brunmeir and Xu 2018; Tian et al. 2014; Floyd and Stephens 2004). As discussed above, these modifications and the upstream signals are tightly related to the metabolic status of cells and might be regulated by mTORC2. Second, PPARγ binds with several co-factors (Viswakarma et al. 2010; Powell, Kuhn, and Xu 2007). These co-factors include HAT (CBP, PCAF) and HDACs/Sirtuins which can alter the acetylation status of nearby histones and/or protein partners. As mentioned above, these HAT/HDACs are sensitive to nuclear-cytoplasmic acetyl-CoA level, so mTORC2 might regulate the co-factor binding and/or activity by changing acetyl-CoA metabolism. Other chromatin-remodeling mechanisms for regulating PPARγ expression and activity during adipogenesis. For example, the mammalian SWI/SNF family of ATP-dependent chromatin remodeler can interact with transcriptional regulatory proteins and previous studies show that SWI/SNF enzymes are required for the induction of differentiation genes including *Pparg2* during adipogenesis (Armstrong, Bieker, and Emerson 1998; Salma et al. 2004). Of noted, several members in SWI/SNF family and their associated proteins are identified as AKT substrates (K. S. J. Foster et al. 2006; Sif et al. 1998). Moreover, histone acetylation also depends directly on acetyl-CoA availability and mTORC2 might also contribute to acetyl-CoA flux. Other than co-factor binding, PPARγ also orchestrates with C/EBPα to regulate gene

expression during differentiation. These two transcription factors share common target genes, bind to adjacent sites and mutually regulate their expression and activity (Lefterova et al. 2014). Whether the PPARγ activity defect is primary or secondary to C/EBPα activity is remained elusive. Finally, there might be a mTORC2-dependent hormonal signal which might reprogram cell metabolism by concurrently regulating these mechanisms.

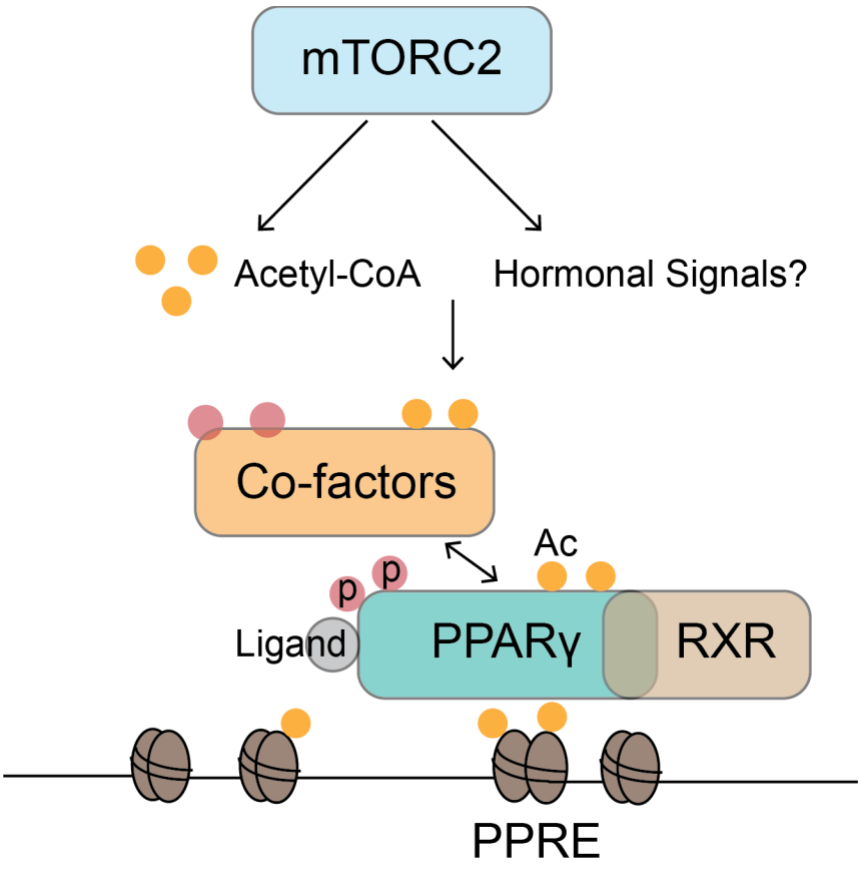

Figure IV-2 The possible mechanisms of how mTORC2 regulates PPARγ activity.

4.4 Genetic tools for studying white adipose tissue development *in vivo*

In this dissertation, I presented a white adipocyte precursor (APC)-targeting *Prx1-Cre* and successfully deleted *Rictor* and *Akt1* in the APC pool of SWAT with this approach. However, there might be some caveats with this Cre driver. Since *Prx1* expresses in mesenchyme during embryogenesis, we as well as other groups observed that *Prx1-Cre* targets bone mesenchymal stem cells which give rise to bone and bone marrow adipose tissue (MATs) (Sanchez-Gurmaches, Hsiao, and Guertin 2015; Krueger et al. 2014). It has been shown that MATs contribute to nearly 10% of whole-body adiposity and secrete adiponectin (Scheller et al. 2016; Cawthorn et al. 2014). MATs are also highly regulated depending on whole-body energy status (Q. Li, Wu, and Kang 2018). In *Rictor*$^{Prx1\text{-}Cre}$ mice, the adiposity in MAT is slightly decreased and long bones are significantly shorter [Table II-2 and II-3]. But how it contributes to the lipodystrophy phenotypes in other depots and systemic insulin sensitivity is unclear. Moreover, decreased bone length is also correlated with reduced muscle volume in these mice, which might also affect systemic metabolism. As mentioned in Chapter I, other APC-targeting Cre drivers are available but have limitations due to profound off-target effects to other organs [Table I-2]. More advances are required in this field for elucidating how white adipose tissue develops *in vivo*.

4.5 Sex differences in adipose tissue

A growing body of evidence suggests that adipose tissue distribution and metabolic functions are distinct between sexes in human and mouse models (Valencak, Osterrieder, and Schulz 2017; Fitzgerald et al. 2018). In general, women before puberty and in reproductive years accumulate more SWAT (e.g. gluteal-femoral fat) compared to the age-matched men. This fat distribution pattern gives rise to pear-like or gynoid body shape (Björntorp 1991). Men, on the hand, tend to store fat in VWAT and have so called apple shape or android type obesity (Karastergiou et al. 2012). These sex-specific fat distribution patterns are in part due to the number of X and Y chromosomes (X. Chen et al. 2013) and circulating sex steroids (Fuente-Martín et al. 2013). Sex steroids also regulate adipose tissue functions. For example, estrogens improve metabolic health by favoring fat deposition in SWAT, reducing inflammatory signals and improving systemic action in post-menopausal women (Brussaard et al. 1997; C. C. Lee, Kasa-Vubu, and Supiano 2003). On the contrary, androgens have negative effects on systemic metabolism by increasing VWAT size, reducing adiponectin production and impairing insulin sensitivity and are associated with a higher risk of developing cardiovascular disease (Zhao et al. 2018; Elbers et al. 1999; Evans et al. 1983; A. Tchernof and Després 2000; Nishizawa et al. 2002). Moreover, adipose tissue in females have more plasticity than that in males. In both human and mouse models, adipose tissue in females are more responsive to browning signals, which might be due to higher estrogen-induced sympathetic

innervation (S.-N. Kim et al. 2016; Quarta et al. 2012). Notably, a female-specific adipocyte, called pink adipocyte which is trans-differentiated from white adipocyte in SWAT, transiently arises during pregnancy through lactation in response to hormonal changes and has milk-secreting function (Giordano et al. 2014; Cinti 2017). How androgens and estrogens mechanistically contribute to these sex-specific observations is still unclear and requires more investigation.

In the past, the majority of studies mainly focused on male animals due to potentially higher metabolic variabilities related to hormonal fluctuations in female mice (Zucker and Beery 2010). An increasing number of studies has appreciated the differential metabolic phenotypes between sexes in many mouse models. For example, knocking out *Noggin*, a gene encoding an extracellular bone morphogenetic proteins (BMPs) which are essential regulators for adipocyte differentiation and function, in mature adipocytes shows that both male and females mice became obese, with reduced thermogenic gene expression significantly in females and impaired adipogenic and lipid metabolic gene expression in males (Blázquez-Medela et al. 2019). Conditional heme oxygenase-1 (OH-1, responsible for the recycling of heme) ablation in adipocytes increased adiposity selectively in females fed with HFD, and only female mice developed hyperglycemia and hyperinsulinemia (Hosick et al. 2017). Genetic deletion of *Acly* in mature adipocytes causes lipodystrophy with hepatic lipid accumulation and insulin resistance particularly in females fed with high sucrose

diet (Fernandez et al. 2019). These animal studies suggest that females might depend more on certain mechanisms, such as DNL, than males for regulating glucose and lipid metabolism. Similarly, I observed that only male *Rictor*$^{Prx1\text{-}Cre}$ mice developed insulin resistance and sex differences exist in bone phenotypes [Figure II-S5 and S6, Table II-2 and II-3]. Whether males are more dependent on mTORC2-PPARγ during adipose tissue development and function remains unclear, and more careful characterization and comparisons between sexes are required to uncover other potential differences in *Rictor*$^{Prx1\text{-}Cre}$ mice. To further explore the mechanisms of sexual dimorphism, sex hormone supplement in combination of ovariectomy/orchidectomy could be considered.

4.6 mTORC2-AKT signaling in adipose tissue development and function

In this dissertation, I conclude that mTORC2 is required for white adipose tissue development and function *in vivo* by selectively deleting *Rictor* in APCs of SWAT using *Rictor*^{prx1cKO} mouse model. The *Rictor*$^{Prx1\text{-}Cre}$ mice develop lipodystrophy in SAT, redistribution of body fat to other depots, and systemic insulin resistance in males. Mechanistically, the *Rictor*-null depots have down-regulation of DNL and PPARγ-targeting lipid metabolism genes with normal PPARγ expression and preserved adipocyte morphology [Figure II-6 and II-7]. These *in vivo* observations are consistent with the findings *in vitro*. I further explored the role of AKT1 in adipose tissue development by generating *Akt1*$^{Prx1\text{-}Cre}$ mice. Interestingly, these mice have slightly reduced adiposity in AKT1-null

SWAT [Figure II-10] and decreased DNL gene expression selectively in females. Figure IV-3 summarizes the working model based on the in *vivo* findings in this thesis. It is the first time the role of mTORC2 and AKT1 in white adipocyte precursors has been addressed *in vivo*. *Rictor* deletion in mature adipocytes under standard chow do not have a lipodystrophy phenotype, but have liver steatosis which contributes in part to the systemic insulin resistance (Tang et al. 2016). This phenotype is not detected in the *Rictor*$^{Prx1\text{-}Cre}$ model. Deleting *Rictor* in brown adipocyte precursors also develop lipodystrophy in targeted depots (Hung et al. 2014a). Notably, these mice are protected from diet-induced obesity at thermoneutrality (at 30 °C, without cold stress) and the *Rictor*-null depots are more thermogenic (Hung et al. 2014a). Consistently, *Rictor*$^{prx1\text{-}Cre}$ mice fed with HFD are also protected from diet-induced weight gain, less glucose intolerance, and the *Rictor*-null SWAT also have higher UCP1 expression, which suggests the depot might be more thermogenic [Figure II-8 and II-9]. More analyses are required to determine the whole-body metabolic status of these mice, e.g. metabolic cage study in response to special diet condition or temperature changes. More mechanistic studies also need to be addressed, such as complete profiles of mTORC2 and AKT signaling as well as mTORC1 signaling, the DNL pathway, lipid metabolism inflammation profiles in these depots. Besides, I observed the link between histone acetylation and PPARγ gene expression *in vitro*. To confirm this *in vivo*, we could utilize NuTRAP to unbiased

approach to correlate the histone modification change and transcriptome profiles simultaneously in adipocytes (Roh et al. 2017).

Whether the phenotypes I detected in *Rictor*-deficient depots are specific AKT isoform-dependent is unclear. Many adipose-specific *Rictor* deletion models do not show significant AKT signaling change determined by immunoblotting for phosphorylation signals of canonical downstream targets (Hung et al. 2014a; Tang et al. 2016; Calejman et al. 2020). In the *Rictor*$^{Prx1\text{-}Cre}$ model, I first identified decreases in phosphorylation of some canonical AKT targets as well as mTORC1 signaling, and a decrease on AKT at T308/309 site [Figure II-7A]. This may be due to reduced total AKT level, especially the AKT2 isoform [Figure II-7A]. It is also the first time I identified the transcriptional regulation of *Akt2* by mTORC2 [Figure II-S7A]. Interestingly, ablating AKT1 in subcutaneous APCs using *Akt1*$^{Prx1\text{-}Cre}$ model causes slightly decreased adipose tissue size in targeted female depot [Figure II-10]. Mechanistically, this *Akt1*-depleted SWAT shows decreased DNL gene and protein expression. These findings provide novel insights of how AKT1 regulates white adipose tissue development *in vivo* because this is the first time I have deleted *Akt1* in white fat precursors. The current understanding is that AKT1 is dispensable for mature white and brown adipose tissue functions as well as brown adipose tissue development (Shearin et al. 2016; Sanchez-Gurmaches et al. 2019), even though some studies suggest AKT1 is required for adipogenesis *in vitro* as discussed in Chapter 1. Moreover,

previous studies mainly focused on male mice, which might overlook the fact that metabolism in adipose tissues are distinct between sexes (White and Tchoukalova 2014).

In conclusion, this dissertation provides a novel insight of how mTORC2 regulates white adipocyte differentiation and function using both *in vitro* and *in vivo* approaches and reveals a potential mechanism of mTORC2 in regulating acetyl-CoA metabolism.

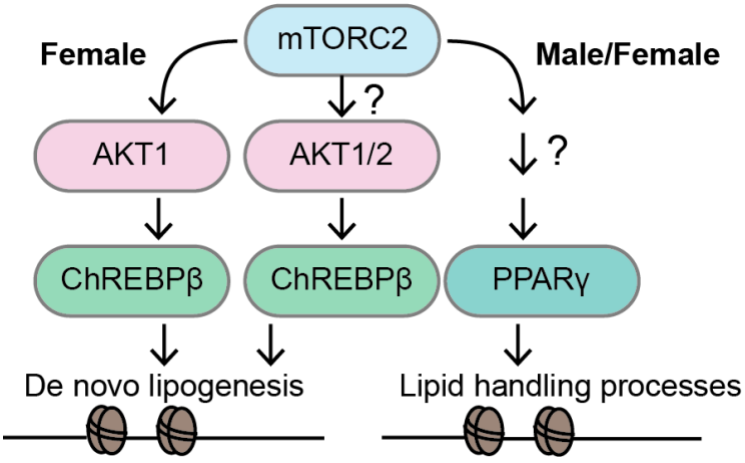

Figure IV-3 Model of how mTORC2 regulates adipose tissue development *in vivo*.

Appendix I: Key Resources Table

REAGENT or RESOURCE	SOURCE	IDENTIFIER
Antibodies		
mTOR	Cell Signaling Technology	Cat# 2972; RRID: AB_330978
RICTOR	Cell Signaling Technology	Cat# 2140; RRID: AB_561245
PPARγ (Western blot)	Cell Signaling Technology	Cat# 2443; RRID: AB_823598
Perilipin1 (IF staining)	Cell Signaling Technology	Cat# 9349; RRID: AB_10829911
C/EBPα	Santa Cruz Biotechnology	Cat# sc-365318; RRID: AB_10846948
α-Tubulin	Cell Signaling Technology	Cat# 2125; RRID: AB_2619646
Phospho-S473-AKT	Cell Signaling Technology	Cat# 4058; RRID: AB_331168
Phospho-T450-AKT	Cell Signaling Technology	Cat# 9267; RRID: AB_823676
Phospho-T308-AKT	Cell Signaling Technology	Cat# 4056; RRID: AB_331163
Phospho-S473-AKT1	Cell Signaling Technology	Cat# 9018; RRID: AB_2629283
Phospho-S474-AKT2	Cell Signaling Technology	Cat# 8599; RRID: AB_2630347
AKT1	Cell Signaling Technology	Cat# 2938; RRID: AB_915788
AKT2	Cell Signaling Technology	Cat# 3063; RRID: AB_2225186
AKT	Cell Signaling Technology	Cat# 9272; RRID: AB_329827
Phospho-T24-FoxO1	Cell Signaling Technology	Cat# 9464; RRID: AB_329842
FoxO1	Cell Signaling Technology	Cat# 2880; RRID: AB_2106495
Phospho-S9-GSK3β	Cell Signaling Technology	Cat# 9322; RRID: AB_2115196
GSK3bβ	Cell Signaling Technology	Cat# 12456; RRID: AB_2636978
Phospho-T246-PRAS40	Cell Signaling Technology	Cat# 2997; RRID: AB_2258110
PRAS40	Cell Signaling Technology	Cat# 2691; RRID: AB_2225033
Phospho-T642-AS160	Cell Signaling Technology	Cat# 8881; RRID: AB_2651042
AS160	EMD Millipore	Cat# 07-741; RRID: AB_492639
Phospho-T389-S6K1	Cell Signaling Technology	Cat# 9205; RRID: AB_330944
S6K1	Santa Cruz Biotechnology	Cat# sc8418

Insulin Receptor(IR)β	Cell Signaling Technology	Cat# 3025; RRID: AB_2280448
ACC	Cell Signaling Technology	Cat# 3676; RRID: AB_2219397
ACLY	Cell Signaling Technology	Cat# 4332; RRID: AB_2223744
FASN	Cell Signaling Technology	Cat# 3180; RRID: AB_2100796
ChREBP	Novus	Cat# NB400-135; RRID: AB_10002435
SREBP	EMD Millipore	Cat# 04-469, RRID:AB_612072
HA	Cell Signaling Technology	Cat# 2367; RRID: AB_10691311
Histone H3	Cell Signaling Technology	Cat# 4499; RRID: AB_10544537
Acetyl-Histone H3 (lys9)	Cell Signaling Technology	Cat# 9649; RRID: AB_823528
PPARγ	Santa Cruz Biotechnology	Cat# sc-7196; RRID: AB_654710
CD36	NOVUS	Cat#: NB400-144SS; RRID: AB_920879
SCD1	Abclonal	Cat# A16429
FABP4	Cell Signaling Technology	Cat# 2120; RRID: AB_2102466
Goat anti-Rabbit IgG (H+L) Cross-Adsorbed Secondary Antibody, Alexa Fluor 568	Thermo Fisher Scientific	Cat# A-11011; RRID: AB_143157
PE-Cy7-conjugated anti-CD31	eBioscience	Cat# 25-0311-82
PE-Cy7-conjugated anti-CD45	eBioscience	Cat# 25-0451-82
A700-conjugated anti-CD29	BioLegend	Cat# 102218
A647-conjugated anti-CD34	BioLegend	Cat# 119314
LybA/E-conjugated anti-Sca1	eBioscience	Cat# 45-0242-82
ACSS2 (AceCS1, for western blot)	Cell Signaling Technology	Cat# 3658
ACSS2 (IF staining)	GeneTex	Cat# GTX#30020
UCP1	Abcam	Cat# ab10983; RRID: AB_2241462
Chemicals, Peptides, and Recombinant Proteins		
4-hydroxy Tamoxifen (4-OHT)	Toronto research chemicals	H954729
Rosiglitazone	Cayman Chemical	71740
Oil Red O	Sigma-Aldrich	O0625
Human insulin, regular	Novo Nordisk	#183302
Insulin	Sigma-Aldrich	I2643
3-isobutyl-1-methylxanthine (IBMX)	Sigma-Aldrich	I5879
Dexamethasone	Sigma-Aldrich	D1756
Osmium tetroxide 2% aqueous solution	Polysciences Inc	#23311
HCS LipidTOX™ Deep Red Neutral Lipid Stain	Invitrogen	H34477

Trichostatin A (TSA)	Sigma-Aldrich	T1952
BODIPY FL C16	Invitrogen	D3821
Propidium iodide	Invitrogen	P3566
[U-13C] glucose	Cambridge Isotope Laboratories, Inc.	CLM-1396-1
[1,2-13C] acetate	Cambridge Isotope Laboratories, Inc.	CLM-440-PK
Dialyzed fetal bovine serum	Gibco	A3382001
Critical Commercial Assays		
Dual-Luciferase Reporter assay system	Promega	E1910
Free Glycerol Reagent	Sigma-Aldrich	F6428
NEBNext® Ultra™ Directional RNA Library Prep Kit for Illumina®	New England Biolabs	E7760
Seahorse XF Glycolysis stress test kit	Agilent Technologies	Cat# 103020-100
Seahorse XF Palmitate Oxidation stress test kit and FAO substrate	Agilent Technologies	Cat# 103693-100 Cat# 102720-100
Deposited Data		
Raw and analyzed data	This study	GSE146470
Experimental Models: Cell Lines		
Immortalized subcutaneous white preadipocytes	(Tang et al. 2016)	N/A
Primary subcutaneous white preadipocytes	This study	N/A
Experimental Models: Organisms/Strains		
Mouse: *Prx1-Cre*	Jackson Labs	005584
Mouse: *Adiponectin-Cre*	Jackson Labs	028020
Mouse: *Rictor^{floxed}*	Jackson Labs	020649
Mouse: *UBC-cre^{ERT2}*	Jackson Labs	007001
Mouse: *Akt1^{floxed}*	From Morrie Birnbaum	N/A
Oligonucleotides		
Mouse primers	IDT	See Appendix II
Recombinant DNA		
pMSCV-Puro	(Akama-Garren et al. 2016)	RRID: Addgene_68469
pMSCV-ChREBPα-Puro	(Witte et al. 2015)	N/A
pMSCV-ChREBPβ-Puro	(Witte et al. 2015)	N/A
pMSCV-HA-PPARγ2-Hygro	This study	N/A
pMSCV-Myc-ACLY-Puro	(Calejman et al. 2020)	N/A
pMSCV-Myc-ACLY-S455D-Puro	(Calejman et al. 2020)	N/A

pMSCV-Myc-ACLY-S455E-Puro	This study	N/A
pMSCV-Myc-ACLY-S455A-Puro	(Calejman et al. 2020)	N/A
PPRE X3-TK-luc	(Kim et al. 1998)	RRID: Addgene_1015
pMSCV-HA-AKT1-Hygro	(Calejman et al. 2020)	N/A
pMSCV-HA-AKT1-S473D-Hygro	(Calejman et al. 2020)	N/A
pMSCV-HA-AKT1-S473A-Hygro	(Calejman et al. 2020)	N/A
pMSCV-HA-AKT2-Hygro	(Calejman et al. 2020)	N/A
pMSCV-HA-AKT2-S474D-Hygro	(Calejman et al. 2020)	N/A
pMSCV-HA-ACSS2	This study	N/A
pMSCV-HA-ACSS2-NLS	This study	N/A
pMSCV-HA-ACSS2-Cyto	This study	N/A
pLenti-CRISPR v2-sgACSS2#1	This study	N/A
pLenti-CRISPR v2-sgACSS2#2	This study	N/A
Software and Algorithms		
ImageJ (Fiji)	(Schindelin et al. 2012)	https://imagej.nih.gov/ij/
Adiposoft Fiji plugin)	(Galarraga et al. 2012)	N/A
star_2.5.3a	(Dobin et al. 2013)	N/A
Ensembl annotation GRCm38.94	(Zerbino et al. 2018)	N/A
featureCounts_1.5.2	(Liao, Smyth, and Shi 2014)	N/A
DESeq2_1.20.0	(Love, Huber, and Anders 2014)	N/A
Other		
ChIP-Atlas	(Oki and Ohta 2016)	N/A
DAVID Bioinformatics Resources 6.8	(D. W. Huang, Sherman, and Lempicki 2009a; 2009b)	https://david.ncifcrf.gov/home.jsp
Cytation™ 5 Image reader	Biotek	N/A
LSRII A-5 laser flow cytometer	BD Biosciences	N/A
Seahorse XFe96 Analyzer	Agilent	N/A

Appendix II: Primer sequences

RT-PCR (mouse)		
Site		Sequence (5'-3')
TBP	Forward	ACGGACAACTGCGTTGATTTT
	Reverse	ACTTAGCTGGGAAGCCCAAC
Pparg2	Forward	TGGCATCTCTGTGTCAACCATG
	Reverse	GCATGGTGCCTTCGCTGA
Cebpa	Forward	CAAGAACAGCAACGAGTACCG
	Reverse	GTCACTGGTCAACTCCAGCAC
Cebpb	Forward	TCGGGACTTGATGCAATCC
	Reverse	AAACATCAACAACCCCGC
Cebpd	Forward	GCTTTGTGGTTGCTGTTGAA
	Reverse	ATCGACTTCAGCGCCTACA
Akt1	Forward	CACGCTACTTCCTCCTCAAG
	Reverse	CTCTGTCTTCATCAGCTGGC
Akt2	Forward	CCTTCCATGTAGACTCTCCAG
	Reverse	CCTCCATCATCTCAGATGTGG
Acly	Forward	CTCACACGGAAGCTCATCAA
	Reverse	ACGCCCTCATAGACACCATC
Acaca	Forward	GGAGATGTACGCTGACCGAGAA
	Reverse	ACCCGACGCATGGTTTTCA
Fasn	Forward	GCTGCGGAAACTTCAGGAAAT
	Reverse	AGAGACGTGTCACTCCTGGACTT
Cd36	Forward	TGGCCTTACTTGGGATTGG
	Reverse	CCAGTGTATATGGCTCATCCA
Fabp4	Forward	GATGCCTTTGTGGGAACCT
	Reverse	CTGTCGTCTGCGGTGATTT
Lpl	Forward	GGCCAGATTCATCAACTGGAT
	Reverse	GCTCCAAGGCTGTACCCTAAG
Glut4	Forward	GTGACTGGAACACTGGTCCTA
	Reverse	CCAGCCAGTTGCATTGTAG
Scd1	Forward	CCCTGCGGATCTTCCTTATC
	Reverse	TGTGTTTCTGAGAACTTGTGGTG
Dgat1	Forward	GAGGCCTCTCTGCCCCTATG
	Reverse	GCCCCTGGACAACACAGACT
Dgat2	Forward	CCGCAAAGGCTTTGTGAAG
	Reverse	GGAATAAGTGGGAACCAGATCA
Hsl	Forward	CAGTGTGACCGCCAGTTC
	Reverse	ACCTCAATCTCAGTGATGTTCC
Mcad	Forward	GCCAAGATCTATCAGATTTATGAAGG
	Reverse	AGCTATGATCAGCCTCTGAATTTGT
Perilipin1	Forward	CTGTGTGCAATGCCTATGAGA

	Reverse	CTGGAGGGTATTGAAGAGCCG	
Adipoq	Forward	TGTTCCTCTTAATCCTGCCCA	
	Reverse	CCAACCTGCACAAGTTCCCTT	
Chrebpa	Forward	CGACACTCACCCACCTCTTC	
	Reverse	TTGTTCAGCCGGATCTTGTC	
Chrebpb	Forward	TCTGCAGATCGCGTGGAG	
	Reverse	CTTGTCCCGGCATAGCAAC	
Pkm2	Forward	TCGCATGCAGCACCTGATT	
	Reverse	CCTCGAATAGCTGCAAGTGGTA	
Rictor	Forward	TCGATCTGACCCGAGAACCTT	
	Reverse	GTTATTCAGATGGCCCAGCTTTT	
Ucp1	Forward	CTGCCAGGACAGTACCCAAG	
	Reverse	TCAGCTGTTCAAAGCACACA	
Acss2	Forward	GGATCACTGGTCATTCCTAC	
	Reverse	GTGCTGTGTAGAACTTGGTC	
gRNA sequences for CRISPR/Cas9 KO			
ACSS2KO-g1		GCTGCACCGGCGTTCTGTGG	
ACSS2KO-g2		GGTCACCTGTAGTGATGAGC	
ChIP-qPCR primers			
Site		Sequence (5'-> 3')	Reference
Cd36-PPRE	Forward	CCAACGGAACTGATTTGAGC	(Lefterova et al. 2010)
	Reverse	TTGCTGCTACACTCCAGCAT	
Fabp4-PPRE	Forward	AATGTCAGGCATCTGGGAAC	(Lefterova et al. 2010)
	Reverse	GACAAAGGCAGAAATGCACA	
H3K9ac-Cd36-PPRE	Forward	GAGCCGCCCCTTCTATACTT	(Lefterova et al. 2010)
	Reverse	TGTTGGGACAGACCAATCAG	
H3K9ac-Fabp4-PPRE	Forward	TTCTGACTCCTGGCCTGAAC	(Lefterova et al. 2010)
	Reverse	TGCCCTCTCAGGTTTCATTT	
Pkm2-PPRE	Forward	GCAGCCAGCCTGTAAGGGCA	(Panasyuk et al. 2012b)
	Reverse	GCGAAGACAGGAAAACAGTGGGT	
Insulin	Forward	CTTCAGCCCAGTTGACCAAT	N/A
	Reverse	AGGGAGGAGGAAAGCAGAAC	
Chr. 15	Forward	AGCGTGGCCTTGGCAGCAAA	(Zhang et al. 2012)
	Reverse	TGCGATTGGCTTCCTCTCCCC	

References

Abel, E. D., O. Peroni, J. K. Kim, Y. B. Kim, O. Boss, E. Hadro, T. Minnemann, G. I. Shulman, and B. B. Kahn. 2001. “Adipose-Selective Targeting of the GLUT4 Gene Impairs Insulin Action in Muscle and Liver.” *Nature* 409 (6821): 729–33. https://doi.org/10.1038/35055575.

Adams, M., M. J. Reginato, D. Shao, M. A. Lazar, and V. K. Chatterjee. 1997. “Transcriptional Activation by Peroxisome Proliferator-Activated Receptor Gamma Is Inhibited by Phosphorylation at a Consensus Mitogen-Activated Protein Kinase Site.” *The Journal of Biological Chemistry* 272 (8): 5128–32. https://doi.org/10.1074/jbc.272.8.5128.

Akama-Garren, Elliot H., Nikhil S. Joshi, Tuomas Tammela, Gregory P. Chang, Bethany L. Wagner, Da-Yae Lee, William M. Rideout III, Thales Papagiannakopoulos, Wen Xue, and Tyler Jacks. 2016. “A Modular Assembly Platform for Rapid Generation of DNA Constructs.” *Scientific Reports* 6 (1). https://doi.org/10.1038/srep16836.

Albert, Verena, Kristoffer Svensson, Mitsugu Shimobayashi, Marco Colombi, Sergio Muñoz, Veronica Jimenez, Christoph Handschin, Fatima Bosch, and Michael N. Hall. 2016. “MTORC2 Sustains Thermogenesis via Akt-Induced Glucose Uptake and Glycolysis in Brown Adipose Tissue.” *EMBO Molecular Medicine* 8 (3): 232–46. https://doi.org/10.15252/emmm.201505610.

Alessi, D. R., M. Andjelkovic, B. Caudwell, P. Cron, N. Morrice, P. Cohen, and B. A. Hemmings. 1996. “Mechanism of Activation of Protein Kinase B by Insulin and IGF-1.” *The EMBO Journal* 15 (23): 6541–51.

Almandoz, J. P., E. Singh, L. A. Howell, K. Grothe, D. T. Vlazny, A. Smailovic, B. A. Irving, R. H. Nelson, and J. M. Miles. 2013. “Spillover of Fatty Acids During Dietary Fat Storage in Type 2 Diabetes: Relationship to Body Fat Depots and Effects of Weight Loss.” *Diabetes* 62 (6): 1897–1903. https://doi.org/10.2337/db12-1407.

Alva, Jackelyn A., Ann C. Zovein, Arnaud Monvoisin, Thomas Murphy, Anthony Salazar, Natasha L. Harvey, Peter Carmeliet, and M. Luisa Iruela-Arispe. 2006. “VE-Cadherin-Cre-Recombinase Transgenic Mouse: A Tool for Lineage Analysis and Gene Deletion in Endothelial Cells.” *Developmental Dynamics: An Official Publication of the American Association of Anatomists* 235 (3): 759–67. https://doi.org/10.1002/dvdy.20643.

Appari, Mahesh, Keith M. Channon, and Eileen McNeill. 2017. “Metabolic Regulation of Adipose Tissue Macrophage Function in Obesity and Diabetes.” *Antioxidants & Redox Signaling* 29 (3): 297–312. https://doi.org/10.1089/ars.2017.7060.

Armstrong, J. A., J. J. Bieker, and B. M. Emerson. 1998. “A SWI/SNF-Related Chromatin Remodeling Complex, E-RC1, Is Required for Tissue-Specific

Transcriptional Regulation by EKLF in Vitro." *Cell* 95 (1): 93–104. https://doi.org/10.1016/s0092-8674(00)81785-7.
Ashcroft, Frances M., and Patrik Rorsman. 2012. "Diabetes Mellitus and the β Cell: The Last Ten Years." *Cell* 148 (6): 1160–71. https://doi.org/10.1016/j.cell.2012.02.010.
Badri, Kameswara Rao, Yuanxiang Zhou, Urmil Dhru, Sreelatha Aramgam, and Lucia Schuger. 2008. "Effects of the SANT Domain of Tension-Induced/Inhibited Proteins (TIPs), Novel Partners of the Histone Acetyltransferase P300, on P300 Activity and TIP-6-Induced Adipogenesis." *Molecular and Cellular Biology* 28 (20): 6358–72. https://doi.org/10.1128/MCB.00333-08.
Barlow, C., M. Schroeder, J. Lekstrom-Himes, H. Kylefjord, C. X. Deng, A. Wynshaw-Boris, B. M. Spiegelman, and K. G. Xanthopoulos. 1997. "Targeted Expression of Cre Recombinase to Adipose Tissue of Transgenic Mice Directs Adipose-Specific Excision of LoxP-Flanked Gene Segments." *Nucleic Acids Research* 25 (12): 2543–45. https://doi.org/10.1093/nar/25.12.2543.
Beg, Muheeb, Nazish Abdullah, Fathima Shazna Thowfeik, Nasser K. Altorki, and Timothy E. McGraw. 2017. "Distinct Akt Phosphorylation States Are Required for Insulin Regulated Glut4 and Glut1-Mediated Glucose Uptake." ELife. June 7, 2017. https://doi.org/10.7554/eLife.26896.
Berry, Ryan, and Matthew S. Rodeheffer. 2013. "Characterization of the Adipocyte Cellular Lineage in Vivo." *Nature Cell Biology* 15 (3): 302–8. https://doi.org/10.1038/ncb2696.
Bjørndal, Bodil, Lena Burri, Vidar Staalesen, Jon Skorve, and Rolf K. Berge. 2011. "Different Adipose Depots: Their Role in the Development of Metabolic Syndrome and Mitochondrial Response to Hypolipidemic Agents." *Journal of Obesity* 2011: 1–15. https://doi.org/10.1155/2011/490650.
Björntorp, P. 1991. "Adipose Tissue Distribution and Function." *International Journal of Obesity* 15 Suppl 2 (September): 67–81.
Blázquez-Medela, Ana M., Medet Jumabay, Prashant Rajbhandari, Tamer Sallam, Yina Guo, Jiayi Yao, Laurent Vergnes, et al. 2019. "Noggin Depletion in Adipocytes Promotes Obesity in Mice." *Molecular Metabolism* 25: 50–63. https://doi.org/10.1016/j.molmet.2019.04.004.
Booth, A. D., A. M. Magnuson, J. Fouts, Y. Wei, D. Wang, M. J. Pagliassotti, and M. T. Foster. 2018. "Subcutaneous Adipose Tissue Accumulation Protects Systemic Glucose Tolerance and Muscle Metabolism." *Adipocyte* 7 (4): 261–72. https://doi.org/10.1080/21623945.2018.1525252.
Brewer, Paul Duffield, Irina Romenskaia, Mark A. Kanow, and Cynthia Corley Mastick. 2011. "Loss of AS160 Akt Substrate Causes Glut4 Protein to Accumulate in Compartments That Are Primed for Fusion in Basal Adipocytes." *The Journal of Biological Chemistry* 286 (30): 26287–97. https://doi.org/10.1074/jbc.M111.253880.

Brunmeir, Reinhard, and Feng Xu. 2018. “Functional Regulation of PPARs through Post-Translational Modifications.” *International Journal of Molecular Sciences* 19 (6). https://doi.org/10.3390/ijms19061738.
Brunn, G. J., C. C. Hudson, A. Sekulić, J. M. Williams, H. Hosoi, P. J. Houghton, J. C. Lawrence, and R. T. Abraham. 1997. “Phosphorylation of the Translational Repressor PHAS-I by the Mammalian Target of Rapamycin.” *Science (New York, N.Y.)* 277 (5322): 99–101. https://doi.org/10.1126/science.277.5322.99.
Brussaard, H. E., J. A. Gevers Leuven, M. Frölich, C. Kluft, and H. M. Krans. 1997. “Short-Term Oestrogen Replacement Therapy Improves Insulin Resistance, Lipids and Fibrinolysis in Postmenopausal Women with NIDDM.” *Diabetologia* 40 (7): 843–49. https://doi.org/10.1007/s001250050758.
Bulusu, Vinay, Sergey Tumanov, Evdokia Michalopoulou, Niels J. van den Broek, Gillian MacKay, Colin Nixon, Sandeep Dhayade, et al. 2017. “Acetate Recapturing by Nuclear Acetyl-CoA Synthetase 2 Prevents Loss of Histone Acetylation during Oxygen and Serum Limitation.” *Cell Reports* 18 (3): 647–58. https://doi.org/10.1016/j.celrep.2016.12.055.
Burnett, P. E., R. K. Barrow, N. A. Cohen, S. H. Snyder, and D. M. Sabatini. 1998. “RAFT1 Phosphorylation of the Translational Regulators P70 S6 Kinase and 4E-BP1.” *Proceedings of the National Academy of Sciences of the United States of America* 95 (4): 1432–37. https://doi.org/10.1073/pnas.95.4.1432.
Cai, Ling, Benjamin M. Sutter, Bing Li, and Benjamin P. Tu. 2011. “Acetyl-CoA Induces Cell Growth and Proliferation by Promoting the Acetylation of Histones at Growth Genes.” *Molecular Cell* 42 (4): 426–37. https://doi.org/10.1016/j.molcel.2011.05.004.
Calejman, C. Martinez, S. Trefely, S. W. Entwisle, A. Luciano, S. M. Jung, W. Hsiao, A. Torres, et al. 2020. “MTORC2-AKT Signaling to ATP-Citrate Lyase Drives Brown Adipogenesis and de Novo Lipogenesis.” *Nature Communications* 11 (1): 1–16. https://doi.org/10.1038/s41467-020-14430-w.
Campbell, Sydney L., and Kathryn E. Wellen. 2018. “Metabolic Signaling to the Nucleus in Cancer.” *Molecular Cell* 71 (3): 398–408. https://doi.org/10.1016/j.molcel.2018.07.015.
Cao, Haiming, Kristin Gerhold, Jared R. Mayers, Michelle M. Wiest, Steven M. Watkins, and Gökhan S. Hotamisligil. 2008. “Identification of a Lipokine, a Lipid Hormone Linking Adipose Tissue to Systemic Metabolism.” *Cell* 134 (6): 933–44. https://doi.org/10.1016/j.cell.2008.07.048.
Cao, Z., R. M. Umek, and S. L. McKnight. 1991. “Regulated Expression of Three C/EBP Isoforms during Adipose Conversion of 3T3-L1 Cells.” *Genes & Development* 5 (9): 1538–52. https://doi.org/10.1101/gad.5.9.1538.
Cariou, Bertrand, Bernard Charbonnel, and Bart Staels. 2012. “Thiazolidinediones and PPARγ Agonists: Time for a Reassessment.”

Trends in Endocrinology and Metabolism: TEM 23 (5): 205–15. https://doi.org/10.1016/j.tem.2012.03.001.
Carrer, Alessandro, Joshua L. D. Parris, Sophie Trefely, Ryan A. Henry, David C. Montgomery, AnnMarie Torres, John M. Viola, et al. 2017. “Impact of a High-Fat Diet on Tissue Acyl-CoA and Histone Acetylation Levels.” *Journal of Biological Chemistry* 292 (8): 3312–22. https://doi.org/10.1074/jbc.M116.750620.
Cawthorn, William P., Erica L. Scheller, Brian S. Learman, Sebastian D. Parlee, Becky R. Simon, Hiroyuki Mori, Xiaomin Ning, et al. 2014. “Bone Marrow Adipose Tissue Is an Endocrine Organ That Contributes to Increased Circulating Adiponectin during Caloric Restriction.” *Cell Metabolism* 20 (2): 368–75. https://doi.org/10.1016/j.cmet.2014.06.003.
Chatzigeorgiou, Antonios, and Triantafyllos Chavakis. 2016. “Immune Cells and Metabolism.” *Handbook of Experimental Pharmacology* 233: 221–49. https://doi.org/10.1007/164_2015_8.
Chau, You-Ying, Roberto Bandiera, Alan Serrels, Ofelia M. Martínez-Estrada, Wei Qing, Martin Lee, Joan Slight, et al. 2014. “Visceral and Subcutaneous Fat Have Different Origins and Evidence Supports a Mesothelial Source.” *Nature Cell Biology* 16 (4): 367–75. https://doi.org/10.1038/ncb2922.
Chau, You-Ying, David Brownstein, Heidi Mjoseng, Wen-Chin Lee, Natalija Buza-Vidas, Claus Nerlov, Sten Eirik Jacobsen, et al. 2011. “Acute Multiple Organ Failure in Adult Mice Deleted for the Developmental Regulator Wt1.” *PLoS Genetics* 7 (12): e1002404. https://doi.org/10.1371/journal.pgen.1002404.
Chen, Jianquan, Nilsson Holguin, Yu Shi, Matthew J. Silva, and Fanxin Long. 2015. “MTORC2 Signaling Promotes Skeletal Growth and Bone Formation in Mice.” *Journal of Bone and Mineral Research: The Official Journal of the American Society for Bone and Mineral Research* 30 (2): 369–78. https://doi.org/10.1002/jbmr.2348.
Chen, Rui, Min Xu, Jason Nagati, and Joseph A. Garcia. 2017. “Coordinate Regulation of Stress Signaling and Epigenetic Events by Acss2 and HIF-2 in Cancer Cells.” *PloS One* 12 (12): e0190241. https://doi.org/10.1371/journal.pone.0190241.
Chen, S., B. A. Johnson, Y. Li, S. Aster, B. McKeever, R. Mosley, D. E. Moller, and G. Zhou. 2000. “Both Coactivator LXXLL Motif-Dependent and -Independent Interactions Are Required for Peroxisome Proliferator-Activated Receptor Gamma (PPARgamma) Function.” *The Journal of Biological Chemistry* 275 (6): 3733–36. https://doi.org/10.1074/jbc.275.6.3733.
Chen, Shuai, David H. Wasserman, Carol MacKintosh, and Kei Sakamoto. 2011. “Mice with AS160/TBC1D4-Thr649Ala Knockin Mutation Are Glucose Intolerant with Reduced Insulin Sensitivity and Altered GLUT4 Trafficking.” *Cell Metabolism* 13 (1): 68–79. https://doi.org/10.1016/j.cmet.2010.12.005.

Chen, W. S., P. Z. Xu, K. Gottlob, M. L. Chen, K. Sokol, T. Shiyanova, I. Roninson, et al. 2001. “Growth Retardation and Increased Apoptosis in Mice with Homozygous Disruption of the Akt1 Gene.” *Genes & Development* 15 (17): 2203–8. https://doi.org/10.1101/gad.913901.

Chen, Xuqi, Rebecca McClusky, Yuichiro Itoh, Karen Reue, and Arthur P. Arnold. 2013. “X and Y Chromosome Complement Influence Adiposity and Metabolism in Mice.” *Endocrinology* 154 (3): 1092–1104. https://doi.org/10.1210/en.2012-2098.

Chen, Yaqing, Jianchang Qian, Qun He, Hui Zhao, Lourdes Toral-Barza, Celine Shi, Xuesai Zhang, Jiang Wu, and Ker Yu. 2016. “MTOR Complex-2 Stimulates Acetyl-CoA and de Novo Lipogenesis through ATP Citrate Lyase in HER2/PIK3CA-Hyperactive Breast Cancer.” *Oncotarget* 7 (18): 25224–40. https://doi.org/10.18632/oncotarget.8279.

Chiu, Sally, Kathleen Mulligan, and Jean-Marc Schwarz. 2018. “Dietary Carbohydrates and Fatty Liver Disease: De Novo Lipogenesis.” *Current Opinion in Clinical Nutrition and Metabolic Care* 21 (4): 277–82. https://doi.org/10.1097/MCO.0000000000000469.

Cho, H., J. L. Thorvaldsen, Q. Chu, F. Feng, and M. J. Birnbaum. 2001. “Akt1/PKBalpha Is Required for Normal Growth but Dispensable for Maintenance of Glucose Homeostasis in Mice.” *The Journal of Biological Chemistry* 276 (42): 38349–52. https://doi.org/10.1074/jbc.C100462200.

Cho, Han, James Mu, Jason K. Kim, Joanne L. Thorvaldsen, Qingwei Chu, E. Bryan Crenshaw, Klaus H. Kaestner, Marisa S. Bartolomei, Gerald I. Shulman, and Morris J. Birnbaum. 2001. “Insulin Resistance and a Diabetes Mellitus-Like Syndrome in Mice Lacking the Protein Kinase Akt2 (PKBβ).” *Science* 292 (5522): 1728–31. https://doi.org/10.1126/science.292.5522.1728.

Choi, Jang Hyun, Alexander S. Banks, Jennifer L. Estall, Shingo Kajimura, Pontus Boström, Dina Laznik, Jorge L. Ruas, et al. 2010. “Anti-Diabetic Drugs Inhibit Obesity-Linked Phosphorylation of PPARgamma by Cdk5.” *Nature* 466 (7305): 451–56. https://doi.org/10.1038/nature09291.

Choi, Jang Hyun, Sun-Sil Choi, Eun Sun Kim, Mark P. Jedrychowski, Yong Ryoul Yang, Hyun-Jun Jang, Pann-Ghill Suh, Alexander S. Banks, Steven P. Gygi, and Bruce M. Spiegelman. 2014. “Thrap3 Docks on Phosphoserine 273 of PPARγ and Controls Diabetic Gene Programming.” *Genes & Development* 28 (21): 2361–69. https://doi.org/10.1101/gad.249367.114.

Cinti, Saverio. 2017. “UCP1 Protein: The Molecular Hub of Adipose Organ Plasticity.” *Biochimie* 134 (March): 71–76. https://doi.org/10.1016/j.biochi.2016.09.008.

Collins, Jennifer M., Matt J. Neville, Katherine E. Pinnick, Leanne Hodson, Bente Ruyter, Theo H. van Dijk, Dirk-Jan Reijngoud, Mark D. Fielding, and Keith N. Frayn. 2011. “De Novo Lipogenesis in the Differentiating Human Adipocyte Can Provide All Fatty Acids Necessary for Maturation.” *Journal of Lipid Research* 52 (9): 1683–92. https://doi.org/10.1194/jlr.M012195.

Comerford, Sarah A., Zhiguang Huang, Xinlin Du, Yun Wang, Ling Cai, Agnes K. Witkiewicz, Holly Walters, et al. 2014. “Acetate Dependence of Tumors.” *Cell* 159 (7): 1591–1602. https://doi.org/10.1016/j.cell.2014.11.020.

Compe, Emmanuel, Pascal Drané, Camille Laurent, Karin Diderich, Cathy Braun, Jan H. J. Hoeijmakers, and Jean-Marc Egly. 2005. “Dysregulation of the Peroxisome Proliferator-Activated Receptor Target Genes by XPD Mutations.” *Molecular and Cellular Biology* 25 (14): 6065–76. https://doi.org/10.1128/MCB.25.14.6065-6076.2005.

Cristancho, Ana G., and Mitchell A. Lazar. 2011. “Forming Functional Fat: A Growing Understanding of Adipocyte Differentiation.” *Nature Reviews. Molecular Cell Biology* 12 (11): 722–34. https://doi.org/10.1038/nrm3198.

Cybulski, Nadine, Pazit Polak, Johan Auwerx, Markus A. Rüegg, and Michael N. Hall. 2009. “MTOR Complex 2 in Adipose Tissue Negatively Controls Whole-Body Growth.” *Proceedings of the National Academy of Sciences of the United States of America* 106 (24): 9902–7. https://doi.org/10.1073/pnas.0811321106.

Daitoku, Hiroaki, Jun-ichi Sakamaki, and Akiyoshi Fukamizu. 2011. “Regulation of FoxO Transcription Factors by Acetylation and Protein–Protein Interactions.” *Biochimica et Biophysica Acta (BBA) - Molecular Cell Research* 1813 (11): 1954–60. https://doi.org/10.1016/j.bbamcr.2011.03.001.

Davies, Michael N., Brennon L. O’Callaghan, and Howard C. Towle. 2008. “Glucose Activates ChREBP by Increasing Its Rate of Nuclear Entry and Relieving Repression of Its Transcriptional Activity.” *Journal of Biological Chemistry* 283 (35): 24029–38. https://doi.org/10.1074/jbc.M801539200.

Deng, Tuo, Joey Liu, Yanru Deng, Laurie Minze, Xiang Xiao, Valerie Wright, Richeng Yu, et al. 2017. “Adipocyte Adaptive Immunity Mediates Diet-Induced Adipose Inflammation and Insulin Resistance by Decreasing Adipose Treg Cells.” *Nature Communications* 8 (July). https://doi.org/10.1038/ncomms15725.

Dentin, Renaud, Lidia Tomas-Cobos, Fabienne Foufelle, Jane Leopold, Jean Girard, Catherine Postic, and Pascal Ferré. 2012. “Glucose 6-Phosphate, Rather than Xylulose 5-Phosphate, Is Required for the Activation of ChREBP in Response to Glucose in the Liver.” *Journal of Hepatology* 56 (1): 199–209. https://doi.org/10.1016/j.jhep.2011.07.019.

Dobin, Alexander, Carrie A. Davis, Felix Schlesinger, Jorg Drenkow, Chris Zaleski, Sonali Jha, Philippe Batut, Mark Chaisson, and Thomas R. Gingeras. 2013. “STAR: Ultrafast Universal RNA-Seq Aligner.” *Bioinformatics* 29 (1): 15–21. https://doi.org/10.1093/bioinformatics/bts635.

Dos D. Sarbassov, Siraj M Ali, Do-Hyung Kim, David A Guertin, Robert R Latek, Hediye Erdjument-Bromage, Paul Tempst, and David M Sabatini. 2004. “Rictor, a Novel Binding Partner of MTOR, Defines a Rapamycin-Insensitive and Raptor-Independent Pathway That Regulates the

Cytoskeleton." *Current Biology* 14 (14): 1296–1302. https://doi.org/10.1016/j.cub.2004.06.054.
Drolet, R., C. Richard, A. D. Sniderman, J. Mailloux, M. Fortier, C. Huot, C. Rhéaume, and A. Tchernof. 2008. "Hypertrophy and Hyperplasia of Abdominal Adipose Tissues in Women." *International Journal of Obesity (2005)* 32 (2): 283–91. https://doi.org/10.1038/sj.ijo.0803708.
Dubikovskaya, Elena, Rostislav Chudnovskiy, Grigory Karateev, Hyo Min Park, and Andreas Stahl. 2014. "Measurement of Long-Chain Fatty Acid Uptake into Adipocytes." *Methods in Enzymology* 538: 107–34. https://doi.org/10.1016/B978-0-12-800280-3.00007-4.
Dummler, B., and B.A. Hemmings. 2007. "Physiological Roles of PKB/Akt Isoforms in Development and Disease." *Biochemical Society Transactions* 35 (2): 231–35. https://doi.org/10.1042/BST0350231.
Eckel, Robert H., Steven E. Kahn, Ele Ferrannini, Allison B. Goldfine, David M. Nathan, Michael W. Schwartz, Robert J. Smith, and Steven R. Smith. 2011. "Obesity and Type 2 Diabetes: What Can Be Unified and What Needs to Be Individualized?" *The Journal of Clinical Endocrinology and Metabolism* 96 (6): 1654–63. https://doi.org/10.1210/jc.2011-0585.
Eguchi, Jun, Xun Wang, Songtao Yu, Erin E. Kershaw, Patricia C. Chiu, Joanne Dushay, Jennifer L. Estall, Ulf Klein, Eleftheria Maratos-Flier, and Evan D. Rosen. 2011. "Transcriptional Control of Adipose Lipid Handling by IRF4." *Cell Metabolism* 13 (3): 249–59. https://doi.org/10.1016/j.cmet.2011.02.005.
Eissing, Leah, Thomas Scherer, Klaus Tödter, Uwe Knippschild, Jan Willem Greve, Wim A. Buurman, Hans O. Pinnschmidt, et al. 2013. "De Novo Lipogenesis in Human Fat and Liver Is Linked to ChREBP-β and Metabolic Health." *Nature Communications* 4: 1528. https://doi.org/10.1038/ncomms2537.
Elbers, J. M., H. Asscheman, J. C. Seidell, and L. J. Gooren. 1999. "Effects of Sex Steroid Hormones on Regional Fat Depots as Assessed by Magnetic Resonance Imaging in Transsexuals." *The American Journal of Physiology* 276 (2): E317-325. https://doi.org/10.1152/ajpendo.1999.276.2.E317.
Evans, David J., Raymond G. Hoffmann, Ronald K. Kalkhoff, and Ahmed H. Kissebah. 1983. "Relationship of Androgenic Activity to Body Fat Topography, Fat Cell Morphology, and Metabolic Aberrations in Premenopausal Women*." *The Journal of Clinical Endocrinology & Metabolism* 57 (2): 304–10. https://doi.org/10.1210/jcem-57-2-304.
Facchinetti, Valeria, Weiming Ouyang, Hua Wei, Nelyn Soto, Adam Lazorchak, Christine Gould, Carolyn Lowry, et al. 2008. "The Mammalian Target of Rapamycin Complex 2 Controls Folding and Stability of Akt and Protein Kinase C." *The EMBO Journal* 27 (14): 1932–43. https://doi.org/10.1038/emboj.2008.120.

Farmer, Stephen R. 2006. “Transcriptional Control of Adipocyte Formation.” *Cell Metabolism* 4 (4): 263–73. https://doi.org/10.1016/j.cmet.2006.07.001.
Fasshauer, M., J. Klein, K. Ueki, K. M. Kriauciunas, M. Benito, M. F. White, and C. R. Kahn. 2000. “Essential Role of Insulin Receptor Substrate-2 in Insulin Stimulation of Glut4 Translocation and Glucose Uptake in Brown Adipocytes.” *The Journal of Biological Chemistry* 275 (33): 25494–501. https://doi.org/10.1074/jbc.M004046200.
Fernandez, Sully, John M. Viola, AnnMarie Torres, Martina Wallace, Sophie Trefely, Steven Zhao, Hayley C. Affronti, et al. 2019. “Adipocyte ACLY Facilitates Dietary Carbohydrate Handling to Maintain Metabolic Homeostasis in Females.” *Cell Reports* 27 (9): 2772-2784.e6. https://doi.org/10.1016/j.celrep.2019.04.112.
Ferrara, Daniele, Fabrizio Montecucco, Franco Dallegri, and Federico Carbone. 2019. “Impact of Different Ectopic Fat Depots on Cardiovascular and Metabolic Diseases.” *Journal of Cellular Physiology*, May. https://doi.org/10.1002/jcp.28821.
Fischer-Posovszky, Pamela, Daniel Tews, Sina Horenburg, Klaus-Michael Debatin, and Martin Wabitsch. 2012. “Differential Function of Akt1 and Akt2 in Human Adipocytes.” *Molecular and Cellular Endocrinology* 358 (1): 135–43. https://doi.org/10.1016/j.mce.2012.03.018.
Fitzgerald, Sarah Jayne, Amol Vijay Janorkar, Allison Barnes, and Rodrigo Oscar Maranon. 2018. “A New Approach to Study the Sex Differences in Adipose Tissue.” *Journal of Biomedical Science* 25 (1): 89. https://doi.org/10.1186/s12929-018-0488-3.
Floyd, Z. Elizabeth, and Jacqueline M. Stephens. 2004. “Control of Peroxisome Proliferator-Activated Receptor Gamma2 Stability and Activity by SUMOylation.” *Obesity Research* 12 (6): 921–28. https://doi.org/10.1038/oby.2004.112.
Foo, Shane S., Christopher J. Turner, Susanne Adams, Amelia Compagni, Deborah Aubyn, Naoko Kogata, Per Lindblom, Moshe Shani, Daniel Zicha, and Ralf H. Adams. 2006. “Ephrin-B2 Controls Cell Motility and Adhesion during Blood-Vessel-Wall Assembly.” *Cell* 124 (1): 161–73. https://doi.org/10.1016/j.cell.2005.10.034.
Foster, K S J, W J McCrary, J S Ross, and C F Wright. 2006. “Members of the HSWI/SNF Chromatin Remodeling Complex Associate with and Are Phosphorylated by Protein Kinase B/Akt.” *Oncogene* 25 (33): 4605–12. https://doi.org/10.1038/sj.onc.1209496.
Foster, M. T., H. Shi, S. Softic, R. Kohli, R. J. Seeley, and S. C. Woods. 2011. “Transplantation of Non-Visceral Fat to the Visceral Cavity Improves Glucose Tolerance in Mice: Investigation of Hepatic Lipids and Insulin Sensitivity.” *Diabetologia* 54 (11): 2890–99. https://doi.org/10.1007/s00125-011-2259-5.
Foster, M. T., S. Softic, J. Caldwell, R. Kohli, A. D. de Kloet, and R. J. Seeley. 2013. “Subcutaneous Adipose Tissue Transplantation in Diet-Induced

Obese Mice Attenuates Metabolic Dysregulation While Removal Exacerbates It." *Physiological Reports* 1 (2). https://doi.org/10.1002/phy2.15.

Fox, Caroline S., Joseph M. Massaro, Udo Hoffmann, Karla M. Pou, Pal Maurovich-Horvat, Chun-Yu Liu, Ramachandran S. Vasan, et al. 2007. "Abdominal Visceral and Subcutaneous Adipose Tissue Compartments: Association with Metabolic Risk Factors in the Framingham Heart Study." *Circulation* 116 (1): 39–48. https://doi.org/10.1161/CIRCULATIONAHA.106.675355.

Fuente-Martín, Esther, Pilar Argente-Arizón, Purificación Ros, Jesús Argente, and Julie A Chowen. 2013. "Sex Differences in Adipose Tissue: It Is Not Only a Question of Quantity and Distribution." *Adipocyte* 2 (3): 128–34. https://doi.org/10.4161/adip.24075.

Fujita, T., Y. Sugiyama, S. Taketomi, T. Sohda, Y. Kawamatsu, H. Iwatsuka, and Z. Suzuoki. 1983. "Reduction of Insulin Resistance in Obese and/or Diabetic Animals by 5-[4-(1-Methylcyclohexylmethoxy)Benzyl]-Thiazolidine-2,4-Dione (ADD-3878, U-63,287, Ciglitazone), a New Antidiabetic Agent." *Diabetes* 32 (9): 804–10. https://doi.org/10.2337/diab.32.9.804.

Galarraga, Miguel, Javier Campión, Arrate Muñoz-Barrutia, Noemí Boqué, Haritz Moreno, José Alfredo Martínez, Fermín Milagro, and Carlos Ortiz-de-Solórzano. 2012. "Adiposoft: Automated Software for the Analysis of White Adipose Tissue Cellularity in Histological Sections." *Journal of Lipid Research* 53 (12): 2791–96. https://doi.org/10.1194/jlr.D023788.

Galdieri, Luciano, Jennifer Chang, Swati Mehrotra, and Ales Vancura. 2013. "Yeast Phospholipase C Is Required for Normal Acetyl-CoA Homeostasis and Global Histone Acetylation." *Journal of Biological Chemistry* 288 (39): 27986–98. https://doi.org/10.1074/jbc.M113.492348.

Galdieri, Luciano, and Ales Vancura. 2012. "Acetyl-CoA Carboxylase Regulates Global Histone Acetylation." *Journal of Biological Chemistry* 287 (28): 23865–76. https://doi.org/10.1074/jbc.M112.380519.

Galdieri, Luciano, Tiantian Zhang, Daniella Rogerson, Rron Lleshi, and Ales Vancura. 2014. "Protein Acetylation and Acetyl Coenzyme A Metabolism in Budding Yeast." *Eukaryotic Cell* 13 (12): 1472–83. https://doi.org/10.1128/EC.00189-14.

García-Martínez, Juan M., and Dario R. Alessi. 2008. "MTOR Complex 2 (MTORC2) Controls Hydrophobic Motif Phosphorylation and Activation of Serum- and Glucocorticoid-Induced Protein Kinase 1 (SGK1)." *Biochemical Journal* 416 (3): 375–85. https://doi.org/10.1042/BJ20081668.

Garofalo, Robert S., Stephen J. Orena, Kristina Rafidi, Anthony J. Torchia, Jeffrey L. Stock, Audrey L. Hildebrandt, Timothy Coskran, et al. 2003. "Severe Diabetes, Age-Dependent Loss of Adipose Tissue, and Mild Growth Deficiency in Mice Lacking Akt2/PKBβ." *Journal of Clinical Investigation* 112 (2): 197–208. https://doi.org/10.1172/JCI16885.

Gearing, K. L., M. Göttlicher, M. Teboul, E. Widmark, and J. A. Gustafsson. 1993. “Interaction of the Peroxisome-Proliferator-Activated Receptor and Retinoid X Receptor.” *Proceedings of the National Academy of Sciences of the United States of America* 90 (4): 1440–44. https://doi.org/10.1073/pnas.90.4.1440.

Gelman, L., G. Zhou, L. Fajas, E. Raspé, J. C. Fruchart, and J. Auwerx. 1999. “P300 Interacts with the N- and C-Terminal Part of PPARgamma2 in a Ligand-Independent and -Dependent Manner, Respectively.” *The Journal of Biological Chemistry* 274 (12): 7681–88. https://doi.org/10.1074/jbc.274.12.7681.

Giordano, Antonio, Arianna Smorlesi, Andrea Frontini, Giorgio Barbatelli, and Saverio Cinti. 2014. “MECHANISMS IN ENDOCRINOLOGY: White, Brown and Pink Adipocytes: The Extraordinary Plasticity of the Adipose Organ.” *European Journal of Endocrinology* 170 (5): R159–71. https://doi.org/10.1530/EJE-13-0945.

Gonzalez, Eva, Emily Flier, Dorothee Molle, Domenico Accili, and Timothy E. McGraw. 2011. “Hyperinsulinemia Leads to Uncoupled Insulin Regulation of the GLUT4 Glucose Transporter and the FoxO1 Transcription Factor.” *Proceedings of the National Academy of Sciences* 108 (25): 10162–67. https://doi.org/10.1073/pnas.1019268108.

Gonzalez, Eva, and Timothy E. McGraw. 2006. “Insulin Signaling Diverges into Akt-Dependent and -Independent Signals to Regulate the Recruitment/Docking and the Fusion of GLUT4 Vesicles to the Plasma Membrane.” *Molecular Biology of the Cell* 17 (10): 4484–93. https://doi.org/10.1091/mbc.E06-07-0585.

———. 2009. “The Akt Kinases: Isoform Specificity in Metabolism and Cancer.” *Cell Cycle* 8 (16): 2502–8. https://doi.org/10.4161/cc.8.16.9335.

Green, H., and M. Meuth. 1974. “An Established Pre-Adipose Cell Line and Its Differentiation in Culture.” *Cell* 3 (2): 127–33. https://doi.org/10.1016/0092-8674(74)90116-0.

Gu, Yanyun, Jill Lindner, Anil Kumar, Weiping Yuan, and Mark A. Magnuson. 2011. “Rictor/MTORC2 Is Essential for Maintaining a Balance between Beta-Cell Proliferation and Cell Size.” *Diabetes* 60 (3): 827–37. https://doi.org/10.2337/db10-1194.

Guerra, C., P. Navarro, A. M. Valverde, M. Arribas, J. Brüning, L. P. Kozak, C. R. Kahn, and M. Benito. 2001. “Brown Adipose Tissue-Specific Insulin Receptor Knockout Shows Diabetic Phenotype without Insulin Resistance.” *The Journal of Clinical Investigation* 108 (8): 1205–13. https://doi.org/10.1172/JCI13103.

Guertin, David A., Deanna M. Stevens, Carson C. Thoreen, Aurora A. Burds, Nada Y. Kalaany, Jason Moffat, Michael Brown, Kevin J. Fitzgerald, and David M. Sabatini. 2006. “Ablation in Mice of the MTORC Components Raptor, Rictor, or MLST8 Reveals That MTORC2 Is Required for

Signaling to Akt-FOXO and PKCα, but Not S6K1." *Developmental Cell* 11 (6): 859–71. https://doi.org/10.1016/j.devcel.2006.10.007.
Guilherme, Adilson, Felipe Henriques, Alexander H. Bedard, and Michael P. Czech. 2019. "Molecular Pathways Linking Adipose Innervation to Insulin Action in Obesity and Diabetes Mellitus." *Nature Reviews. Endocrinology* 15 (4): 207–25. https://doi.org/10.1038/s41574-019-0165-y.
Guilherme, Adilson, David J. Pedersen, Elizabeth Henchey, Felipe S. Henriques, Laura V. Danai, Yuefei Shen, Batuhan Yenilmez, et al. 2017. "Adipocyte Lipid Synthesis Coupled to Neuronal Control of Thermogenic Programming." *Molecular Metabolism* 6 (8): 781–96. https://doi.org/10.1016/j.molmet.2017.05.012.
Guilherme, Adilson, Joseph V. Virbasius, Vishwajeet Puri, and Michael P. Czech. 2008. "Adipocyte Dysfunctions Linking Obesity to Insulin Resistance and Type 2 Diabetes." *Nature Reviews. Molecular Cell Biology* 9 (5): 367–77. https://doi.org/10.1038/nrm2391.
Guo, Zhixin, Keyu Zhao, Xue Feng, Dandan Yan, Ruiyuan Yao, Yuhao Chen, Lili Bao, and Zhigang Wang. 2019. "MTORC2 Regulates Lipogenic Gene Expression through PPARγ to Control Lipid Synthesis in Bovine Mammary Epithelial Cells." *BioMed Research International* 2019 (May). https://doi.org/10.1155/2019/5196028.
Guri, Yakir, Marco Colombi, Eva Dazert, Sravanth K. Hindupur, Jason Roszik, Suzette Moes, Paul Jenoe, et al. 2017. "MTORC2 Promotes Tumorigenesis via Lipid Synthesis." *Cancer Cell* 32 (6): 807-823.e12. https://doi.org/10.1016/j.ccell.2017.11.011.
Hagiwara, Asami, Marion Cornu, Nadine Cybulski, Pazit Polak, Charles Betz, Francesca Trapani, Luigi Terracciano, Markus H. Heim, Markus A. Rüegg, and Michael N. Hall. 2012. "Hepatic MTORC2 Activates Glycolysis and Lipogenesis through Akt, Glucokinase, and SREBP1c." *Cell Metabolism* 15 (5): 725–38. https://doi.org/10.1016/j.cmet.2012.03.015.
Hales, CM, MD Carroll, CD Fryar, and CL Ogden. 2017. "Prevalence o Fobesity among Adults and Youth: United States, 2015-2016." *NCHS Data Brief*, Hyattsville, MD:NAtional Center for Health statistics, 288.
Hammarstedt, Ann, Ismail Syed, Archana Vijayakumar, Björn Eliasson, Silvia Gogg, Barbara B. Kahn, and Ulf Smith. 2018. "Adipose Tissue Dysfunction Is Associated with Low Levels of the Novel Palmitic Acid Hydroxystearic Acids." *Scientific Reports* 8 (1): 15757. https://doi.org/10.1038/s41598-018-34113-3.
Hanahan, Douglas, and Robert A. Weinberg. 2011. "Hallmarks of Cancer: The next Generation." *Cell* 144 (5): 646–74. https://doi.org/10.1016/j.cell.2011.02.013.
Harada, Naomoto, Zenjun Oda, Yoshikazu Hara, Koji Fujinami, Mayumi Okawa, Katsuya Ohbuchi, Mari Yonemoto, et al. 2007. "Hepatic de Novo Lipogenesis Is Present in Liver-Specific ACC1-Deficient Mice." *Molecular*

and Cellular Biology 27 (5): 1881–88. https://doi.org/10.1128/MCB.01122-06.
Hauner, Hans. 2002. “The Mode of Action of Thiazolidinediones.” *Diabetes/Metabolism Research and Reviews* 18 Suppl 2 (April): S10-15. https://doi.org/10.1002/dmrr.249.
He, Weimin, Yaacov Barak, Andrea Hevener, Peter Olson, Debbie Liao, Jamie Le, Michael Nelson, Estelita Ong, Jerrold M. Olefsky, and Ronald M. Evans. 2003. “Adipose-Specific Peroxisome Proliferator-Activated Receptor Gamma Knockout Causes Insulin Resistance in Fat and Liver but Not in Muscle.” *Proceedings of the National Academy of Sciences of the United States of America* 100 (26): 15712–17. https://doi.org/10.1073/pnas.2536828100.
Helenius, Katja, Ying Yang, Jukka Alasaari, and Tomi P. Mäkelä. 2009. “Mat1 Inhibits Peroxisome Proliferator-Activated Receptor Gamma-Mediated Adipocyte Differentiation.” *Molecular and Cellular Biology* 29 (2): 315–23. https://doi.org/10.1128/MCB.00347-08.
Herman, Mark A., Odile D. Peroni, Jorge Villoria, Michael R. Schön, Nada A. Abumrad, Matthias Blüher, Samuel Klein, and Barbara B. Kahn. 2012. “A Novel ChREBP Isoform in Adipose Tissue Regulates Systemic Glucose Metabolism.” *Nature* 484 (7394): 333–38. https://doi.org/10.1038/nature10986.
Hiraoka, D., E. Okumura, and T. Kishimoto. 2011. “Turn Motif Phosphorylation Negatively Regulates Activation Loop Phosphorylation in Akt.” *Oncogene* 30 (44): 4487–97. https://doi.org/10.1038/onc.2011.155.
Hocking, S. L., D. J. Chisholm, and D. E. James. 2008. “Studies of Regional Adipose Transplantation Reveal a Unique and Beneficial Interaction between Subcutaneous Adipose Tissue and the Intra-Abdominal Compartment.” *Diabetologia* 51 (5): 900–902. https://doi.org/10.1007/s00125-008-0969-0.
Hosick, Peter, Mary Weeks, Michael Hankins, Kyle Moore, and David Stec. 2017. “Sex-Dependent Effects of HO-1 Deletion from Adipocytes in Mice.” *International Journal of Molecular Sciences* 18 (3): 611. https://doi.org/10.3390/ijms18030611.
Hresko, Richard C., and Mike Mueckler. 2005. “MTOR·RICTOR Is the Ser473 Kinase for Akt/Protein Kinase B in 3T3-L1 Adipocytes.” *Journal of Biological Chemistry* 280 (49): 40406–16. https://doi.org/10.1074/jbc.M508361200.
Hu, E., J. B. Kim, P. Sarraf, and B. M. Spiegelman. 1996. “Inhibition of Adipogenesis through MAP Kinase-Mediated Phosphorylation of PPARgamma.” *Science (New York, N.Y.)* 274 (5295): 2100–2103. https://doi.org/10.1126/science.274.5295.2100.
Huang, Da Wei, Brad T. Sherman, and Richard A. Lempicki. 2009a. “Systematic and Integrative Analysis of Large Gene Lists Using DAVID Bioinformatics

Resources.” *Nature Protocols* 4 (1): 44–57. https://doi.org/10.1038/nprot.2008.211.
———. 2009b. “Bioinformatics Enrichment Tools: Paths toward the Comprehensive Functional Analysis of Large Gene Lists.” *Nucleic Acids Research* 37 (1): 1–13. https://doi.org/10.1093/nar/gkn923.
Huang, Zhiguang, Menglu Zhang, Abigail A. Plec, Sandi Jo Estill, Ling Cai, Joyce J. Repa, Steven L. McKnight, and Benjamin P. Tu. 2018a. “ACSS2 Promotes Systemic Fat Storage and Utilization through Selective Regulation of Genes Involved in Lipid Metabolism.” *Proceedings of the National Academy of Sciences of the United States of America* 115 (40): E9499–9506. https://doi.org/10.1073/pnas.1806635115.
———. 2018b. “ACSS2 Promotes Systemic Fat Storage and Utilization through Selective Regulation of Genes Involved in Lipid Metabolism.” *Proceedings of the National Academy of Sciences* 115 (40): E9499–9506. https://doi.org/10.1073/pnas.1806635115.
Huh, Jin Young, Yoon Jeong Park, Mira Ham, and Jae Bum Kim. 2014. “Crosstalk between Adipocytes and Immune Cells in Adipose Tissue Inflammation and Metabolic Dysregulation in Obesity.” *Molecules and Cells* 37 (5): 365–71. https://doi.org/10.14348/molcells.2014.0074.
Hung, Chien-Min, Camila Martinez Calejman, Joan Sanchez-Gurmaches, Huawei Li, Clary B. Clish, Simone Hettmer, Amy J. Wagers, and David A. Guertin. 2014a. “Rictor/MTORC2 Loss in the Myf5 Lineage Reprograms Brown Fat Metabolism and Protects Mice against Obesity and Metabolic Disease.” *Cell Reports* 8 (1): 256–71. https://doi.org/10.1016/j.celrep.2014.06.007.
———. 2014b. “Rictor/MTORC2 Loss in the Myf5 Lineage Reprograms Brown Fat Metabolism and Protects Mice against Obesity and Metabolic Disease.” *Cell Reports* 8 (1): 256–71. https://doi.org/10.1016/j.celrep.2014.06.007.
Iankova, Irena, Rasmus K. Petersen, Jean-Sébastien Annicotte, Carine Chavey, Jacob B. Hansen, Irina Kratchmarova, David Sarruf, Monsef Benkirane, Karsten Kristiansen, and Lluis Fajas. 2006. “Peroxisome Proliferator-Activated Receptor Gamma Recruits the Positive Transcription Elongation Factor b Complex to Activate Transcription and Promote Adipogenesis.” *Molecular Endocrinology (Baltimore, Md.)* 20 (7): 1494–1505. https://doi.org/10.1210/me.2005-0222.
Iizuka, Katsumi, Richard K. Bruick, Guosheng Liang, Jay D. Horton, and Kosaku Uyeda. 2004. “Deficiency of Carbohydrate Response Element-Binding Protein (ChREBP) Reduces Lipogenesis as Well as Glycolysis.” *Proceedings of the National Academy of Sciences of the United States of America* 101 (19): 7281–86. https://doi.org/10.1073/pnas.0401516101.
IJpenberg, A., E. Jeannin, W. Wahli, and B. Desvergne. 1997. “Polarity and Specific Sequence Requirements of Peroxisome Proliferator-Activated Receptor (PPAR)/Retinoid X Receptor Heterodimer Binding to DNA. A

Functional Analysis of the Malic Enzyme Gene PPAR Response Element." *The Journal of Biological Chemistry* 272 (32): 20108–17. https://doi.org/10.1074/jbc.272.32.20108.
Ikeda, Kenji, Pema Maretich, and Shingo Kajimura. 2018. "The Common and Distinct Features of Brown and Beige Adipocytes." *Trends in Endocrinology & Metabolism* 29 (3): 191–200. https://doi.org/10.1016/j.tem.2018.01.001.
Ikenoue, Tsuneo, Ken Inoki, Qian Yang, Xiaoming Zhou, and Kun-Liang Guan. 2008. "Essential Function of TORC2 in PKC and Akt Turn Motif Phosphorylation, Maturation and Signalling." *The EMBO Journal* 27 (14): 1919–31. https://doi.org/10.1038/emboj.2008.119.
Jackson, Robert M., Beth A. Griesel, Jami M. Gurley, Luke I. Szweda, and Ann Louise Olson. 2017. "Glucose Availability Controls Adipogenesis in Mouse 3T3-L1 Adipocytes via up-Regulation of Nicotinamide Metabolism." *Journal of Biological Chemistry* 292 (45): 18556–64. https://doi.org/10.1074/jbc.M117.791970.
Jennewein, Carla, Anne-Marie Kuhn, Martina Victoria Schmidt, Virginie Meilladec-Jullig, Andreas von Knethen, Frank J. Gonzalez, and Bernhard Brüne. 2008. "Sumoylation of Peroxisome Proliferator-Activated Receptor Gamma by Apoptotic Cells Prevents Lipopolysaccharide-Induced NCoR Removal from KappaB Binding Sites Mediating Transrepression of Proinflammatory Cytokines." *Journal of Immunology (Baltimore, Md.: 1950)* 181 (8): 5646–52. https://doi.org/10.4049/jimmunol.181.8.5646.
Ji, Suena, Sang Yoon Park, Jürgen Roth, Hoe Suk Kim, and Jin Won Cho. 2012. "O-GlcNAc Modification of PPARγ Reduces Its Transcriptional Activity." *Biochemical and Biophysical Research Communications* 417 (4): 1158–63. https://doi.org/10.1016/j.bbrc.2011.12.086.
Jing, Enxuan, Stephane Gesta, and C. Ronald Kahn. 2007. "SIRT2 Regulates Adipocyte Differentiation through FoxO1 Acetylation/Deacetylation." *Cell Metabolism* 6 (2): 105–14. https://doi.org/10.1016/j.cmet.2007.07.003.
Joffe, Barry I., Vanessa R. Panz, and Frederick J. Raal. 2001. "From Lipodystrophy Syndromes to Diabetes Mellitus." *The Lancet* 357 (9266): 1379–81. https://doi.org/10.1016/S0140-6736(00)04616-X.
Jouihan, Hani. 2012. "Measurement of Liver Triglyceride Content." *BIO-PROTOCOL* 2 (13). https://doi.org/10.21769/BioProtoc.223.
Jung, Su Myung, Chien-Min Hung, Samuel R. Hildebrand, Joan Sanchez-Gurmaches, Barbara Martinez-Pastor, Jivani M. Gengatharan, Martina Wallace, et al. 2019. "Non-Canonical MTORC2 Signaling Regulates Brown Adipocyte Lipid Catabolism through SIRT6-FoxO1." *Molecular Cell* 75 (4): 807-822.e8. https://doi.org/10.1016/j.molcel.2019.07.023.
Kabashima, T., T. Kawaguchi, B. E. Wadzinski, and K. Uyeda. 2003. "Xylulose 5-Phosphate Mediates Glucose-Induced Lipogenesis by Xylulose 5-Phosphate-Activated Protein Phosphatase in Rat Liver." *Proceedings of*

the National Academy of Sciences 100 (9): 5107–12. https://doi.org/10.1073/pnas.0730817100.
Kaelin, William G., and Steven L. McKnight. 2013. “Influence of Metabolism on Epigenetics and Disease.” *Cell* 153 (1): 56–69. https://doi.org/10.1016/j.cell.2013.03.004.
Kahn, C. Ronald, Guoxiao Wang, and Kevin Y. Lee. 2019. “Altered Adipose Tissue and Adipocyte Function in the Pathogenesis of Metabolic Syndrome.” *Journal of Clinical Investigation* 129 (10): 3990–4000. https://doi.org/10.1172/JCI129187.
Kang, Yea Eun, Ji Min Kim, Kyong Hye Joung, Ju Hee Lee, Bo Ram You, Min Jeong Choi, Min Jeong Ryu, et al. 2016. “The Roles of Adipokines, Proinflammatory Cytokines, and Adipose Tissue Macrophages in Obesity-Associated Insulin Resistance in Modest Obesity and Early Metabolic Dysfunction.” *PLOS ONE* 11 (4): e0154003. https://doi.org/10.1371/journal.pone.0154003.
Karastergiou, Kalypso, Steven R. Smith, Andrew S. Greenberg, and Susan K. Fried. 2012. “Sex Differences in Human Adipose Tissues - the Biology of Pear Shape.” *Biology of Sex Differences* 3 (1): 13. https://doi.org/10.1186/2042-6410-3-13.
Kawaguchi, T., M. Takenoshita, T. Kabashima, and K. Uyeda. 2001. “Glucose and CAMP Regulate the L-Type Pyruvate Kinase Gene by Phosphorylation/Dephosphorylation of the Carbohydrate Response Element Binding Protein.” *Proceedings of the National Academy of Sciences* 98 (24): 13710–15. https://doi.org/10.1073/pnas.231370798.
Kawaguchi, Takumi, Kiyoshi Osatomi, Hiromi Yamashita, Tsutomu Kabashima, and Kosaku Uyeda. 2002. “Mechanism for Fatty Acid ‘Sparing’ Effect on Glucose-Induced Transcription: REGULATION OF CARBOHYDRATE-RESPONSIVE ELEMENT-BINDING PROTEIN BY AMP-ACTIVATED PROTEIN KINASE.” *Journal of Biological Chemistry* 277 (6): 3829–35. https://doi.org/10.1074/jbc.M107895200.
Kearney, Alison L., Kristen C. Cooke, Dougall M. Norris, Armella Zadoorian, James R. Krycer, Daniel J. Fazakerley, James G. Burchfield, and David E. James. 2019. “Serine 474 Phosphorylation Is Essential for Maximal Akt2 Kinase Activity in Adipocytes.” *Journal of Biological Chemistry*, September, jbc.RA119.010036. https://doi.org/10.1074/jbc.RA119.010036.
Kim, Hyeonhui, Minki Kim, Sun-Kyoung Im, and Sungsoon Fang. 2018. “Mouse Cre-LoxP System: General Principles to Determine Tissue-Specific Roles of Target Genes.” *Laboratory Animal Research* 34 (4): 147–59. https://doi.org/10.5625/lar.2018.34.4.147.
Kim, Jae Bum, Harold M. Wright, Margaret Wright, and Bruce M. Spiegelman. 1998. “ADD1/SREBP1 Activates PPARγ through the Production of Endogenous Ligand.” *Proceedings of the National Academy of Sciences* 95 (8): 4333–37. https://doi.org/10.1073/pnas.95.8.4333.

Kim, Sang-Nam, Young-Suk Jung, Hyun-Jung Kwon, Je Kyung Seong, James G. Granneman, and Yun-Hee Lee. 2016. “Sex Differences in Sympathetic Innervation and Browning of White Adipose Tissue of Mice.” *Biology of Sex Differences* 7 (1). https://doi.org/10.1186/s13293-016-0121-7.

Krueger, Katherine C., Maria José Costa, Hongqing Du, and Brian J. Feldman. 2014. “Characterization of Cre Recombinase Activity for in Vivo Targeting of Adipocyte Precursor Cells.” *Stem Cell Reports* 3 (6): 1147–58. https://doi.org/10.1016/j.stemcr.2014.10.009.

Krycer, James R., Katsuyuki Yugi, Akiyoshi Hirayama, Daniel J. Fazakerley, Lake-Ee Quek, Richard Scalzo, Satoshi Ohno, et al. 2017. “Dynamic Metabolomics Reveals That Insulin Primes the Adipocyte for Glucose Metabolism.” *Cell Reports* 21 (12): 3536–47. https://doi.org/10.1016/j.celrep.2017.11.085.

Kuda, Ondrej, Marie Brezinova, Martina Rombaldova, Barbora Slavikova, Martin Posta, Petr Beier, Petra Janovska, et al. 2016. “Docosahexaenoic Acid-Derived Fatty Acid Esters of Hydroxy Fatty Acids (FAHFAs) With Anti-Inflammatory Properties.” *Diabetes* 65 (9): 2580–90. https://doi.org/10.2337/db16-0385.

Kumar, Anil, Thurl E. Harris, Susanna R. Keller, Kin M. Choi, Mark A. Magnuson, and John C. Lawrence. 2008. “Muscle-Specific Deletion of Rictor Impairs Insulin-Stimulated Glucose Transport and Enhances Basal Glycogen Synthase Activity.” *Molecular and Cellular Biology* 28 (1): 61–70. https://doi.org/10.1128/MCB.01405-07.

Kumar, Anil, John C. Lawrence, Dae Young Jung, Hwi Jin Ko, Susanna R. Keller, Jason K. Kim, Mark A. Magnuson, and Thurl E. Harris. 2010. “Fat Cell-Specific Ablation of Rictor in Mice Impairs Insulin-Regulated Fat Cell and Whole-Body Glucose and Lipid Metabolism.” *Diabetes* 59 (6): 1397–1406. https://doi.org/10.2337/db09-1061.

Kumar, Chandra C., and Vincent Madison. 2005. “AKT Crystal Structure and AKT-Specific Inhibitors.” *Oncogene* 24 (50): 7493–7501. https://doi.org/10.1038/sj.onc.1209087.

Kursawe, Romy, Sonia Caprio, Cosimo Giannini, Deepak Narayan, Aiping Lin, Ebe D’Adamo, Melissa Shaw, Bridget Pierpont, Samuel W. Cushman, and Gerald I. Shulman. 2013. “Decreased Transcription of ChREBP-α/β Isoforms in Abdominal Subcutaneous Adipose Tissue of Obese Adolescents With Prediabetes or Early Type 2 Diabetes: Associations With Insulin Resistance and Hyperglycemia.” *Diabetes* 62 (3): 837–44. https://doi.org/10.2337/db12-0889.

Kusminski, Christine M., Perry E. Bickel, and Philipp E. Scherer. 2016. “Targeting Adipose Tissue in the Treatment of Obesity-Associated Diabetes.” *Nature Reviews. Drug Discovery* 15 (9): 639–60. https://doi.org/10.1038/nrd.2016.75.

Kwok, Kelvin H. M., Karen S. L. Lam, and Aimin Xu. 2016. “Heterogeneity of White Adipose Tissue: Molecular Basis and Clinical Implications.”

Experimental & Molecular Medicine 48 (March): e215. https://doi.org/10.1038/emm.2016.5.
Kwon, Hyokjoon, and Jeffrey E. Pessin. 2013. “Adipokines Mediate Inflammation and Insulin Resistance.” *Frontiers in Endocrinology* 4 (June). https://doi.org/10.3389/fendo.2013.00071.
Lang, Deborah, Min Min Lu, Li Huang, Kurt A. Engleka, Maozhen Zhang, Emily Y. Chu, Shari Lipner, Arthur Skoultchi, Sarah E. Millar, and Jonathan A. Epstein. 2005. “Pax3 Functions at a Nodal Point in Melanocyte Stem Cell Differentiation.” *Nature* 433 (7028): 884–87. https://doi.org/10.1038/nature03292.
Lee, Cathy C., Josephine Z. Kasa-Vubu, and Mark A. Supiano. 2003. “Differential Effects of Raloxifene and Estrogen on Insulin Sensitivity in Postmenopausal Women.” *Journal of the American Geriatrics Society* 51 (5): 683–88. https://doi.org/10.1034/j.1600-0579.2003.00214.x.
Lee, Joyce V., Alessandro Carrer, Supriya Shah, Nathaniel W. Snyder, Shuanzeng Wei, Sriram Venneti, Andrew J. Worth, et al. 2014. “Akt-Dependent Metabolic Reprogramming Regulates Tumor Cell Histone Acetylation.” *Cell Metabolism* 20 (2): 306–19. https://doi.org/10.1016/j.cmet.2014.06.004.
Lee, Joyce V., Supriya A. Shah, and Kathryn E. Wellen. 2013. “Obesity, Cancer, and Acetyl-CoA Metabolism.” *Drug Discovery Today. Disease Mechanisms* 10 (1–2): e55–61. https://doi.org/10.1016/j.ddmec.2013.03.005.
Lee, Mi-Jeong, Yuanyuan Wu, and Susan K. Fried. 2013. “Adipose Tissue Heterogeneity: Implication of Depot Differences in Adipose Tissue for Obesity Complications.” *Molecular Aspects of Medicine* 34 (1): 1–11. https://doi.org/10.1016/j.mam.2012.10.001.
Lee, Peter L., Su Myung Jung, and David A. Guertin. 2017. “The Complex Roles of Mechanistic Target of Rapamycin in Adipocytes and Beyond.” *Trends in Endocrinology and Metabolism: TEM* 28 (5): 319–39. https://doi.org/10.1016/j.tem.2017.01.004.
Lefterova, Martina I., Anders K. Haakonsson, Mitchell A. Lazar, and Susanne Mandrup. 2014. “PPARγ and the Global Map of Adipogenesis and Beyond.” *Trends in Endocrinology and Metabolism: TEM* 25 (6): 293–302. https://doi.org/10.1016/j.tem.2014.04.001.
Lefterova, Martina I., David J. Steger, David Zhuo, Mohammed Qatanani, Shannon E. Mullican, Geetu Tuteja, Elisabetta Manduchi, Gregory R. Grant, and Mitchell A. Lazar. 2010. “Cell-Specific Determinants of Peroxisome Proliferator-Activated Receptor Gamma Function in Adipocytes and Macrophages.” *Molecular and Cellular Biology* 30 (9): 2078–89. https://doi.org/10.1128/MCB.01651-09.
Lefterova, Martina I., Yong Zhang, David J. Steger, Michael Schupp, Jonathan Schug, Ana Cristancho, Dan Feng, et al. 2008. “PPARgamma and C/EBP Factors Orchestrate Adipocyte Biology via Adjacent Binding on a

Genome-Wide Scale." *Genes & Development* 22 (21): 2941–52. https://doi.org/10.1101/gad.1709008.
Lepper, Christoph, Simon J. Conway, and Chen-Ming Fan. 2009. "Adult Satellite Cells and Embryonic Muscle Progenitors Have Distinct Genetic Requirements." *Nature* 460 (7255): 627–31. https://doi.org/10.1038/nature08209.
Lepper, Christoph, and Chen-Ming Fan. 2010. "Inducible Lineage Tracing of Pax7-Descendant Cells Reveals Embryonic Origin of Adult Satellite Cells." *Genesis* 48 (7): 424–36. https://doi.org/10.1002/dvg.20630.
Lessard, Julie, and André Tchernof. 2012. "Depot- and Obesity-Related Differences in Adipogenesis." *Clinical Lipidology* 7 (5): 587–96. https://doi.org/10.2217/clp.12.49.
Li, Qiwen, Yunshu Wu, and Ning Kang. 2018. "Marrow Adipose Tissue: Its Origin, Function, and Regulation in Bone Remodeling and Regeneration." Research article. Stem Cells International. 2018. https://doi.org/10.1155/2018/7098456.
Li, Xinjian, Willie Yu, Xu Qian, Yan Xia, Yanhua Zheng, Jong-Ho Lee, Wei Li, et al. 2017. "Nucleus-Translocated ACSS2 Promotes Gene Transcription for Lysosomal Biogenesis and Autophagy." *Molecular Cell* 66 (5): 684-697.e9. https://doi.org/10.1016/j.molcel.2017.04.026.
Liao, Y., G. K. Smyth, and W. Shi. 2014. "FeatureCounts: An Efficient General Purpose Program for Assigning Sequence Reads to Genomic Features." *Bioinformatics* 30 (7): 923–30. https://doi.org/10.1093/bioinformatics/btt656.
Liu, Dong-Mei, Lin Zhao, Ting-Ting Liu, Pei-Lin Jiao, Dian-Dian Zhao, Mei-Shu Shih, Bei Tao, Li-Hao Sun, Hong-Yan Zhao, and Jian-Min Liu. 2016. "Rictor/MTORC2 Loss in Osteoblasts Impairs Bone Mass and Strength." *Bone* 90: 50–58. https://doi.org/10.1016/j.bone.2016.05.010.
Liu, Weiyi, Yaqin Liu, Xinsheng Lai, and Shihuan Kuang. 2012. "Intramuscular Adipose Is Derived from a Non-Pax3 Lineage and Required for Efficient Regeneration of Skeletal Muscles." *Developmental Biology* 361 (1): 27–38. https://doi.org/10.1016/j.ydbio.2011.10.011.
Logan, Malcolm, James F. Martin, Andras Nagy, Corrinne Lobe, Eric N. Olson, and Clifford J. Tabin. 2002. "Expression of Cre Recombinase in the Developing Mouse Limb Bud Driven by a Prxl Enhancer." *Genesis (New York, N.Y.: 2000)* 33 (2): 77–80. https://doi.org/10.1002/gene.10092.
Longo, Michele, Federica Zatterale, Jamal Naderi, Luca Parrillo, Pietro Formisano, Gregory Alexander Raciti, Francesco Beguinot, and Claudia Miele. 2019. "Adipose Tissue Dysfunction as Determinant of Obesity-Associated Metabolic Complications." *International Journal of Molecular Sciences* 20 (9). https://doi.org/10.3390/ijms20092358.
Love, Michael I, Wolfgang Huber, and Simon Anders. 2014. "Moderated Estimation of Fold Change and Dispersion for RNA-Seq Data with

DESeq2." *Genome Biology* 15 (12). https://doi.org/10.1186/s13059-014-0550-8.
Luo, Liping, and Meilian Liu. 2016. "Adipose Tissue in Control of Metabolism." *Journal of Endocrinology* 231 (3): R77–99. https://doi.org/10.1530/JOE-16-0211.
Macotela, Yazmín, Brice Emanuelli, Marcelo A. Mori, Stephane Gesta, Tim J. Schulz, Yu-Hua Tseng, and C. Ronald Kahn. 2012. "Intrinsic Differences in Adipocyte Precursor Cells from Different White Fat Depots." *Diabetes* 61 (7): 1691–99. https://doi.org/10.2337/db11-1753.
Manning, Brendan D., and Lewis C. Cantley. 2007. "AKT/PKB Signaling: Navigating Downstream." *Cell* 129 (7): 1261–74. https://doi.org/10.1016/j.cell.2007.06.009.
Mashimo, Tomoyuki, Kumar Pichumani, Vamsidhara Vemireddy, Kimmo J. Hatanpaa, Dinesh Kumar Singh, Shyam Sirasanagandla, Suraj Nannepaga, et al. 2014. "Acetate Is a Bioenergetic Substrate for Human Glioblastoma and Brain Metastases." *Cell* 159 (7): 1603–14. https://doi.org/10.1016/j.cell.2014.11.025.
Masui, Kenta, Webster K. Cavenee, and Paul S. Mischel. 2014. "MTORC2 in the Center of Cancer Metabolic Reprogramming." *Trends in Endocrinology and Metabolism: TEM* 25 (7): 364–73. https://doi.org/10.1016/j.tem.2014.04.002.
McLaughlin, Tracey, Cindy Lamendola, Alice Liu, and Fahim Abbasi. 2011. "Preferential Fat Deposition in Subcutaneous versus Visceral Depots Is Associated with Insulin Sensitivity." *The Journal of Clinical Endocrinology and Metabolism* 96 (11): E1756-1760. https://doi.org/10.1210/jc.2011-0615.
McLaughlin Tracey, Liu Li-Fen, Lamendola Cindy, Shen Lei, Morton John, Rivas Homero, Winer Daniel, et al. 2014. "T-Cell Profile in Adipose Tissue Is Associated With Insulin Resistance and Systemic Inflammation in Humans." *Arteriosclerosis, Thrombosis, and Vascular Biology* 34 (12): 2637–43. https://doi.org/10.1161/ATVBAHA.114.304636.
Miard, S., and L. Fajas. 2005. "Atypical Transcriptional Regulators and Cofactors of PPARgamma." *International Journal of Obesity (2005)* 29 Suppl 1 (March): S10-12. https://doi.org/10.1038/sj.ijo.0802906.
Mîinea, Cristinel P., Hiroyuki Sano, Susan Kane, Eiko Sano, Mitsunori Fukuda, Johan Peränen, William S. Lane, and Gustav E. Lienhard. 2005. "AS160, the Akt Substrate Regulating GLUT4 Translocation, Has a Functional Rab GTPase-Activating Protein Domain." *Biochemical Journal* 391 (Pt 1): 87–93. https://doi.org/10.1042/BJ20050887.
Mondoux, Michelle A., Dona C. Love, Salil K. Ghosh, Tetsunari Fukushige, Michelle Bond, Gayani R. Weerasinghe, John A. Hanover, and Michael W. Krause. 2011. "O-Linked-N-Acetylglucosamine Cycling and Insulin Signaling Are Required for the Glucose Stress Response in

Caenorhabditis Elegans." *Genetics* 188 (2): 369–82. https://doi.org/10.1534/genetics.111.126490.
Monvoisin, Arnaud, Jackelyn A. Alva, Jennifer J. Hofmann, Ann C. Zovein, Timothy F. Lane, and M. Luisa Iruela-Arispe. 2006. "VE-Cadherin-CreERT2 Transgenic Mouse: A Model for Inducible Recombination in the Endothelium." *Developmental Dynamics: An Official Publication of the American Association of Anatomists* 235 (12): 3413–22. https://doi.org/10.1002/dvdy.20982.
Morigny, Pauline, Marianne Houssier, Etienne Mouisel, and Dominique Langin. 2016. "Adipocyte Lipolysis and Insulin Resistance." *Biochimie* 125 (June): 259–66. https://doi.org/10.1016/j.biochi.2015.10.024.
Muka, T., J. Nano, T. Voortman, K. V. E. Braun, S. Ligthart, S. Stranges, W. M. Bramer, et al. 2016. "The Role of Global and Regional DNA Methylation and Histone Modifications in Glycemic Traits and Type 2 Diabetes: A Systematic Review." *Nutrition, Metabolism, and Cardiovascular Diseases: NMCD* 26 (7): 553–66. https://doi.org/10.1016/j.numecd.2016.04.002.
Mullican, Shannon E., Takuya Tomaru, Christine A. Gaddis, Lindsey C. Peed, Anand Sundaram, and Mitchell A. Lazar. 2013. "A Novel Adipose-Specific Gene Deletion Model Demonstrates Potential Pitfalls of Existing Methods." *Molecular Endocrinology (Baltimore, Md.)* 27 (1): 127–34. https://doi.org/10.1210/me.2012-1267.
Nakatani, Kaname, Hiroshi Sakaue, Devon A. Thompson, Ronald J. Weigel, and Richard A. Roth. 1999. "Identification of a Human Akt3 (Protein Kinase B γ) Which Contains the Regulatory Serine Phosphorylation Site." *Biochemical and Biophysical Research Communications* 257 (3): 906–10. https://doi.org/10.1006/bbrc.1999.0559.
Nishizawa, Hitoshi, Iichiro Shimomura, Ken Kishida, Norikazu Maeda, Hiroshi Kuriyama, Hiroyuki Nagaretani, Morihiro Matsuda, et al. 2002. "Androgens Decrease Plasma Adiponectin, an Insulin-Sensitizing Adipocyte-Derived Protein." *Diabetes* 51 (9): 2734–41. https://doi.org/10.2337/diabetes.51.9.2734.
Ohshima, Takayuki, Hiroshi Koga, and Kunitada Shimotohno. 2004. "Transcriptional Activity of Peroxisome Proliferator-Activated Receptor Gamma Is Modulated by SUMO-1 Modification." *The Journal of Biological Chemistry* 279 (28): 29551–57. https://doi.org/10.1074/jbc.M403866200.
Oki, S, and T Ohta. 2016. "ChIP-Atlas." https://doi.org/10.18908/lsdba.nbdc01558-000.
Olefsky, Jerrold M., and Christopher K. Glass. 2010. "Macrophages, Inflammation, and Insulin Resistance." *Annual Review of Physiology* 72: 219–46. https://doi.org/10.1146/annurev-physiol-021909-135846.
Oliva-Olivera, Wilfredo, Said Lhamyani, Leticia Coín-Aragüez, Juan Alcaide-Torres, Fernando Cardona, Rajaa El Bekay, and Francisco J. Tinahones. 2018. "Involvement of Acetyl-CoA-Producing Enzymes in the Deterioration of the Functional Potential of Adipose-Derived Multipotent Cells from

Subjects with Metabolic Syndrome." *Metabolism: Clinical and Experimental* 88: 12–21. https://doi.org/10.1016/j.metabol.2018.08.004.
Ortega-Prieto, Paula, and Catherine Postic. 2019. "Carbohydrate Sensing Through the Transcription Factor ChREBP." *Frontiers in Genetics* 10: 472. https://doi.org/10.3389/fgene.2019.00472.
Panasyuk, Ganna, Catherine Espeillac, Céline Chauvin, Ludivine A. Pradelli, Yasuo Horie, Akira Suzuki, Jean-Sebastien Annicotte, et al. 2012a. "PPARγ Contributes to PKM2 and HK2 Expression in Fatty Liver." *Nature Communications* 3 (1). https://doi.org/10.1038/ncomms1667.
———. 2012b. "PPARγ Contributes to PKM2 and HK2 Expression in Fatty Liver." *Nature Communications* 3 (February): 672. https://doi.org/10.1038/ncomms1667.
Park, Seung Yoon, Jiwon Ryu, and Wan Lee. 2005. "O -GlcNAc Modification on IRS-1 and Akt2 by PUGNAc Inhibits Their Phosphorylation and Induces Insulin Resistance in Rat Primary Adipocytes." *Experimental & Molecular Medicine* 37 (3): 220–29. https://doi.org/10.1038/emm.2005.30.
Parlee, Sebastian D., Stephen I. Lentz, Hiroyuki Mori, and Ormond A. MacDougald. 2014. "Quantifying Size and Number of Adipocytes in Adipose Tissue." *Methods in Enzymology* 537: 93–122. https://doi.org/10.1016/B978-0-12-411619-1.00006-9.
Pascual, Gabriel, Amy L. Fong, Sumito Ogawa, Amir Gamliel, Andrew C. Li, Valentina Perissi, David W. Rose, Timothy M. Willson, Michael G. Rosenfeld, and Christopher K. Glass. 2005. "A SUMOylation-Dependent Pathway Mediates Transrepression of Inflammatory Response Genes by PPAR-Gamma." *Nature* 437 (7059): 759–63. https://doi.org/10.1038/nature03988.
Peng, Xiao-Ding, Pei-Zhang Xu, Mei-Ling Chen, Annett Hahn-Windgassen, Jennifer Skeen, Joel Jacobs, Deepa Sundararajan, et al. 2003. "Dwarfism, Impaired Skin Development, Skeletal Muscle Atrophy, Delayed Bone Development, and Impeded Adipogenesis in Mice Lacking Akt1 and Akt2." *Genes & Development* 17 (11): 1352–65. https://doi.org/10.1101/gad.1089403.
Perrot, Valérie, and Matthew M. Rechler. 2005. "The Coactivator P300 Directly Acetylates the Forkhead Transcription Factor Foxo1 and Stimulates Foxo1-Induced Transcription." *Molecular Endocrinology* 19 (9): 2283–98. https://doi.org/10.1210/me.2004-0292.
Pietrocola, Federico, Lorenzo Galluzzi, José Manuel Bravo-San Pedro, Frank Madeo, and Guido Kroemer. 2015. "Acetyl Coenzyme A: A Central Metabolite and Second Messenger." *Cell Metabolism* 21 (6): 805–21. https://doi.org/10.1016/j.cmet.2015.05.014.
Pope, Benjamin D., Curtis R. Warren, Kevin Kit Parker, and Chad A. Cowan. 2016. "Microenvironmental Control of Adipocyte Fate and Function." *Trends in Cell Biology* 26 (10): 745–55. https://doi.org/10.1016/j.tcb.2016.05.005.

Powell, Emily, Peter Kuhn, and Wei Xu. 2007. “Nuclear Receptor Cofactors in PPAR γ -Mediated Adipogenesis and Adipocyte Energy Metabolism.” *PPAR Research* 2007: 1–11. https://doi.org/10.1155/2007/53843.

Primeau, V., L. Coderre, A. D. Karelis, M. Brochu, M.-E. Lavoie, V. Messier, R. Sladek, and R. Rabasa-Lhoret. 2011. “Characterizing the Profile of Obese Patients Who Are Metabolically Healthy.” *International Journal of Obesity* 35 (7): 971–81. https://doi.org/10.1038/ijo.2010.216.

Qian, Hui, Yuanying Chen, Zongqian Nian, Lu Su, Haoyong Yu, Feng-Jung Chen, Xiuqin Zhang, et al. 2017. “HDAC6-Mediated Acetylation of Lipid Droplet-Binding Protein CIDEC Regulates Fat-Induced Lipid Storage.” *The Journal of Clinical Investigation* 127 (4): 1353–69. https://doi.org/10.1172/JCI85963.

Quarta, Carmelo, Roberta Mazza, Renato Pasquali, and Uberto Pagotto. 2012. “Role of Sex Hormones in Modulation of Brown Adipose Tissue Activity.” *Journal of Molecular Endocrinology* 49 (1): R1–7. https://doi.org/10.1530/JME-12-0043.

Ramm, Georg, Mark Larance, Michael Guilhaus, and David E. James. 2006. “A Role for 14-3-3 in Insulin-Stimulated GLUT4 Translocation through Its Interaction with the RabGAP AS160.” *Journal of Biological Chemistry* 281 (39): 29174–80. https://doi.org/10.1074/jbc.M603274200.

Roberts, R., L. Hodson, A. L. Dennis, M. J. Neville, S. M. Humphreys, K. E. Harnden, K. J. Micklem, and K. N. Frayn. 2009. “Markers of de Novo Lipogenesis in Adipose Tissue: Associations with Small Adipocytes and Insulin Sensitivity in Humans.” *Diabetologia* 52 (5): 882–90. https://doi.org/10.1007/s00125-009-1300-4.

Rodeheffer, Matthew S., Kivanç Birsoy, and Jeffrey M. Friedman. 2008. “Identification of White Adipocyte Progenitor Cells in Vivo.” *Cell* 135 (2): 240–49. https://doi.org/10.1016/j.cell.2008.09.036.

Roesch, Karin, Ashutosh P. Jadhav, Jeffrey M. Trimarchi, Michael B. Stadler, Botond Roska, Ben B. Sun, and Constance L. Cepko. 2008. “The Transcriptome of Retinal Müller Glial Cells.” *The Journal of Comparative Neurology* 509 (2): 225–38. https://doi.org/10.1002/cne.21730.

Roh, Hyun Cheol, Linus T.-Y. Tsai, Anna Lyubetskaya, Danielle Tenen, Manju Kumari, and Evan D. Rosen. 2017. “Simultaneous Transcriptional and Epigenomic Profiling from Specific Cell Types within Heterogeneous Tissues In Vivo.” *Cell Reports* 18 (4): 1048–61. https://doi.org/10.1016/j.celrep.2016.12.087.

Rosen, Evan D., and Bruce M. Spiegelman. 2014. “What We Talk About When We Talk About Fat.” *Cell* 156 (1): 20–44. https://doi.org/10.1016/j.cell.2013.12.012.

Salma, Nunciada, Hengyi Xiao, Elisabetta Mueller, and Anthony N. Imbalzano. 2004. “Temporal Recruitment of Transcription Factors and SWI/SNF Chromatin-Remodeling Enzymes during Adipogenic Induction of the Peroxisome Proliferator-Activated Receptor Gamma Nuclear Hormone

Receptor." *Molecular and Cellular Biology* 24 (11): 4651–63. https://doi.org/10.1128/MCB.24.11.4651-4663.2004.
Samuel, Varman T., and Gerald I. Shulman. 2012. "Mechanisms for Insulin Resistance: Common Threads and Missing Links." *Cell* 148 (5): 852–71. https://doi.org/10.1016/j.cell.2012.02.017.
Sanchez-Gurmaches, Joan, Wen-Yu Hsiao, and David A. Guertin. 2015. "Highly Selective In Vivo Labeling of Subcutaneous White Adipocyte Precursors with Prx1-Cre." *Stem Cell Reports* 4 (4): 541–50. https://doi.org/10.1016/j.stemcr.2015.02.008.
Sanchez-Gurmaches, Joan, Chien-Min Hung, and David A. Guertin. 2016. "Emerging Complexities in Adipocyte Origins and Identity." *Trends in Cell Biology* 26 (5): 313–26. https://doi.org/10.1016/j.tcb.2016.01.004.
Sanchez-Gurmaches, Joan, Chien-Min Hung, Cynthia A. Sparks, Yuefeng Tang, Huawei Li, and David A. Guertin. 2012. "PTEN Loss in the Myf5 Lineage Redistributes Body Fat and Reveals Subsets of White Adipocytes That Arise from Myf5 Precursors." *Cell Metabolism* 16 (3): 348–62. https://doi.org/10.1016/j.cmet.2012.08.003.
Sanchez-Gurmaches, Joan, Camila Martinez Calejman, Su Myung Jung, Huawei Li, and David A. Guertin. 2019. "Brown Fat Organogenesis and Maintenance Requires AKT1 and AKT2." *Molecular Metabolism* 23 (February): 60–74. https://doi.org/10.1016/j.molmet.2019.02.004.
Sanders, Francis W. B., and Julian L. Griffin. 2016. "De Novo Lipogenesis in the Liver in Health and Disease: More than Just a Shunting Yard for Glucose." *Biological Reviews of the Cambridge Philosophical Society* 91 (2): 452–68. https://doi.org/10.1111/brv.12178.
Santi, Stacey A., and Hoyun Lee. 2010. "The Akt Isoforms Are Present at Distinct Subcellular Locations." *American Journal of Physiology-Cell Physiology* 298 (3): C580–91. https://doi.org/10.1152/ajpcell.00375.2009.
Sarbassov, D. D., David A. Guertin, Siraj M. Ali, and David M. Sabatini. 2005. "Phosphorylation and Regulation of Akt/PKB by the Rictor-MTOR Complex." *Science (New York, N.Y.)* 307 (5712): 1098–1101. https://doi.org/10.1126/science.1106148.
Sattar, Naveed, and Jason MR Gill. 2014. "Type 2 Diabetes as a Disease of Ectopic Fat?" *BMC Medicine* 12 (1). https://doi.org/10.1186/s12916-014-0123-4.
Saxton, Robert A., and David M. Sabatini. 2017. "MTOR Signaling in Growth, Metabolism, and Disease." *Cell* 169 (2): 361–71. https://doi.org/10.1016/j.cell.2017.03.035.
Scheller, Erica L., Aaron A. Burr, Ormond A. MacDougald, and William P. Cawthorn. 2016. "Inside out: Bone Marrow Adipose Tissue as a Source of Circulating Adiponectin." *Adipocyte* 5 (3): 251–69. https://doi.org/10.1080/21623945.2016.1149269.
Scheller, Erica L., Casey R. Doucette, Brian S. Learman, William P. Cawthorn, Shaima Khandaker, Benjamin Schell, Brent Wu, et al. 2015. "Region-

Specific Variation in the Properties of Skeletal Adipocytes Reveals Regulated and Constitutive Marrow Adipose Tissues." *Nature Communications* 6 (August): 7808. https://doi.org/10.1038/ncomms8808.
Scheller, Erica L., Nancy Troiano, Joshua N. VanHoutan, Mary A. Bouxsein, Jackie A. Fretz, Yougen Xi, Tracy Nelson, et al. 2014. "Use of Osmium Tetroxide Staining with Microcomputerized Tomography to Visualize and Quantify Bone Marrow Adipose Tissue In Vivo." In *Methods in Enzymology*, 537:123–39. Elsevier. https://doi.org/10.1016/B978-0-12-411619-1.00007-0.
Scherer, Philipp E. 2019. "The Many Secret Lives of Adipocytes: Implications for Diabetes." *Diabetologia* 62 (2): 223–32. https://doi.org/10.1007/s00125-018-4777-x.
Schindelin, Johannes, Ignacio Arganda-Carreras, Erwin Frise, Verena Kaynig, Mark Longair, Tobias Pietzsch, Stephan Preibisch, et al. 2012. "Fiji: An Open-Source Platform for Biological-Image Analysis." *Nature Methods* 9 (7): 676–82. https://doi.org/10.1038/nmeth.2019.
Schoonjans, K., G. Martin, B. Staels, and J. Auwerx. 1997. "Peroxisome Proliferator-Activated Receptors, Orphans with Ligands and Functions." *Current Opinion in Lipidology* 8 (3): 159–66. https://doi.org/10.1097/00041433-199706000-00006.
Schoonjans, K., B. Staels, and J. Auwerx. 1996. "Role of the Peroxisome Proliferator-Activated Receptor (PPAR) in Mediating the Effects of Fibrates and Fatty Acids on Gene Expression." *Journal of Lipid Research* 37 (5): 907–25.
Schug, Zachary T., Barrie Peck, Dylan T. Jones, Qifeng Zhang, Shaun Grosskurth, Israt S. Alam, Louise M. Goodwin, et al. 2015. "Acetyl-CoA Synthetase 2 Promotes Acetate Utilization and Maintains Cancer Cell Growth under Metabolic Stress." *Cancer Cell* 27 (1): 57–71. https://doi.org/10.1016/j.ccell.2014.12.002.
Sebo, Zachary L., Elise Jeffery, Brandon Holtrup, and Matthew S. Rodeheffer. 2018. "A Mesodermal Fate Map for Adipose Tissue." *Development (Cambridge, England)* 145 (17). https://doi.org/10.1242/dev.166801.
Sebo, Zachary L., and Matthew S. Rodeheffer. 2019. "Assembling the Adipose Organ: Adipocyte Lineage Segregation and Adipogenesis in Vivo." *Development (Cambridge, England)* 146 (7). https://doi.org/10.1242/dev.172098.
Sharma, Sorabh, and Rajeev Taliyan. 2016. "Histone Deacetylase Inhibitors: Future Therapeutics for Insulin Resistance and Type 2 Diabetes." *Pharmacological Research* 113 (November): 320–26. https://doi.org/10.1016/j.phrs.2016.09.009.
Shearin, Abigail L., Bobby R. Monks, Patrick Seale, and Morris J. Birnbaum. 2016. "Lack of AKT in Adipocytes Causes Severe Lipodystrophy." *Molecular Metabolism* 5 (7): 472–79. https://doi.org/10.1016/j.molmet.2016.05.006.

Shi, Lei, and Benjamin P. Tu. 2015. “Acetyl-CoA and the Regulation of Metabolism: Mechanisms and Consequences.” *Current Opinion in Cell Biology* 33 (April): 125–31. https://doi.org/10.1016/j.ceb.2015.02.003.
Shiota, Chiyo, Jeong-Taek Woo, Jill Lindner, Kathy D. Shelton, and Mark A. Magnuson. 2006. “Multiallelic Disruption of the Rictor Gene in Mice Reveals That MTOR Complex 2 Is Essential for Fetal Growth and Viability.” *Developmental Cell* 11 (4): 583–89. https://doi.org/10.1016/j.devcel.2006.08.013.
Sif, S., P. T. Stukenberg, M. W. Kirschner, and R. E. Kingston. 1998. “Mitotic Inactivation of a Human SWI/SNF Chromatin Remodeling Complex.” *Genes & Development* 12 (18): 2842–51. https://doi.org/10.1101/gad.12.18.2842.
Sivanand, Sharanya, Isabella Viney, and Kathryn E. Wellen. 2018. “Spatiotemporal Control of Acetyl-CoA Metabolism in Chromatin Regulation.” *Trends in Biochemical Sciences* 43 (1): 61–74. https://doi.org/10.1016/j.tibs.2017.11.004.
Snel, M., J. T. Jonker, J. Schoones, H. Lamb, A. de Roos, H. Pijl, J. W. A. Smit, A. E. Meinders, and I. M. Jazet. 2012. “Ectopic Fat and Insulin Resistance: Pathophysiology and Effect of Diet and Lifestyle Interventions.” *International Journal of Endocrinology* 2012: 1–18. https://doi.org/10.1155/2012/983814.
Song, Ziyi, Alus M. Xiaoli, and Fajun Yang. 2018. “Regulation and Metabolic Significance of De Novo Lipogenesis in Adipose Tissues.” *Nutrients* 10 (10). https://doi.org/10.3390/nu10101383.
Stanford, Kristin I., Roeland J.W. Middelbeek, Kristy L. Townsend, Min-Young Lee, Hirokazu Takahashi, Kawai So, Kristen M. Hitchcox, et al. 2015. “A Novel Role for Subcutaneous Adipose Tissue in Exercise-Induced Improvements in Glucose Homeostasis.” *Diabetes* 64 (6): 2002–14. https://doi.org/10.2337/db14-0704.
Steger, David J., Gregory R. Grant, Michael Schupp, Takuya Tomaru, Martina I. Lefterova, Jonathan Schug, Elisabetta Manduchi, Christian J. Stoeckert, and Mitchell A. Lazar. 2010. “Propagation of Adipogenic Signals through an Epigenomic Transition State.” *Genes & Development* 24 (10): 1035–44. https://doi.org/10.1101/gad.1907110.
Stephens, M. 2017. “False Discovery Rates: A New Deal.” *Biostatistics*. https://doi.org/10.1093/biostatistics/kxw041.
Strawford, A., F. Antelo, M. Christiansen, and M. K. Hellerstein. 2004. “Adipose Tissue Triglyceride Turnover, de Novo Lipogenesis, and Cell Proliferation in Humans Measured with 2H2O.” *American Journal of Physiology. Endocrinology and Metabolism* 286 (4): E577-588. https://doi.org/10.1152/ajpendo.00093.2003.
Sullivan, Patrick W., Elaine H. Morrato, Vahram Ghushchyan, Holly R. Wyatt, and James O. Hill. 2005. “Obesity, Inactivity, and the Prevalence of Diabetes and Diabetes-Related Cardiovascular Comorbidities in the U.S.,

2000-2002." *Diabetes Care* 28 (7): 1599–1603. https://doi.org/10.2337/diacare.28.7.1599.
Sun, Chao, Jin Shang, Yuan Yao, Xiaohong Yin, Minghan Liu, Huan Liu, and Yue Zhou. 2016. "O-GlcNAcylation: A Bridge between Glucose and Cell Differentiation." *Journal of Cellular and Molecular Medicine* 20 (5): 769–81. https://doi.org/10.1111/jcmm.12807.
Sun, Weiwei, Yu Shi, Wen-Chih Lee, Seung-Yon Lee, and Fanxin Long. 2016. "Rictor Is Required for Optimal Bone Accrual in Response to Anti-Sclerostin Therapy in the Mouse." *Bone* 85 (April): 1–8. https://doi.org/10.1016/j.bone.2016.01.013.
Syed, Ismail, Jennifer Lee, Pedro M. Moraes-Vieira, Cynthia J. Donaldson, Alexandra Sontheimer, Pratik Aryal, Kerry Wellenstein, et al. 2018. "Palmitic Acid Hydroxystearic Acids Activate GPR40, Which Is Involved in Their Beneficial Effects on Glucose Homeostasis." *Cell Metabolism* 27 (2): 419-427.e4. https://doi.org/10.1016/j.cmet.2018.01.001.
Tabák, Adam G., Christian Herder, Wolfgang Rathmann, Eric J. Brunner, and Mika Kivimäki. 2012. "Prediabetes: A High-Risk State for Developing Diabetes." *Lancet* 379 (9833): 2279–90. https://doi.org/10.1016/S0140-6736(12)60283-9.
Takahashi, Hidekazu, J. Michael McCaffery, Rafael A. Irizarry, and Jef D. Boeke. 2006. "Nucleocytosolic Acetyl-Coenzyme a Synthetase Is Required for Histone Acetylation and Global Transcription." *Molecular Cell* 23 (2): 207–17. https://doi.org/10.1016/j.molcel.2006.05.040.
Tallquist, M. D., K. E. Weismann, M. Hellström, and P. Soriano. 2000. "Early Myotome Specification Regulates PDGFA Expression and Axial Skeleton Development." *Development (Cambridge, England)* 127 (23): 5059–70.
Tang, Wei, Daniel Zeve, Jae Myoung Suh, Darko Bosnakovski, Michael Kyba, Robert E. Hammer, Michelle D. Tallquist, and Jonathan M. Graff. 2008. "White Fat Progenitor Cells Reside in the Adipose Vasculature." *Science (New York, N.Y.)* 322 (5901): 583–86. https://doi.org/10.1126/science.1156232.
Tang, Yuefeng, Martina Wallace, Joan Sanchez-Gurmaches, Wen-Yu Hsiao, Huawei Li, Peter L. Lee, Santiago Vernia, Christian M. Metallo, and David A. Guertin. 2016. "Adipose Tissue MTORC2 Regulates ChREBP-Driven de Novo Lipogenesis and Hepatic Glucose Metabolism." *Nature Communications* 7 (April): 11365. https://doi.org/10.1038/ncomms11365.
Tchernof, A., and J. P. Després. 2000. "Sex Steroid Hormones, Sex Hormone-Binding Globulin, and Obesity in Men and Women." *Hormone and Metabolic Research = Hormon- Und Stoffwechselforschung = Hormones Et Metabolisme* 32 (11–12): 526–36. https://doi.org/10.1055/s-2007-978681.
Tchernof, André, and Jean-Pierre Després. 2013. "Pathophysiology of Human Visceral Obesity: An Update." *Physiological Reviews* 93 (1): 359–404. https://doi.org/10.1152/physrev.00033.2011.

Tchoukalova, Yourka D, Christina Koutsari, Susanne B Votruba, Tamara Tchkonia, Nino Giorgadze, Thomas Thomou, James L. Kirkland, and Michael D Jensen. 2010. “Sex- and Depot-Dependent Differences in Adipogenesis in Normal Weight Humans.” *Obesity (Silver Spring, Md.)* 18 (10): 1875–80. https://doi.org/10.1038/oby.2010.56.

Tian, Lifeng, Chenguang Wang, Fred K. Hagen, Michael Gormley, Sankar Addya, Raymond Soccio, Mathew C. Casimiro, et al. 2014. “Acetylation-Defective Mutant of Pparγ Is Associated with Decreased Lipid Synthesis in Breast Cancer Cells.” *Oncotarget* 5 (17): 7303–15. https://doi.org/10.18632/oncotarget.2371.

Tontonoz, P., R. A. Graves, A. I. Budavari, H. Erdjument-Bromage, M. Lui, E. Hu, P. Tempst, and B. M. Spiegelman. 1994. “Adipocyte-Specific Transcription Factor ARF6 Is a Heterodimeric Complex of Two Nuclear Hormone Receptors, PPAR Gamma and RXR Alpha.” *Nucleic Acids Research* 22 (25): 5628–34. https://doi.org/10.1093/nar/22.25.5628.

Tramunt, Blandine, Sarra Smati, Naia Grandgeorge, Françoise Lenfant, Jean-François Arnal, Alexandra Montagner, and Pierre Gourdy. 2019. “Sex Differences in Metabolic Regulation and Diabetes Susceptibility.” *Diabetologia*, November. https://doi.org/10.1007/s00125-019-05040-3.

Tran, Khanh-Van, Olga Gealekman, Andrea Frontini, Maria Cristina Zingaretti, Manrico Morroni, Antonio Giordano, Arianna Smorlesi, et al. 2012. “The Vascular Endothelium of the Adipose Tissue Gives Rise to Both White and Brown Fat Cells.” *Cell Metabolism* 15 (2): 222–29. https://doi.org/10.1016/j.cmet.2012.01.008.

Tran, Thien T., Yuji Yamamoto, Stephane Gesta, and C. Ronald Kahn. 2008. “Beneficial Effects of Subcutaneous Fat Transplantation on Metabolism.” *Cell Metabolism* 7 (5): 410–20. https://doi.org/10.1016/j.cmet.2008.04.004.

Trefely, Sophie, Peter Ashwell, and Nathaniel W. Snyder. 2016. “FluxFix: Automatic Isotopologue Normalization for Metabolic Tracer Analysis.” *BMC Bioinformatics* 17 (1): 485. https://doi.org/10.1186/s12859-016-1360-7.

Tulloch-Reid, Marshall K., Robert L. Hanson, Nancy G. Sebring, James C. Reynolds, Ahalya Premkumar, David J. Genovese, and Anne E. Sumner. 2004. “Both Subcutaneous and Visceral Adipose Tissue Correlate Highly with Insulin Resistance in African Americans.” *Obesity Research* 12 (8): 1352–59. https://doi.org/10.1038/oby.2004.170.

Unger, Roger H., Gregory O. Clark, Philipp E. Scherer, and Lelio Orci. 2010. “Lipid Homeostasis, Lipotoxicity and the Metabolic Syndrome.” *Biochimica et Biophysica Acta (BBA) - Molecular and Cell Biology of Lipids*, Lipotoxicity, 1801 (3): 209–14. https://doi.org/10.1016/j.bbalip.2009.10.006.

Valencak, Teresa G., Anne Osterrieder, and Tim J. Schulz. 2017. “Sex Matters: The Effects of Biological Sex on Adipose Tissue Biology and Energy

Metabolism." *Redox Biology* 12 (August): 806–13. https://doi.org/10.1016/j.redox.2017.04.012.
Van Gaal, Luc F., Ilse L. Mertens, and Christophe E. De Block. 2006. "Mechanisms Linking Obesity with Cardiovascular Disease." *Nature* 444 (7121): 875–80. https://doi.org/10.1038/nature05487.
Veilleux, Alain, Maude Caron-Jobin, Suzanne Noël, Philippe Y. Laberge, and André Tchernof. 2011. "Visceral Adipocyte Hypertrophy Is Associated With Dyslipidemia Independent of Body Composition and Fat Distribution in Women." *Diabetes* 60 (5): 1504–11. https://doi.org/10.2337/db10-1039.
Verboven, K., K. Wouters, K. Gaens, D. Hansen, M. Bijnen, S. Wetzels, C. D. Stehouwer, et al. 2018. "Abdominal Subcutaneous and Visceral Adipocyte Size, Lipolysis and Inflammation Relate to Insulin Resistance in Male Obese Humans." *Scientific Reports* 8 (1): 4677. https://doi.org/10.1038/s41598-018-22962-x.
Vijayakumar, Archana, Pratik Aryal, Jennifer Wen, Ismail Syed, Reema P. Vazirani, Pedro M. Moraes-Vieira, Joao Paulo Camporez, et al. 2017. "Absence of Carbohydrate Response Element Binding Protein in Adipocytes Causes Systemic Insulin Resistance and Impairs Glucose Transport." *Cell Reports* 21 (4): 1021–35. https://doi.org/10.1016/j.celrep.2017.09.091.
Vishvanath, Lavanya, and Rana K. Gupta. 2019. "Contribution of Adipogenesis to Healthy Adipose Tissue Expansion in Obesity." *Journal of Clinical Investigation* 129 (10): 4022–31. https://doi.org/10.1172/JCI129191.
Viswakarma, Navin, Yuzhi Jia, Liang Bai, Aurore Vluggens, Jayme Borensztajn, Jianming Xu, and Janardan K. Reddy. 2010. "Coactivators in PPAR-Regulated Gene Expression." *PPAR Research* 2010: 1–21. https://doi.org/10.1155/2010/250126.
Vysochan, Anna, Arjun Sengupta, Aalim M. Weljie, James C. Alwine, and Yongjun Yu. 2017. "ACSS2-Mediated Acetyl-CoA Synthesis from Acetate Is Necessary for Human Cytomegalovirus Infection." *Proceedings of the National Academy of Sciences of the United States of America* 114 (8): E1528–35. https://doi.org/10.1073/pnas.1614268114.
Wang, Qiong A, Caroline Tao, Rana K Gupta, and Philipp E Scherer. 2013. "Tracking Adipogenesis during White Adipose Tissue Development, Expansion and Regeneration." *Nature Medicine* 19 (10): 1338–44. https://doi.org/10.1038/nm.3324.
Wang, Xiao, Zhimin Wang, Qing Wang, Hao Liang, and Dongjun Liu. 2019. "Trichostatin A and Vorinostat Promote Adipogenic Differentiation through H3K9 Acetylation and Dimethylation." *Research in Veterinary Science* 126 (October): 207–12. https://doi.org/10.1016/j.rvsc.2019.09.002.
Wang, Xiaoqing, Lai Wang, Yizheng Sun, Ruiping Li, Jinbo Deng, and Jiexin Deng. 2017. "DNA Methylation and Histone Deacetylation Regulating Insulin Sensitivity Due to Chronic Cold Exposure." *Cryobiology* 74: 36–42. https://doi.org/10.1016/j.cryobiol.2016.12.006.

Wang, Zhao V., Yingfeng Deng, Qiong A. Wang, Kai Sun, and Philipp E. Scherer. 2010. “Identification and Characterization of a Promoter Cassette Conferring Adipocyte-Specific Gene Expression.” *Endocrinology* 151 (6): 2933–39. https://doi.org/10.1210/en.2010-0136.

Ward, Patrick S., and Craig B. Thompson. 2012. “Metabolic Reprogramming: A Cancer Hallmark Even Warburg Did Not Anticipate.” *Cancer Cell* 21 (3): 297–308. https://doi.org/10.1016/j.ccr.2012.02.014.

Wellen, Kathryn E., Georgia Hatzivassiliou, Uma M. Sachdeva, Thi V. Bui, Justin R. Cross, and Craig B. Thompson. 2009. “ATP-Citrate Lyase Links Cellular Metabolism to Histone Acetylation.” *Science (New York, N.Y.)* 324 (5930): 1076–80. https://doi.org/10.1126/science.1164097.

Wellen, Kathryn E., and Craig B. Thompson. 2012. “A Two-Way Street: Reciprocal Regulation of Metabolism and Signalling.” *Nature Reviews. Molecular Cell Biology* 13 (4): 270–76. https://doi.org/10.1038/nrm3305.

Wells, L., K. Vosseller, and G. W. Hart. 2003. “A Role for N-Acetylglucosamine as a Nutrient Sensor and Mediator of Insulin Resistance.” *Cellular and Molecular Life Sciences: CMLS* 60 (2): 222–28.

Whelan, Stephen A., Wagner B. Dias, Lakshmanan Thiruneelakantapillai, M. Daniel Lane, and Gerald W. Hart. 2010. “Regulation of Insulin Receptor Substrate 1 (IRS-1)/AKT Kinase-Mediated Insulin Signaling by O-Linked β-N-Acetylglucosamine in 3T3-L1 Adipocytes.” *Journal of Biological Chemistry* 285 (8): 5204–11. https://doi.org/10.1074/jbc.M109.077818.

White, Ursula A., and Yourka D. Tchoukalova. 2014. “Sex Dimorphism and Depot Differences in Adipose Tissue Function.” *Biochimica et Biophysica Acta (BBA) - Molecular Basis of Disease* 1842 (3): 377–92. https://doi.org/10.1016/j.bbadis.2013.05.006.

Willett, Walter C., William H. Dietz, and Graham A. Colditz. 1999. “Guidelines for Healthy Weight.” *New England Journal of Medicine* 341 (6): 427–34. https://doi.org/10.1056/NEJM199908053410607.

Witte, Nicole, Matthias Muenzner, Janita Rietscher, Miriam Knauer, Steffi Heidenreich, Alli M. Nuotio-Antar, Franziska A. Graef, et al. 2015. “The Glucose Sensor ChREBP Links De Novo Lipogenesis to PPARγ Activity and Adipocyte Differentiation.” *Endocrinology* 156 (11): 4008–19. https://doi.org/10.1210/EN.2015-1209.

Wollaston-Hayden, Edith E., Ruth B. S. Harris, Bingqiang Liu, Robert Bridger, Ying Xu, and Lance Wells. 2014. “Global O-GlcNAc Levels Modulate Transcription of the Adipocyte Secretome during Chronic Insulin Resistance.” *Frontiers in Endocrinology* 5: 223. https://doi.org/10.3389/fendo.2014.00223.

Wong, Roger HF, and Hei Sook Sul. 2010. “Insulin Signaling in Fatty Acid and Fat Synthesis: A Transcriptional Perspective.” *Current Opinion in Pharmacology* 10 (6): 684–91. https://doi.org/10.1016/j.coph.2010.08.004.

Xia, Chang, Xiaoquan Rao, and Jixin Zhong. 2017. “Role of T Lymphocytes in Type 2 Diabetes and Diabetes-Associated Inflammation.” Research

article. Journal of Diabetes Research. 2017. https://doi.org/10.1155/2017/6494795.
Xie, Yun, Canqi Cui, Aifang Nie, Yan Wang, Qicheng Ni, Yun Liu, Qinglei Yin, et al. 2017. “The MTORC2/PKC Pathway Sustains Compensatory Insulin Secretion of Pancreatic β Cells in Response to Metabolic Stress.” *Biochimica et Biophysica Acta (BBA) - General Subjects* 1861 (8): 2039–47. https://doi.org/10.1016/j.bbagen.2017.04.008.
Xu, Huifen, Jun Luo, Gongzhen Ma, Xueying Zhang, Dawei Yao, Ming Li, and Juan J. Loor. 2018. “Acyl-CoA Synthetase Short-Chain Family Member 2 (ACSS2) Is Regulated by SREBP-1 and Plays a Role in Fatty Acid Synthesis in Caprine Mammary Epithelial Cells.” *Journal of Cellular Physiology* 233 (2): 1005–16. https://doi.org/10.1002/jcp.25954.
Yang, Qin, Archana Vijayakumar, and Barbara B. Kahn. 2018. “Metabolites as Regulators of Insulin Sensitivity and Metabolism.” *Nature Reviews Molecular Cell Biology* 19 (10): 654. https://doi.org/10.1038/s41580-018-0044-8.
Ye, Jianping. 2013. “Improving Insulin Sensitivity With HDAC Inhibitor.” *Diabetes* 62 (3): 685–87. https://doi.org/10.2337/db12-1354.
Yki-Järvinen, Hannele. 2004. “Thiazolidinediones.” *The New England Journal of Medicine* 351 (11): 1106–18. https://doi.org/10.1056/NEJMra041001.
Yoo, Hyuntae, Gregory Stephanopoulos, and Joanne K. Kelleher. 2004. “Quantifying Carbon Sources for de Novo Lipogenesis in Wild-Type and IRS-1 Knockout Brown Adipocytes.” *Journal of Lipid Research* 45 (7): 1324–32. https://doi.org/10.1194/jlr.M400031-JLR200.
Yore, Mark M., Ismail Syed, Pedro M. Moraes-Vieira, Tejia Zhang, Mark A. Herman, Edwin A. Homan, Rajesh T. Patel, et al. 2014. “Discovery of a Class of Endogenous Mammalian Lipids with Anti-Diabetic and Anti-Inflammatory Effects.” *Cell* 159 (2): 318–32. https://doi.org/10.1016/j.cell.2014.09.035.
Yu, Deyang, Jay L. Tomasiewicz, Shany E. Yang, Blake R. Miller, Matthew H. Wakai, Dawn S. Sherman, Nicole E. Cummings, et al. 2019. “Calorie-Restriction-Induced Insulin Sensitivity Is Mediated by Adipose MTORC2 and Not Required for Lifespan Extension.” *Cell Reports* 29 (1): 236-248.e3. https://doi.org/10.1016/j.celrep.2019.08.084.
Yuan, Minsheng, Elizabeth Pino, Lianfeng Wu, Michael Kacergis, and Alexander A. Soukas. 2012. “Identification of Akt-Independent Regulation of Hepatic Lipogenesis by Mammalian Target of Rapamycin (MTOR) Complex 2.” *The Journal of Biological Chemistry* 287 (35): 29579–88. https://doi.org/10.1074/jbc.M112.386854.
Yun, Sung-Ji, Eun-Kyoung Kim, David F. Tucker, Chi Dae Kim, Morris J. Birnbaum, and Sun Sik Bae. 2008. “Isoform-Specific Regulation of Adipocyte Differentiation by Akt/Protein Kinase Bα.” *Biochemical and Biophysical Research Communications* 371 (1): 138–43. https://doi.org/10.1016/j.bbrc.2008.04.029.

Zebisch, Katja, Valerie Voigt, Martin Wabitsch, and Matthias Brandsch. 2012. "Protocol for Effective Differentiation of 3T3-L1 Cells to Adipocytes." *Analytical Biochemistry* 425 (1): 88–90. https://doi.org/10.1016/j.ab.2012.03.005.

Zerbino, Daniel R., Premanand Achuthan, Wasiu Akanni, M. Ridwan Amode, Daniel Barrell, Jyothish Bhai, Konstantinos Billis, et al. 2018. "Ensembl 2018." *Nucleic Acids Research* 46 (D1): D754–61. https://doi.org/10.1093/nar/gkx1098.

Zhang, Qiongyi, Muhammad Khairul Ramlee, Reinhard Brunmeir, Claudio J. Villanueva, Daniel Halperin, and Feng Xu. 2012. "Dynamic and Distinct Histone Modifications Modulate the Expression of Key Adipogenesis Regulatory Genes." *Cell Cycle (Georgetown, Tex.)* 11 (23): 4310–22. https://doi.org/10.4161/cc.22224.

Zhao, Di, Eliseo Guallar, Pamela Ouyang, Vinita Subramanya, Dhananjay Vaidya, Chiadi E. Ndumele, Joao A. Lima, et al. 2018. "Endogenous Sex Hormones and Incident Cardiovascular Disease in Post-Menopausal Women." *Journal of the American College of Cardiology* 71 (22): 2555–66. https://doi.org/10.1016/j.jacc.2018.01.083.

Zlotorynski, Eytan. 2017. "Gene Expression: ACSS2 Boosts Local Histone Acetylation." *Nature Reviews Molecular Cell Biology* 18 (June): 405. https://doi.org/10.1038/nrm.2017.61.

Zucker, Irving, and Annaliese K. Beery. 2010. "Males Still Dominate Animal Studies." *Nature* 465 (7299): 690. https://doi.org/10.1038/465690a.